

**OFFSHORE TECHNOLOGY
REPORT OTO 1999 022**

**Fatigue Life Implications for Design and Inspection
for Single Sided Welds at Tubular Joints**

MSL Engineering Limited
MSL House, 5-7 High Street,
Sunninghill, Ascot, Berks

Date of Issue: June 1999

Health and Safety Executive

This report is made available by the Health and Safety Executive as part of a series of reports of work which has been supported by funds provided by the Executive. Neither the Executive, nor the contractors concerned assume any liability for the reports nor do they necessarily reflect the views or policy of the Executive.

Reports in the OTO series can be obtained from
Research Strategy Unit, Magdalen House, Bootle, Merseyside L20 3DL
Fax: 0151 951 3098

SUMMARY

In offshore structures, tubular brace members are sometimes connected to the chord by single-sided welds. This may introduce defects at the weld root which remain undetected due to the difficulty of internal inspection. Such undetected defects may act as crack initiators under fatigue loading. The propensity of fatigue cracking to initiate and grow from the internal weld root rather than the external weld toe depends on the ratio (R) of the SCF at the root to that at the toe, and on the applicable S-N curves for the two sites.

This document reviews the available data on internal SCFs and pertinent S-N data, such that the impact of single-sided welding can be assessed. Formulations for the SCF ratio (R) are developed for simple joint types and load cases. The impact of single-sided welding is explored by two analyses of a typical structure; one analysis assuming single-sided welding and the other not. It is concluded that single-sided welded joints can give lower fatigue lives at the root than at the toe, but there are indications that this would only rarely constitute a problem because of the long lives of the affected joints.

CONTENTS

SUMMARY

CONTENTS

1. INTRODUCTION.....	1
2. AVAILABLE DATA ON INTERNAL SCFs.....	3
2.1 General.....	3
2.2 K Joints.....	4
2.3 X/DT Joints	4
2.4 Y/T Joints.....	5
3. INTERPOLATION FUNCTIONS FOR INTERNAL/EXTERNAL SCF RATIO.....	7
3.1 Methodology.....	7
3.2 K Joints	8
3.3 X/DT Joints	10
3.4 Y/T Joints.....	12
3.5 Summary of Fitted R Formulations	13
4. SELECTION OF S-N CURVE	17
5. IMPACT ON JACKET ANALYSIS	19
5.1 General.....	19
5.2 Description of Jacket Structure.....	19
5.3 Analysis Results.....	19
6. CONCLUSIONS	25
7. REFERENCES	

FIGURES

APPENDIX A DATABASES

APPENDIX B SCF PLOTS

1. INTRODUCTION

In many regions of the world, tubular brace members in offshore structures are connected directly to the chord by single sided welds. This method of fabrication, sometimes referred to as point-to-point construction, is cheaper and quicker than the alternative of separately fabricating nodal joints with brace stubs connected by double sided welding. The main issue with single sided welding is the occurrence of undetected notches and cracks in the weld root, where inspection possibilities are limited. Such undetected defects may act as crack initiators under fatigue conditions.

In the North Sea, current fabrication practice is to use brace stubs with double sided welding. This leads to an improved quality of weld at the root, thereby inhibiting fatigue crack formation. If the cheaper single sided welding techniques are to be permitted, it is necessary to show that the increased propensity for fatigue cracking at the weld root is acceptable. This becomes even more important in cases where weld improvement has been carried out, as such improvement can only be made to the external, visible, part of the weld and not to the hidden root.

The likelihood of fatigue cracking to initiate and grow from the weld root rather than the weld toe is a function of two aspects:

- the relative ratio of the SCF at the root compared to that at the toe (the 'R' value), and
- the applicable S-N curves for the two sites.

There is little in the way of codified guidance specifically addressing single sided welding at tubular joints. The HSE Guidance Notes⁽¹⁾ including Amendment No 3, suggests various classification details for assessing fatigue strength. The Guidance Notes makes reference to single-side welds in two clauses.

In Section A21.2.12a of the Guidance Notes, type 7.1(b) classification detail would suggest a classification factor of 1.34P whereas type 7.5(d) suggests 1.52P (these are equivalent to the old F and F2 classifications respectively). Assuming that the same thickness correction applies on both the outer and inner surface (which is true for the great majority of joints since the maximum internal and external SCF occur on the same member), a limiting R value can be calculated from the S-N curve such that the root life is equal to the toe life. For 1.34P and 1.52P classification factors, the limiting R values are respectively 0.55 and 0.49. If R is greater than the limiting value, it would indicate internal cracking is more likely. However, these limiting R values are not tenable as they are too low. Many joints in practice have geometries which give R values greater than these limits, yet have not suffered cracking. It is interesting to note that, according to Reference 2, the previous version of the Guidance Notes gives a limiting R value of 0.72, which is more in keeping with the ISO⁽³⁾ recommended value of 0.7.

It may also be noted that many, if not the majority, of the tubular joint fatigue specimens on which the 'T' curve was derived were, in fact, fabricated using single sided welding. It could be argued, therefore, that the T curve is applicable to single-sided welding implying a limiting value of R = 1.0. One may still wish to downgrade the root life on the basis of no access for inspection leading to an effective lowering of the limiting R from unity. However, this is a separate issue.

The purpose of this report is to review the available data on internal SCFs, derive appropriate formulations for estimating R, suggest an appropriate S-N curve, demonstrate the impact of single sided welding by analysing a typical structure, and to draw conclusions and make recommendations based on the findings.

2. AVAILABLE DATA ON INTERNAL SCFs

2.1 General

All SCF studies on single-sided welded joints to date have been based on the finite element method.

Bærheim⁽⁴⁾ found that the stresses at the weld root were always smaller than toe stresses for overlapped KT joints. Some analysed joints, however, showed that the root stresses could be as much as 80% of the stresses at the toe.

In 1994, Statoil initiated a preliminary program to examine root stresses for simple gapped K joints. Nine joints plus one validation joint were analysed by DNV and MSL Engineering Limited. The results were published in 1996⁽⁵⁾, together with a simple parametric equation for the ratio of root to toe stress. The database was limited, however, and it was decided to extend it. Hansen⁽⁶⁾ analysed 21 K joints and K Bærheim analysed 17 X joints, all results being summarised in Reference 7. This reference also contains parametric equations for K joints ($\theta = 45^\circ$ only) and X joints. For the K joints, parametric formulae were given for balanced axial loads, balanced in-plane bending and balanced out-of-plane bending. (The more important moment cases of unbalanced bending were not investigated.) For the X joints, a parametric formula was developed for (balanced) axial loading only.

Work has also been conducted at the University of Wales Swansea⁽²⁾. Data and parametric equations were generated for T/Y and X joints. A subsidiary study on K joints examined the effect of θ to complement the Statoil work above. The Swansea work encompassed axial and moment (IPB and OPB) load cases.

In the above parametric studies, the matrix of FE models were designed to explore the effect of each parameter (β , γ , θ etc.) in isolation. It was not possible, therefore, to capture the possibility of coupling effects between the parameters except in a few isolated instances.

Parametric formulae are generally given for the ratio R defined as:

$$R = \frac{\text{maximum internal SCF (chord or brace side)}}{\text{maximum external SCF (chord or brace side)}}$$

Thus, when this R value is multiplied by the external SCFs for the chord and brace sides (for which parametric equations are already available), the maximum internal SCF is captured. Information on whether an internal crack is more likely to form on the chord or brace side of the weld root is lost. However, there is no information on actual incidences of internal crack initiation and growth and it is possible that a crack initiating in one member could eventually grow into the other member.

One further comment should be made and this concerns extrapolation of stresses to the weld. For outside surfaces, SCF determination is based on a linear extrapolation of stresses from defined points which have been in use for two decades. This is to avoid the local notch effects at the weld toe (these are accounted for in the SN curve). There are no generally accepted principles for determining SCFs for internal surfaces. Researchers have therefore established the interior extrapolation points at the same distances from the weld as used on the outer surfaces. No studies have been conducted to verify whether this is entirely appropriate.

The results from the parametric studies are summarised in the databases in Appendix A, according to joint type (K, X, Y) and load case (axial, in-plane bending and out-of-plane bending). The SCF data, together with Efthymiou predictions for chord and brace external values, are plotted in the figures given in Appendix B. A more detailed examination of the available data, based on type of joint, is given in the following subsections.

2.2 K Joints

Figure 2.1 shows the scope of preliminary analyses conducted by MSL and DNV on behalf of Statoil. In the diagrams on this figure, and in those that follow, the full listing of the non-dimensional geometric parameters is shown only for one ‘parent’ specimen, e.g. specimen M1 in the case of MSL study. Variations to the parent specimen to produce ‘offspring’ specimens are indicated by the arrows. For instance varying γ , but keeping other parameters constant, produces specimens M2 and M4.

The MSL/DNV studies were limited, not only in the range of geometric parameters but also in that only balanced axial loaded K joints were investigated. Although the results have been recorded herein, see Table A1 in Appendix A, their use has been restricted to confirming the trends (which they do) noted in the more complete studies discussed below. The results are therefore not mentioned further.

The principal parametric study on K joints subjected to either balanced axial loading, balanced in-plane bending or balanced out-of-plane bending was reported in Reference 6. This considered 45° braces. A supplementary study conducted at Swansea, designed to be complementary to the Statoil study, investigated the effect of varying the brace angle for selected geometries and load cases.

The scope of the combined studies is indicated in Figure 2.2. It can be seen that the Swansea specimens investigating θ variations are based on specimens K1, K13 and K36 of the main study. The letters A, I and O to the right of the relevant boxes in Figure 2 represent the load cases (Axial, balanced IPB and balanced OPB) that were run. It may also be observed that the gap parameter ζ ($= g/D$) has been systematically varied for two different β values, ie. for $\beta = 0.6$ (specimens K0, K31 to K36) and $\beta = 0.9$ (specimens K3, K41 to K44). This allows the exploration of possible coupling effects between β and ζ , and this is addressed in Section 3.2. Four additional specimens (K100, K101, K102 and Valid 3) were run. These specimens have variations in at least two parameters compared to any other specimen and were originally used, as is the case in this study, to check on the robustness of formulations developed for R.

The full results, in terms of SCFs inferred from the Finite Element studies, SCFs calculated from Efthymiou parametric equations and the resulting R values, are given in the databases in Appendix A. Plots of SCF against the geometric parameters are provided in Appendix B. These plots generally show the chord SCFs (the internal and external values from the finite element analyses (FEA) and the Efthymiou value which is only applicable to the external surface). Where the brace SCFs become governing, as is sometimes the case for IPB, then these too are plotted. The SCF plots perform a useful function in checking the validity of the FEA values against the Efthymiou predictions.

2.3 X/DT Joints

Two separate parametric studies have been conducted on X/DT joints. Statoil’s study⁽⁶⁾ considered axial compression only whilst that of Swansea⁽²⁾ examined the behaviour under axial tension, in-plane bending and out-of-plane bending.

Figure 2.3 illustrates the scopes of the two studies. The original references have used the same specimen identification system (ie. X1, X2, etc.). To avoid possible confusion here, the Swansea original specimen identifications have been modified by adding a tick mark (ie. X1’, X2’, etc.). It can be seen that the studies overlap each other with respect to geometric parameters. This enables cross-checking of the axial results, as discussed in Section 3.3, to be made. (The SCF values should be the same for compression and tension, assuming sufficiently small loads were used in the analyses to avoid geometric or material non-linearities.) At the same time, investigation on possible coupling effects between the geometric parameters are possible as the pivot specimens (X1’ and X4 for Swansea’s and Statoil’s studies respectively) are of different geometries.

As for the K joints, the X/DT SCF results are tabulated in the databases in Appendix A and the SCF variations with geometric parameters are plotted in Appendix B.

2.4 Y/T Joints

Y/T joints have been analysed at Swansea under axial tension, in-plane bending and out-of-plane bending. For Y joints, the in-plane bending load was orientated such that the extreme fibres of the brace were under tension at the crown heel and in compression at the crown toe.

The scope of the parametric studies for T joints and Y joints are illustrated in Figure 2.4. Note specimen T1 (a T joint) is included as a special case of a Y joint as specimens T1, Y2 and Y1 are the main group available for determining the role of θ effects.

The SCF results are tabulated and plotted in Appendices A and B respectively.

3. INTERPOLATION FUNCTIONS FOR INTERNAL/EXTERNAL SCF RATIO

3.1 Methodology

Selection of R Ratio

This Section 3 describes the development of fitted functions for estimating the ratio of the internal SCF to the external SCF, based on the finite element analysis (FEA) data presented in Section 2. There are a number of ways in which the ratio (R) can be defined. This is because there are, in general, four different SCFs that have been extracted from the FEA results (ie. internal and external values for both the chord and brace members). In addition, there are external brace and chord SCF predictions obtained from parametric equations such as those due to Efthymiou. The most useful definitions of R which might be considered are:

- $R1 = \text{FEA.int (CH)} / \text{FEA.ext (CH)}$
- $R2 = \text{FEA.int (BR)} / \text{FEA.ext (BR)}$
- $R3 = \text{MAX \{FEA.int (CH) or FEA.int (BR)\}} / \text{MAX \{FEA.ext (CH) or FEA.ext (BR)\}}$
- $R4 = \text{FEA.int (CH)} / \text{Efth.ext (CH)}$
- $R5 = \text{FEA.int (BR)} / \text{Efth.ext (BR)}$
- $R6 = \text{MAX \{FEA.int (CH) or FEA.int (BR)\}} / \text{MAX \{Efth.ext (CH) or Efth.ext (BR)\}}$

In the above, (CH) and (BR) stand for chord and brace respectively, int and ext for internal and external SCF values respectively, and Efth for Efthymiou SCF prediction.

Definitions R1 to R3 and R4 to R6 constitute two groups, depending on whether the external SCFs are based on FEA values or parametric equation (eg. Efthymiou) values. The definitions in the former group (R1 to R3) are considered to be the more appropriate in the present study because:

- they are independent of any one particular set of parametric SCF formulations; the definitions in the second group are necessarily tied to Efthymiou's parametric equations
- modelling inaccuracies in the FEA studies will, to some extent, be cancelled out when the ratio R is taken
- the ratios R1 to R3, when used in conjunction with an appropriate SN curve, will give a more reliable indication of the propensity of cracks to form internally rather than externally.

In traditional fatigue analysis, such as is carried out during design, both the brace and chord members are checked at several locations around each joint intersection. This requires parametric equations for both the brace and chord sides of the weld. In principle the same approach could be used to check for internal locations, by using definitions R1 and R2 above in conjunction with existing (external) parametric equations. Unfortunately, however, the available data are not sufficient to derive R2 for all joint/load types as sometimes only the maximum SCF values, which most often occur on the chord, are quoted. Therefore, in this study, the definition used is R3 throughout.

Thus, applying R3 to both the chord and brace SCF parametric equation predictions will ensure the maximum internal SCF is captured. The disadvantages of this approach are that:

- Information as to which member (chord or brace) has the highest internal SCF is lost. This is not considered to be too much of an impediment in itself though; what is important is to identify whether cracking can occur internally, its precise position is secondary.
- For $\tau (= t/T)$ values other than unity, different corrections to account for the thickness effect will apply to the chord and brace members. The R3 definition does not identify which is the relevant member to which the thickness effect should be applied in calculating internal life. This is actually not much of a problem as the great majority of FEA data indicate that the maximum external and the maximum internal SCF occur on the same member. Therefore, the thickness effect cancels out when the internal life is given as a ratio of the external life.

- In some instances, and for in-plane bending in particular, there is a transition from the chord being the critical member to the brace as τ is decreased. The bounding R surface is therefore the lower of two independent surfaces describing chord behaviour and brace behaviour. This could, in turn, introduce complications in the R3 fitting function as it tries to model the two surfaces. More discussion of this aspect is given in later sections of this report.

Curve Fitting

As mentioned previously, nearly all the FEA studies were designed with a ‘pivot’ specimen, and the effects of the various geometric parameters (β , γ , τ , etc.) were investigated by varying each parameter in turn, keeping the other geometric parameters constant at their pivot values. Thus, by looking at only those specimens where a given parameter alone was varied, its effect can be ascertained. Each parameter is assumed to be uncoupled to other parameters. The R ratio is therefore found in the form of the following expression:

$$R = \text{constant} \cdot f(\beta) \cdot f(\gamma) \cdot f(\tau) \cdot f(\zeta) \cdot f(\theta)$$

where $f(\beta)$ to $f(\theta)$ are the separately fitted expressions for the effect of each parameter. The leading constant is fitted last, to give the best overall fit to the data. Nine formulations for R were developed to account for the matrix of three joint types (K, X/DT, Y/T) and three load types (axial, IPB, OPB). The results are summarised in Section 3.5.

In a few instances, it was possible to check for possible coupling effects (eg. between β and ζ for K joints and β and γ for X joints). It is confirmed in the following subsections that the coupling effects, if any, must be of a minor degree except for Y joints.

In fitting the R formulations, and the individual parameter expressions $f(\beta)$ etc. in particular, simple expression forms such as linear or parabolic were selected. These generally gave sufficient accuracy bearing in mind that the FEA data contains elements of uncertainty due to:

- FE modelling – mesh density, element types etc.
- SCF extrapolation technique.

A comparison of Statoil and Swansea data indicates that the overall difference (in R) is of the order 10%. This value may be taken as indicative of a good fit between R formulations and the FEA data.

3.2 K Joints

K joints: balanced axial loading

Using the methodology cited in Section 3.1, plots were made of the R ratio (maximum internal SCF divided by maximum external SCF) against individual parameters and expressions were fitted to the data. These plots and expressions are shown in Figures 3.1 to 3.5 for the parameters β , γ , τ , ζ and θ respectively.

The data, in all cases, appear well ordered and no particular difficulties were encountered during curve fitting. The chosen function for β is parabolic (Figure 3.1), and a parabola appears best suited not only for K joints under balanced axial loading but also for other joint types and load types. Initially a parabola was also used for γ , but other joint and load types favoured a linear function and therefore this was finally selected. A fair fit was obtained, see Figure 3.2.

Except for the data point at the lowest τ value ($= 0.2$), a linear function also fits the τ data well, see Figure 3.3. The low τ data point was excluded when the linear fit was obtained. The reason for drop in R at low τ can be seen in the SCF plot (Figure B3 in Appendix B). Inspection of the SCF plot shows that the maximum external SCF generally occurs on the chord surface except at low τ . The transition of the maximum external SCF from the chord to the brace surface occurs at $\tau = 0.27$ for the FEA results, or at $\tau = 0.4$ for the Efthymiou predictions. It is apparent, therefore, that R is based on chord behaviour except at low τ values when it is related to brace behaviour. Strictly R should be defined as the lower of the values given by two separate functions, one for the chord and the other for the brace. It was decided, however, that this was not necessary as the transition occurs at a τ value on the limit of the practical range. It is also noted that adopting a R based on the chord behaviour throughout is conservative. Furthermore, the SCFs at small τ are relatively low and therefore do not give rise to fatigue problems. A further difficulty in defining two separate functions is that the transition point is uncertain, both with respect to different sets of analyses producing different results (ie. 0.27 versus 0.4 above) and that it may vary in an unknown fashion with other parameters (β , γ , etc.).

Figure 3.4 presents the variation of R with respect to ζ ($=$ gap/chord diameter). Reference to Figure 2.2 shows that ζ variation was investigated at two values of β ($= 0.6$ and 0.9). To enable the two sets of results to be compared on a common basis, the R results pertaining to $\beta = 0.6$ were normalised by scaling them by the factor $f(\beta = 0.9) / f(\beta = 0.6)$ where $f(\beta)$ is the fitted function for β obtained earlier. The scaled results for $\beta = 0.6$ are almost identical (and is identical at the common pivot value of $\zeta = 0.075$) to the $\beta = 0.9$ data. This close matching of results demonstrates that β and ζ are uncoupled, at least for K joints under balanced axial loading. This observation lends weight to the basic assumption stated in Section 3.1 that all parameters are uncoupled.

The role of θ is shown in Figure 3.5. The results of K joints under OPB are also given, as these were found to align closely to the axial results and a common θ function could be derived. Both the axial and OPB results were extracted from Swansea data, the Swansea study being complementary to the Statoil primary study, see Section 2.1. The results in Figure 3.5 have therefore been normalised to give an R value of unity at $\theta = 45^\circ$. A linear fitted function was deemed suitable.

Having fitted functions to the individual parameters, the functions were multiplied together with a leading constant. An overall fit was then conducted to find the value of the leading constant which minimised the sum of the squares of the errors between predicted and calculated (from FEA) R values. The resulting overall formulation is given, along with those for other load cases and joint types, in Section 3.5.

Figure 3.6 presents a bar chart of the ratios of predicted R, using the overall formulation, to the calculated R from FEA data. Apart from one result for model K10, all results lie within a band of $\pm 5\%$ of unity. Model K10 has a low τ value (0.2) and was deliberately excluded from the fitting process as discussed above. The R function can nevertheless be conservatively used for this model.

K joints: in-plane bending

The development of R functions for K joints under IPB followed a similar pattern as for axial loaded K joints. Figures 3.7 to 3.11 show the fitted functions for the effect of individual parameters on R.

The role of γ , Figure 3.8, was again deemed to be linear but, for IPB, a suitable approximation was a horizontal line across the plot, ie. the equation of the line was simply a constant. This constant was absorbed into the leading constant of the overall R formulation in the tabulated functions in Section 3.5.

The transition of maximum SCF from chord to brace at low τ values was again observed, Figure 3.9. Figure 3.10 confirms that there is no significant coupling between β and ζ .

The effect of θ on K joints under IPB is quite different to K joints under balanced axial loading or OPB, compare Figures 3.11 and 3.5. For IPB, two series were used to study θ effects: the series differed with respect to both τ and ζ , see Figure 2.2. The two series give very similar results for brace angles between 45° and 60° , but diverge at angles less than 45° . Since the R ratios decrease for low brace angles, a linear fit between 45° and 60° provides a conservative estimate of R for lower angles.

The final overall R formulation is given in Section 3.5, and the bar chart of predicted R to calculated R is shown in Figure 3.12. In general, a satisfactory fit has been obtained, with the exception of the low τ (≈ 0.2) model K10.

K joints: out-of-plane bending

The effect of β , γ , τ and ζ parameters on R are shown in Figures 3.13 to 3.17 respectively. The effect of θ is similar to that for K joints under balanced axial loading, as discussed above.

As observed in axial and IPB loaded joints, transitional behaviour occurs at low τ values (see Figure 3.14) and β and ζ were found to be uncoupled (Figure 3.15).

The bar chart of ratios of predicted R (given in Section 3.5) to calculated R is shown in Figure 3.18. Once again, apart from the low τ model, satisfactory agreement of predicted to calculated values have been obtained.

3.3 X/DT Joints

X/DT joints: axial loading

As discussed in Section 2.3, there are two sets of FEA data available for exploring the internal SCF behaviour of axially loaded X/DT joints. The studies overlap to a large extent and this led to a modification in the methodology cited in Section 3.1 with respect to developing the R formulations. In essence, the two sets of data were initially treated as being independent, and two sets of fitted functions for the geometric parameters (β , γ , etc.) were derived. The R values for each set of data were then normalised using these initial functions to a common basis taking a ‘pivot’ specimen with $\beta = 0.5$, $\gamma = 20$, $\tau = 0.5$ and $\theta = 90^\circ$. Inspection of Figure 2.3 shows that this pivot specimen is essentially an average of the actual pivot specimens used in the original studies (X1’ and X4 for Swansea and Statoil respectively). As an example, the normalised R values (R_{mod}) for exploring β effects were:

$$R_{mod} \text{ (Swansea data)} = R \cdot \frac{f'(\gamma = 20) \cdot f'(\tau = 0.5)}{f'(\gamma = 21) \cdot f'(\tau = 0.35)}$$

$$R_{mod} \text{ (Statoil data)} = R \cdot \frac{f(\gamma = 20) \cdot f(\tau = 0.5)}{f(\gamma = 18.75) \cdot f(\tau = 0.5)}$$

In the above $f'(\gamma)$ and $f'(\tau)$ are the individual fitted functions considering the Swansea data alone, and $f(\gamma)$ and $f(\tau)$ are those corresponding to the Statoil data. The R_{mod} values for exploring the effects of other parameters were similarly obtained, cycling through the f' and f functions.

The R_{mod} values from the Swansea and Statoil data could then be plotted together on a common basis and the curve fitting exercise repeated for the combined data set.

Figure 3.19 presents the R_{mod} data and fitted functions for β . Three fitted functions are shown, one is the function (normalised in a similar manner as explained above) that is the best fit to the Statoil data alone, the second is the best fit to the Swansea data alone, and the third is the fit to the combined data. The third function constitutes part of the overall R formulation in Section 3.5. It can be observed that there is fair agreement between the Statoil and Swansea sets of data with respect to the impact of changing β . However, the respective fitted curves do diverge somewhat when extrapolated to $\beta = 1.0$.

Figure 3.20 corresponds to γ variations. Although the magnitude of R_{mod} values are similar between Statoil and Swansea, their functional relationship to γ are indicated to be different. Inspection of the relevant SCF plots (Figures B18 and B19 in Appendix B) indicates some variability in external SCF values, particularly for the Statoil data. It was therefore considered appropriate to fit a linear function, especially since linear relationships hold for other joint and load types.

Fair agreement between the two sets of data with respect to τ is indicated in Figure 3.21, when the low τ data point representing transitional behaviour is ignored.

Only one set of data is available for studying the role of θ , see Figure 3.22. The data point at $\theta = 45^\circ$ was omitted in conducting the curve fit. The internal SCF appears to be too high, and the external SCF possibly too low, from Figure B22 in Appendix B.

The overall fitted R formulation is given in Section 3.5 and the bar chart of the ratios of predicted R to calculated R is shown in Figure 3.23. A number of models have ratios with significant departures from unity; these are highlighted in the figure. Swansea Model X8' has a τ ratio of 0.2 and thus is affected by the maximum external SCF being on the brace (transitional behaviour). Statoil Models X7 and X9 are respectively at high γ and β ratios. These models are known to drift from the fitted curves for the combined data, see Figures 3.20 and 3.19. Similarly, Model X12 at $\theta = 45^\circ$ lies above the fitted θ function, see Figure 3.22. Model X2 lies 10% above the unity line, and therefore R is conservatively predicted, but no reason for this relatively high result could be ascertained.

X/DT joints: in-plane bending

X/DT joints under IPB were studied by Swansea only, see Figure 2.3.

Curve fitting against the geometric parameters proved to be straight forward and the results are shown in Figures 3.24 to 3.26. Once again, the transitional behaviour for low τ ratios occurs, see Figure 3.26 and Figure B25 in Appendix B.

No data are available for studying the effect of θ for X joints under IPB. In the overall R formulation in Section 3.5, the K joint IPB θ function has been assumed to apply, this being conservative with respect to the alternative, the Y joint IPB θ function, for angles down to about 60° . The range $60^\circ - 90^\circ$ is more important than lower angles for actual structures.

As can be seen in Figure 3.27, the overall R formulation gives good predictions, ignoring the data point for low τ ratio.

X/DT joints: out-of-plane bending

The study of X/DT joints under OPB was very similar to that under IPB. Figures 3.28 to 3.30 present the individual fitted functions.

Again, there are no data available for ascertaining the effect of θ . By analogy with K joint behaviour where it was found the role of θ was similar for axial and OPB loading, the X/DT θ -function for axial behaviour has been assumed to apply here.

Figure 3.31 shows the goodness of fit of the overall R function.

3.4 Y/T Joints

In many respects, fitting functions to the Y/T data proved most difficult. This was because the data indicated that strong coupling effects exist between θ and the other parameters. It is possible that such coupling effects exist for other joint types, but the data for other joint types are not extensive enough to check this conjecture out. In the case of Y/T joints, the other parameters are varied both for $\theta = 90^\circ$ and $\theta = 30^\circ$, see Figure 2.4. This allowed such coupling effects to be identified.

Y/T joints: axial loading

The T and Y joints were initially examined separately. The T joint parametric functions for β , γ and τ are shown in Figures 3.32 to 3.34. The corresponding Y joint ones are shown in Figures 3.35 to 3.37, and the effect of θ alone is indicated in Figure 3.38. Superimposed on the Y joint plots are the T joint functions which have been suitably normalised. The normalising process used is similar to that described for X/DT joints under axial loading.

Inspection of Figure 3.35 shows that the normalised T curve provides an excellent fit to the Y joint data. This indicates β and θ are uncoupled. Figure 3.36 indicates a significant amount of coupling between γ and θ whilst Figure 3.37 shows a moderate amount of coupling between τ and θ .

A coupled equation was developed for the γ - θ interaction on the assumption that the γ -function at $\theta = 90^\circ$ changes to that at $\theta = 30^\circ$ in a linear manner. The resulting coupled equation can be found in Section 3.5. It was decided not to develop a coupled equation for τ - θ interaction on the basis that $\theta = 30^\circ$ represents an extreme practical angle and that an 'averaged' τ function would suffice.

Figure 3.39 presents the bar chart of the ratios of predicted to calculated R values. The agreement is reasonable, although the highlighted Models Y6 and Y7 are 10% below the unity line. These models are 'low' because of the approximation of not coupling τ - θ as discussed above. The low results are compensated by the 'high' results of the corresponding T joint Models T6 and T7.

Y/T joints: in-plane bending

The variations of R with β , γ and τ are shown in Figures 3.40 to 3.42 respectively for T joints and in Figures 3.43 to 3.45 for Y joints. The T joint functions have been normalised and re-plotted on the Y joint figures to allow comparisons to be made. Figure 3.46 shows the variation of R with θ .

It can be seen in Figure 3.43 that the role of β for Y joints ($\theta = 30^\circ$) is different to that for T joints. This suggests a coupling effect for β - θ . A coupling between γ - θ is suggested in Figure 3.44. However an examination of the fit of the T curve in Figure 3.41 shows the Y and T data only differ at the lowest γ ratio of 15. A strong coupling between τ - θ is indicated in Figure 3.45.

It would appear that the effects of the parameters for IPB is completely different to axial loaded Y/T joints. Parameters which are uncoupled, or only moderately so, in the axial case are coupled in IPB, and vice versa.

There are insufficient data to derive coupled equations for β - θ and τ - θ in the IPB case. In the recommended overall R formulation in Section 3.5, the T joint functions have been used as a basis together with the θ -function from Figure 3.46. Rather poor predictions for Y joints ensue, as seen in the bar chart for ratios of predicted to calculated R values, Figure 3.47. Attempts were made to derive a more robust R formulation by referring to Efthymiou parametric equations but to no avail. It is understood that Efthymiou, too, had a limited database, for Y joints under IPB, to work on when deriving his parametric equations. It is possible that some of the above difficulties are only apparent for the low θ angle (30°) studied. It was felt appropriate to limit the application of the R formulation to angles greater than 60° .

Y/T joints: out-of-plane bending

The behaviour of Y/T joints under OPB is not as erratic as either for the axial or the IPB cases. The T joint parametric plots, Figure 3.48 to 3.50, have been normalised and replotted on the Y joint curves, Figures 3.51 to 3.54, as before.

An examination of Figures 3.51 to 3.53 show that the T joints and corresponding Y joints behave in a similar manner. The effect of θ , Figure 3.54, is well approximated by a linear function.

The bar chart of the ratios of predicted to calculated R, Figure 3.55, shows a reasonable fit. Model T7 lies 8% above the unity line and Model Y7 lies 13% below.

3.5 Summary of Fitted R Formulations

The fitted function described in the previous subsections have all been collated here for convenience of application. They are presented in Table 3.1. The R formulations are meant to be applied to the maximum external SCF (whether this be on the brace or chord) to estimate the maximum internal SCF value. Note that the K and X formulations have been based on balanced axial and balanced moment loading conditions.

The validity ranges of the various parameters are given in Table 3.2. In general, the validity ranges have been based on the ranges of data generated in the FEA studies, except that τ and β values have been extrapolated to unity. In some instances more onerous limits have been applied where the reliability of the R formulation is questionable, this applies especially to joints of low angles. A limit of $\tau = 0.3$ has generally been applied to the R formulations as they become overly conservative for lower values, see Note 1 to Table 3.2.

It should be emphasised that the design of the FEA studies was such that there was little opportunity to confirm that the parameters are uncoupled. However, for Y joints, the data indicate that coupling of some parameters does exist although the data are not sufficiently extensive to develop robust coupled formulations. The Y joints (though not necessarily the T joints) predictions are considered to be relatively unreliable.

The goodness of fit of the predicted R values using the formulations to the calculated values from FEA studies has been shown in various bar charts presented in previous subsections. Figure 3.56 presents a composite histogram for all joint and load types when Tables 3.1 and especially 3.2 are strictly applied. In particular the majority of Y joints under IPB are excluded and the limit of $\tau = 0.3$ has been used to estimate the R values of low τ models. It can be observed that the great majority of data fall near unity and the shape of the distribution appears to be log-normal. The mean bias and the standard deviation of the data are 1.012 and 0.064 respectively.

Table 3.1: Summary of R Formulations

Joint Type	Load Case	Formulation
K	Axial	$R = 3.03(-1.29\beta^2+1.65\beta+0.2)(0.001\gamma+0.69)(-0.47\tau+0.96)(1.56(1-0.008\theta))(9\zeta^2-2.5\zeta+0.775)$
	IPB	$R = 3.05(-0.51\beta^2+0.54\beta+0.45)(-0.43\tau+0.77)(0.0222\theta)(1.0-0.15\zeta^{-0.4})$
	OPB	$R = 4.75(0.58\beta^2-\beta+1)(\gamma^{0.177})(-0.53\tau+0.85)(1.56(1-0.008\theta))(-0.17\zeta+0.61)$
X	Axial	$R = 5.20(-1.7\beta^2+1.5\beta+0.27)(0.002\gamma+0.53)(-0.63\tau+0.91)(0.002\theta+0.38)$
	IPB	$R = 1.25(0.24\beta^2+0.6)(0.008\gamma+0.47)(-0.52\tau+0.81)(0.0222\theta)$
	OPB	$R = 4.22(-1.2\beta^2+\beta+0.45)(0.004\gamma+0.56)(-0.58\tau+0.85)(0.002\theta+0.38)$
Y	Axial	$R = 2.40(-1.9\beta^2+1.7\beta+0.27)(0.03\gamma-0.1+\theta(0.0067-0.00025\gamma))(-0.43\tau + 0.78)$
	IPB	$R = 3.06(0.5\beta^2-0.44\beta+0.78)(0.005\gamma+0.55)(-0.64\tau+0.91)(0.0005\theta^2-0.066\theta+2.6)$
	OPB	$R = 4.00(-\beta^2+0.8\beta+0.48)(0.003\gamma+0.58)(-0.52\tau+0.81)(-0.0023\theta+0.84)$

Notes:

1. θ should be in degrees
2. See table 3.2 for validity ranges

Table 3.2: Validity Ranges for R Formulations

Joint Type	Load Case	Validity Range of Parameters				
K	Axial	$0.2 \leq \beta \leq 1.0$	$10 \leq \gamma \leq 30$	$0.3 \leq \tau \leq 1.0(1)$	$30^\circ \leq \theta \leq 60^\circ$	$0.04 \leq \zeta \leq 0.2$
	IPB	$0.2 \leq \beta \leq 1.0$	$10 \leq \gamma \leq 30$	$0.3 \leq \tau \leq 1.0(1)$	$30^\circ \leq \theta \leq 60^\circ(2)$	$0.04 \leq \zeta \leq 0.2$
	OPB	$0.2 \leq \beta \leq 1.0$	$10 \leq \gamma \leq 30$	$0.3 \leq \tau \leq 1.0(1)$	$30^\circ \leq \theta \leq 60^\circ$	$0.04 \leq \zeta \leq 0.2$
X	Axial	$0.2 \leq \beta \leq 1.0$	$10 \leq \gamma \leq 30$	$0.3 \leq \tau \leq 1.0(1)$	$50^\circ \leq \theta \leq 90^\circ$	
	IPB	$0.2 \leq \beta \leq 1.0$	$15 \leq \gamma \leq 30(3)$	$0.3 \leq \tau \leq 1.0(1)$	$30^\circ \leq \theta \leq 90^\circ(4)$	
	OPB	$0.2 \leq \beta \leq 1.0$	$15 \leq \gamma \leq 30$	$0.3 \leq \tau \leq 1.0(1)$	$50^\circ \leq \theta \leq 90^\circ(5)$	
Y	Axial	$0.3 \leq \beta \leq 1.0$	$15 \leq \gamma \leq 30$	$0.3 \leq \tau \leq 1.0(1)$	$30^\circ \leq \theta \leq 90^\circ$	
	IPB	$0.3 \leq \beta \leq 1.0$	$15 \leq \gamma \leq 30$	$0.3 \leq \tau \leq 1.0(1)$	$60^\circ \leq \theta \leq 90^\circ(6)$	
	OPB	$0.3 \leq \beta \leq 1.0$	$15 \leq \gamma \leq 30$	$0.3 \leq \tau \leq 1.0(1)$	$30^\circ \leq \theta \leq 90^\circ$	

Notes:

1. For all joint and load types, the formulations can be used for lower τ ratios by setting $\tau = 0.3$.
2. For K IPB, the formulation is conservative for $\theta \leq 45^\circ$.
3. For X IPB, indicated γ limits reflect the available data which demonstrates that γ does not appear to affect R.
4. No θ data exist for X IPB, extrapolation of K joint behaviour assumed.
5. No θ data exist for X OPB, X axial behaviour assumed (similarity of OPB and axial behaviour is observed for K joints).
6. The Y IPB R formulation becomes unreliable for low θ angles.

4. SELECTION OF S-N CURVE

To evaluate the fatigue performance of single sided welds, the product of the nominal stress and a stress concentration factor, usually obtained from a recommended parametric equation, is used in conjunction with an appropriate S-N curve. As a result of failures in member closure welds, the 1.34P=F or 1.52P=F2 curve is recommended in the HSE Guidance Notes⁽¹⁾, depending on whether the full penetration single-sided weld is made with or without a permanent backing strip respectively.

For tubular joint connections, it is recommended in the Guidance Notes that the F curve (1.34P) in conjunction with an appropriate internal SCF should be considered, in addition to the T' curve in conjunction with an appropriate external weld SCF.

In virtually all fatigue tests reported for tubular joints, fatigue cracking has occurred at the weld toes either in the brace or more usually the chord, without evidence of root cracking. The HSE T' curve was derived from joints of chord wall thickness of 16mm, welded from one side and from tests in the UK (UKORSP I/II data) and European Programmes (French and Dutch data). Tubular joints were manufactured at the time to specifications for weld profiles as defined in AWS D1.1 with the basic guidelines to weld concavity and toe blending being followed by the fabricator. All of the joints failed at the chord weld toe without any root cracking being observed.

Some larger tubular joint specimens (ie. chords with 914mm/1828mm diameters and chord wall thickness of 32mm/75mm respectively) were tested in the same above programmes. These were welded from one side and were subjected to the dime test in the region of the anticipated hot spot stress. The larger sized joints provided some of the better profiles and the performance of these joints were similar to those used to derive the T' curve (when corrected for thickness) and failure occurred externally without root cracking.

A review of the tubular joint database used to derive the basic T' curve and larger joints (i.e. as mentioned above) from the HSE Fatigue background document⁽⁸⁾ was undertaken to determine the R ratios using the equations given in Table 3.1 for the different joint types, loading modes and geometries. In many cases the R ratios predicted were low, ie. $R < 0.2$. However, a number of joints did have R ratios > 0.6 . The data for these joints were a mix of different joint types, wall thicknesses, loading modes and geometries. The fatigue results for these joints using both the external measured hot spot stress range and predicted internal hot spot stresses are compared to the T' curve and other S-N Classes (i.e. D, E and F) as shown in Figure 4.1.

It can be seen from Figure 4.1 that the fatigue lives based on the external hot spot stress range lie above the T' curve. However, when based on the internal hot spot stress range (using the same number of cycles to failure as obtained externally) the data tend to lie above the D curve although one data point lies just below the E curve. It should be noted that these data points have been plotted assuming that fatigue cracking and failure has occurred internally at the root which was not found in the tests. On this basis, the internal life would be higher and therefore it is considered appropriate to recommend a Class D for internal welds.

This justification is supported by reference to other sources of data on the fatigue behaviour of fillet welded tubular joints and single-sided girth welded joints as follows:

Single sided girth welded joints

Recently, data has been published by Maddox and Razamjo⁽⁹⁾ on the performance of large scale girth welded joints fabricated using different welding techniques and made from one or both sides. The general conclusions from the results were as follows:

- There was no difference in the performance of girth welds made from one or two sides.
- The results indicated that the current S-N classification F/F2 for girth welds could be increased to Class D.

The data for those joints welded from one side are shown in Figure 4.1. It can be seen that the data lie above the D curve.

Fillet welded tubular joint data

A limited amount of fatigue data are available for tubular joints fabricated using fillet welds⁽¹⁰⁾ which have predicted R ratios >0.5.

The tests were conducted to identify whether failure would occur from the root. However, even with toe grinding being carried on the external welds for some of these joints, failure still occurred externally. The results using the external measured hot spot stresses and the predicted internal hot spot stresses are shown in Figure 4.1. When based on external hot spot stress range the results lie above the T' curve. When based on using the predicted internal hot spot stress range the results lie above the D curve.

From the above assessments it is considered appropriate that a Class D (=P) curve should be used to determine the internal weld fatigue life for tubular joints.

5. IMPACT ON JACKET ANALYSIS

5.1 General

Having derived suitable R formulations (Section 3) and a suggested S-N curve for the root of single sided welds in tubular joints (Section 4), it is pertinent to assess the implications for jacket analysis. In order to have indicative results, a typical structure has been analysed and the fatigue lives of the joints established, firstly considering only the outside toes and then also the roots of the welds.

The selected structure is described in subsection 5.2. The results of the analysis, and their implications for jacket analyses in general, are given in subsection 5.3.

5.2 Description of Jacket Structure

The analysed structure was adapted from an existing platform operating in some 75m water depth in the Central North Sea. The platform supports a topside load of about 20,000 tonnes and has a design life of 25 years. A spectral fatigue analysis of the platform, conducted at the design stage, found that fatigue requirements governed the size of most joints and some members in and around the splash zone. Leg node sizes and stubs at all four plan levels were also governed by fatigue. The platform was therefore deemed suitable for the purposes of this study.

The original structural model was modified for this study in two main respects:

- reduction in problem size by removal of appurtenances and secondary plan bracing members (equivalent loads were applied however) from the computer model.
- adjustment to some of the framing arrangements to include K, X and Y primary joints.

The resulting jacket model is illustrated in Figures 5.1 and 5.2 which respectively indicate the node and element numbering system.

5.3 Analysis Results

A spectral fatigue analysis was carried out using a wave spectrum applicable to the platform site. The stress results were further processed to estimate joint fatigue lives as follows:

- (i) The lives were estimated using the HSE T' curve in conjunction with stresses factored by Efthymiou SCF predictions. These lives can therefore be considered to be indicative of present-day practice.
- (ii) The lives were estimated using the HSE D curve in conjunction with stresses factored by the products of Efthymiou SCF predictions and calculated R factors. These lives are therefore the internal (root) lives assuming all joints to be single side welded.

The fatigue life estimates have been collated and are presented in Tables 5.1 to 5.3 using the following basis:

- Table 5.1 shows the results ordered according to the toe lives (present-day practice, assessment (i) above).
- Table 5.2 shows the results ordered according to the root lives (internal lives, assessment (ii) above).
- Table 5.3 shows the results ordered according to the ratios of root life to toe life.

Only the uppermost 50 entries are included in each table. The following observations can be made from an inspection of the tables:

- The lowest fatigue life for a weld toe (external) is 53 years, being just above the target life of 2 x 25 years. However, the fatigue life for the weld root (internal) of this joint is 309 years, ie. 5.8 times higher.

- The lowest fatigue life for a root weld is 215 years. This life is well above the 50 year target life for the structure.
- The lowest ratio of the life of the weld root to the weld toe of a joint is 0.19, and this applies to two joints. However, these joints have very long fatigue lives being approximately 4,720 years for the toe and 910 for the root.
- There are over 30 joints where the ratio of root to toe life is under unity, see Table 5.3. For these joints there is a higher propensity for any fatigue cracking to occur internally rather than externally. The lowest internal fatigue life for this group of joints is 444 years (node 238 at a life ratio = 0.48).
- Although perhaps influenced by the relative numbers of K, X and Y joints in the structure, there are indications that internal lives are more of an issue for K/KT joints than other joint types.

The above observations are specific to the analysed structure and may not always be appropriate for other structures. However, the trends appear to be very evident and therefore should be applicable for the vast majority of other structures.

Further mention should be made of the fact that inspection possibilities are limited for detecting internal cracks, even to the extent that the weld root can be deemed, for practical purposes, uninspectable. Industry is presently setting a penalty factor for uninspectability, figures of around 2 to 3 on life are being mooted. (A penalty factor based on the criticality of the joint to overall structural integrity is also being discussed, but this presumably would apply equally to both internal and external life estimates and so not need be considered here). A simplistic view would be to divide all internal lives by the penalty factor. Adopting a penalty factor of 3 would then give a lowest internal life of $215/3 \approx 72$ years for the subject structure. This is above the 50 year target life and thus is acceptable.

However, it is possible to hypothesise another structure, again with a target fatigue life of 50 years, in which a particular joint had an external life of 51 years but an internal life of, say, 120 years. Applying the penalty factor, the 120 year life would be downgraded to 40 years and, on the simplistic basis, be deemed unacceptable. This approach ignores the greater reliability of the joint against failing by internal cracking than by external cracking. External cracking is more likely to appear prior to internal cracking and therefore the non-detection of external cracking is also good evidence of no internal cracking. Thus, in a sense, external inspection can also give evidence about the internal situation. Further work, possibly involving reliability analysis, is required to fully resolve this aspect.

Node	Element	Joint type	Fatigue Life		
			Toe	Root	Ratio
415	403	KT	53.12	309.29	5.82
315	301	KT	53.36	310.19	5.81
315	303	KT	54.53	328.06	6.02
415	401	KT	54.64	328.65	6.01
1411	409	K	79.77	228.17	2.86
1311	309	K	81.67	232.57	2.85
115	103	KT	82.23	404.8	4.92
215	201	KT	82.72	405.57	4.90
2411	209	K	102.3	262.68	2.57
115	101	KT	102.82	524.21	5.10
215	203	KT	104.74	521.24	4.98
1411	109	K	106.33	268.54	2.53
2311	310	K	109.37	214.83	1.96
2411	410	K	113.66	221.49	1.95
138	108	KT	122.74	1288.78	10.50
238	208	KT	126.91	1327.72	10.46
1311	110	K	139.95	245.88	1.76
2311	210	K	142.62	248.83	1.74
148	107	KT	154.49	921.63	5.97
248	207	KT	155.56	915.22	5.88
238	308	KT	197.06	1670.73	8.48
248	408	KT	199.53	1654.04	8.29
415	4211	T	200.19	3172.85	15.85
315	4209	T	202.39	3181.92	15.72
217	2203	Y	227.83	4996.2	21.93
117	2204	Y	229.02	5212.84	22.76
415	4207	KT	235.55	11210	47.59
315	4204	KT	237.88	11317	47.57
315	4210	T	241.4	3535.44	14.65
315	4203	KT	241.68	11377	47.07
415	4212	T	242.66	3559.97	14.67
415	4208	KT	244.77	11525	47.09
215	4211	T	247.88	3688.05	14.88
317	2204	Y	248.02	5425.66	21.88
417	2201	Y	248.48	5256.6	21.16
148	407	KT	253.56	1197.09	4.72
115	4209	T	254	3720.31	14.65
138	307	KT	258.3	1194.46	4.62
235	4204	T	266.76	482.82	1.81
145	4208	T	276.3	495.45	1.79
317	2203	Y	306.3	4108.43	13.41
115	4212	T	314.44	4183.92	13.31
215	4210	T	318.27	4236.39	13.31
245	4207	T	329.88	569.12	1.73
135	4203	T	335.15	576.06	1.72
417	2202	Y	341.47	4009.72	11.74
117	2201	Y	383.58	4498.73	11.73
215	4206	KT	411.61	16034	38.95
115	4202	KT	416.18	16021	38.50
215	4205	KT	420.45	16278	38.72

Table 5.1: Analysis results ranked according to toe life

Node	Element	Joint type	Fatigue Life		
			Toe	Root	Ratio
2311	310	K	109.37	214.83	1.96
2411	410	K	113.66	221.49	1.95
1411	409	K	79.77	228.17	2.86
1311	309	K	81.67	232.57	2.85
1311	110	K	139.95	245.88	1.76
2311	210	K	142.62	248.83	1.74
2411	209	K	102.3	262.68	2.57
1411	109	K	106.33	268.54	2.53
415	403	KT	53.12	309.29	5.82
315	301	KT	53.36	310.19	5.81
315	303	KT	54.53	328.06	6.02
415	401	KT	54.64	328.65	6.01
115	103	KT	82.23	404.8	4.92
215	201	KT	82.72	405.57	4.90
238	306	KT	927.3	444.05	0.48
148	404	KT	937.52	455.93	0.49
238	206	KT	919.3	477.85	0.52
235	4204	T	266.76	482.82	1.81
148	104	KT	959.58	489.34	0.51
145	4208	T	276.3	495.45	1.79
215	203	KT	104.74	521.24	4.98
115	101	KT	102.82	524.21	5.10
248	406	KT	989.58	525.22	0.53
138	304	KT	1007.01	533.04	0.53
245	4207	T	329.88	569.12	1.73
248	204	KT	1176.26	574.29	0.49
135	4203	T	335.15	576.06	1.72
138	106	KT	1223.4	578.34	0.47
235	4205	T	424.16	670.77	1.58
145	4201	T	432.59	677	1.56
135	4202	T	607.77	840.35	1.38
245	4206	T	609.56	848.62	1.39
132	7003	K	4721.86	910.01	0.19
142	7008	K	4543.65	910.49	0.20
232	7004	K	4554.89	911.6	0.20
242	7007	K	4723.26	912.06	0.19
248	207	KT	155.56	915.22	5.88
148	107	KT	154.49	921.63	5.97
315	306	KT	616.61	1079.05	1.75
415	404	KT	640.68	1101.65	1.72
242	403	K	1750.6	1186.84	0.68
132	301	K	1754.72	1189.09	0.68
138	307	KT	258.3	1194.46	4.62
148	407	KT	253.56	1197.09	4.72
115	104	KT	675.73	1200.56	1.78
142	401	K	1791.85	1209.71	0.68
232	303	K	1801.2	1210.83	0.67
215	206	KT	713.59	1229.32	1.72
138	108	KT	122.74	1288.78	10.50
238	208	KT	126.91	1327.72	10.46

Table 5.2: Analysis results ranked according to root life

Node	Element	Joint type	Fatigue Life		Ratio
			Toe	Root	
132	7003	K	4721.86	910.01	0.19
242	7007	K	4723.26	912.06	0.19
2311	1204	K	96075	18998	0.20
232	7004	K	4554.89	911.6	0.20
142	7008	K	4543.65	910.49	0.20
2411	1207	K	91639	19028	0.21
1411	1208	K	87874	19910	0.23
1311	1203	K	87742	20011	0.23
2311	1205	K	89634	24836	0.28
2411	1206	K	80184	25454	0.32
1311	1202	K	74921	25529	0.34
1411	1201	K	68396	24895	0.36
142	101	K	4214.85	1956.64	0.46
232	203	K	4139.47	1955.31	0.47
138	106	KT	1223.4	578.34	0.47
132	103	K	4006.79	1906.78	0.48
238	306	KT	927.3	444.05	0.48
242	201	K	3898.77	1889.25	0.48
148	404	KT	937.52	455.93	0.49
248	204	KT	1176.26	574.29	0.49
148	104	KT	959.58	489.34	0.51
238	206	KT	919.3	477.85	0.52
138	304	KT	1007.01	533.04	0.53
248	406	KT	989.58	525.22	0.53
232	303	K	1801.2	1210.83	0.67
142	401	K	1791.85	1209.71	0.68
132	301	K	1754.72	1189.09	0.68
242	403	K	1750.6	1186.84	0.68
414	7009	K	41245	35795	0.87
314	7011	K	38502	34471	0.90
317	307	X	68068	61067	0.90
238	1304	KT	4230.71	4199.2	0.99
417	407	X	62500	62391	1.00
217	210	X	34187	34604	1.01
248	1307	KT	4027.17	4192.73	1.04
414	7012	K	27686	29136	1.05
148	1308	KT	4010.26	4306.75	1.07
314	7010	K	27250	29349	1.08
117	110	X	30930	34492	1.12
138	1303	KT	3713.31	4329.25	1.17
217	207	X	43127	51622	1.20
117	107	X	42587	51206	1.20
214	7011	K	17872	23831	1.33
114	7009	K	17598	23694	1.35
135	4202	T	607.77	840.35	1.38
245	4206	T	609.56	848.62	1.39
214	7012	K	14415	20808	1.44
114	7010	K	14503	21034	1.45
215	204	KT	1009.45	1556.61	1.54
315	304	KT	870.03	1361.05	1.56

Table 5.3: Analysis results ranked according to root/toe life ratio conclusions

6. CONCLUSIONS

A complete review has been undertaken of available data on stress concentration factors (SCFs) occurring on the inside of brace or on the chord plug region of tubular joints. A number of studies have been undertaken using finite element analysis (FEA), mainly by Statoil and University of Wales, Swansea, which cover simple joint types (K, X, Y) and load cases (axial, IPB and OPB). Data from the studies have been extracted and tabulated in Appendix A. The internal and external SCFs have been plotted on the figures in Appendix B.

A small proportion of the respective studies overlap and comparisons have shown that different investigators report different SCFs. Nevertheless, the calculated ratios of internal SCF to external SCF (R ratios) are broadly similar for the different studies and generally, although not always, indicated the same dependency of R on given tubular joint geometric variables.

The FEA studies were usually designed such that there was little opportunity to study possible interaction effects on R between the geometric variables. Where opportunity did arise, the following observations could be made:

- There is no coupling between β and ζ for K joints subjected to balanced axial load, balanced IPB or balanced OPB.
- There is little coupling between θ and other parameters (β , γ and τ) for Y joints under OPB.
- There is little β - θ coupling, strong γ - θ coupling and moderate τ - θ coupling for axially loaded Y joints.
- There are moderate β - θ and γ - θ couplings and a strong τ - θ coupling for Y joints under IPB.

Curve fitting exercises were conducted to give R formulations for the three joint types and three load cases. The nine R formulations, and the validity ranges of the pertinent geometric variables, are given in Tables 3.1 and 3.2 in Section 3.5 respectively. Difficulty was found in fitting Y joints under axial loads and especially under IPB. This was due to the above coupling effects without there being sufficient data to clarify the true nature of the interaction surface. Overall, reasonable predictions appear to be provided by the R formulations. Taking all joint and load types together, the R formulations give a mean bias of 1.012 and a standard deviation of 6.4%. However, it should be noted that these statistics apply to the data from which the R formulations were derived and thus a good fit should be expected.

A review of pertinent S-N data has been carried out, see Section 4. Both tubular joint and girth weld data were examined in the review. It was concluded that a Class D S-N curve might be appropriate for single sided welds.

To assess the impact of single sided welding, a typical North Sea structure was subject to a fatigue analysis. All tubular joints were assumed to be single side welded, and SCFs were established on the external surface (toe of weld) and internally (weld root). Using the HSE T' curve for the weld toes, and the suggested D curve for the weld root, the internal and external lives for each joint were derived. The results, detailed in Section 5, led to the following observations:

- The lowest toe life (ie. the lowest life that would be established by present day design practice) is 53 years. The internal life for the same joint is 309 years.
- The lowest internal life anywhere is 215 years.
- Over 30 joints have internal lives less than the external lives. Of these joints the lowest life was 444 years.

It may be concluded that, for this structure, internal fatigue life would not have given any problem even had all joints been single side welded. It is appropriate, however, that further consideration should be given to two issues. The first concerns weld improvement by such techniques as weld profiling, toe grinding and hammer peening. These techniques necessarily only lead to a life enhancement for the external weld, the internal life remains unaffected. The second issue concerns inspectability; the weld root is hidden and for practical purposes is not inspectable. A penalty factor of around 2 to 3 is

presently being mooted by the industry for uninspectable joints. Neither issue, taken alone, leads to any difficulty for the subject structure. However, other structures may present concerns. This does not apply so much to the design of the new structures, for which double sided welding can be specified, as to the assessment of existing structures. It is noted that some information on the likely state of the internal weld can be gleaned from an external inspection. That is if no external crack is found, then it is likely that no internal crack is present where the ratio of internal life to external life (on the basis that no inspection penalty factor is applied) is greater than unity. It is recommended that reliability studies should be conducted to explore this further.

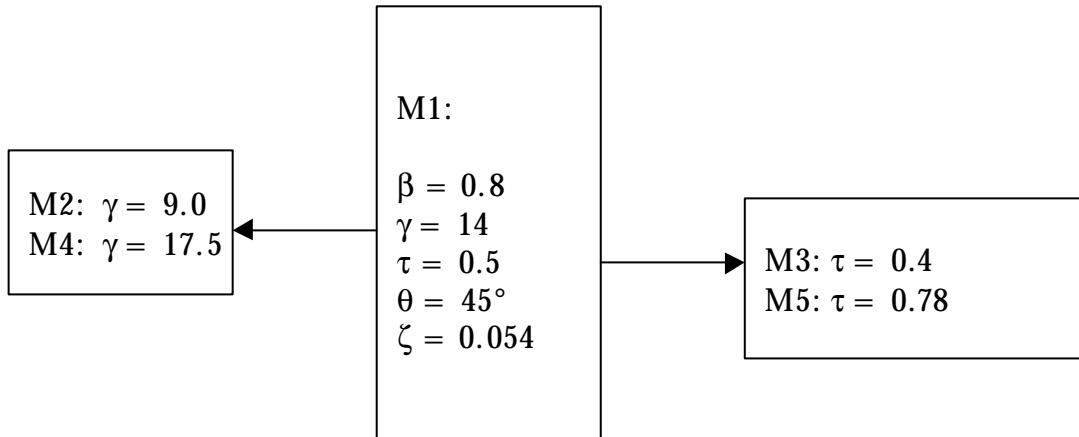
In conclusion, it would appear that single side welded joints can give lower fatigue lives at the root than at the toe, especially if a penalty factor is applied, but the indications are that this would only rarely constitute a problem because of the long lives of the affected joints.

7. REFERENCES

1. HEALTH AND SAFETY EXECUTIVE
Offshore Installations: Guidance on Design, Construction and Certification
4th Edition (1990) plus Amendment No 3, February 1995.
2. LEE, M. M. K., MORGAN, M. R. AND LEA, F.
Stress Concentrations in Single-sided Welds in Offshore Tubular Joints
Offshore Technology Report OTO 98 044, Health and Safety Executive, May 1998.
3. ISO TC67/SC7/WG3 PANEL 3 TECHNICAL CORE GROUP JOINTS
Draft Code Provisions and Commentary for Section F: Fatigue Strength of Connections
Revision R4, December 1997.
4. BÆRHEIM, M.
Stress Concentrations in Overlapped KT Joints
Tubular Structures Conference, den Haag, 1991.
5. BÆRHEIM, M.
Stress Concentrations in Tubular Joints Welded from One Side
International Offshore and Polar Engineering (ISOPE) Conference, Los Angeles, 1996.
6. HANSEN, K
Single Side Welded Tubular Joints in Offshore Structures – A Study of the Stress Concentrations at the Weld Root
Høgskolen in Stavanger, 1996.
7. BÆRHEIM, M., HANSEN, K., BÆRHEIM, K. AND GUDMESTAD, O. T
Single Sided Welded Tubular Joints – Stress Concentrations at the Weld Root
17th International Conference on Offshore Mechanics and Arctic Engineering, Lisbon, 1998.
8. MaTSU
Fatigue Background Guidance Document
OTH 92 390 (Draft).
9. MADDOX, S.J. AND RAZMJOO, G.R
Fatigue Performance of Large Girth Welded Steel Tubes
17th International Conference on Offshore Mechanics and Arctic Engineering, Lisbon, 1998.
10. AD HOC DATA RELEASED TO ISO TC67/SC7/WG3/P3
Technical Core Group for Tubular Joints

FIGURES

MSL



DNV

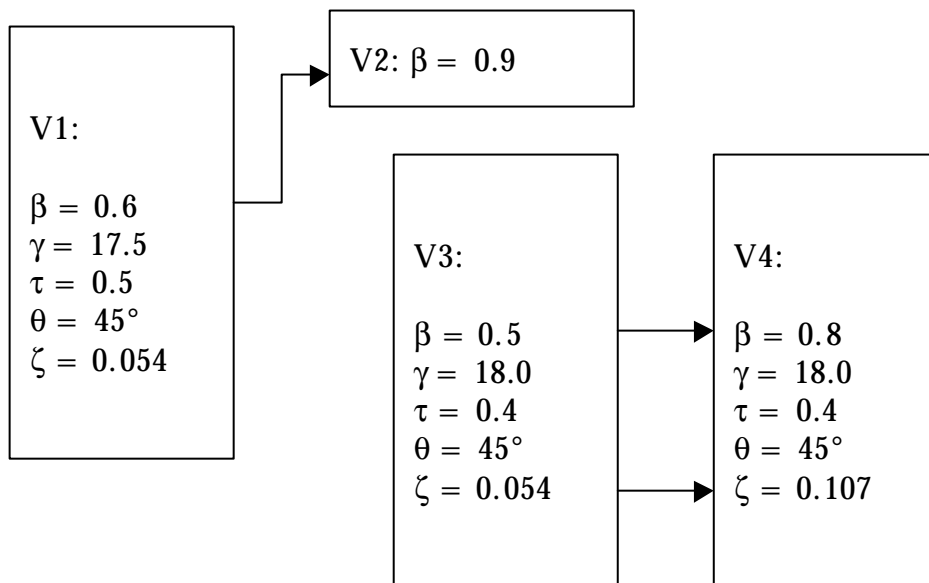


Figure 2.1: MSL and DNV preliminary study⁽⁵⁾ for K joints under balanced axial loading

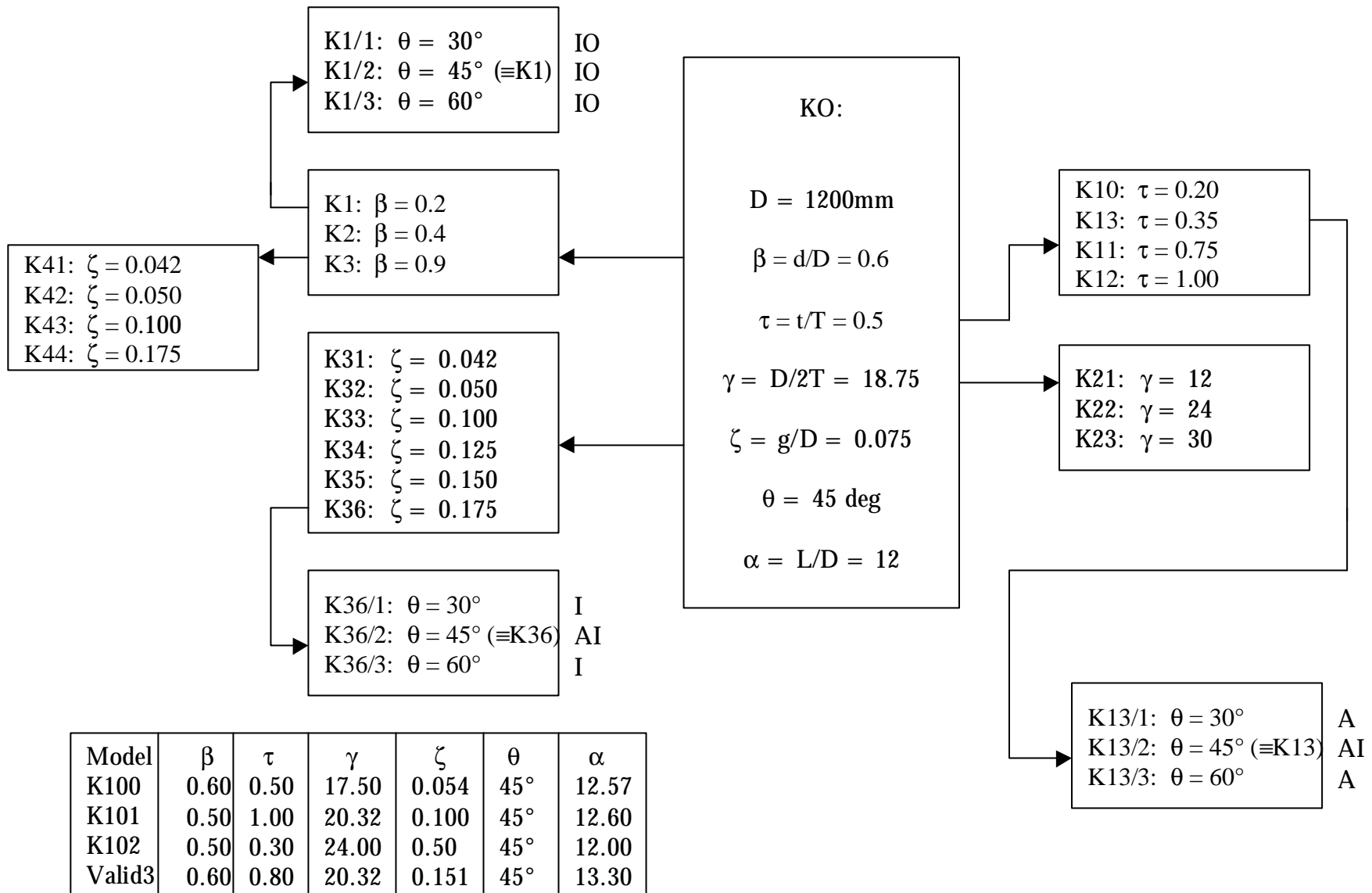
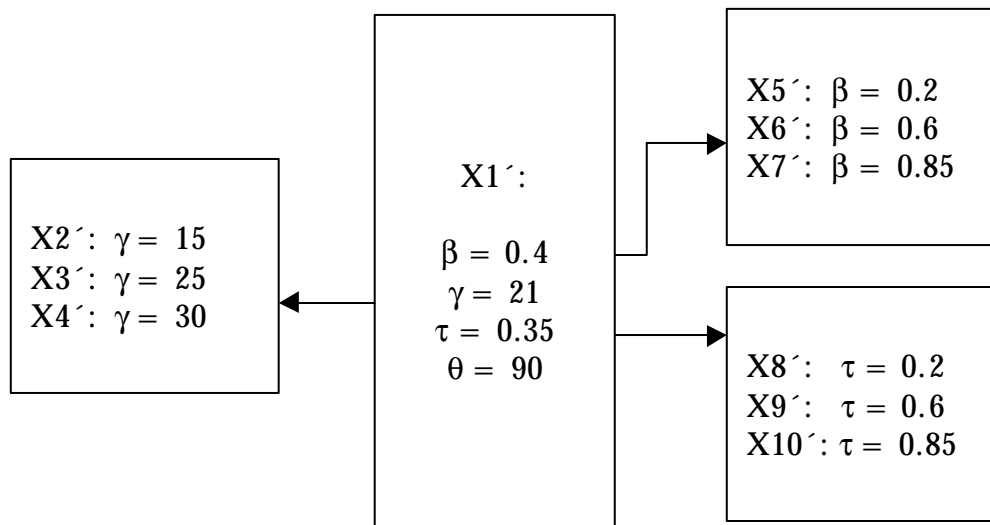


Figure 2.2: Parametric studies on K joints^(2 and 6) under balanced axial loading, balanced in-plane bending and balanced out-of-plane bending (Note for θ variations, only indicated cases run)

Swansea Study - axial tension, IPB, OPB⁽²⁾



Statoil study - axial compression only⁽⁶⁾

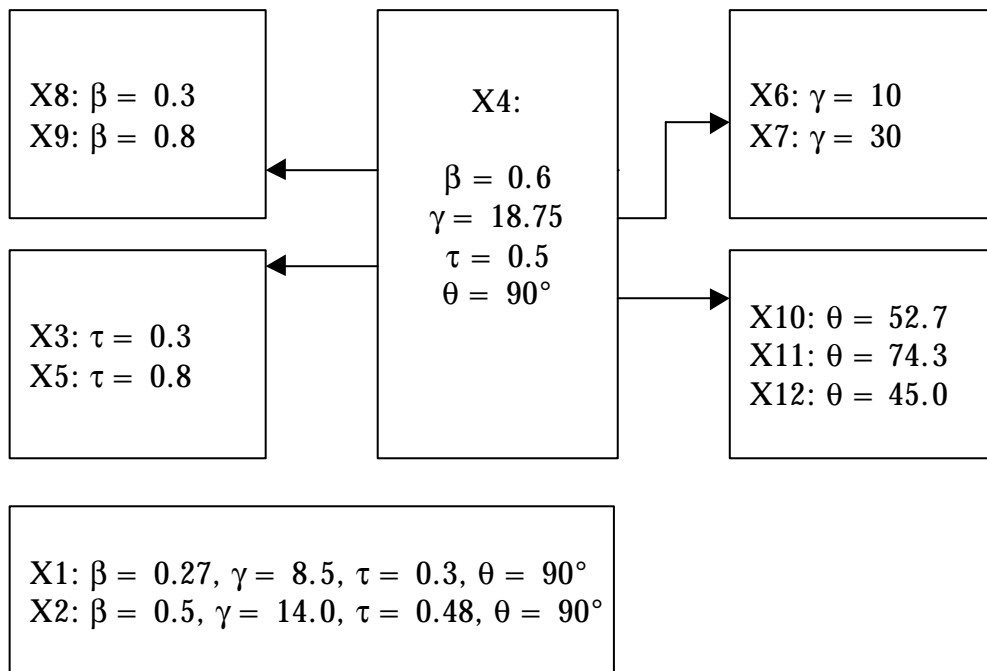
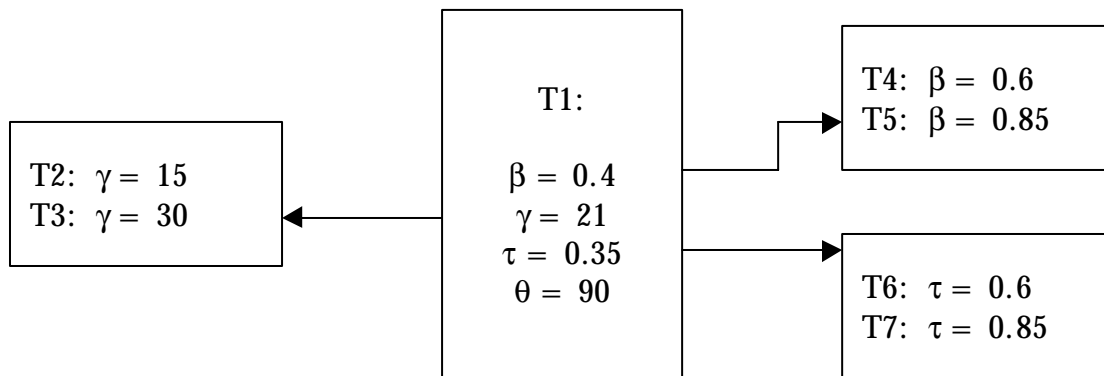


Figure 2.3: Parametric studies on X/DT joints^(2 and 6)

T-Joints



Y - Joints

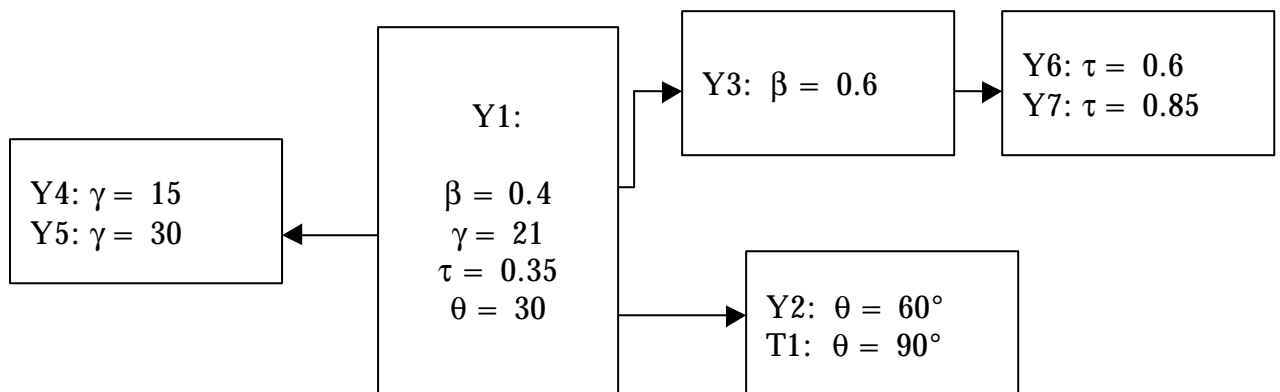


Figure 2.4: Parametric studies on Y/T joints⁽²⁾ under axial, in-plane bending and out-of-plane bending

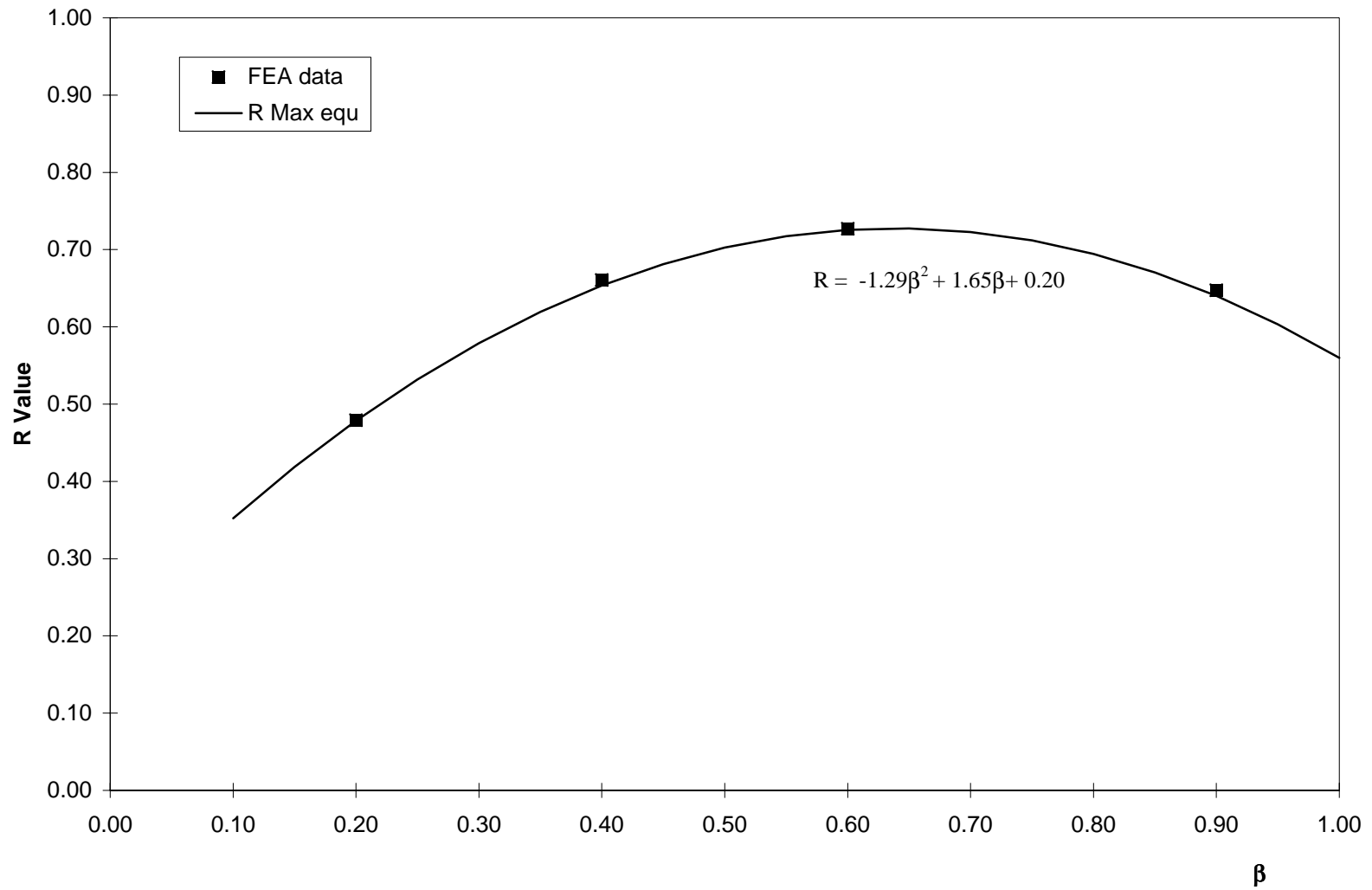


Figure 3.1: K joints under balanced axial loading, R v. β
 $\gamma = 18.75, \tau = 0.5, \zeta = 0.075, \theta = 45^\circ$

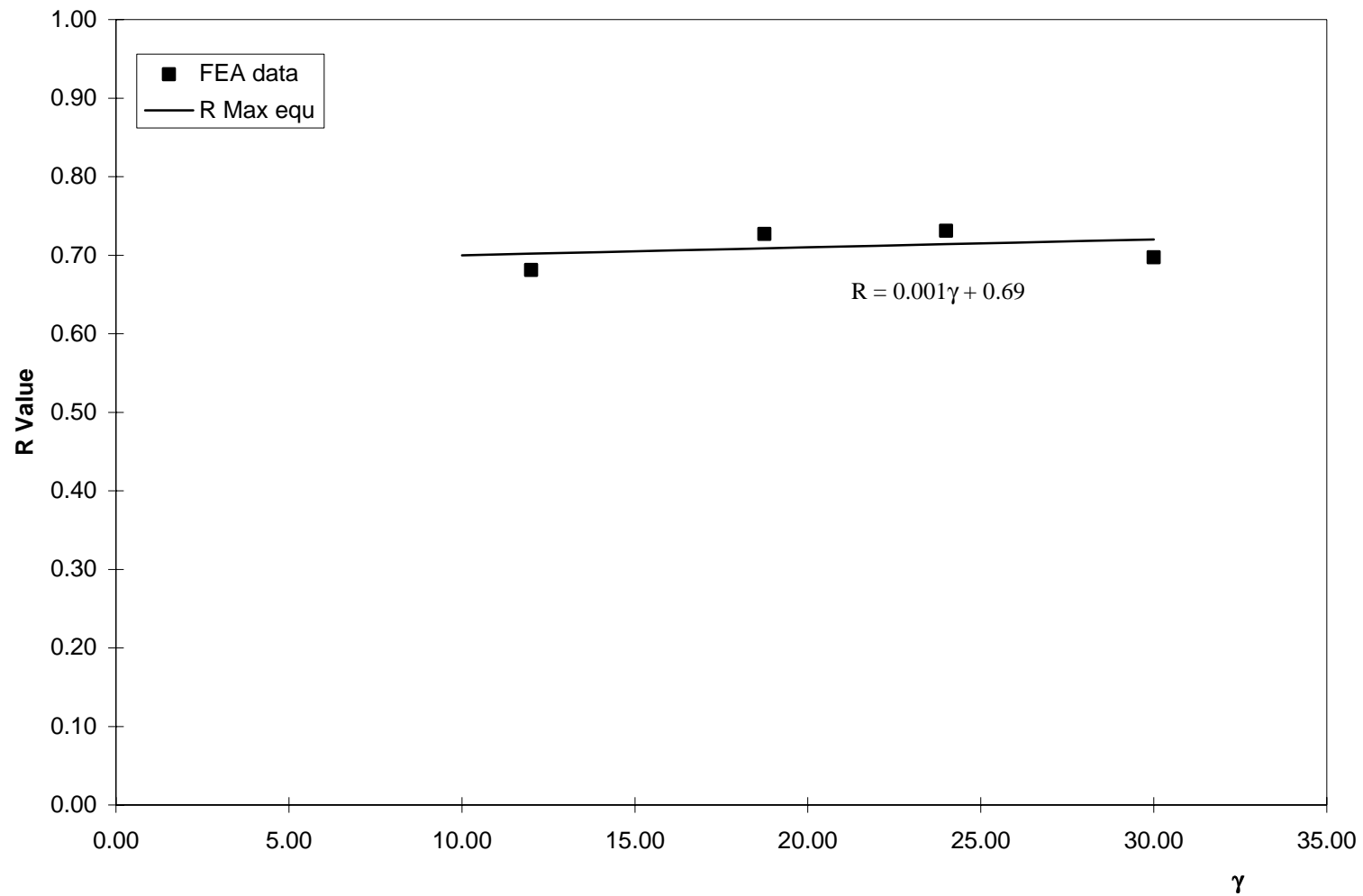


Figure 3.2: K joints under balanced axial loading, R v. γ
 $\beta = 0.6, \tau = 0.5, \zeta = 0.075, \theta = 45^\circ$

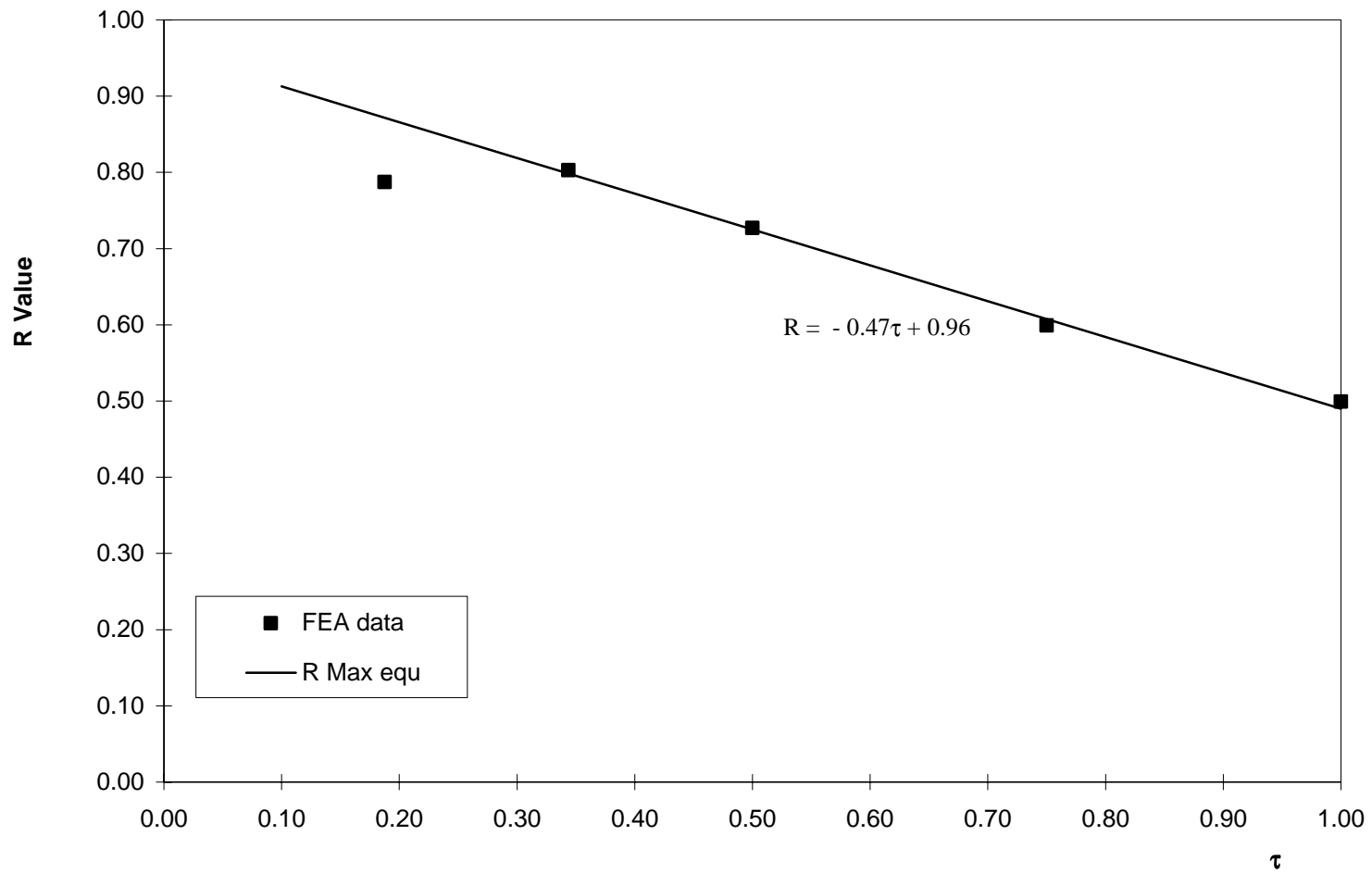


Figure 3.3: K joints under balanced axial loading, R v. τ
 $\beta = 0.6, \gamma = 18.75, \zeta = 0.075, \theta = 45^\circ$

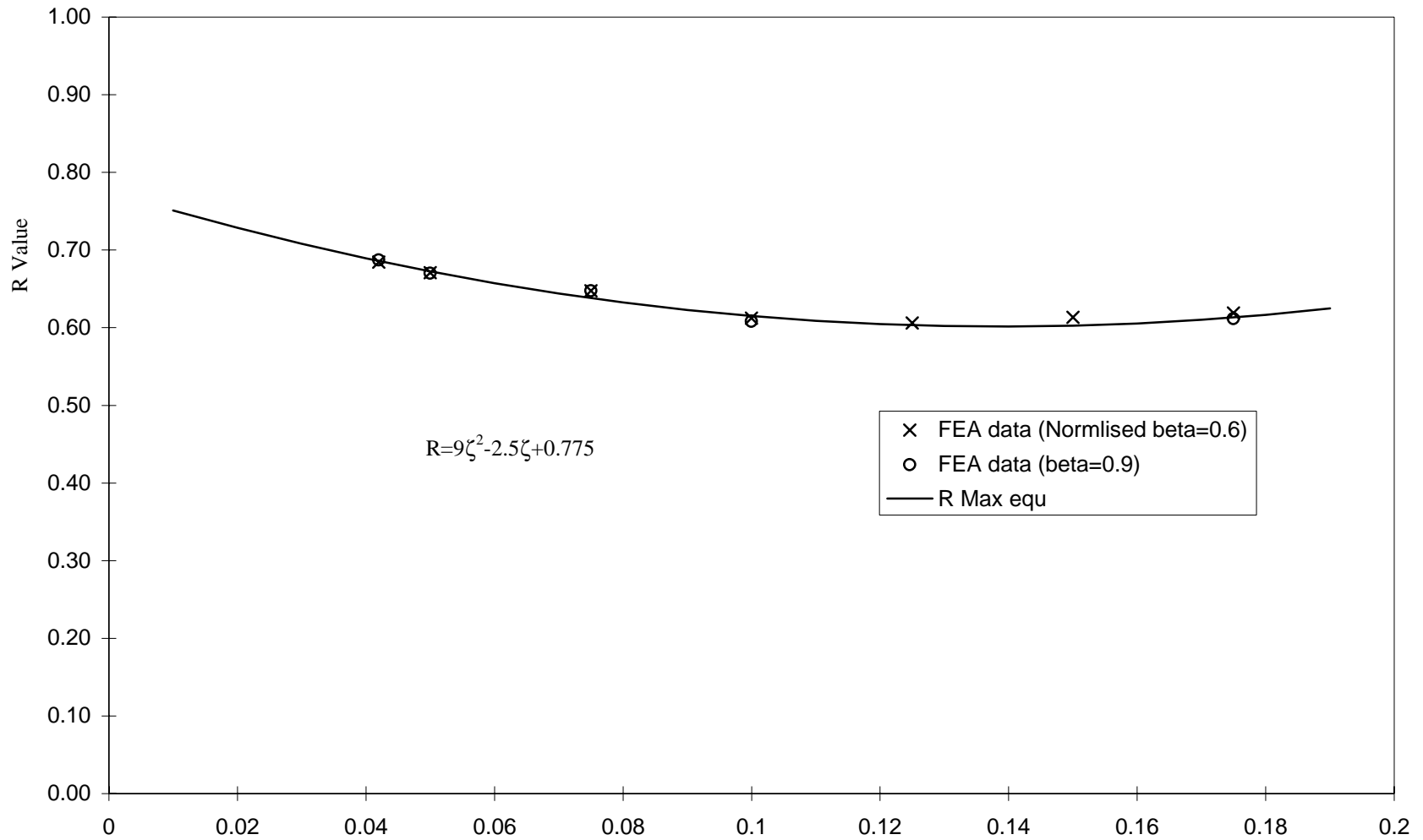


Figure 3.4: K joints under balanced axial loading, R v. ζ
 $\beta=0.6$ and 0.9 , $\gamma=18.75$, $\tau=0.5$, $\theta=45^\circ$

ζ

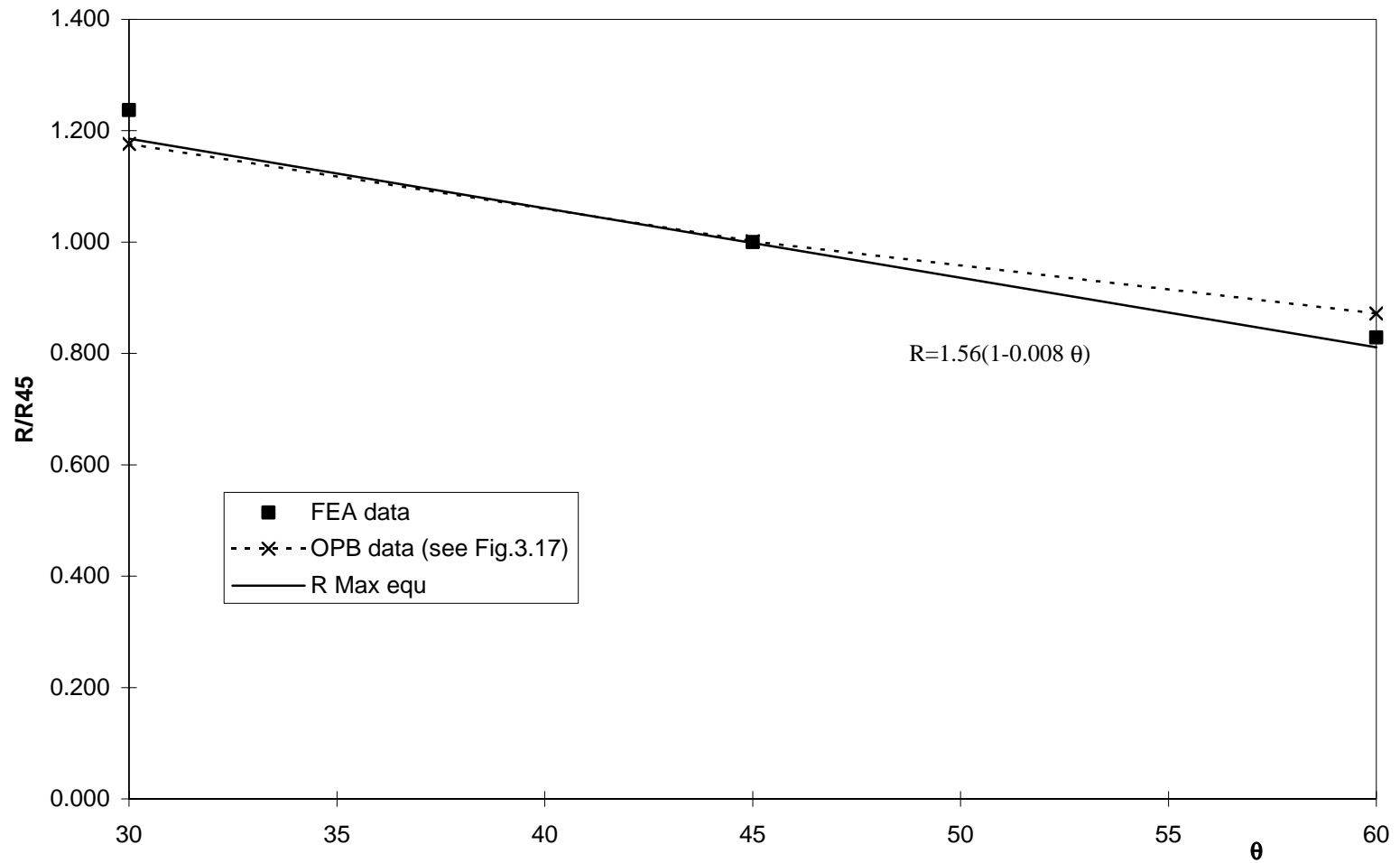


Figure 3.5: K joints under balanced axial loading, R v. θ
 $\beta=0.6, \gamma=18.75, \tau=0.35, \zeta=0.075$

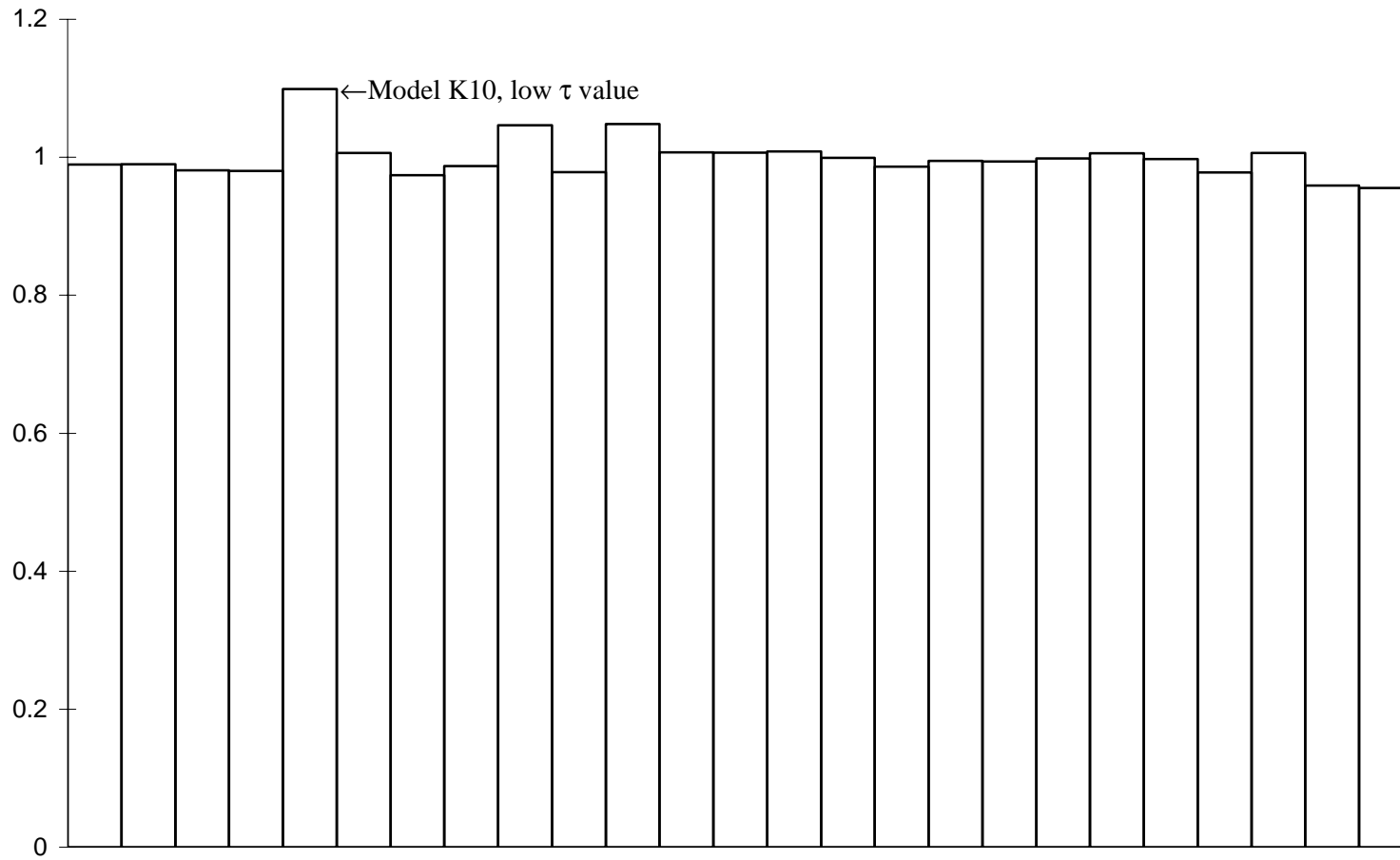


Figure 3.6: K joints under axial loading; Histogram of predicted to calculated R values

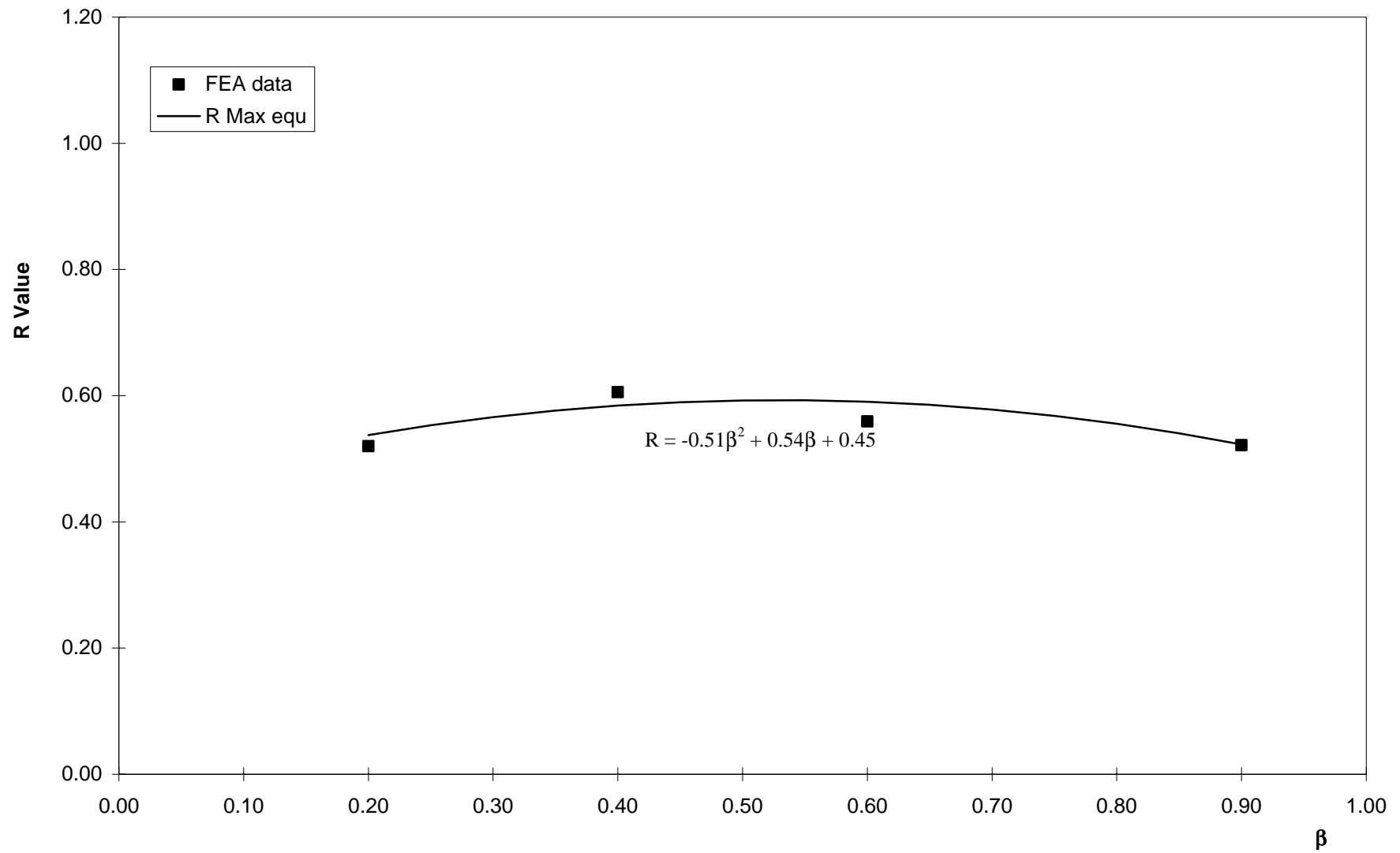


Figure 3.7: K joints under IPB loading, R v. β , $\gamma = 18.75$, $\tau = 0.5$, $\zeta = 0.075$, $\theta = 45^\circ$

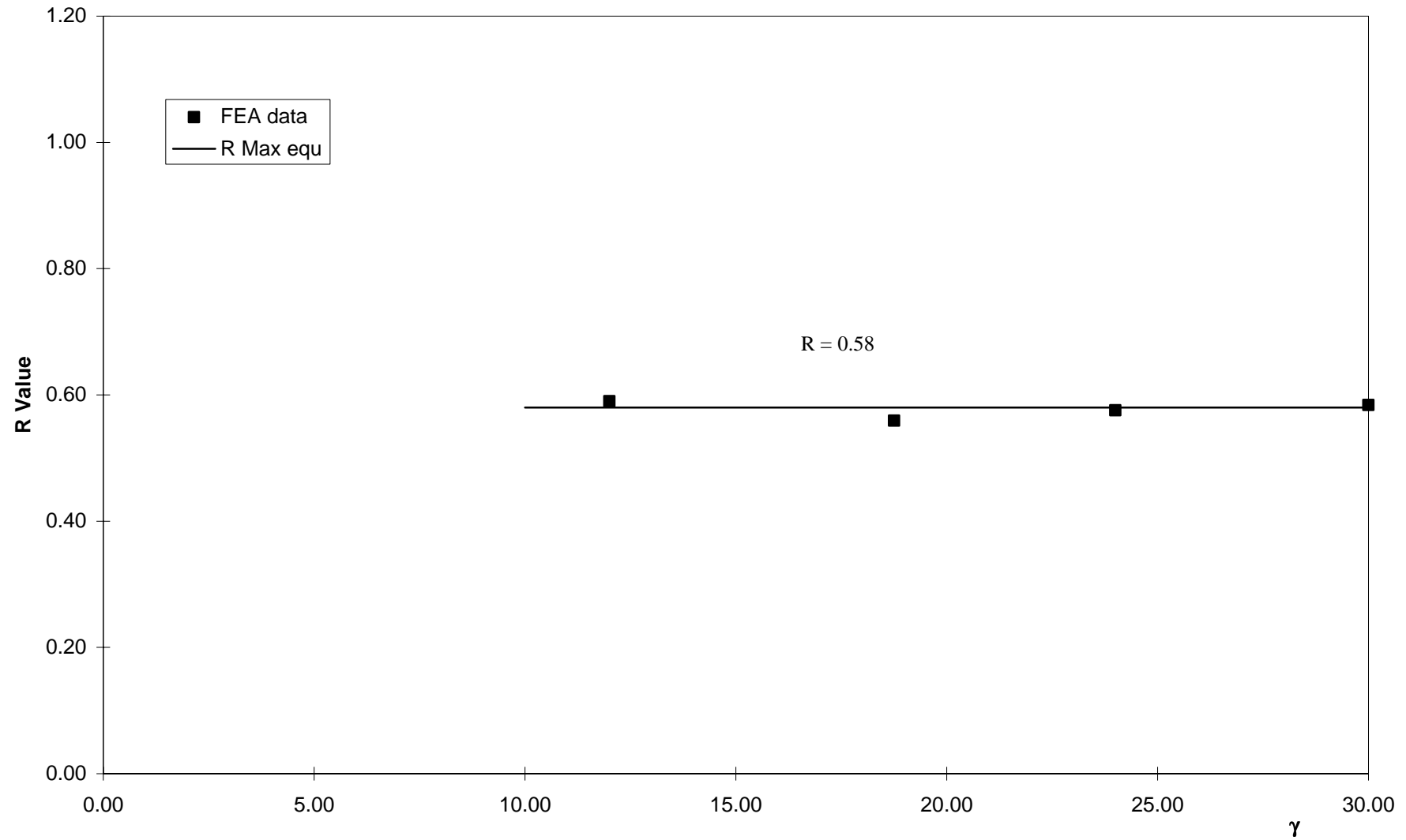


Figure 3.8: K joints under IPB loading, R v. γ , $\beta = 0.6$, $\tau = 0.5$, $\zeta = 0.075$, $\theta = 45^\circ$

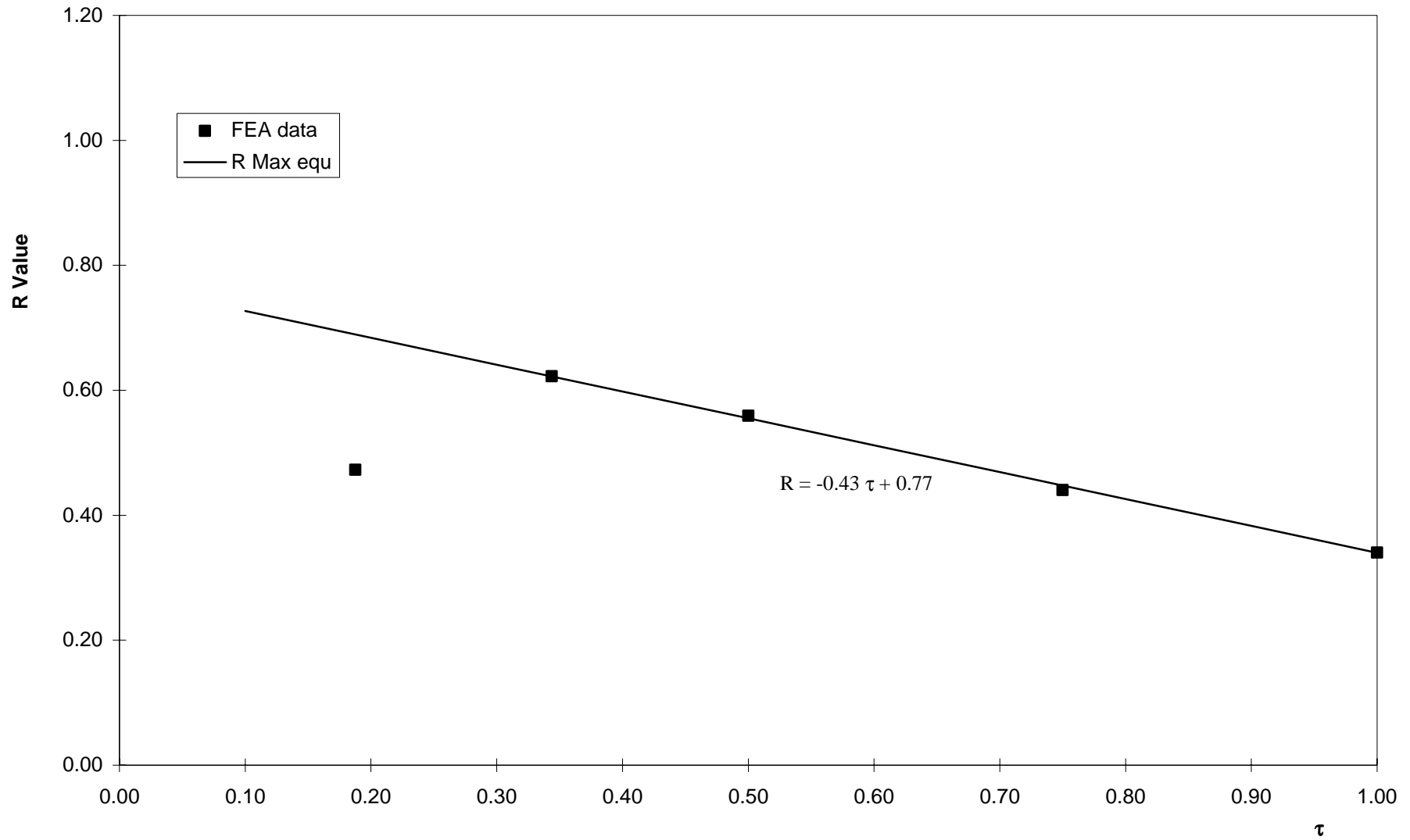


Figure 3.9: K joints under IPB loading, R v. τ , $\beta = 0.6$, $\gamma = 18.75$, $\zeta = 0.075$, $\theta = 45^\circ$

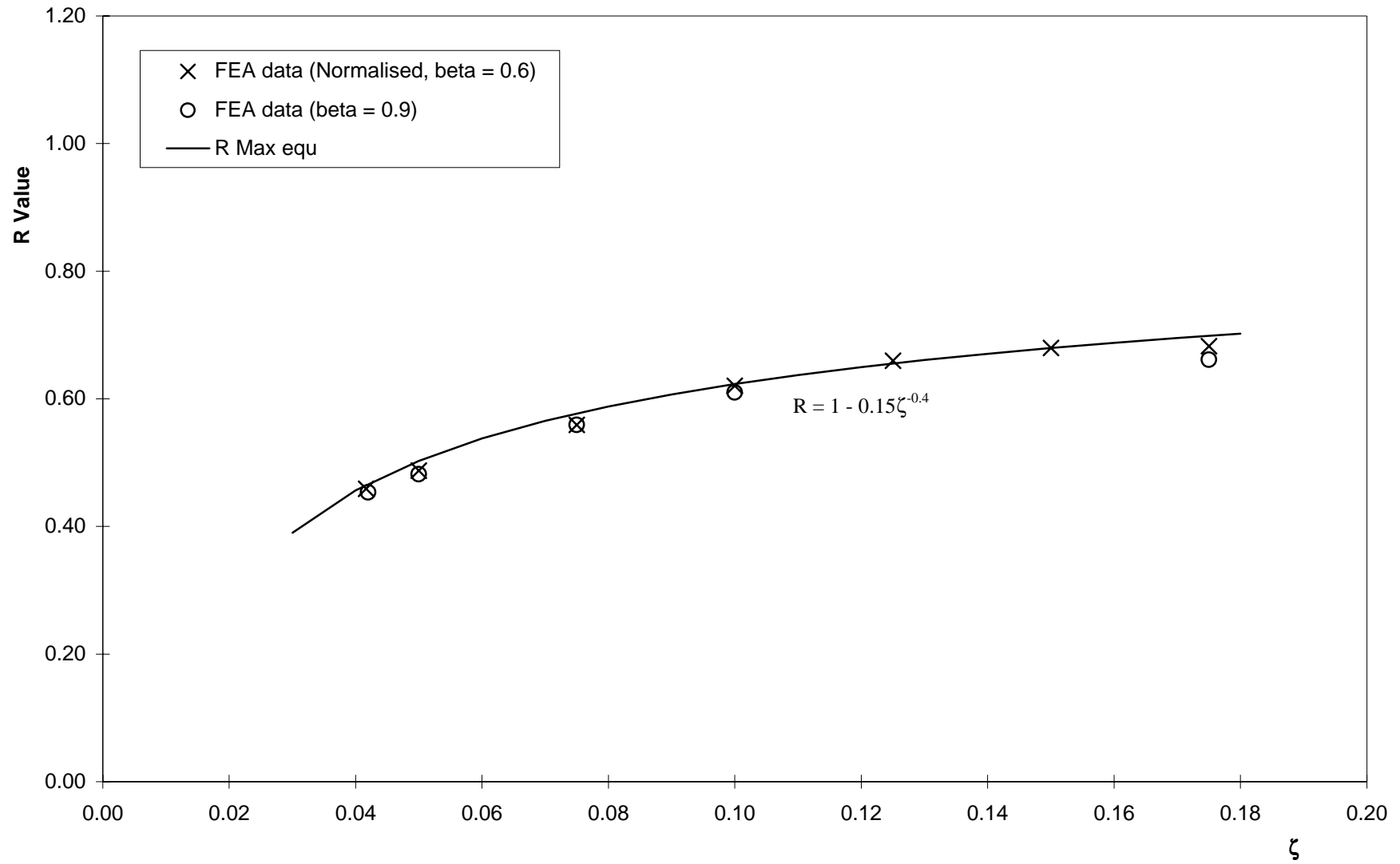


Figure 3.10: K joints under IPB loading, R v. ζ
 $\beta = 0.6$ and 0.9 , $\gamma = 18.75$, $\tau = 0.5$, $\theta = 45^\circ$

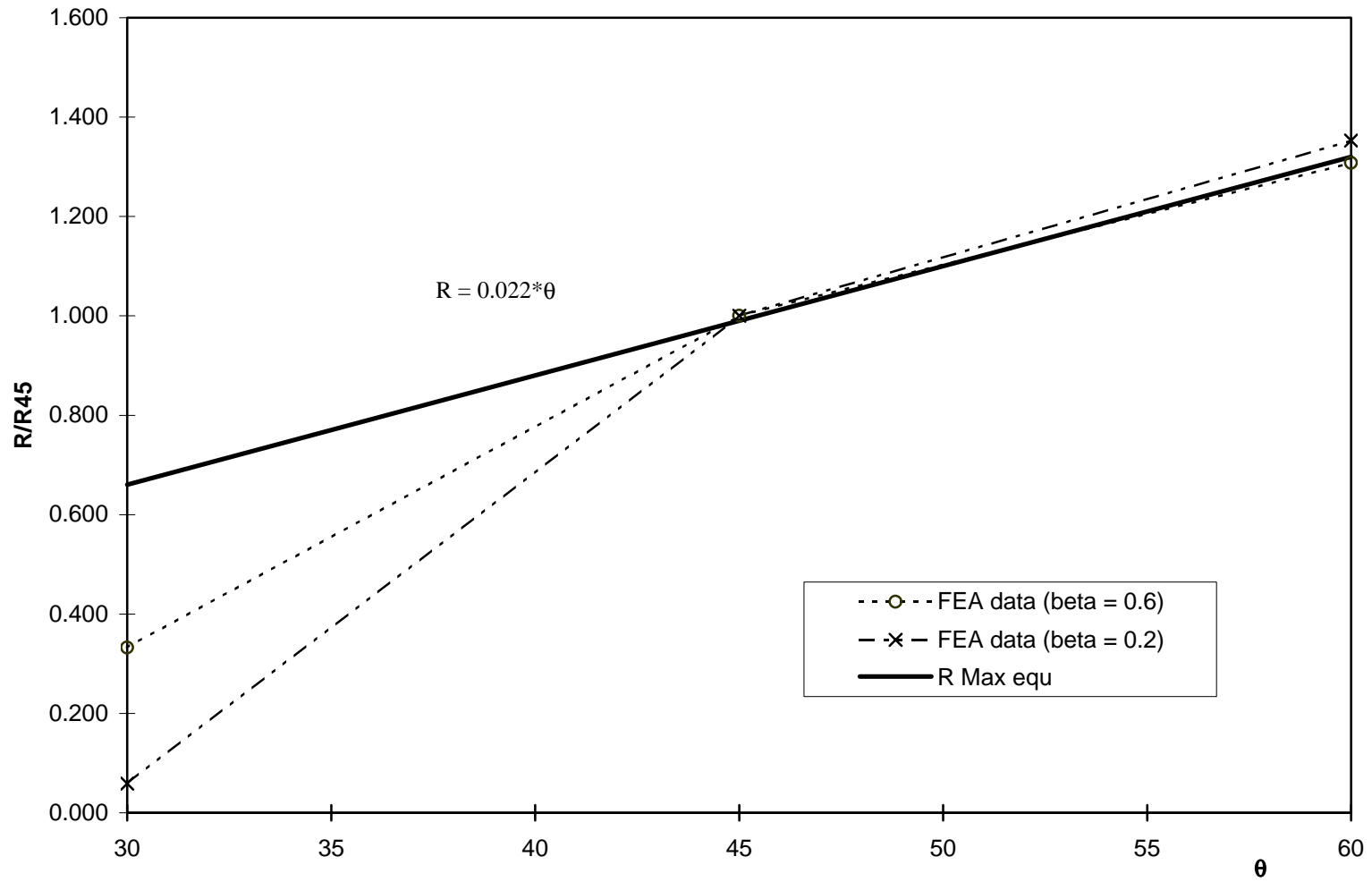


Figure 3.11: K joints under IPB loading, R v. θ
 $\beta=0.6, \gamma=18.75, \tau=0.5, \zeta=0.175$ and $\beta=0.2, \gamma=18.75, \tau=0.5, \zeta=0.075$

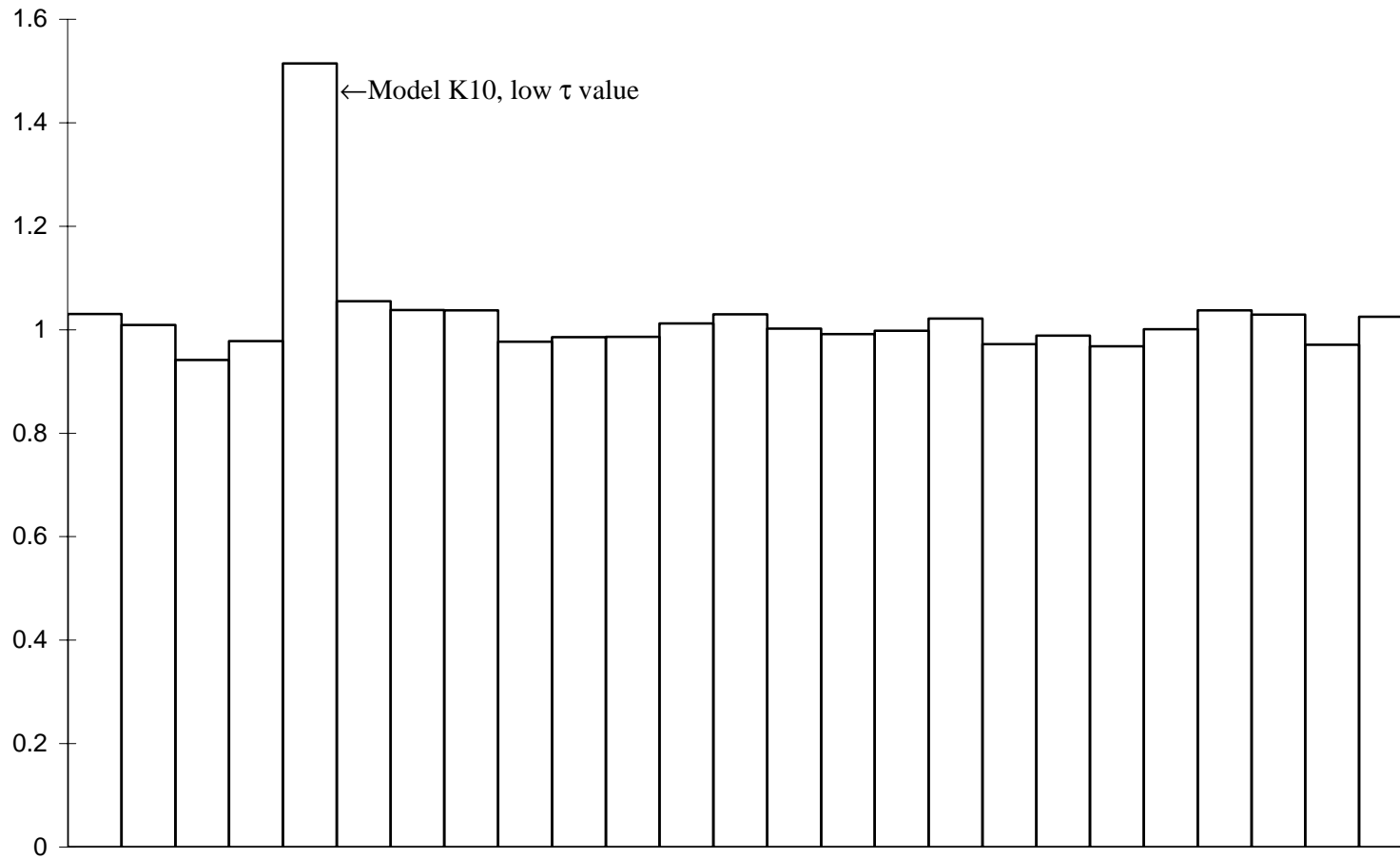


Figure 3.12: K joints under IPB loading; Histogram of predicted to calculated R values

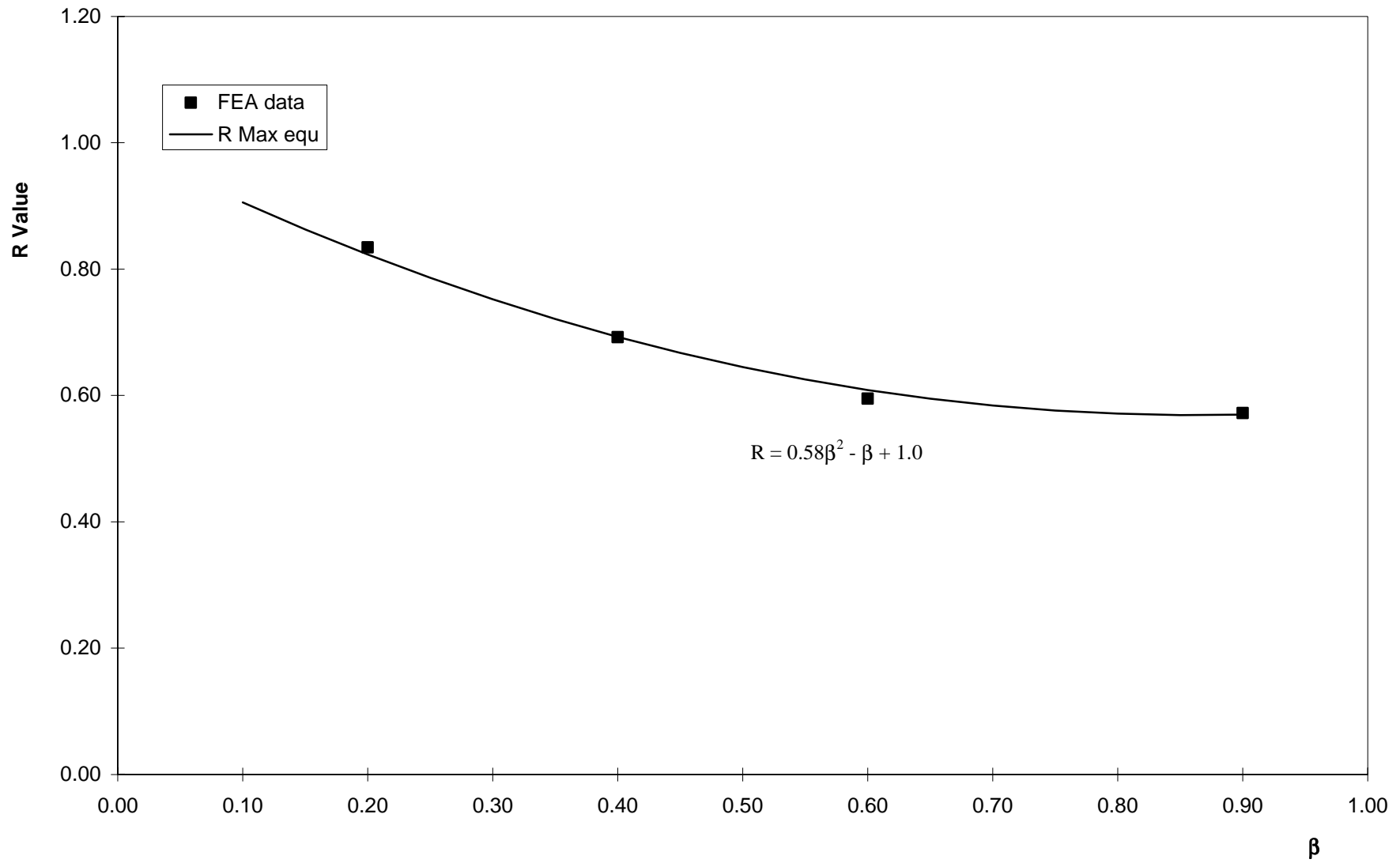


Figure 3.13: K joints under OPB loading, R v. β , $\gamma=18.75$, $\tau = 0.5$, $\zeta = 0.075$, $\theta = 45^\circ$

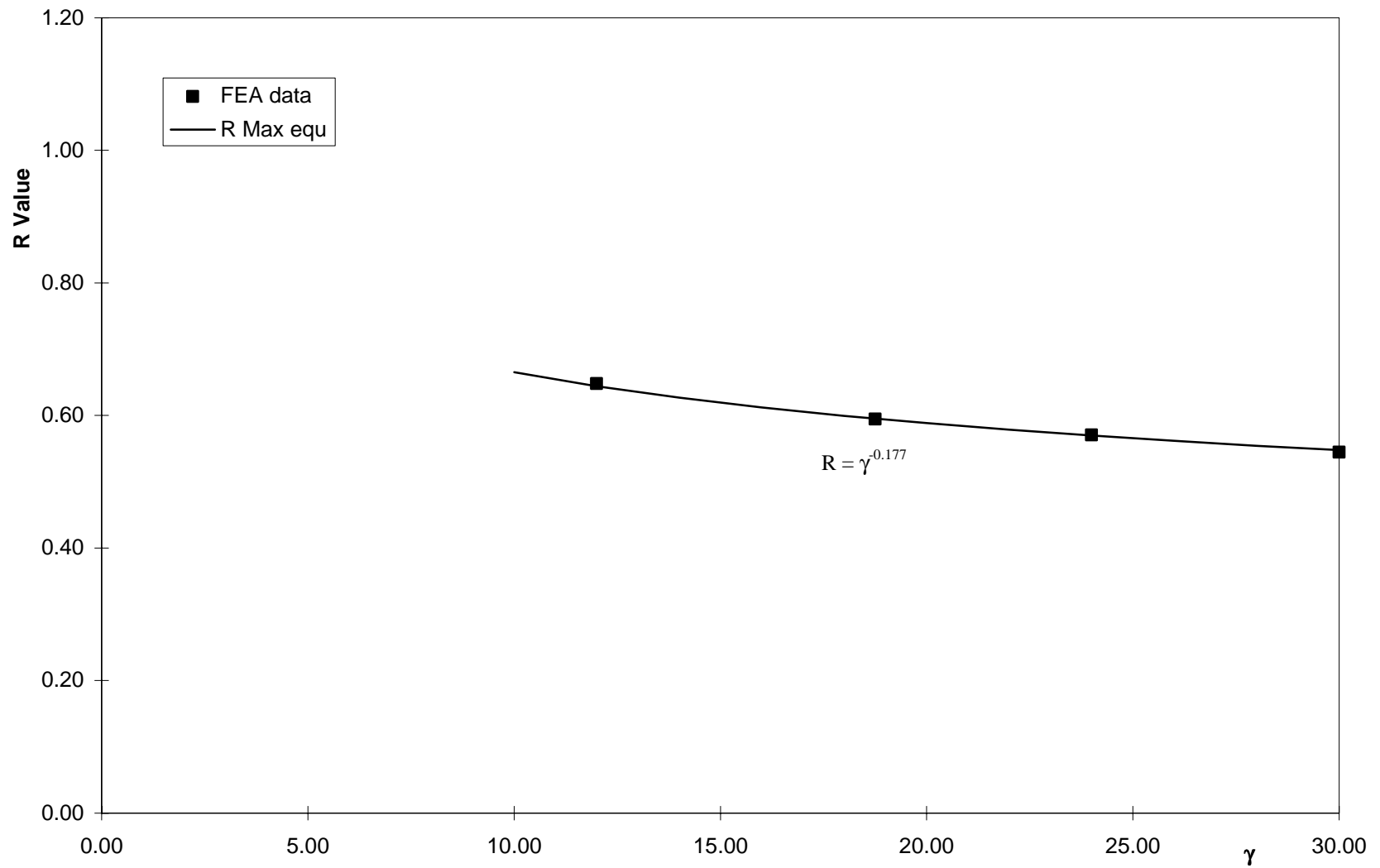


Figure 3.14: K joints under OPB loading, R v. γ , $\beta = 0.6$, $\tau = 0.5$, $\zeta = 0.075$, $\theta = 45^\circ$

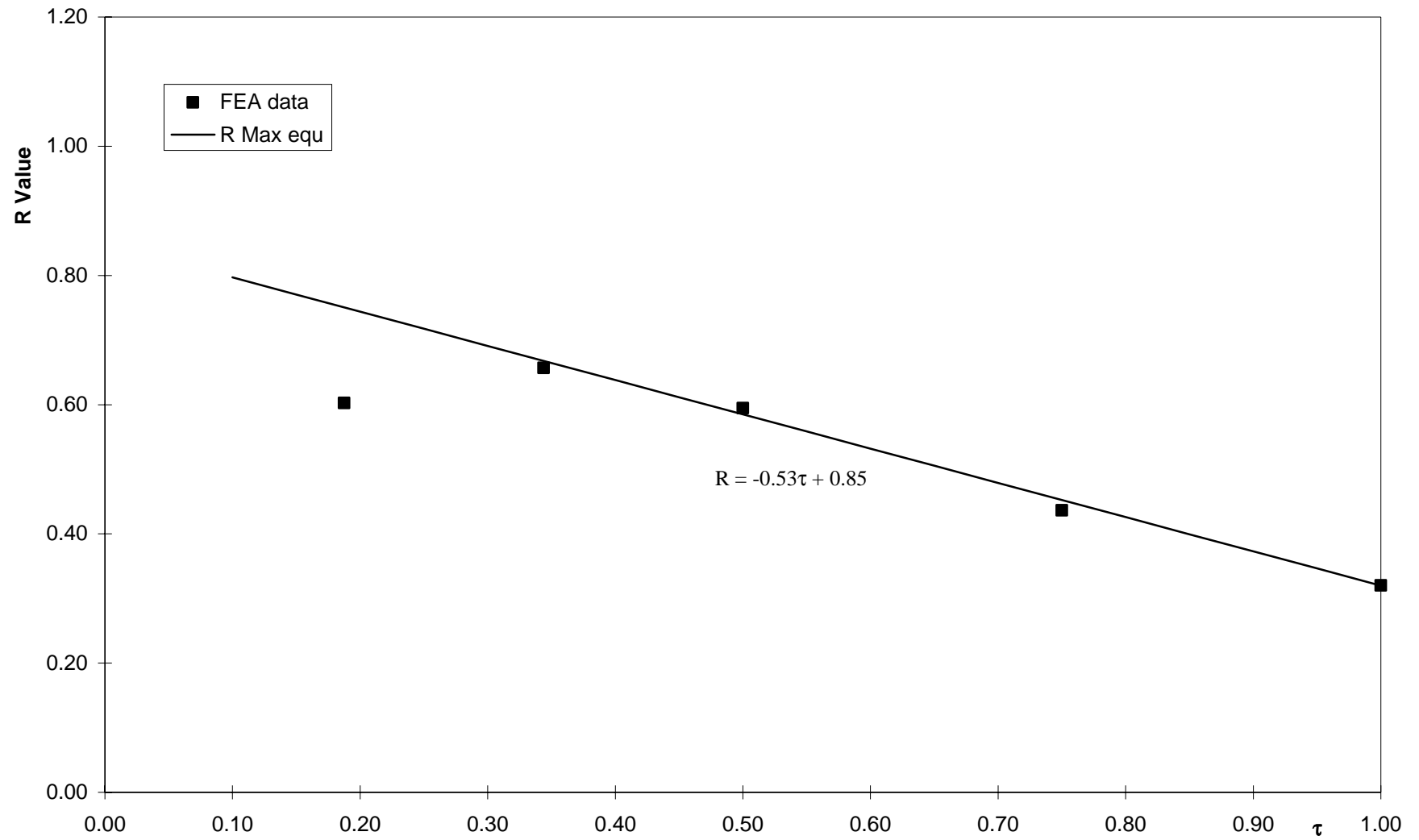


Figure 3.15: K joints under OPB loading, R v. τ , $\beta = 0.6$, $\gamma = 18.75$, $\zeta = 0.075$, $\theta = 45^\circ$

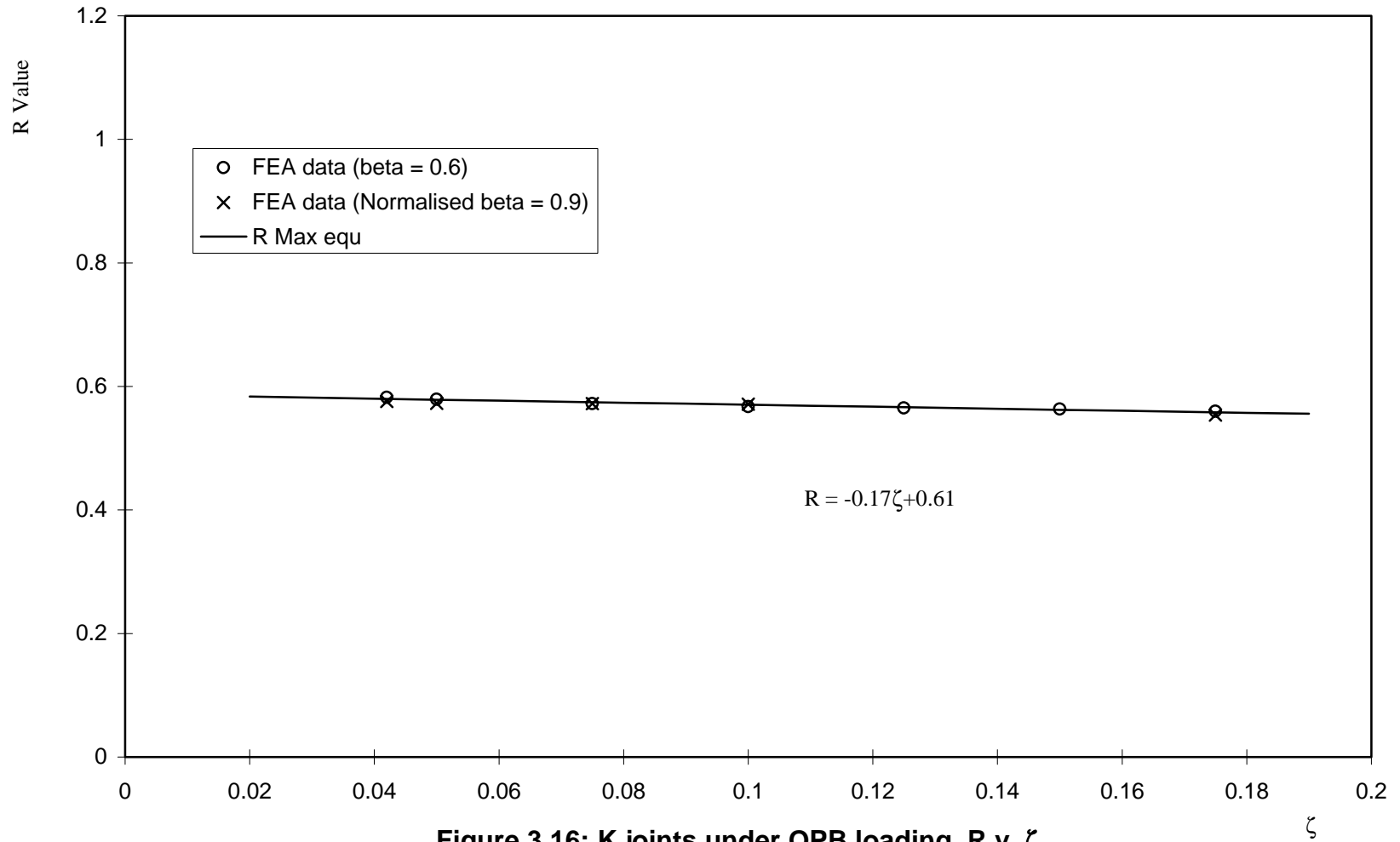


Figure 3.16: K joints under OPB loading, R v. ζ
β=0.6 and 0.9, γ=18.75, τ=0.5, θ=45°

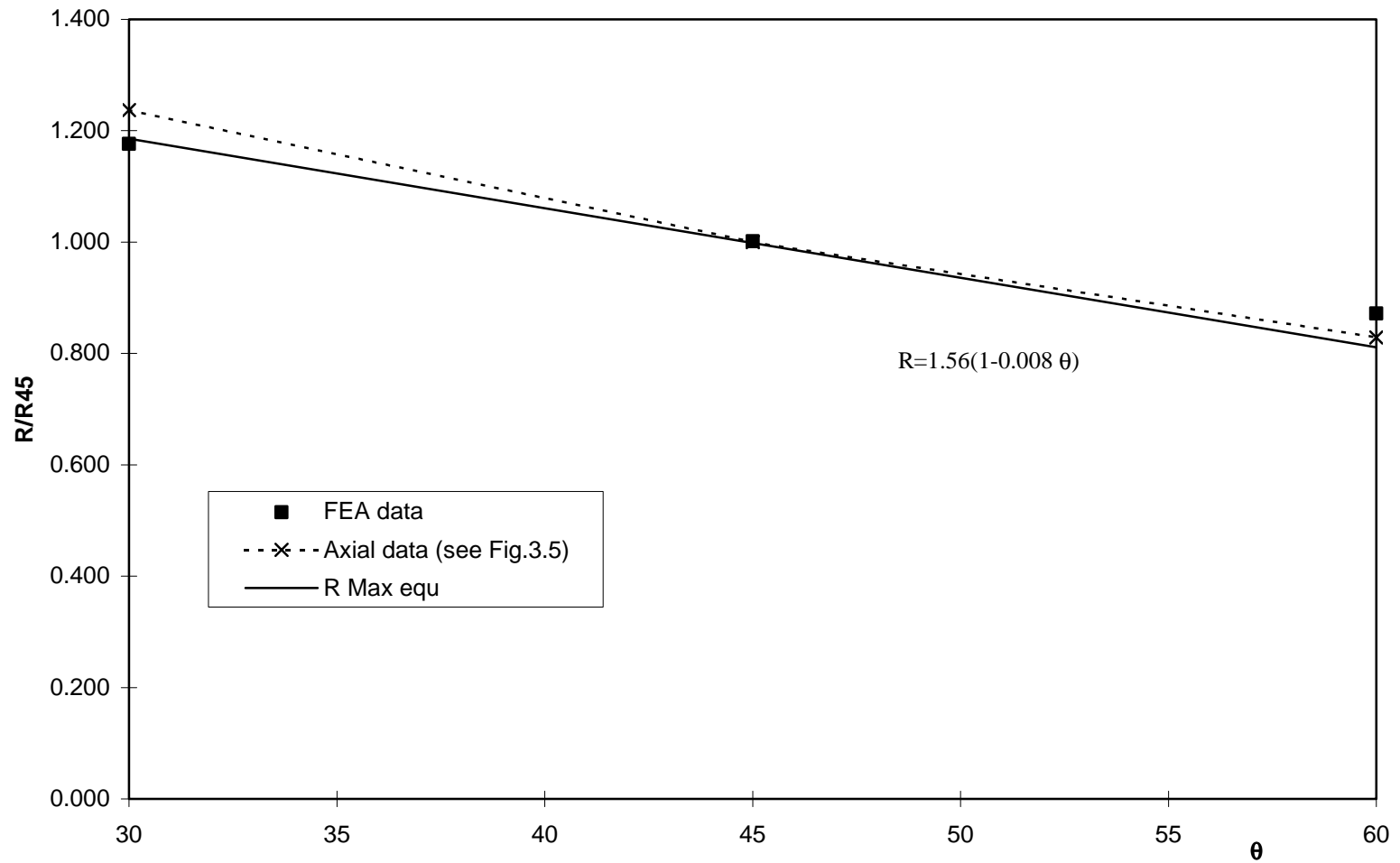


Figure 3.17: K joints under OPB loading, R v. θ
 $\beta=0.2, \gamma=18.75, \tau=0.5, \zeta=0.075$

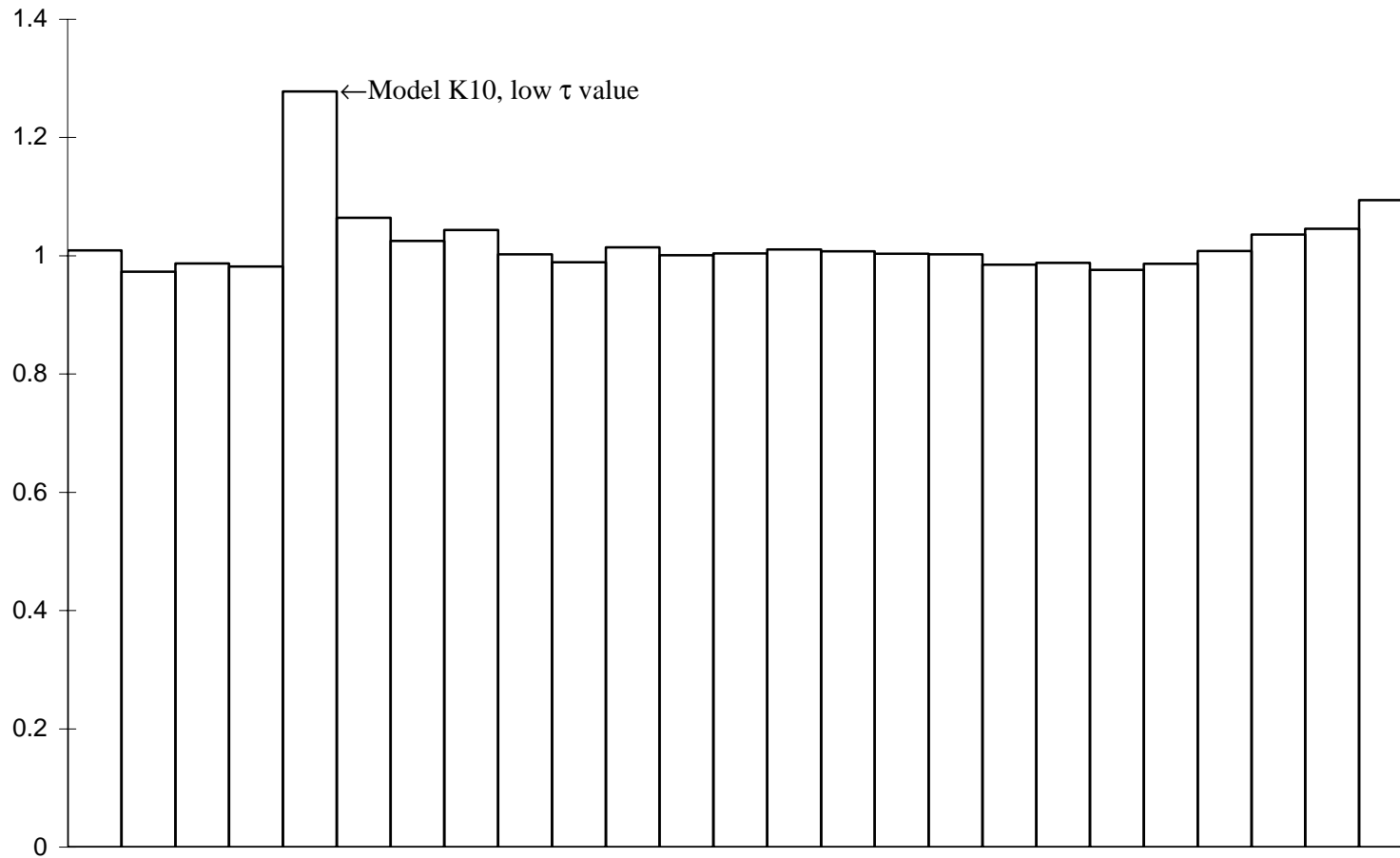


Figure 3.18: K joints under OPB loading; Histogram of predicted to calculated R values

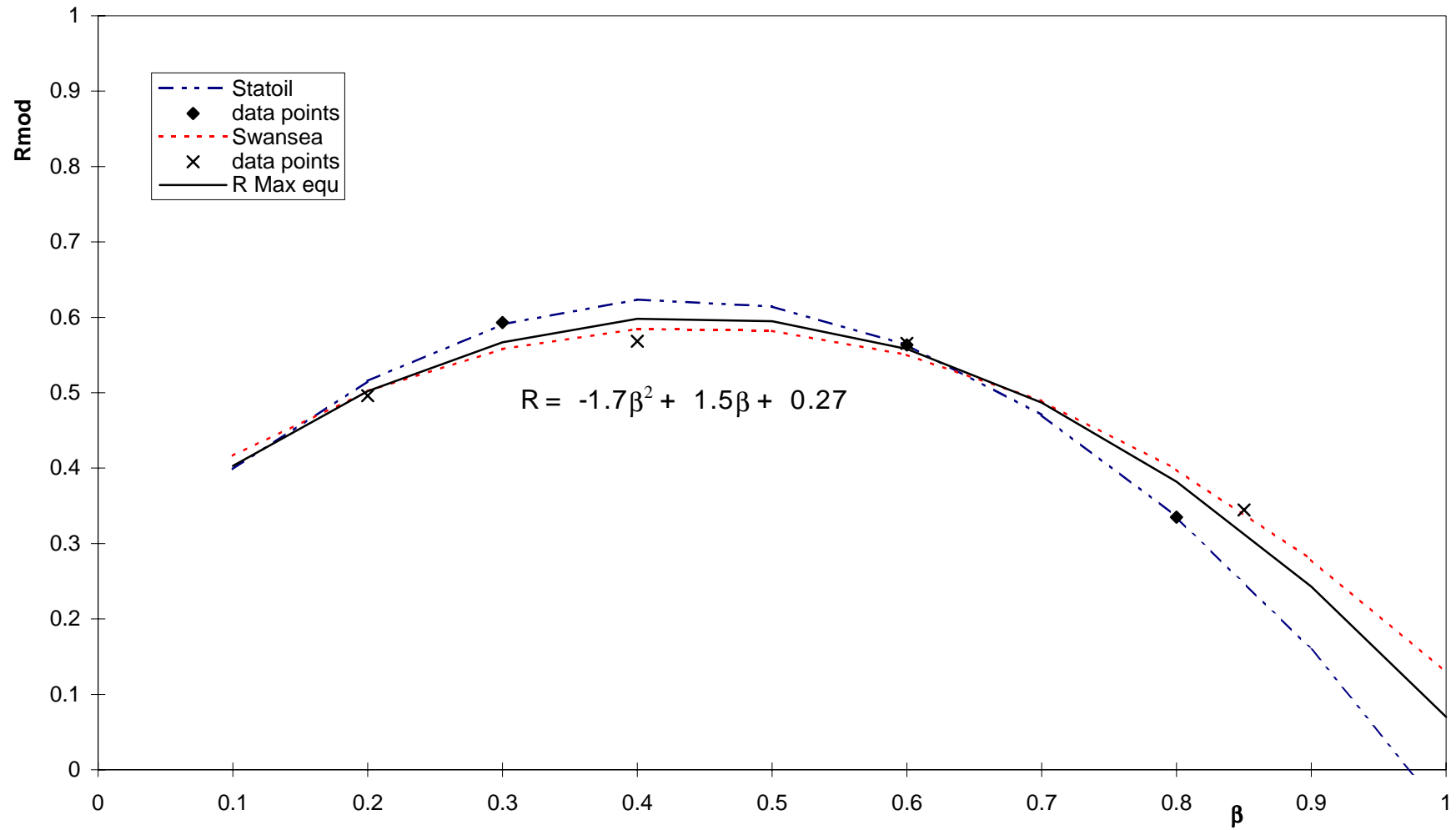


Figure 3.19: X joints under axial loading, R v. β , data normalised to $\gamma=20$, $\tau=0.5$ and $\theta=90^\circ$

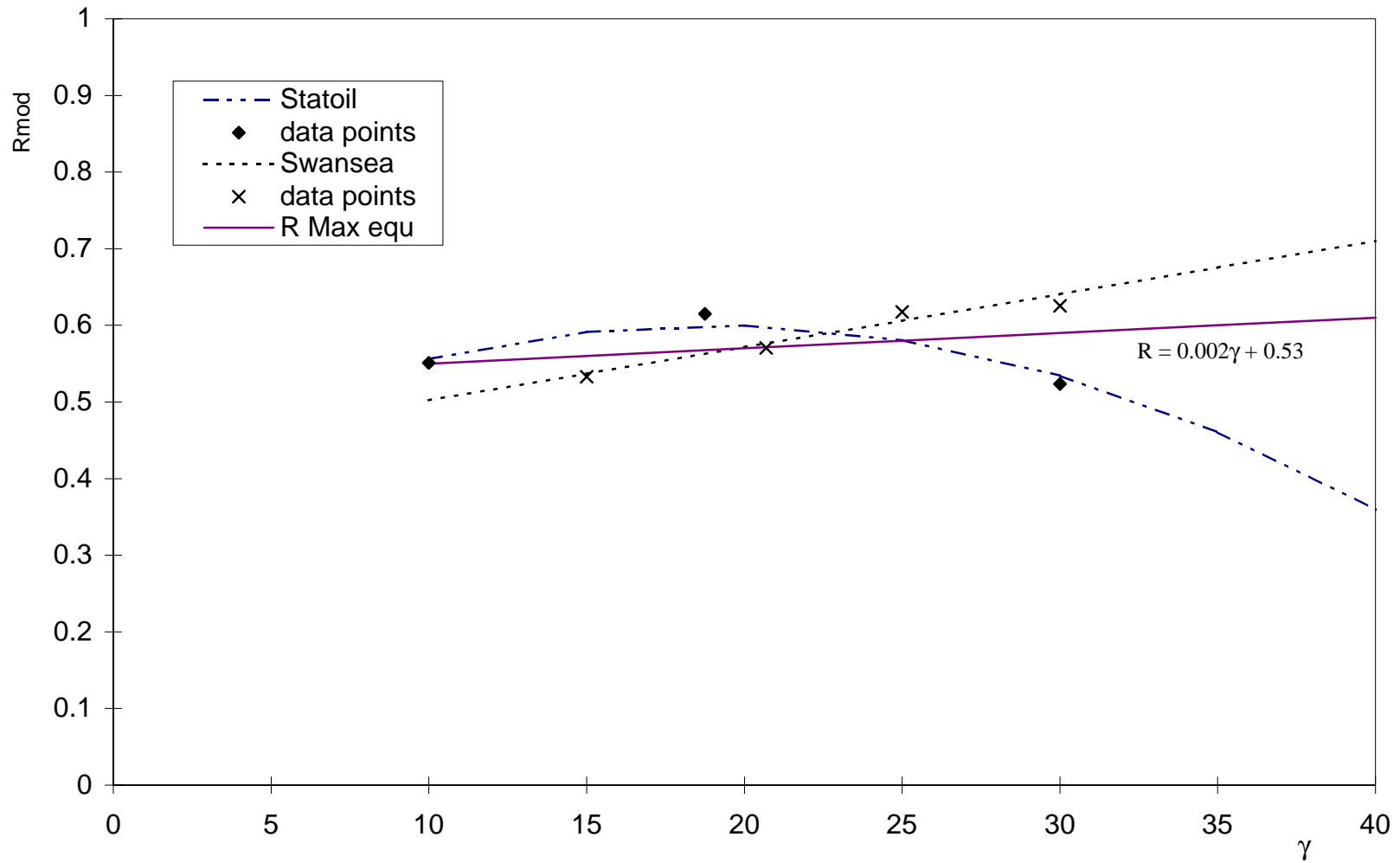


Figure 3.20: X joints under axial loading, R v. γ , data normalised to $\beta=0.5$, $\tau=0.5$ and $\theta=90^\circ$

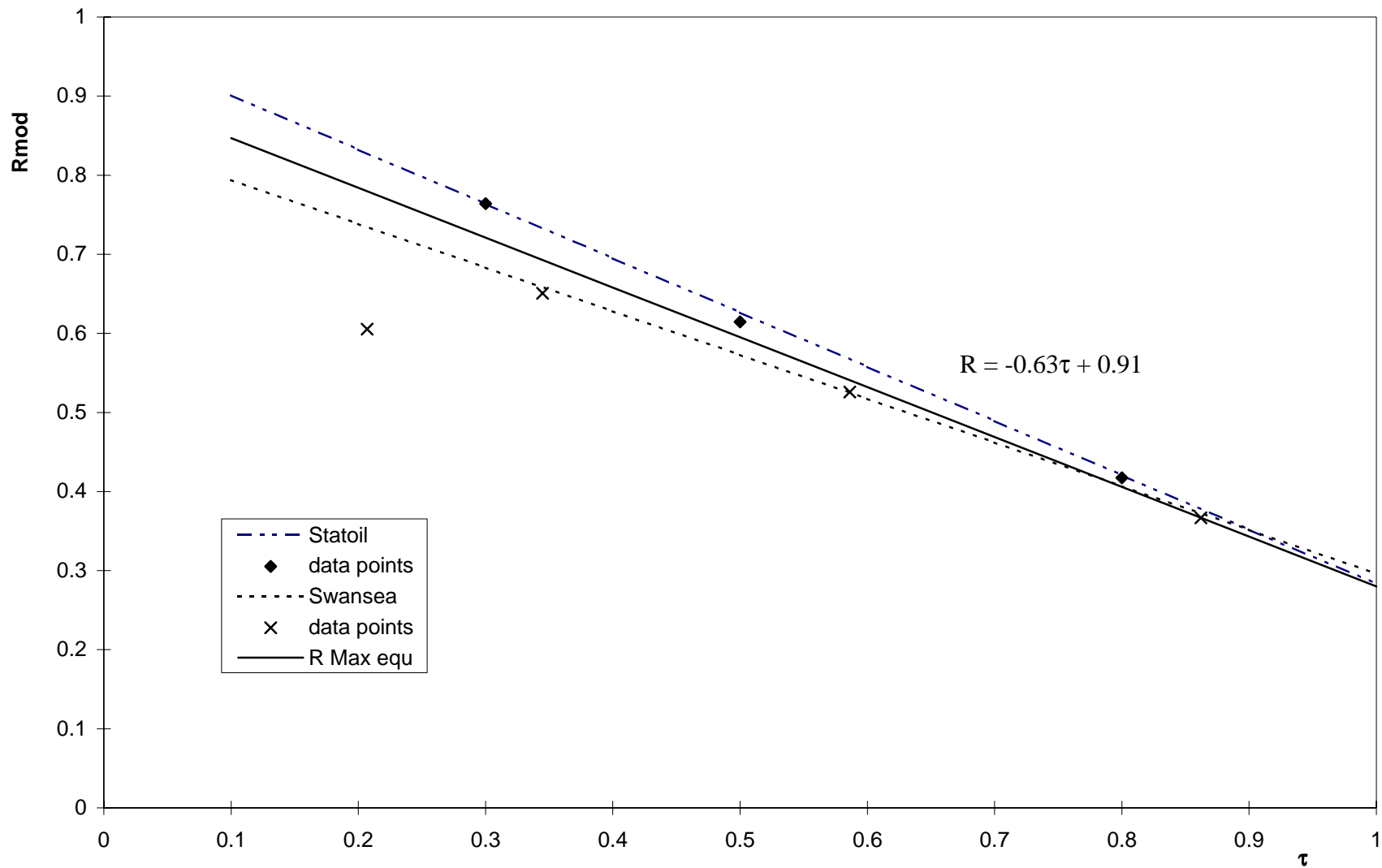
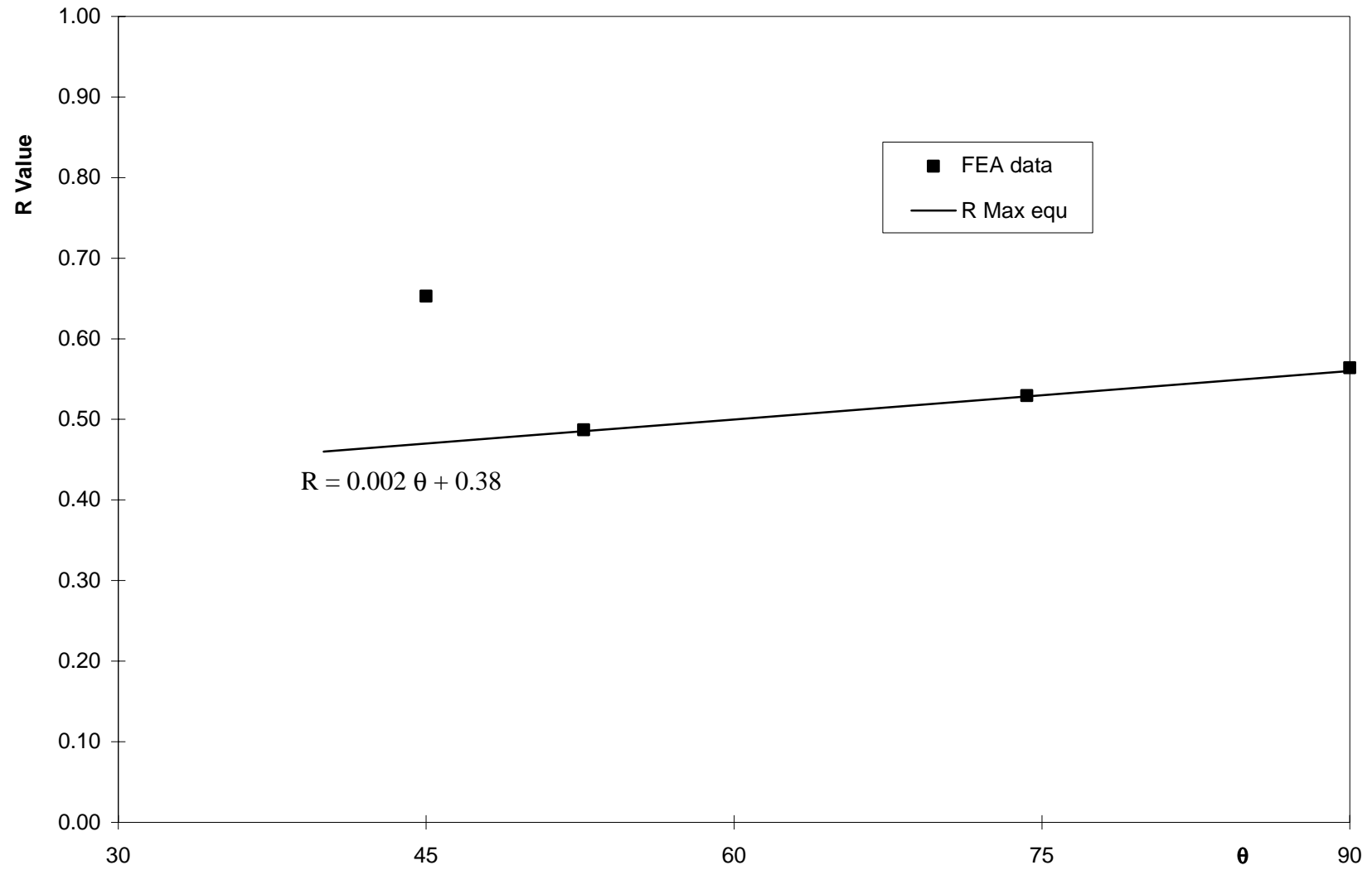


Figure 3.21: X joints under axial loading, R v. τ , data normalised to $\beta=0.5$, $\gamma=20$ and $\theta=90^\circ$



**Figure 3.22: X joints under axial loading, R v. θ ,
 $\beta=0.6$, $\theta=18.75$, $\tau=0.35$**

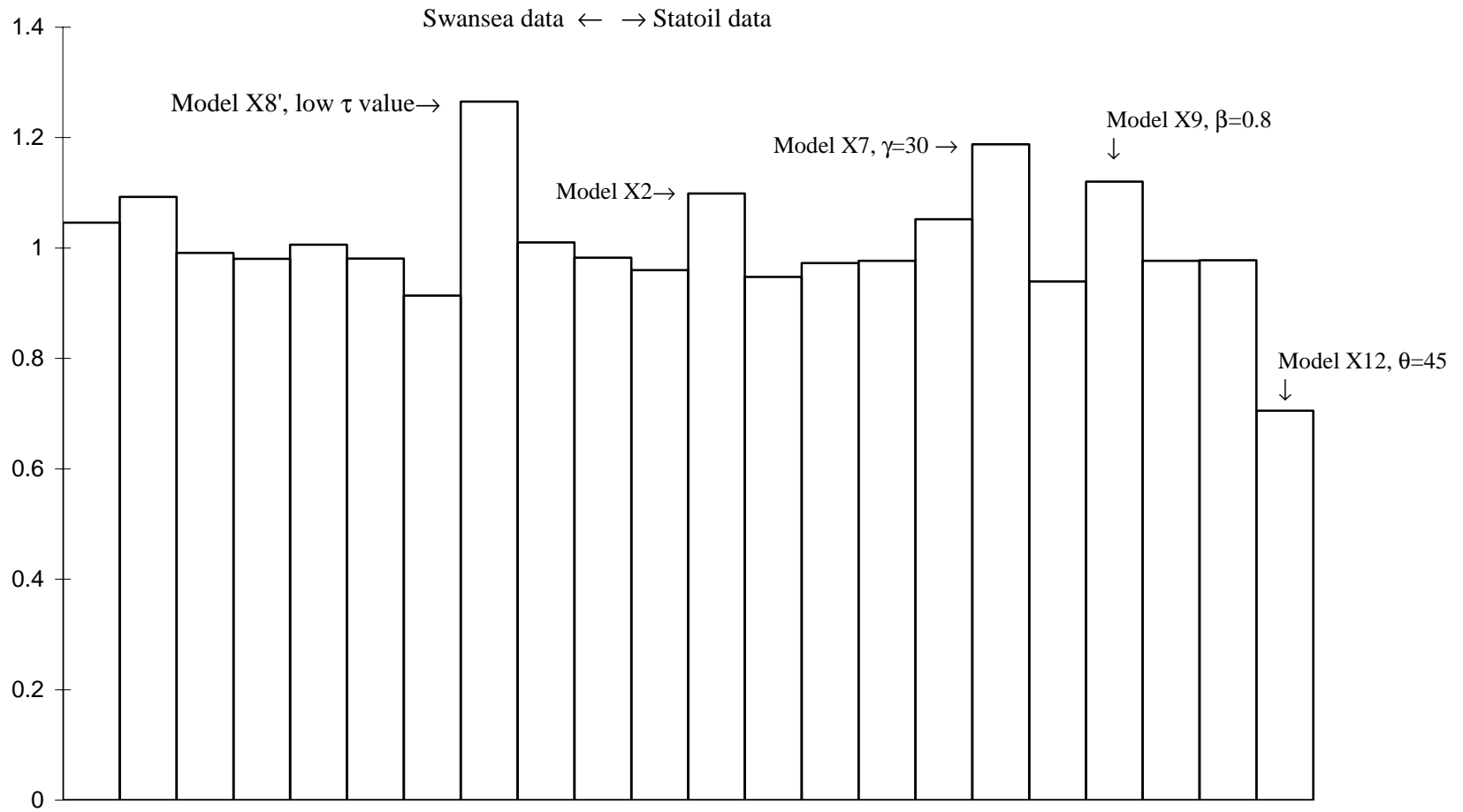


Figure 3.23: X/DT joints under axial loading; Bar chart of predicted to calculated R values

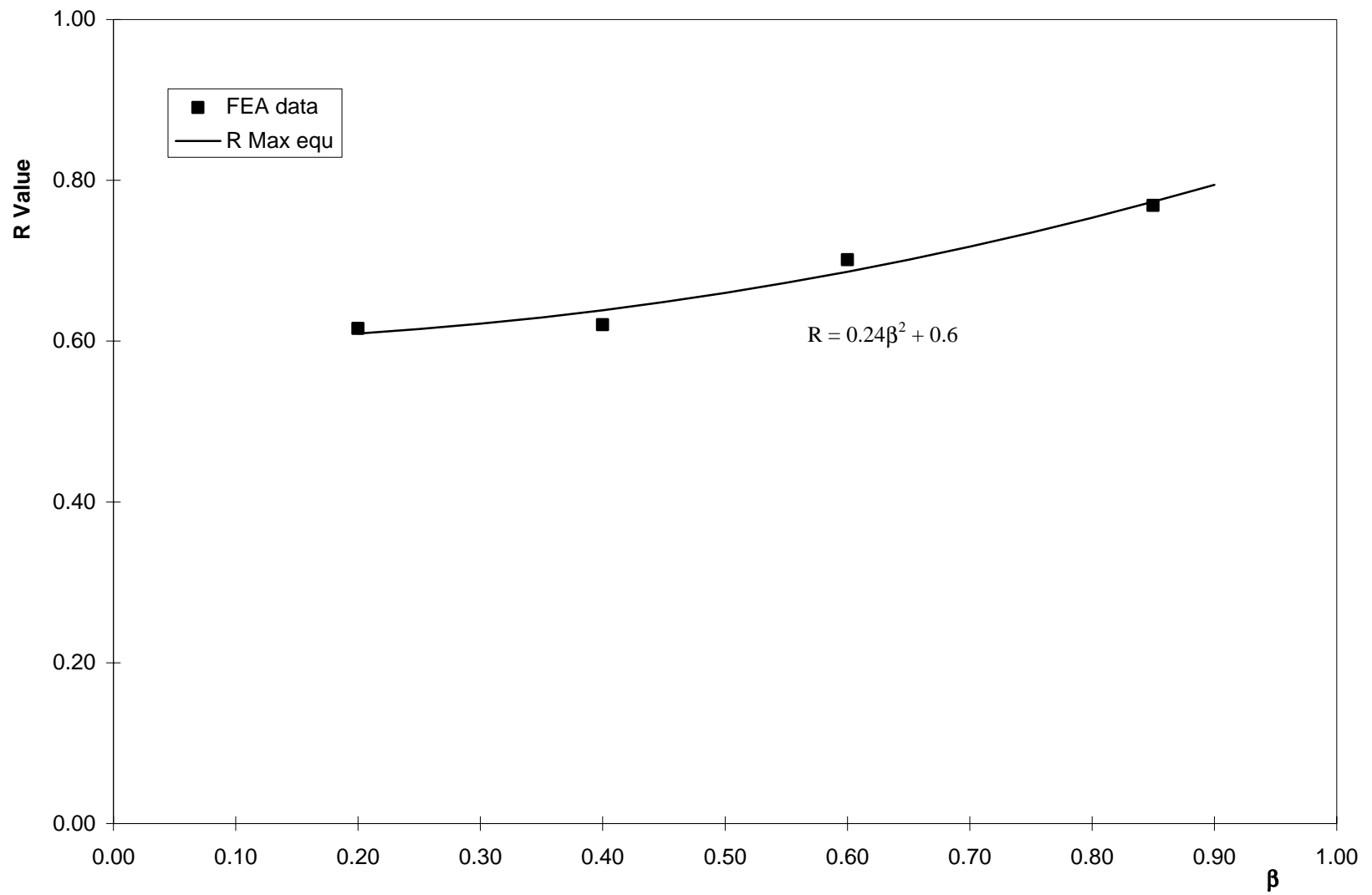


Figure 3.24: X joints under IPB loading, R v. β , $\gamma=21$, $\tau = 0.35$, $\theta = 90^\circ$

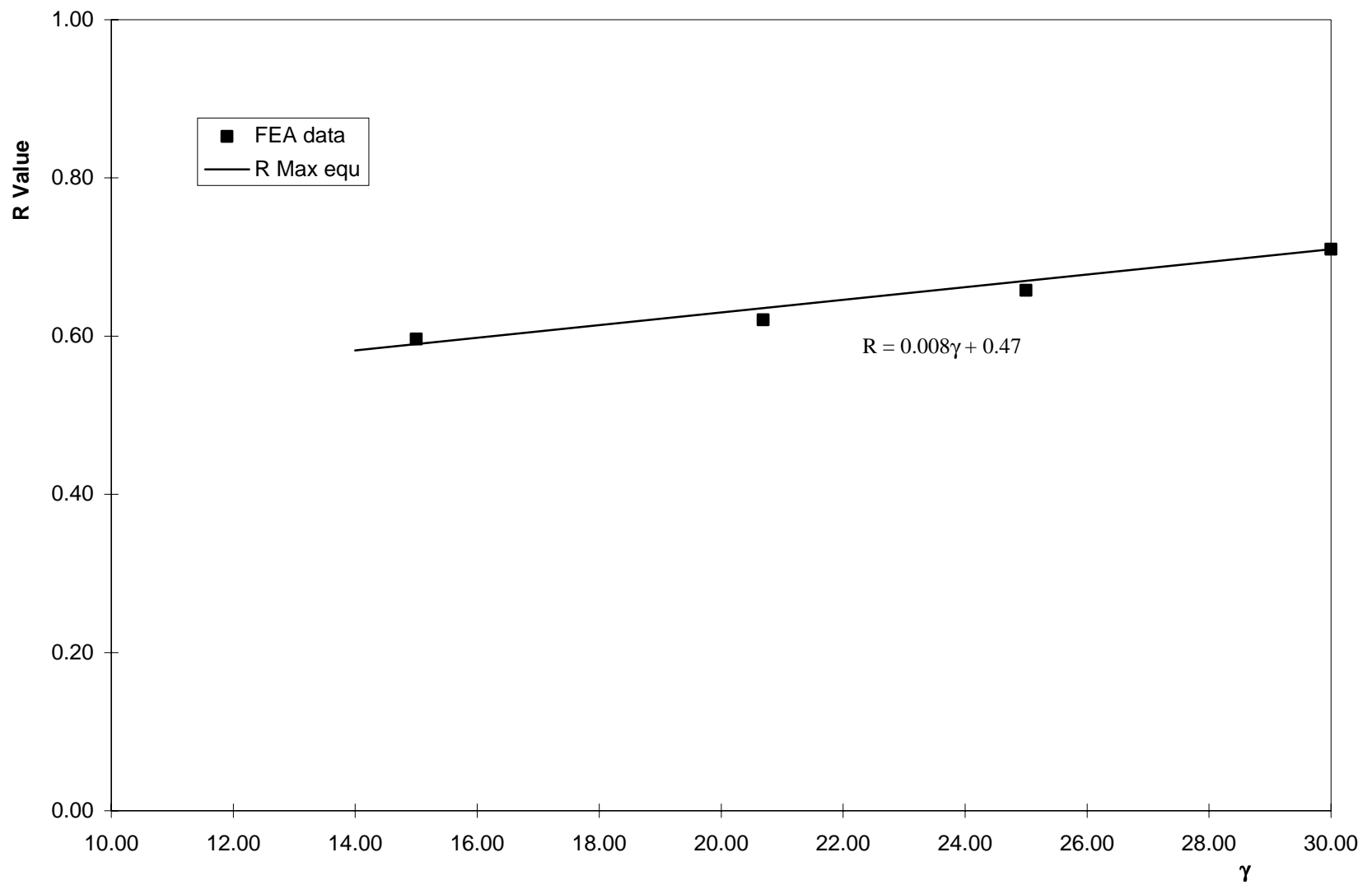


Figure 3.25: X joints under IPB loading, R v. γ , $\beta = 0.4$, $\tau = 0.35$, $\theta = 90^\circ$

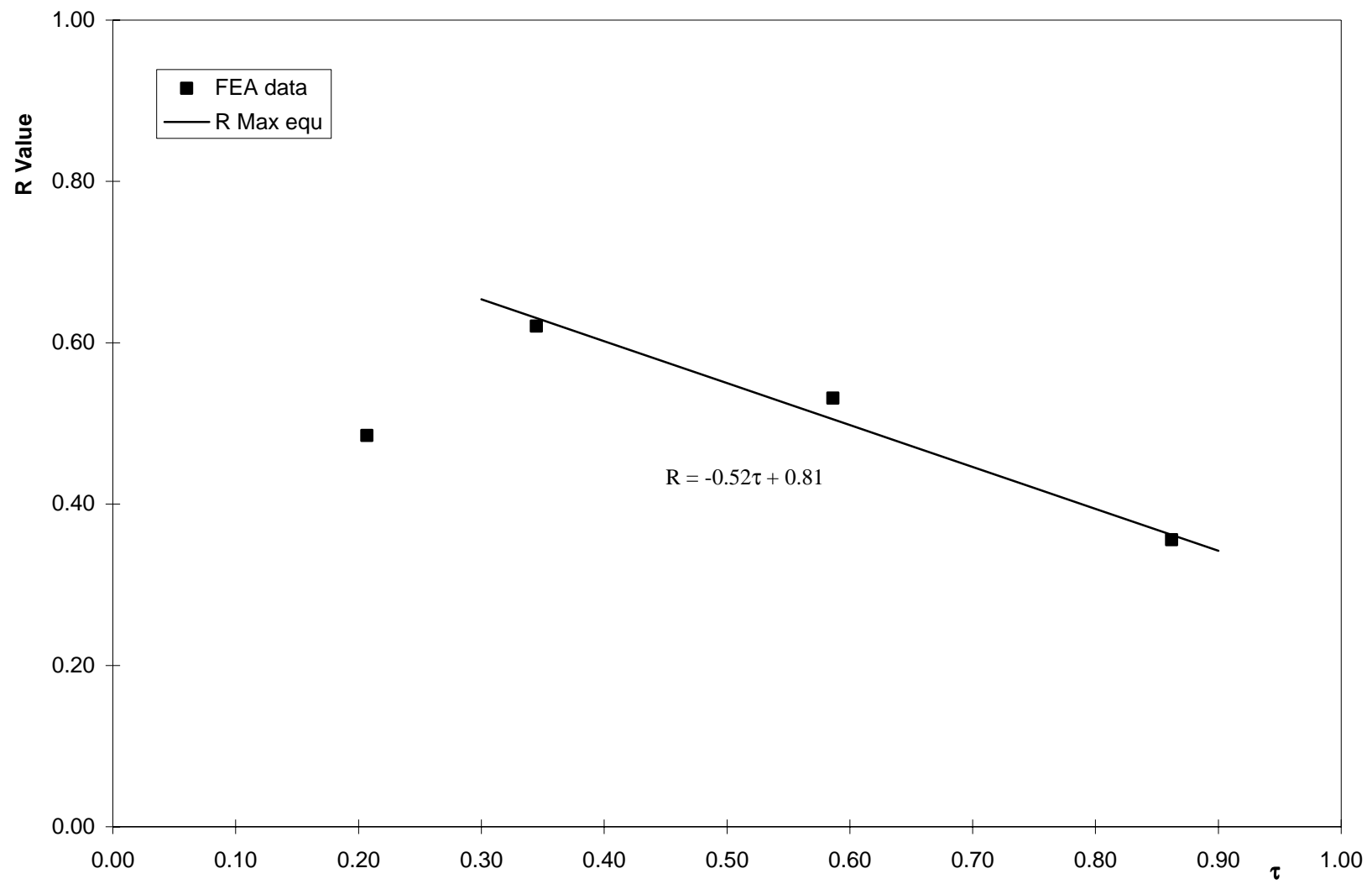


Figure 3.26: X joints under IPB loading, R v. τ , $\beta = 0.4$, $\gamma = 21$, $\theta = 90^\circ$

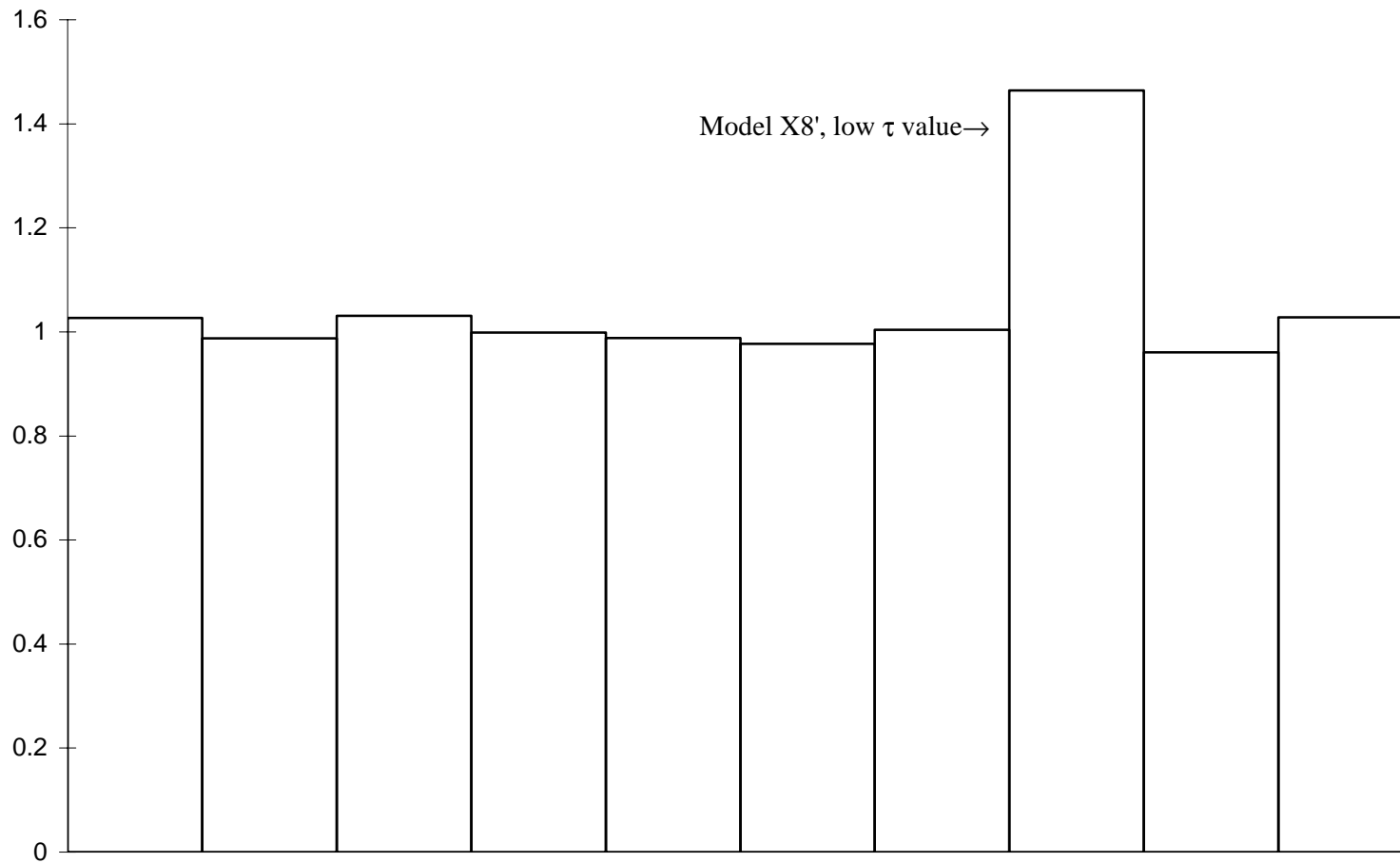


Figure 3.27: X/DT joints under IPB loading; Bar chart of predicted to calculated R values

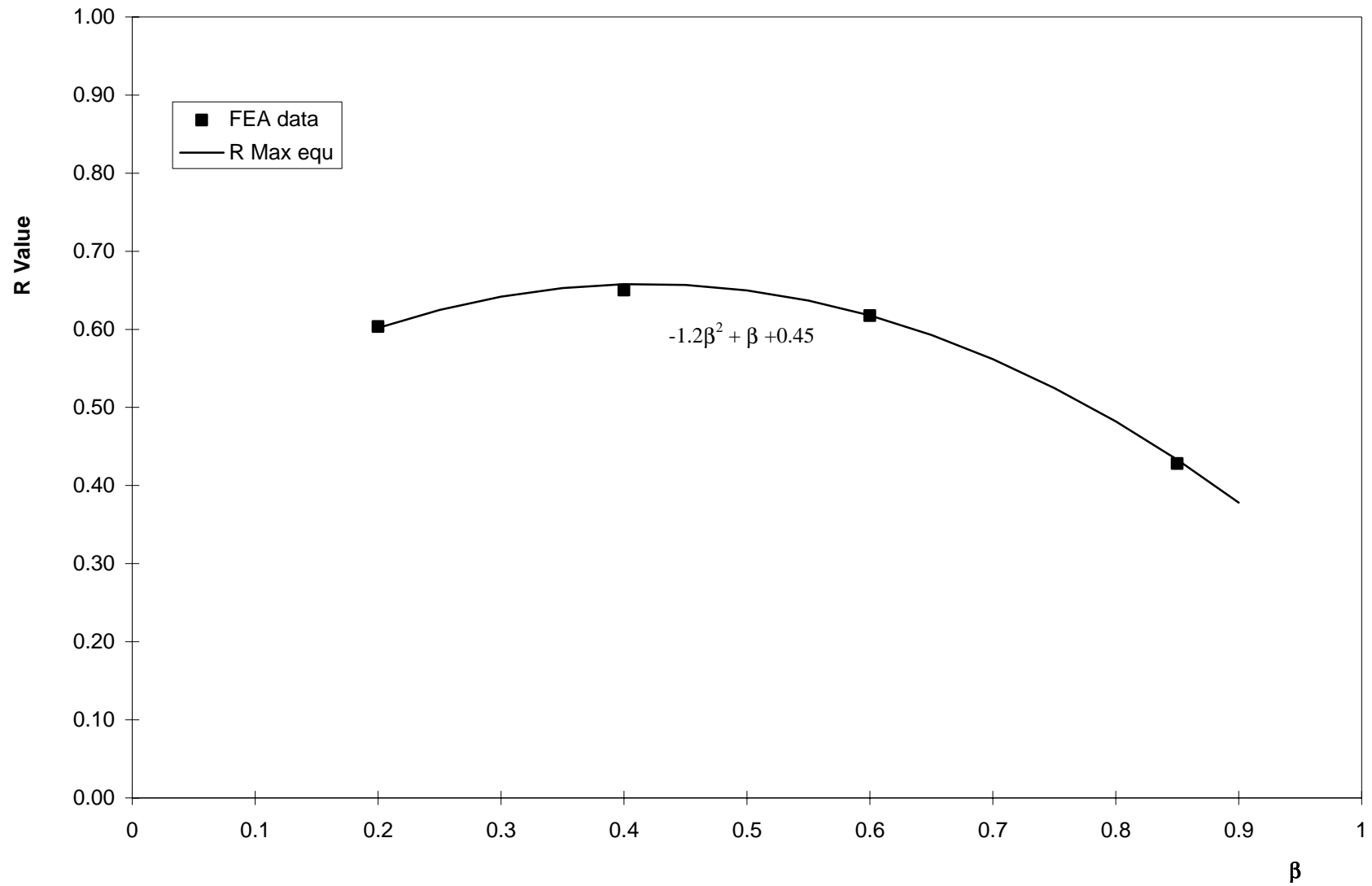


Figure 3.28: X joints under OPB loading, R v. β , $\gamma = 21$, $\tau = 0.35$, $\theta = 90^\circ$

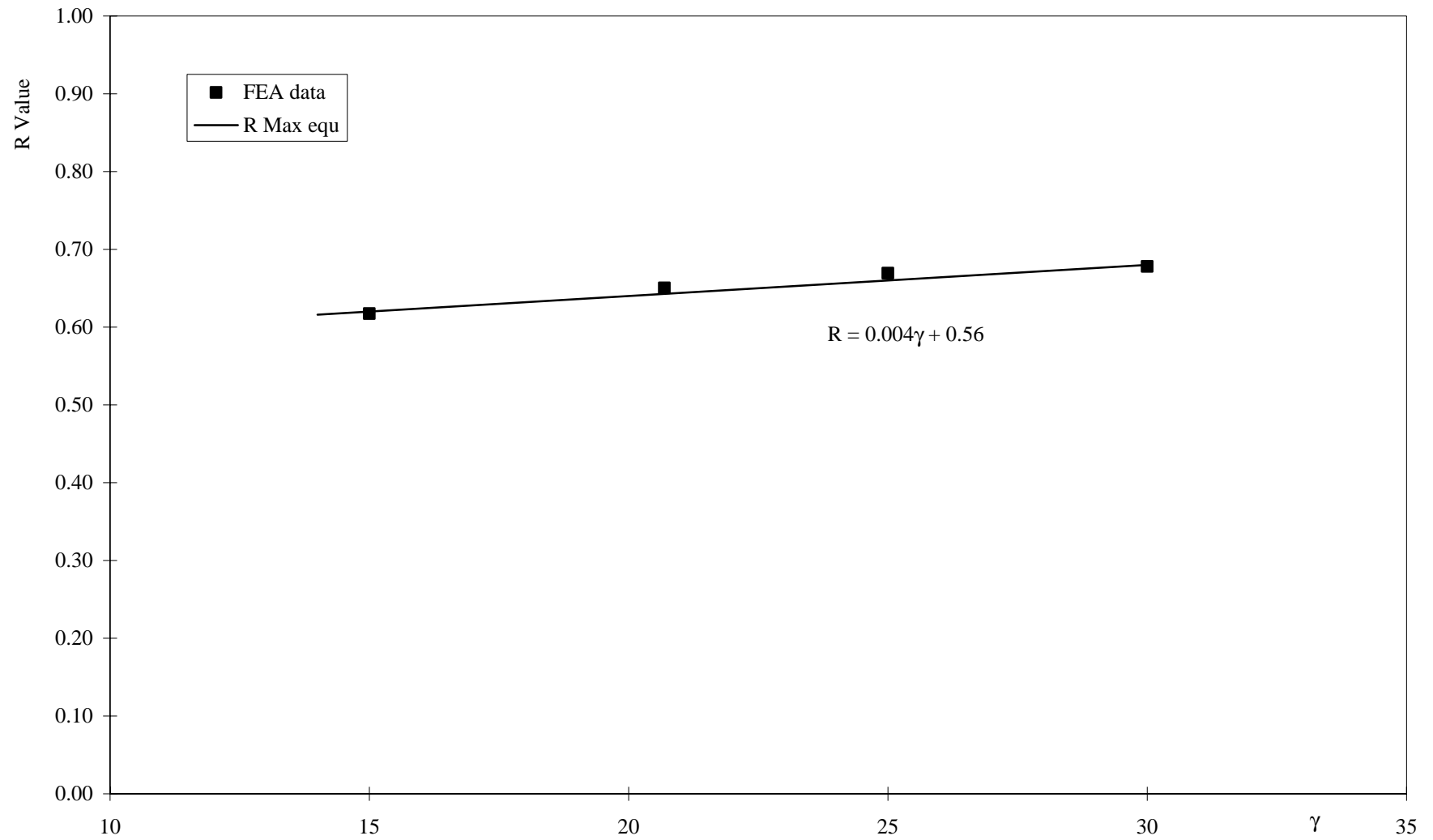


Figure 3.29: X joints under OPB loading, R v. γ , $\beta = 0.4$, $\tau = 0.35$, $\theta = 90^\circ$

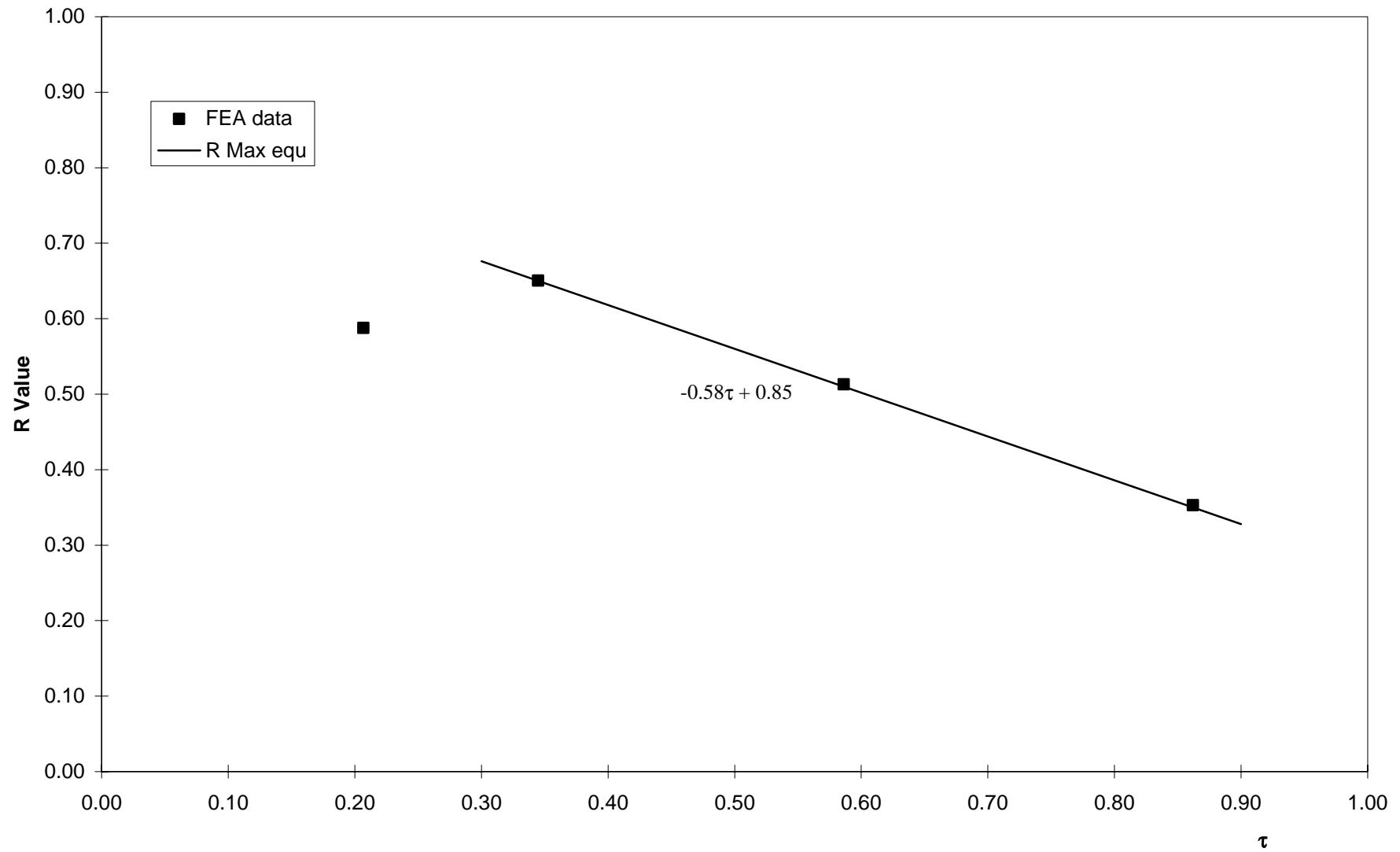


Figure 3.30: X joints under OPB loading, R v. τ , $\beta = 0.4$, $\gamma = 21$, $\theta = 90^\circ$

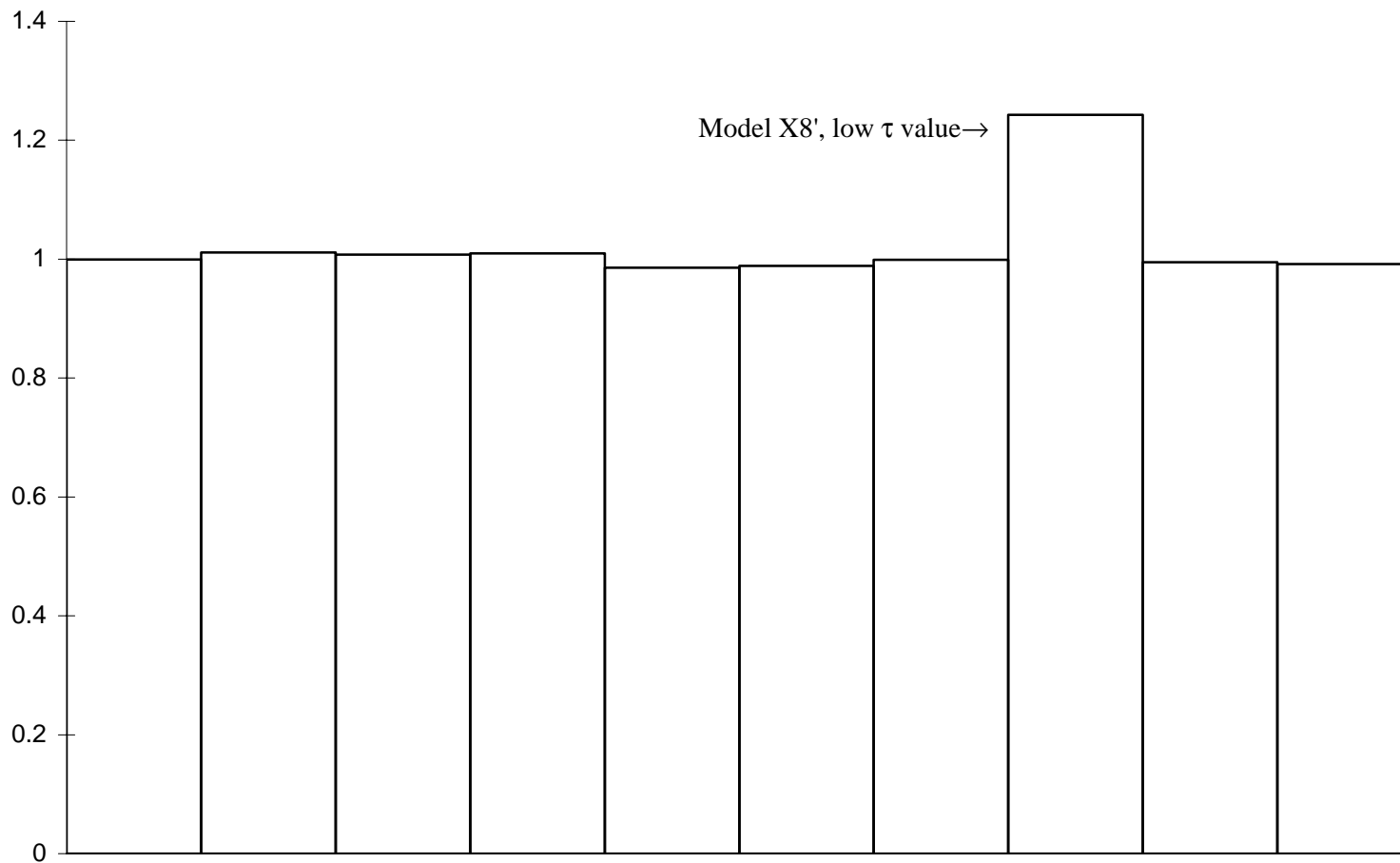


Figure 3.31: X/DT joints under OPB loading; Bar chart of predicted to calculated R values

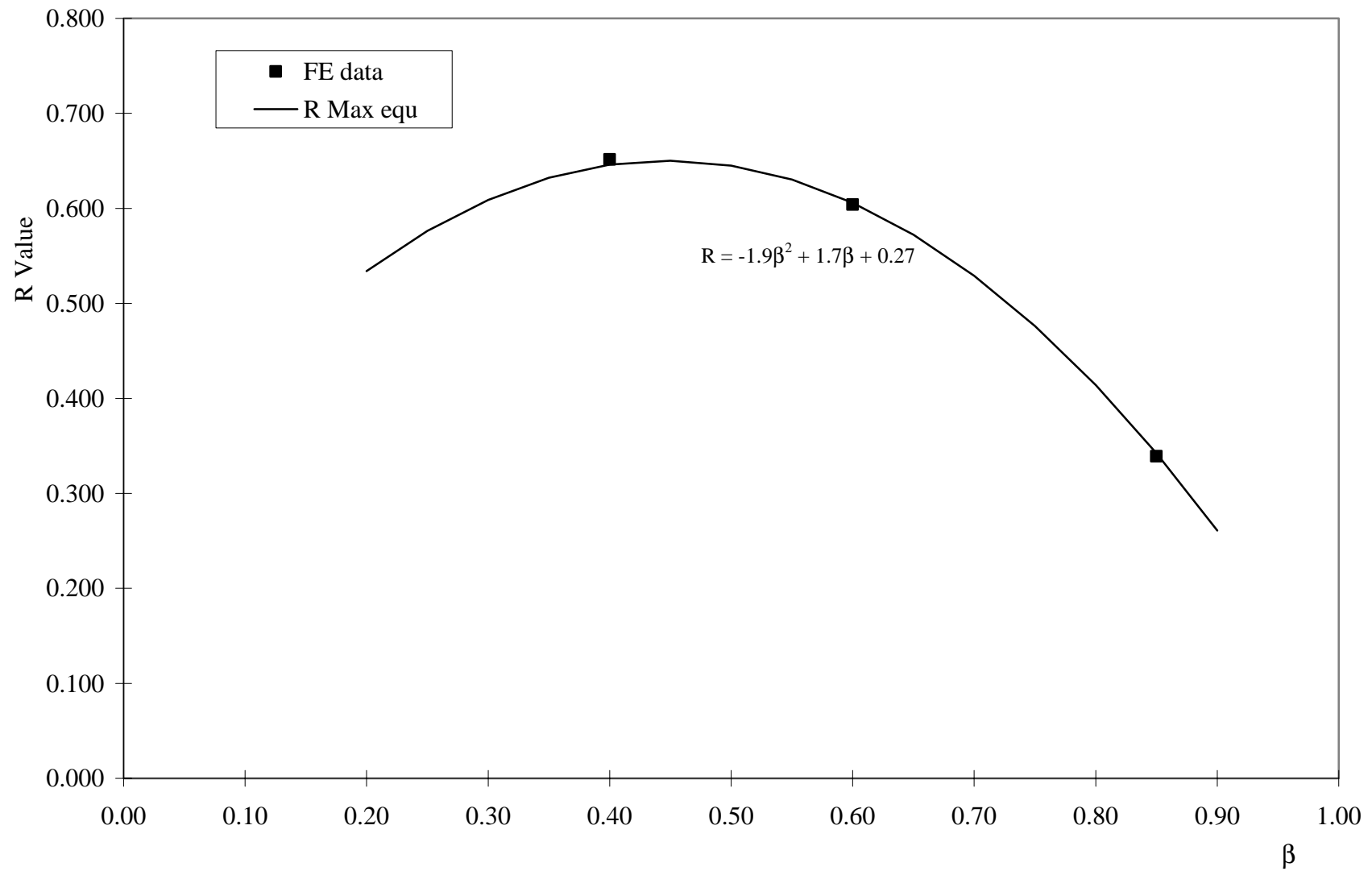


Figure 3.32: T Joints under axial loading, R v. β , $\gamma = 20.69$, $\tau = 0.34$, $\theta = 90^\circ$

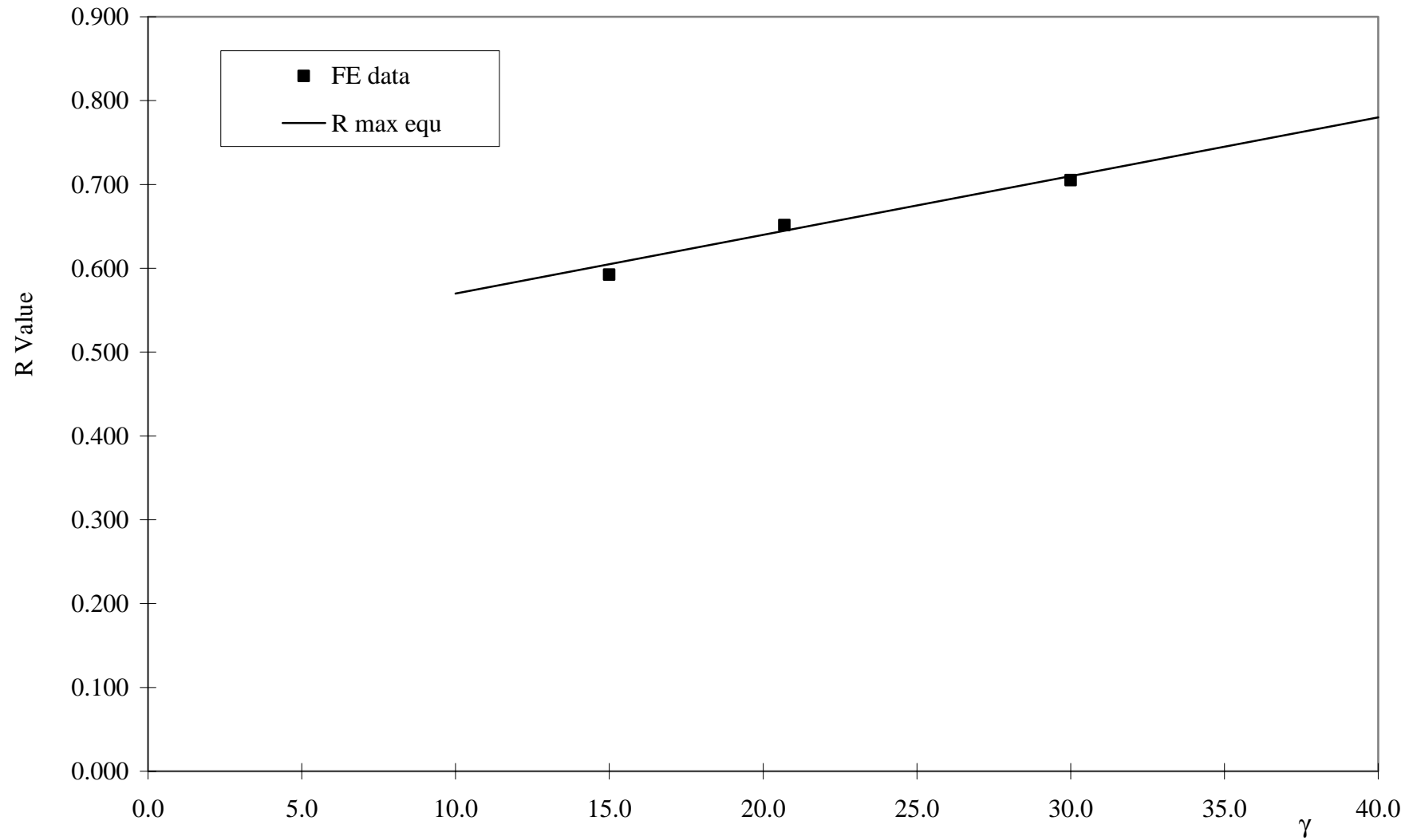


Figure 3.33: T Joints under axial loading, R v. γ , $\beta = 0.4$, $\tau = 0.35$, $\theta = 90^\circ$

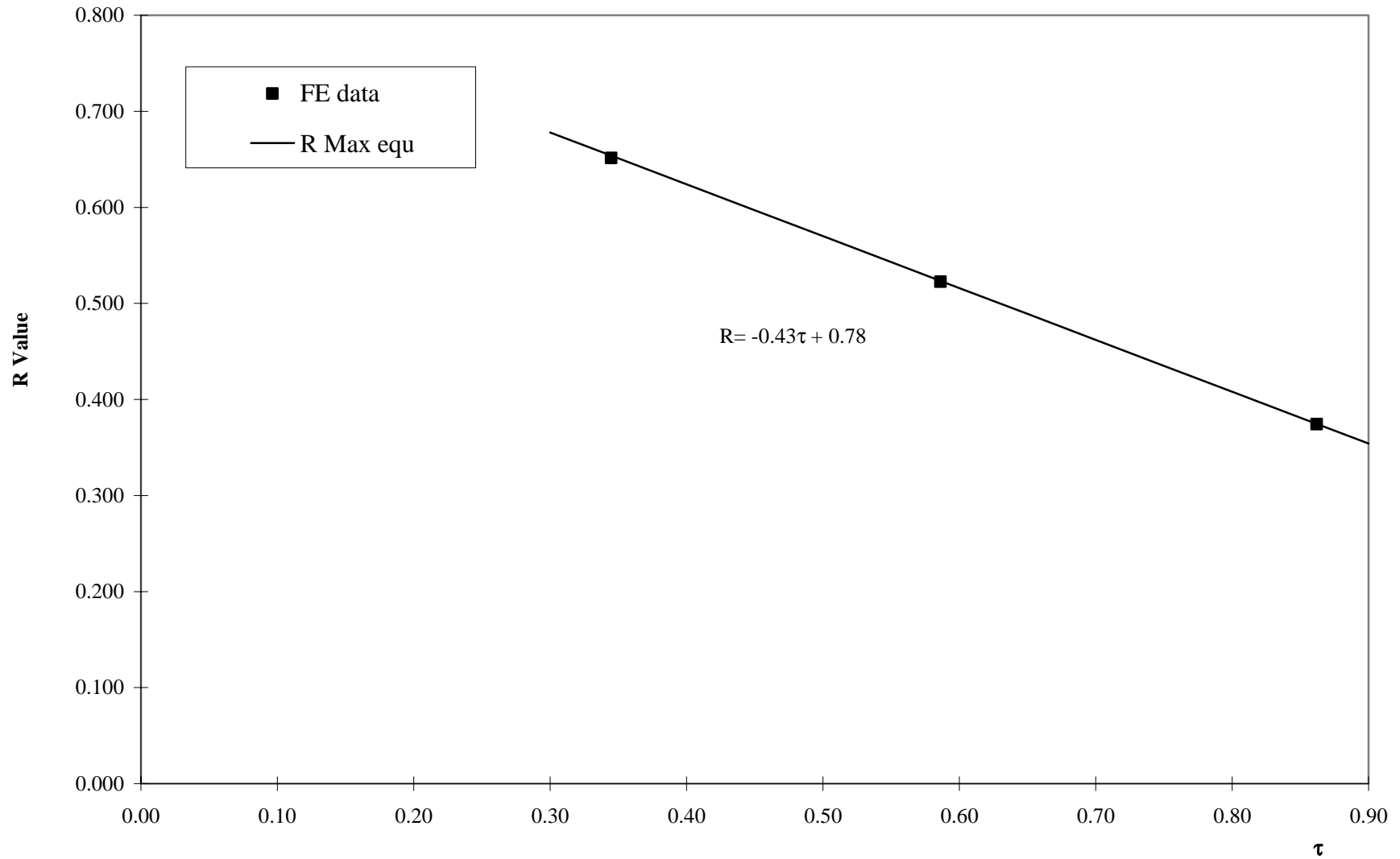


Figure 3.34: T Joints under axial loading, R v. τ , $\gamma = 20.69$, $\tau = 0.34$, $\theta = 90^\circ$

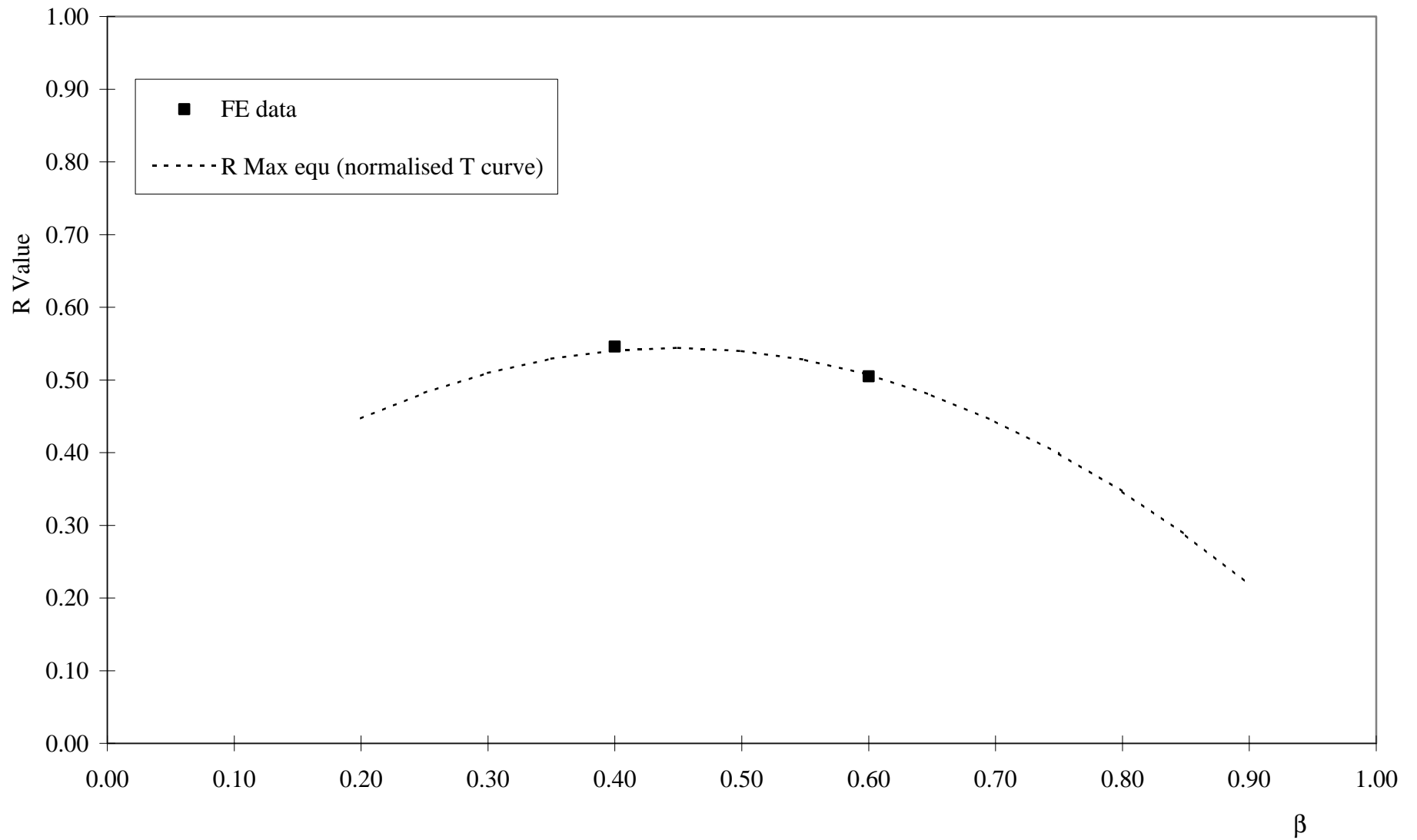


Figure 3.35: Y Joints under axial loading, R v. β , $\gamma = 21.00$, $\tau = 0.35$, $\theta = 30^\circ$

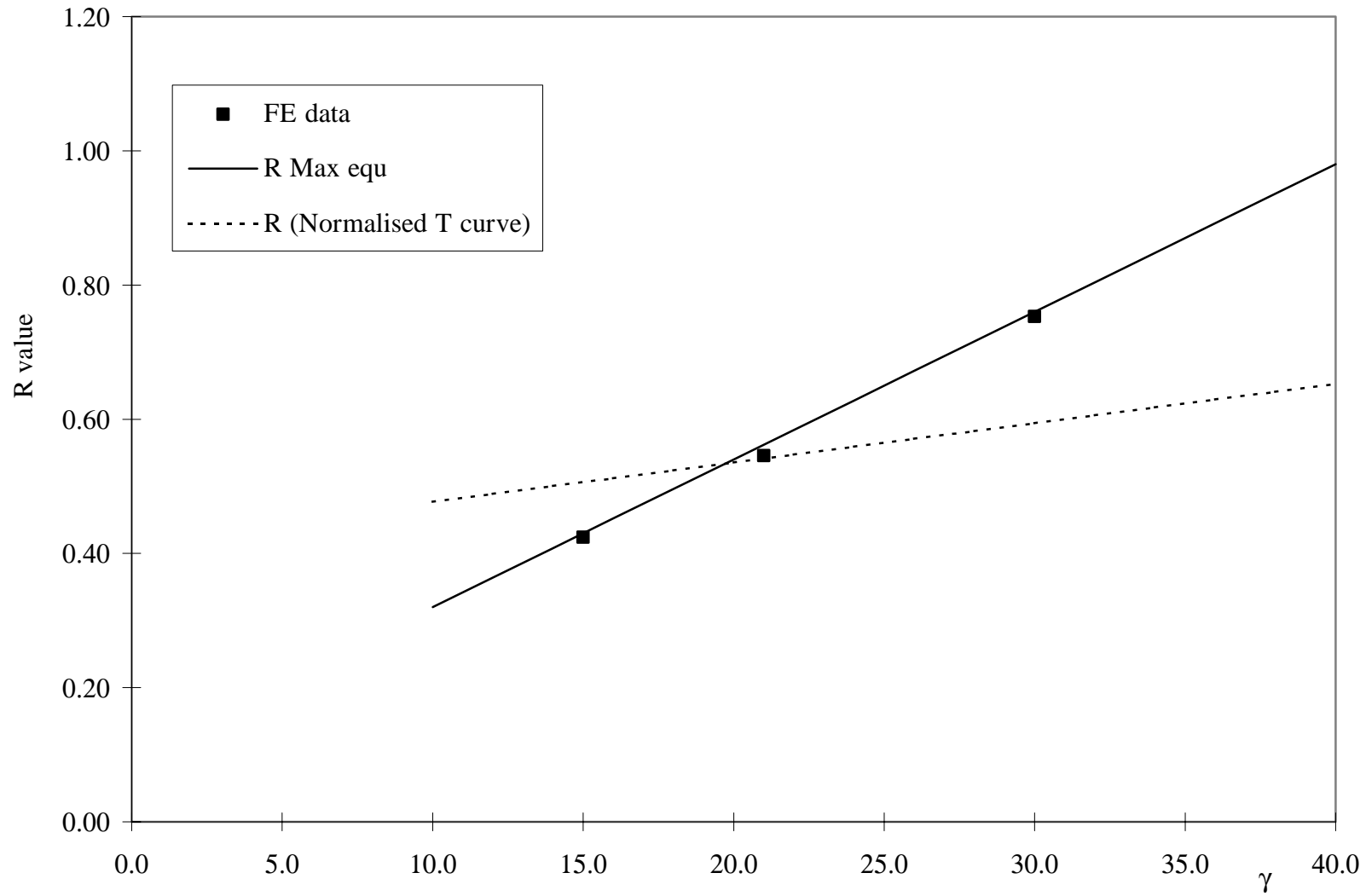


Figure 3.36: Y Joints under axial loading, R v. γ , $\beta = 0.4$, $\tau = 0.35$, $\theta = 30^\circ$

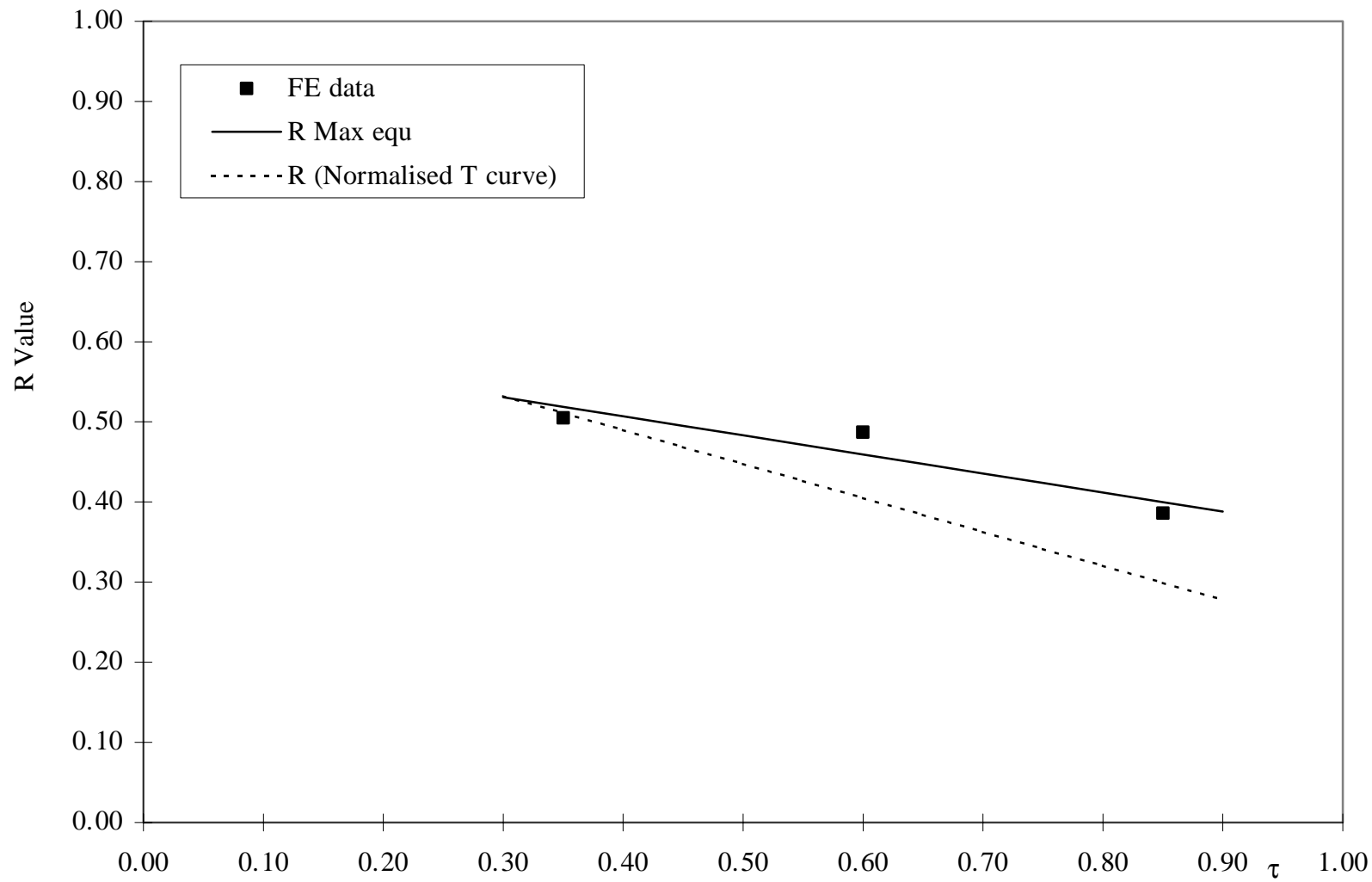


Figure 3.37: Y Joints under axial loading, R v. τ , $\beta = 0.6$, $\gamma = 21.00$, $\theta = 30^\circ$

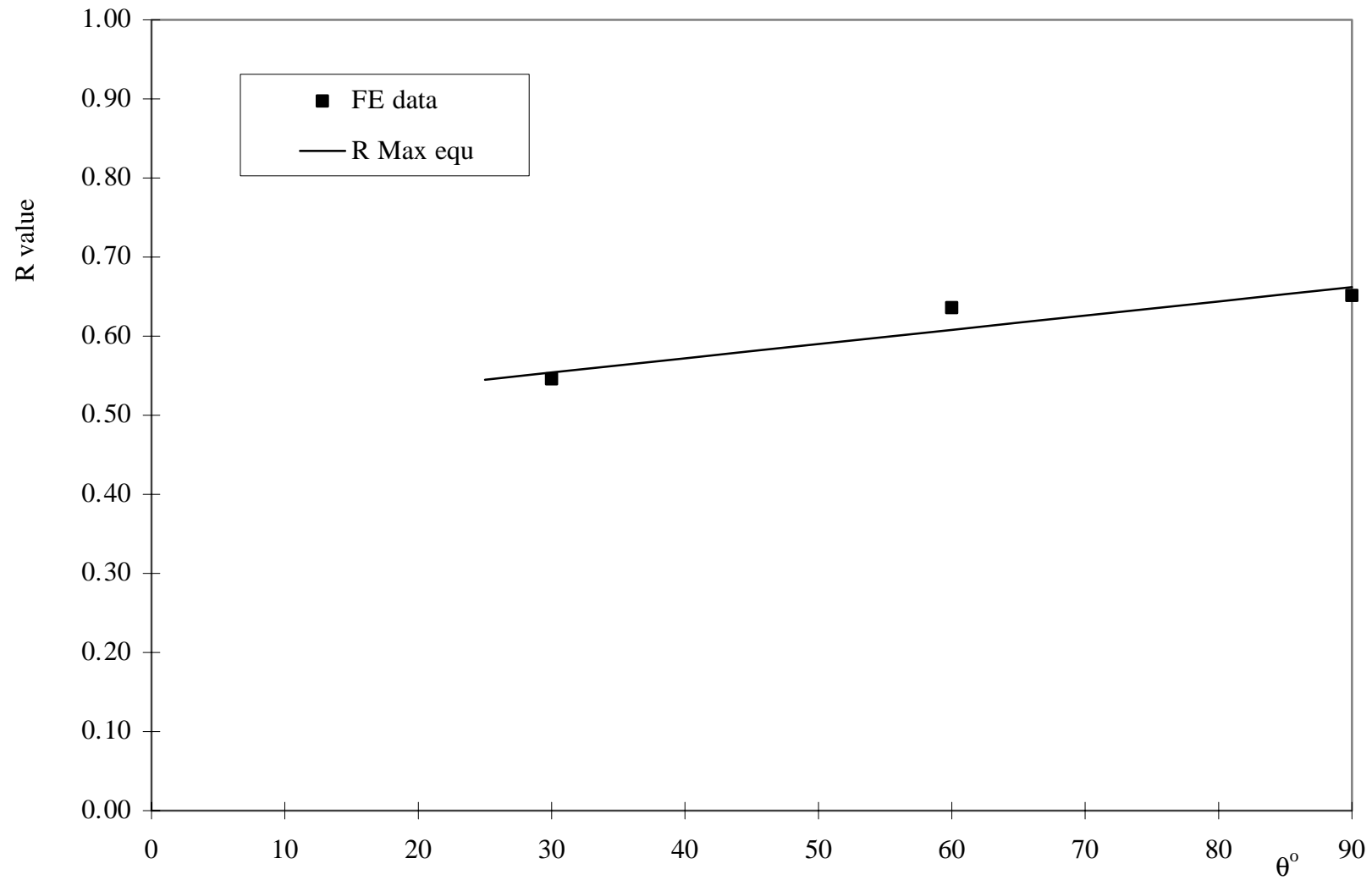


Figure 3.38: Y Joints under axial loading, R v. θ , $\beta = 0.4$, $\gamma = 21.0$, $\tau = 0.35$

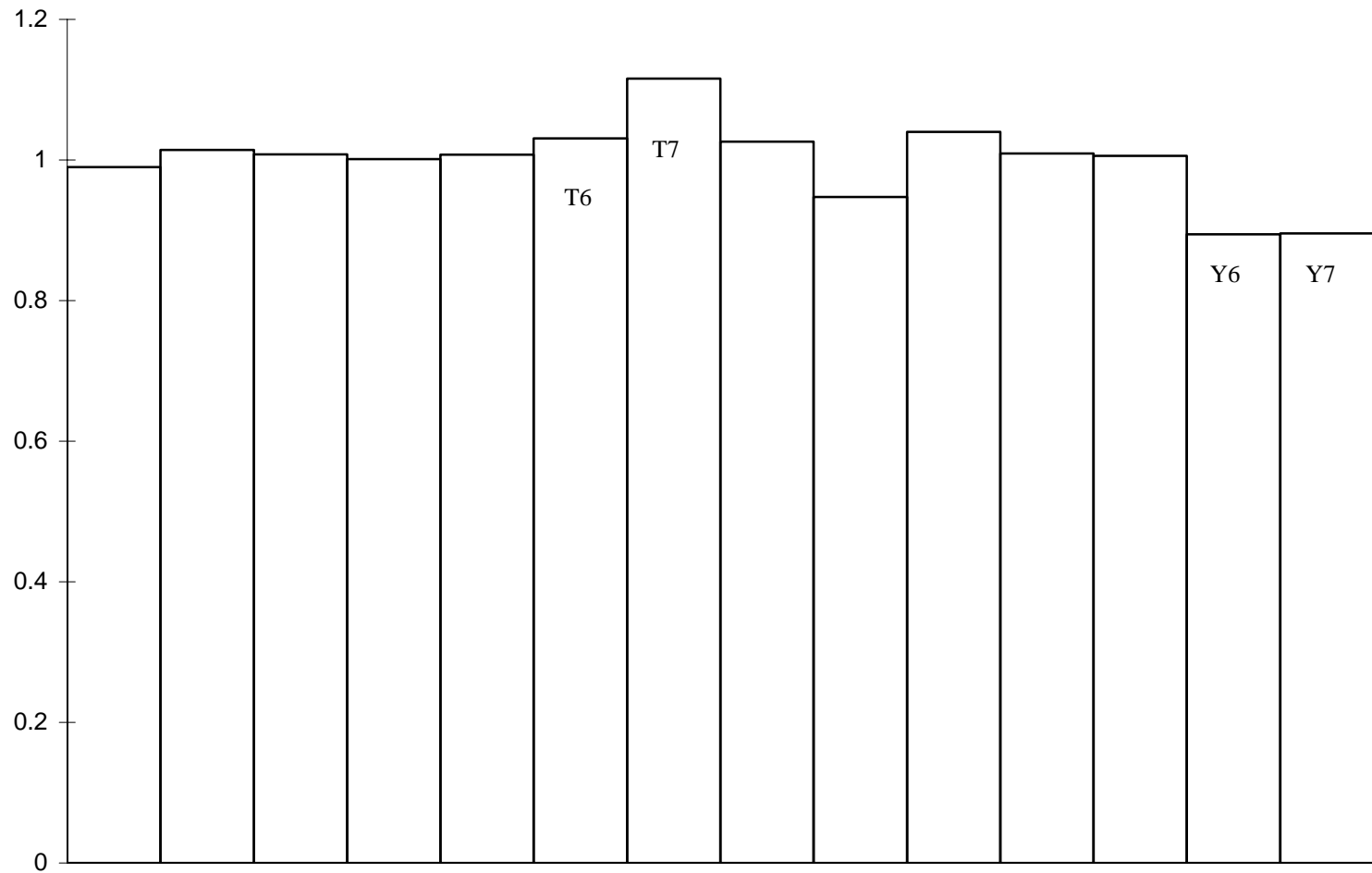


Figure 3.39: Y/T joints under axial loading; Bar chart of predicted to calculated R values

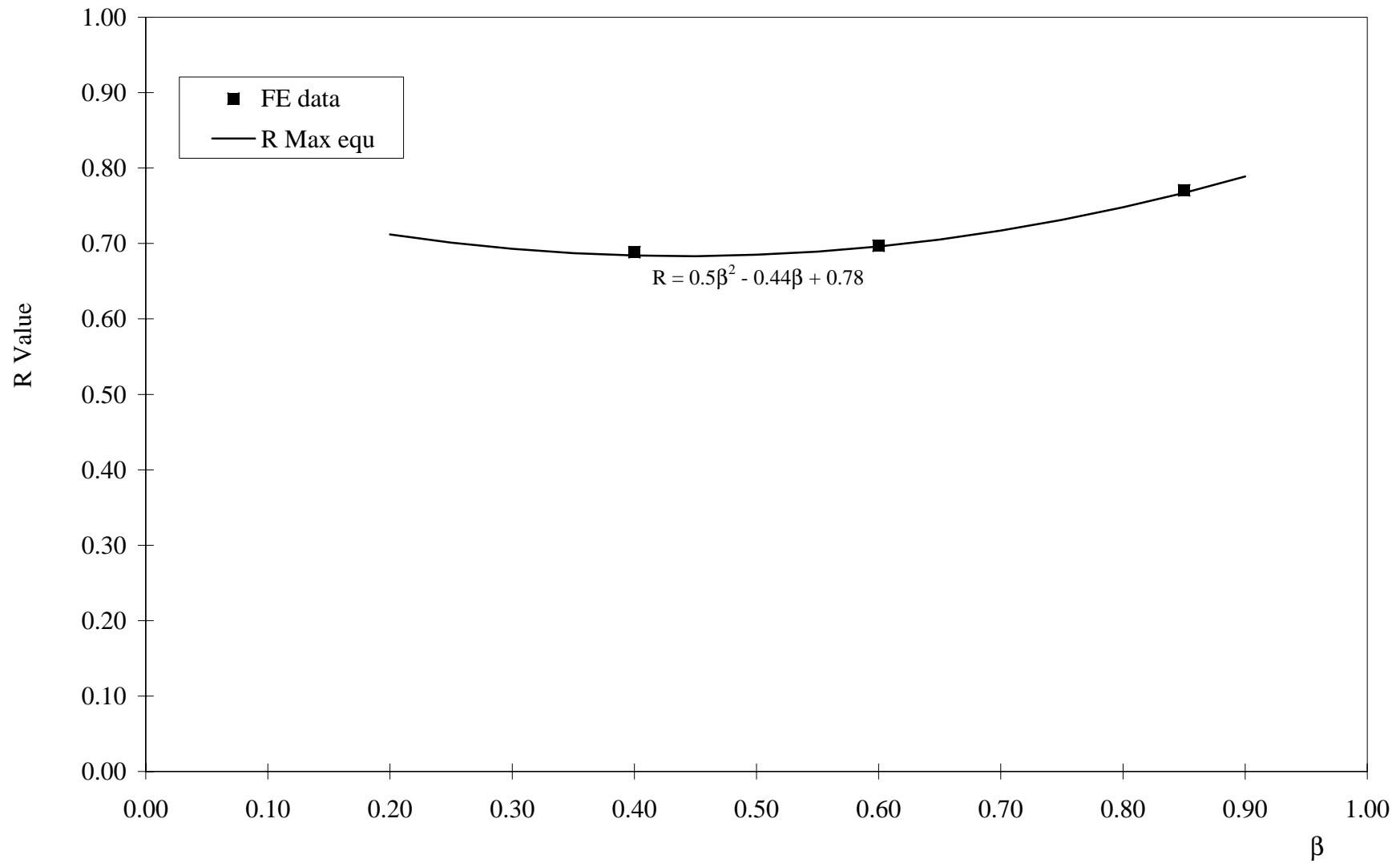


Figure 3.40: T Joints under IPB loading, R v. β , $\gamma = 20.69$, $\tau = 0.34$, $\theta = 90^\circ$

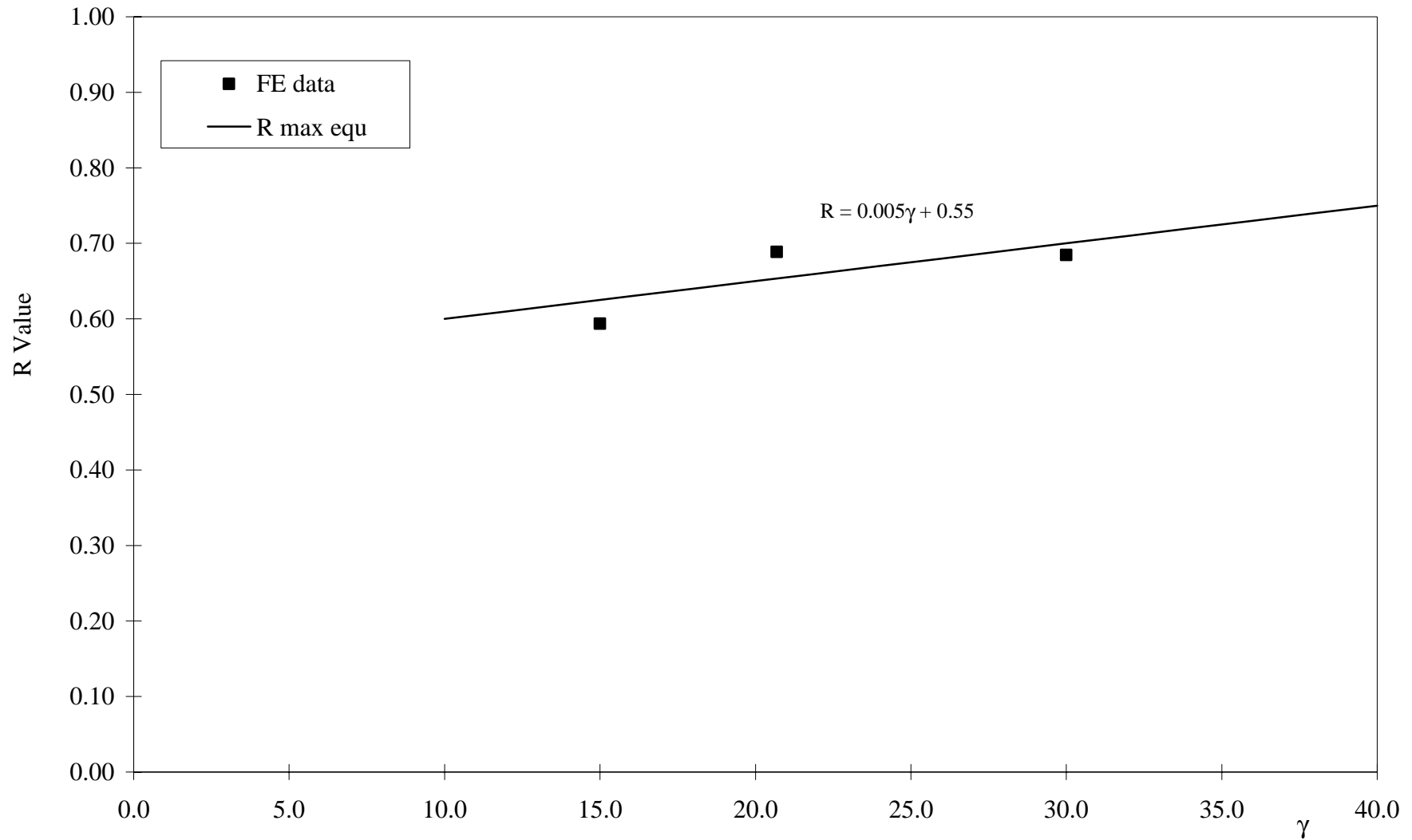


Figure 3.41: T Joints under IPB loading, R v. γ , $\beta = 0.4$, $\tau = 0.35$, $\theta = 90^\circ$

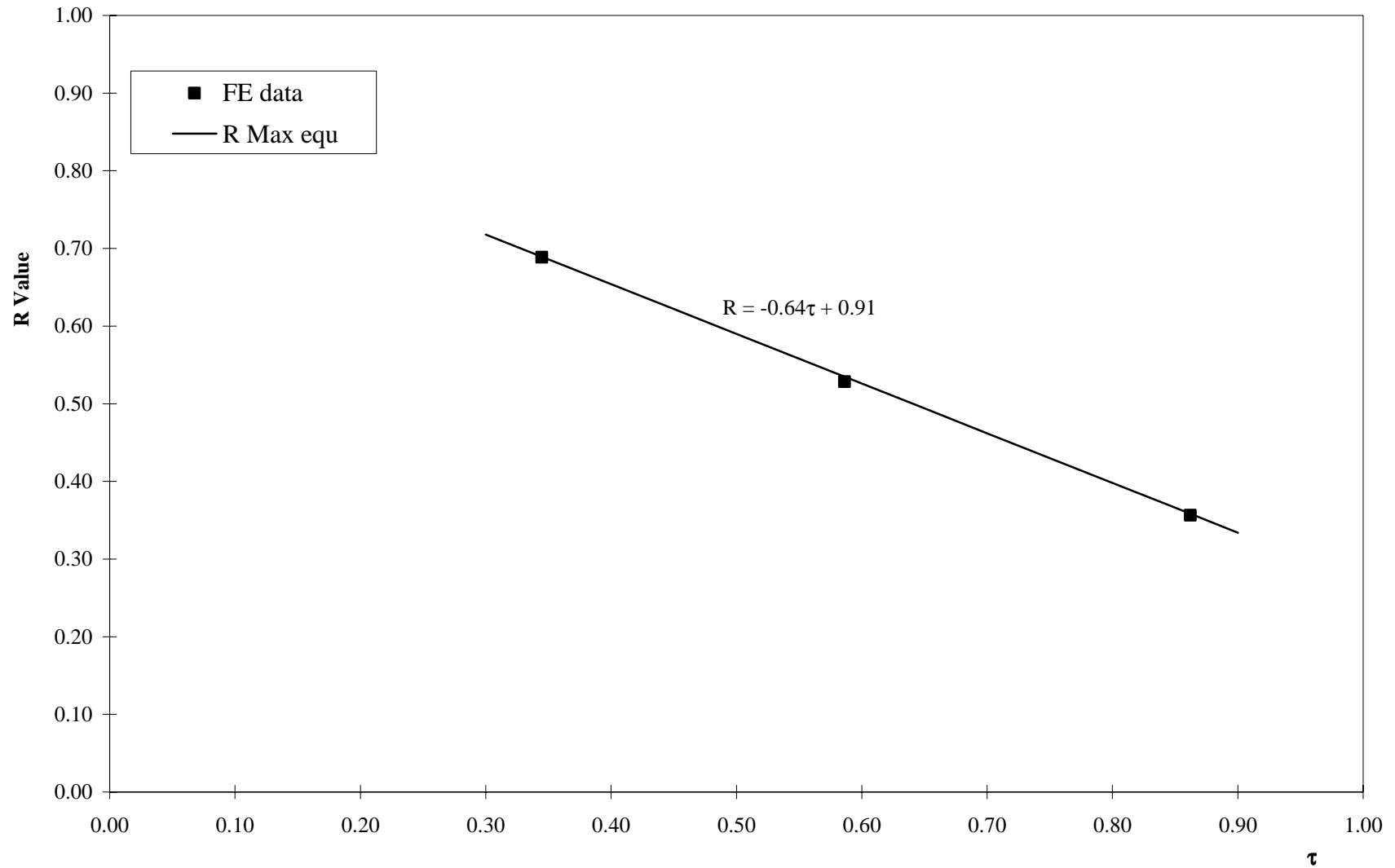


Figure 3.42: T Joints under IPB loading, R v. τ , $\beta = 0.4$, $\gamma = 20.69$, $\theta = 90^\circ$

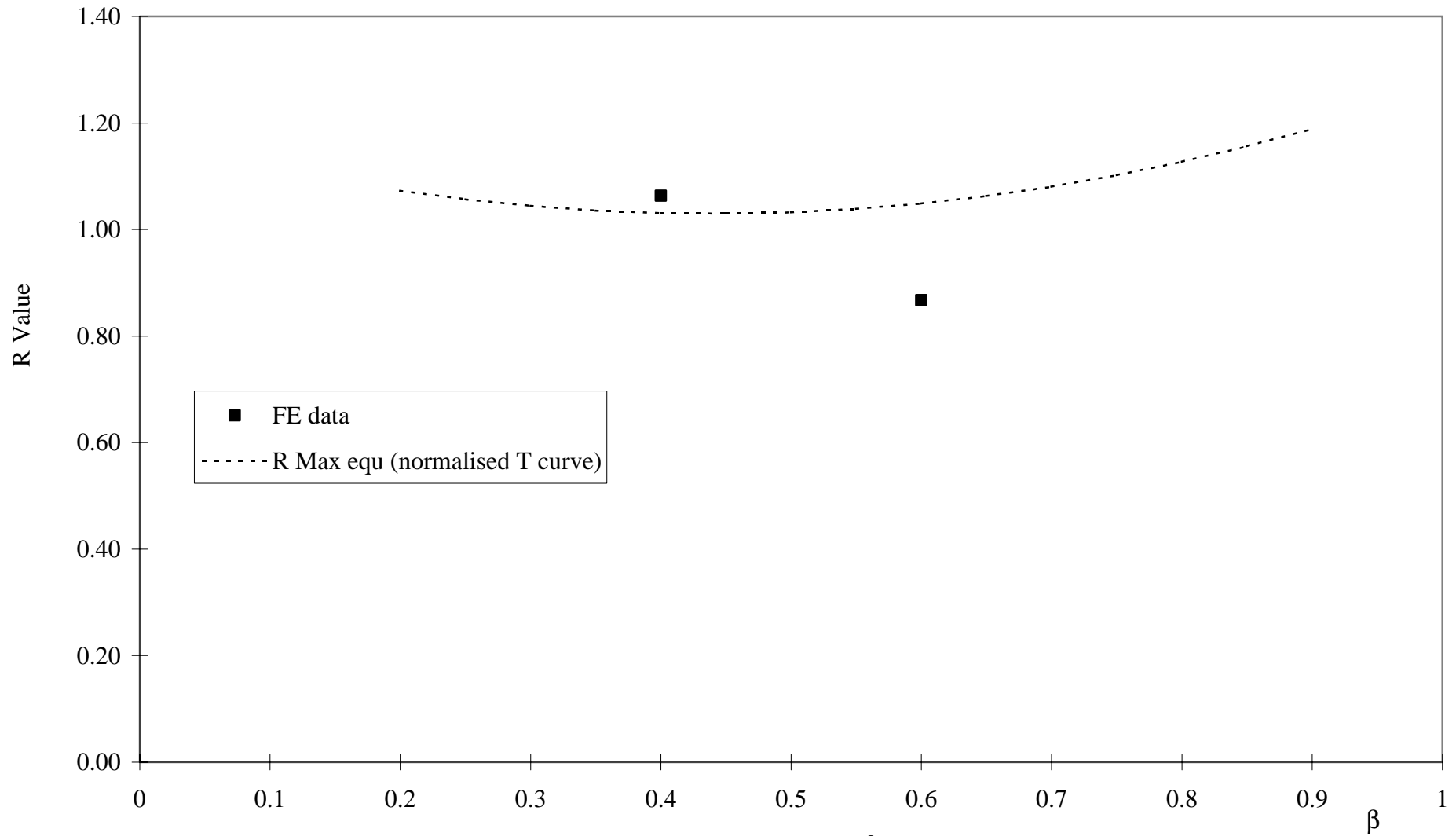


Figure 3.43: Y Joints under IPB loading, R v. β , $\gamma = 21.00$, $\tau = 0.35$, $\theta = 30^\circ$

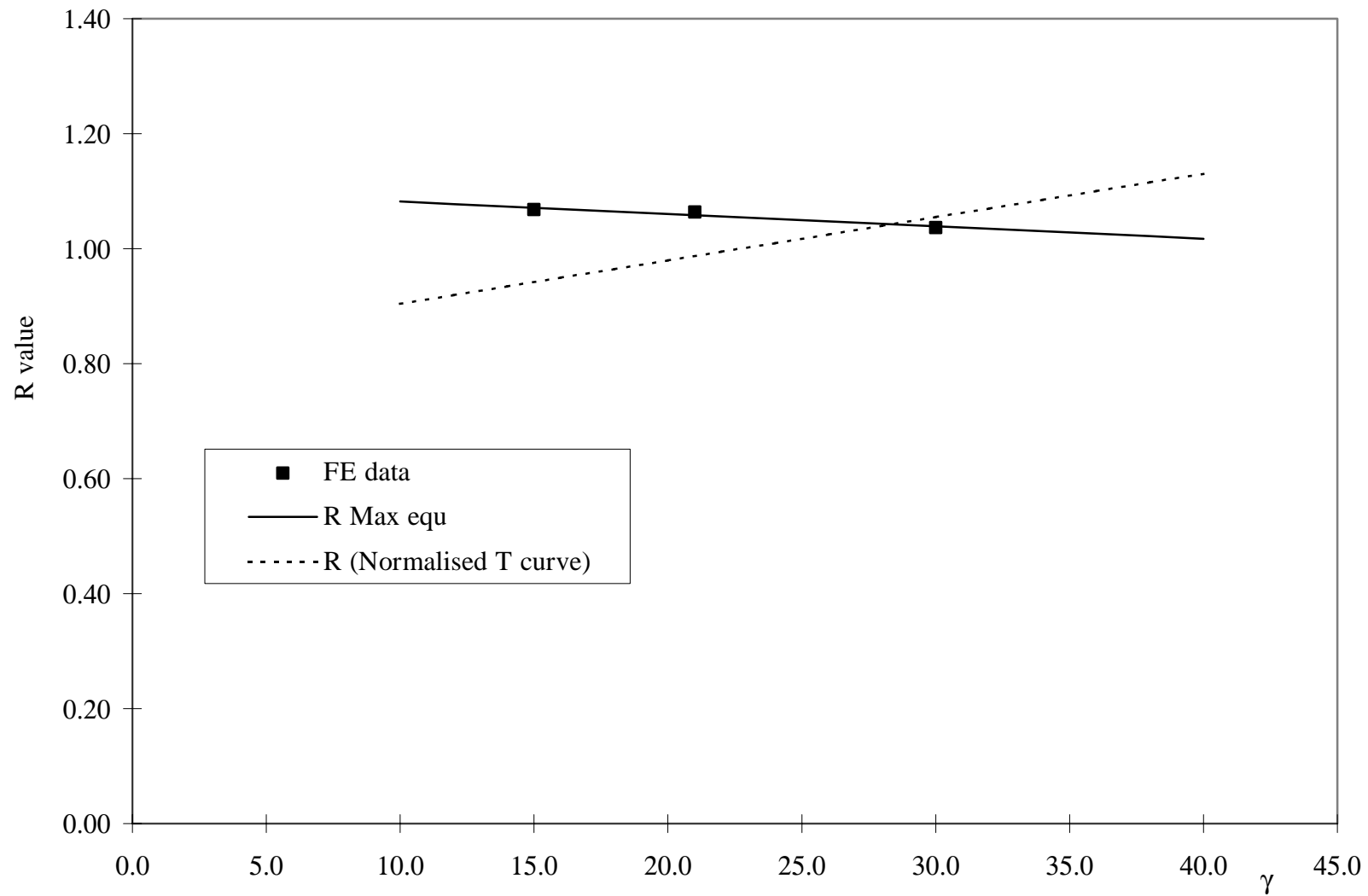


Figure 3.44: Y Joints under IPB loading, R v. γ , $\beta = 0.4$, $\tau = 0.35$, $\theta = 30^\circ$

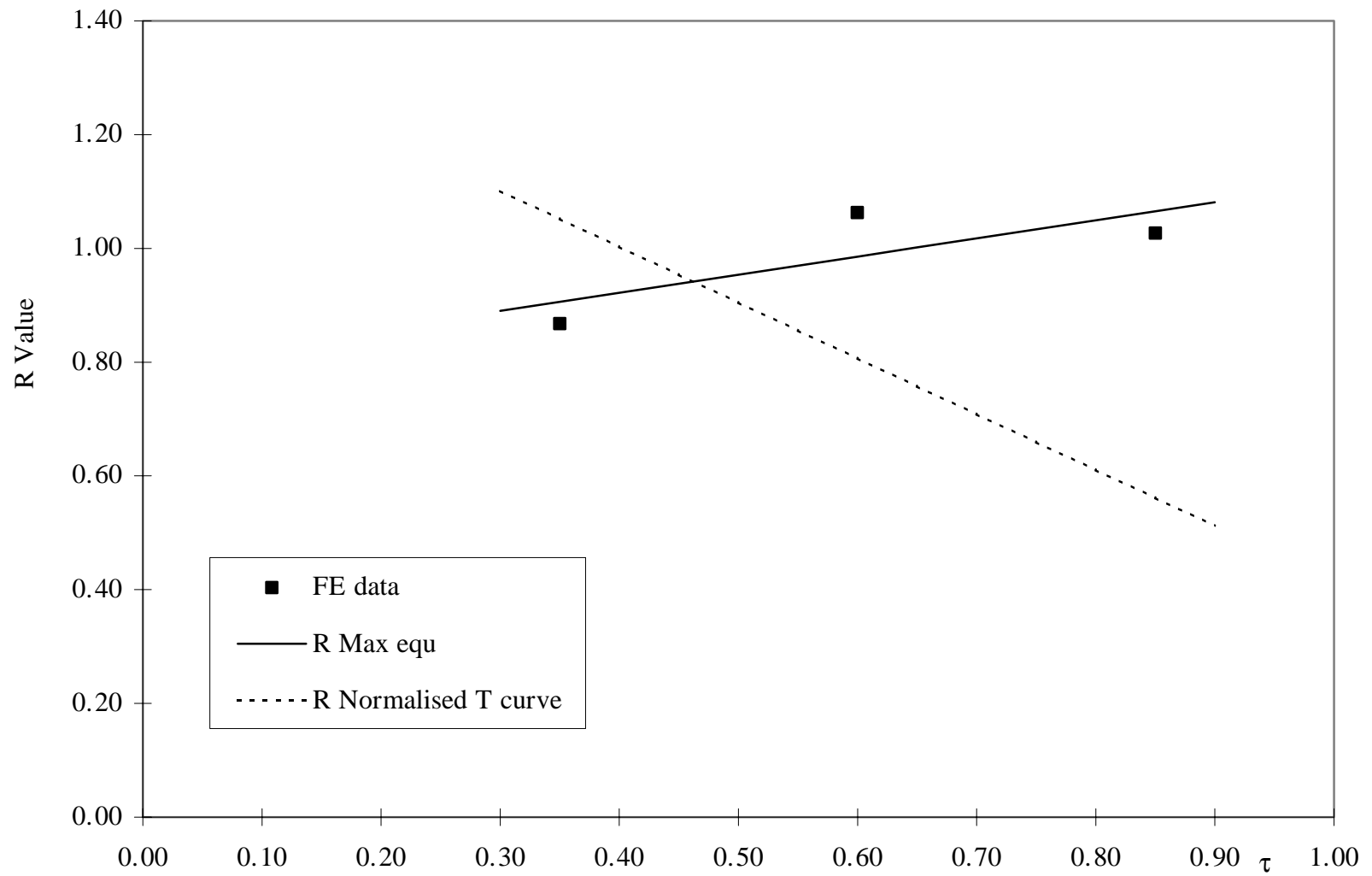


Figure 3.45: Y Joints under IPB loading, R v. τ , $\beta = 0.6$, $\gamma = 21.00$, $\theta = 30^\circ$

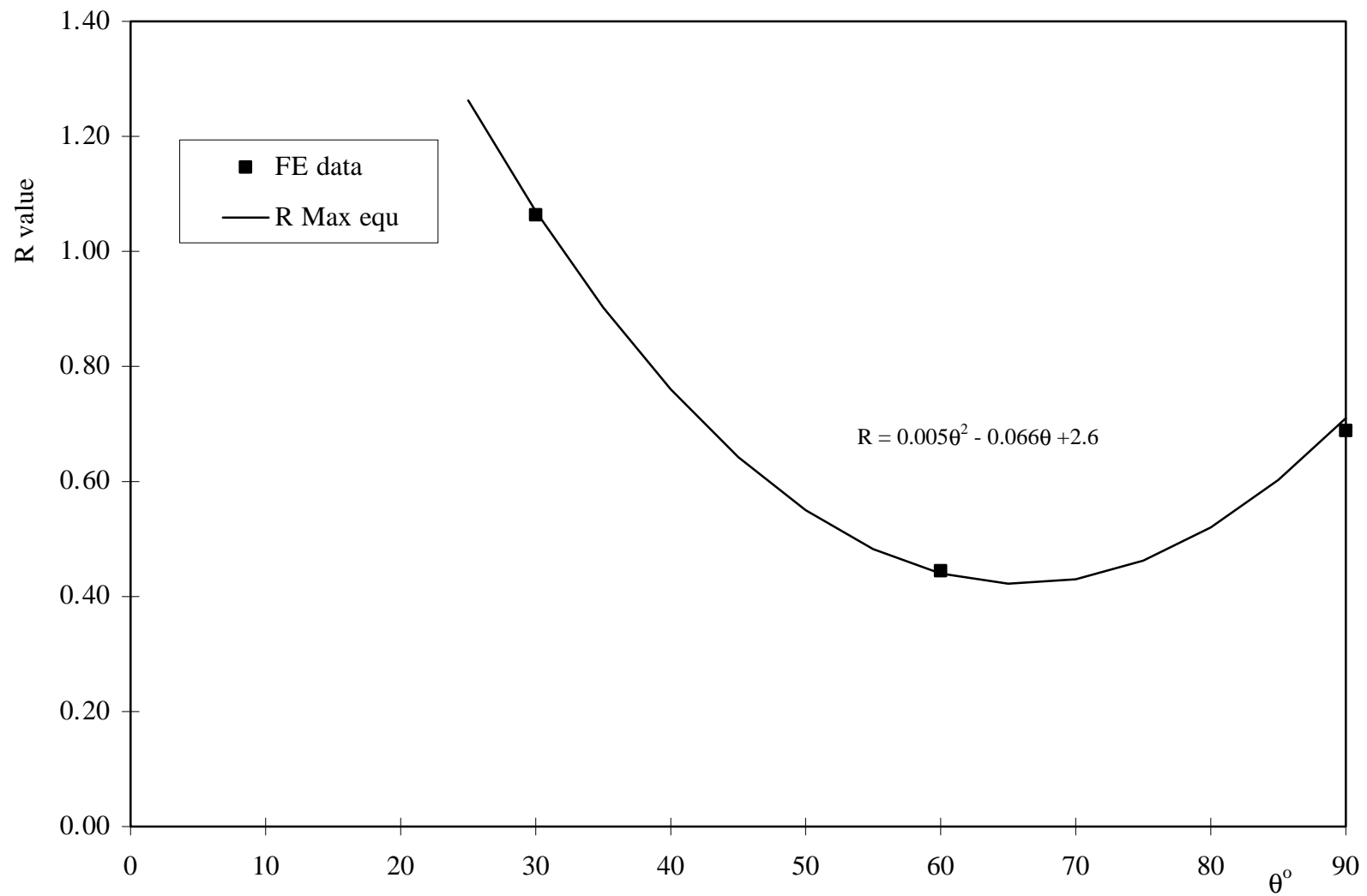


Figure 3.46: Y Joints under IPB loading, R v. θ , $\beta = 0.4$, $\gamma = 21.0$, $\tau = 0.35$

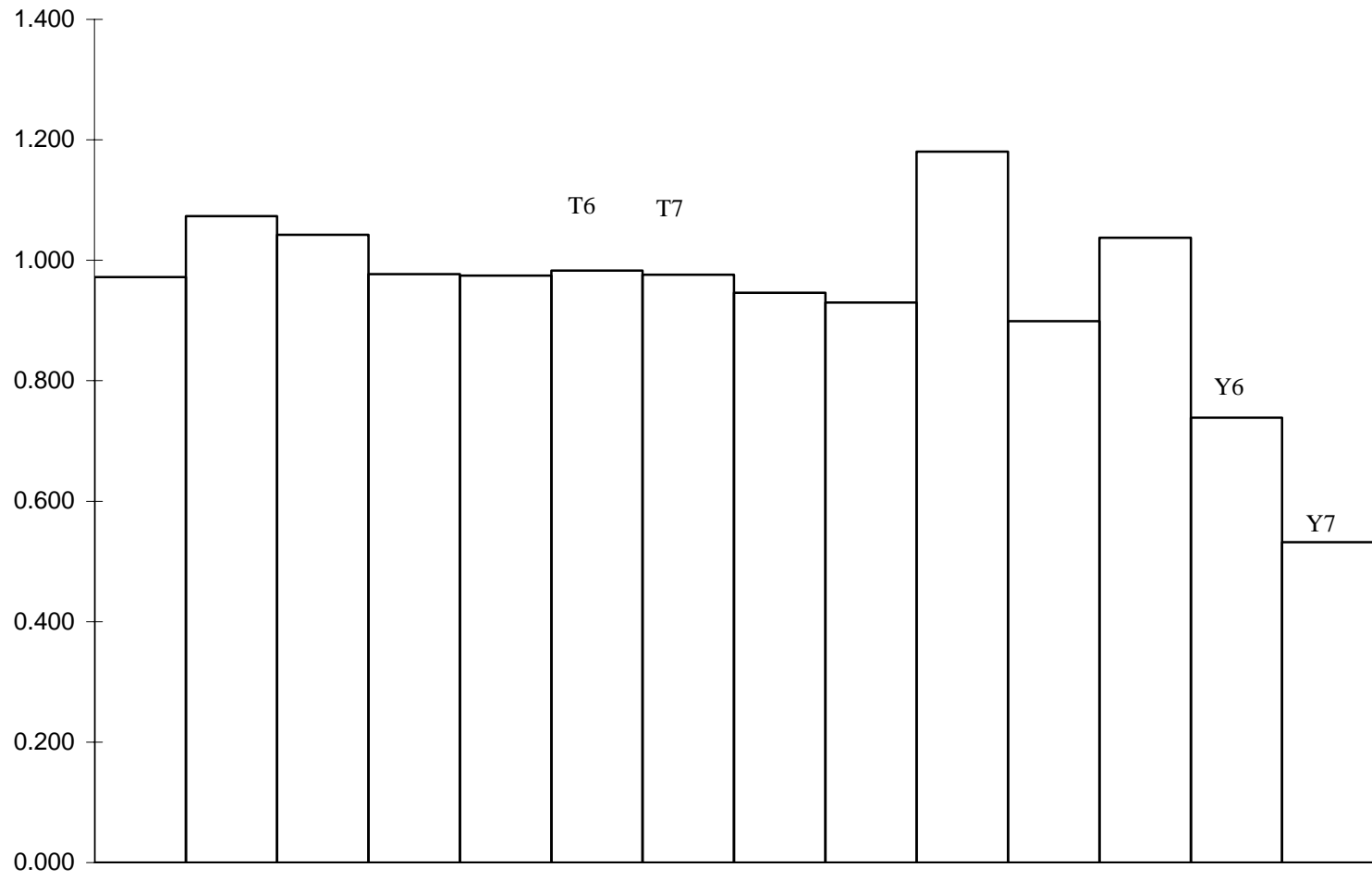


Figure 3.47: Y/T joints under IPB loading; Bar chart of predicted to calculated R values

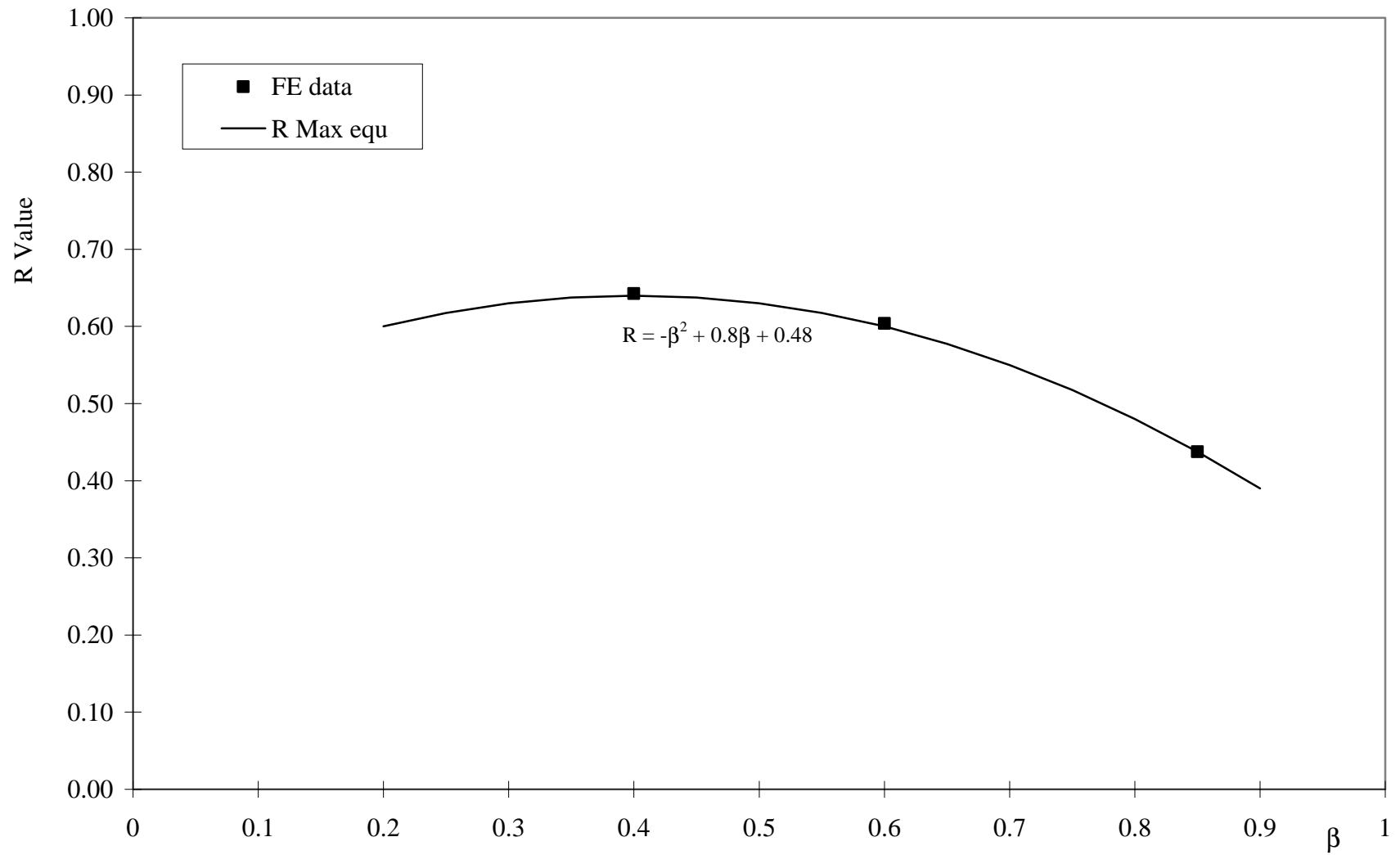


Figure 3.48: T Joints under OPB loading, R v. β , $\gamma = 20.69$, $\tau = 0.34$, $\theta = 90^\circ$

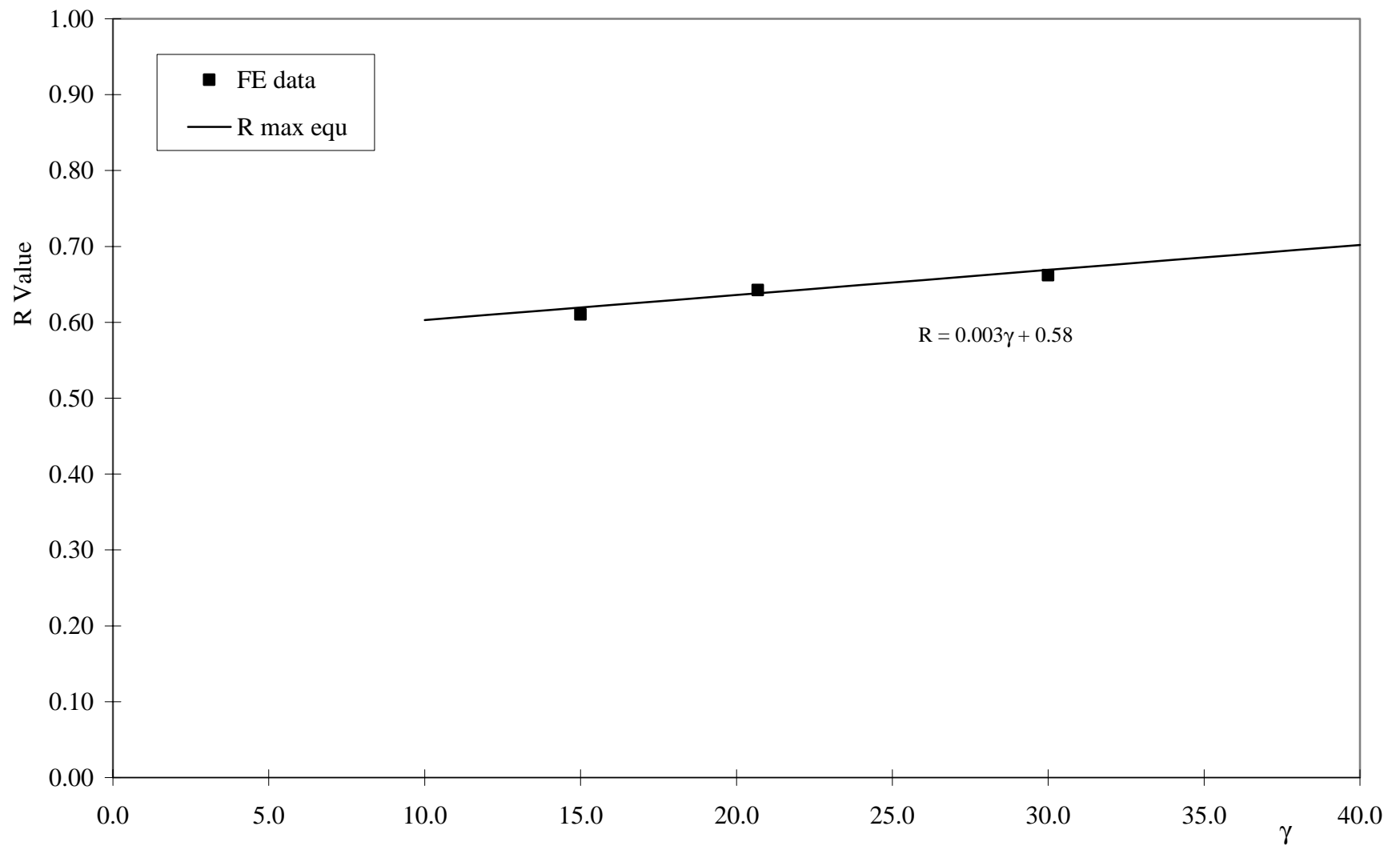


Figure 3.49: T Joints under OPB loading, R v. γ , $\beta = 0.4$, $\tau = 0.35$, $\theta = 90^\circ$

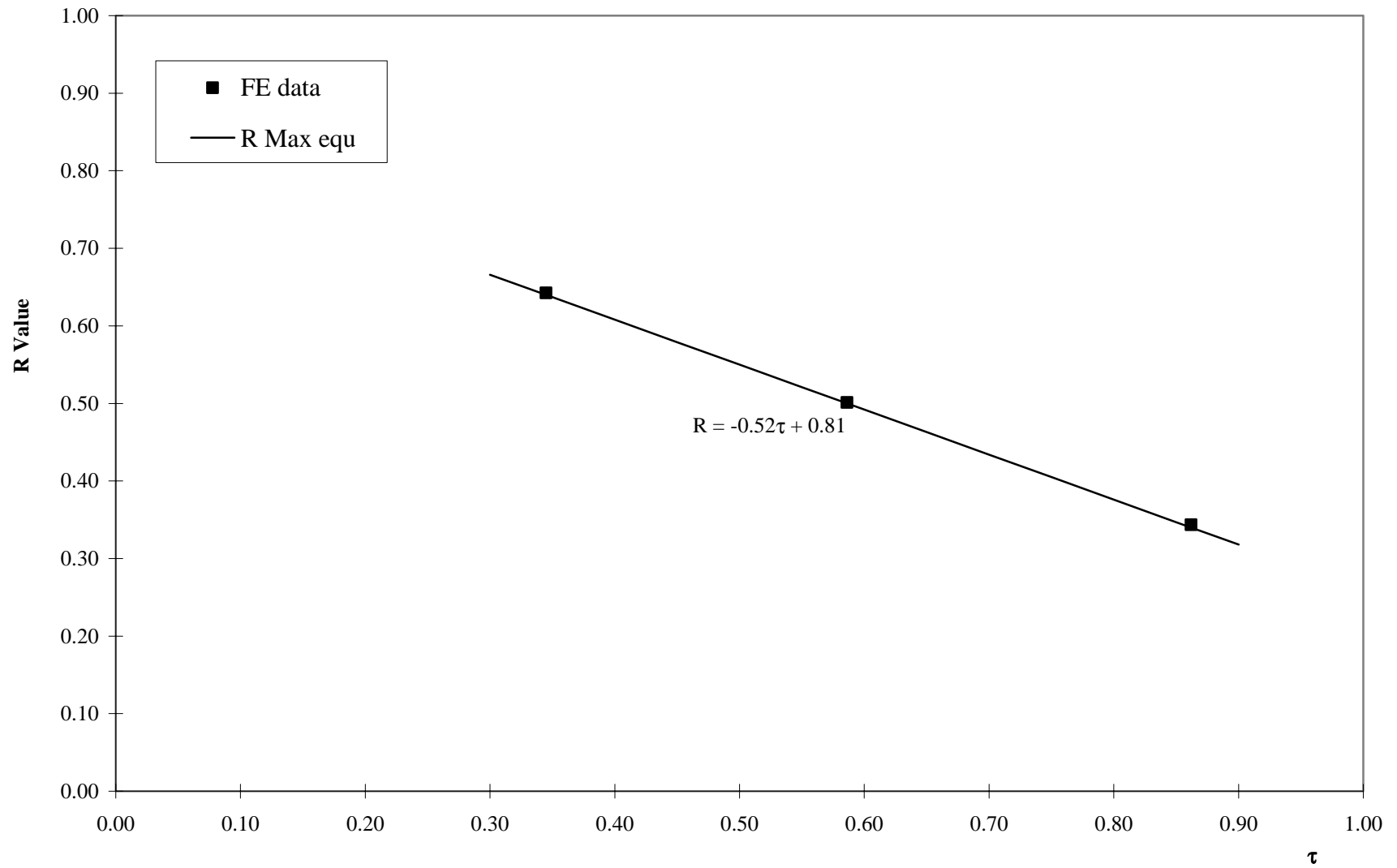


Figure 3.50: T Joints under OPB loading, R v. τ , $\gamma = 20.69$, $\tau = 0.34$, $\theta = 90^\circ$

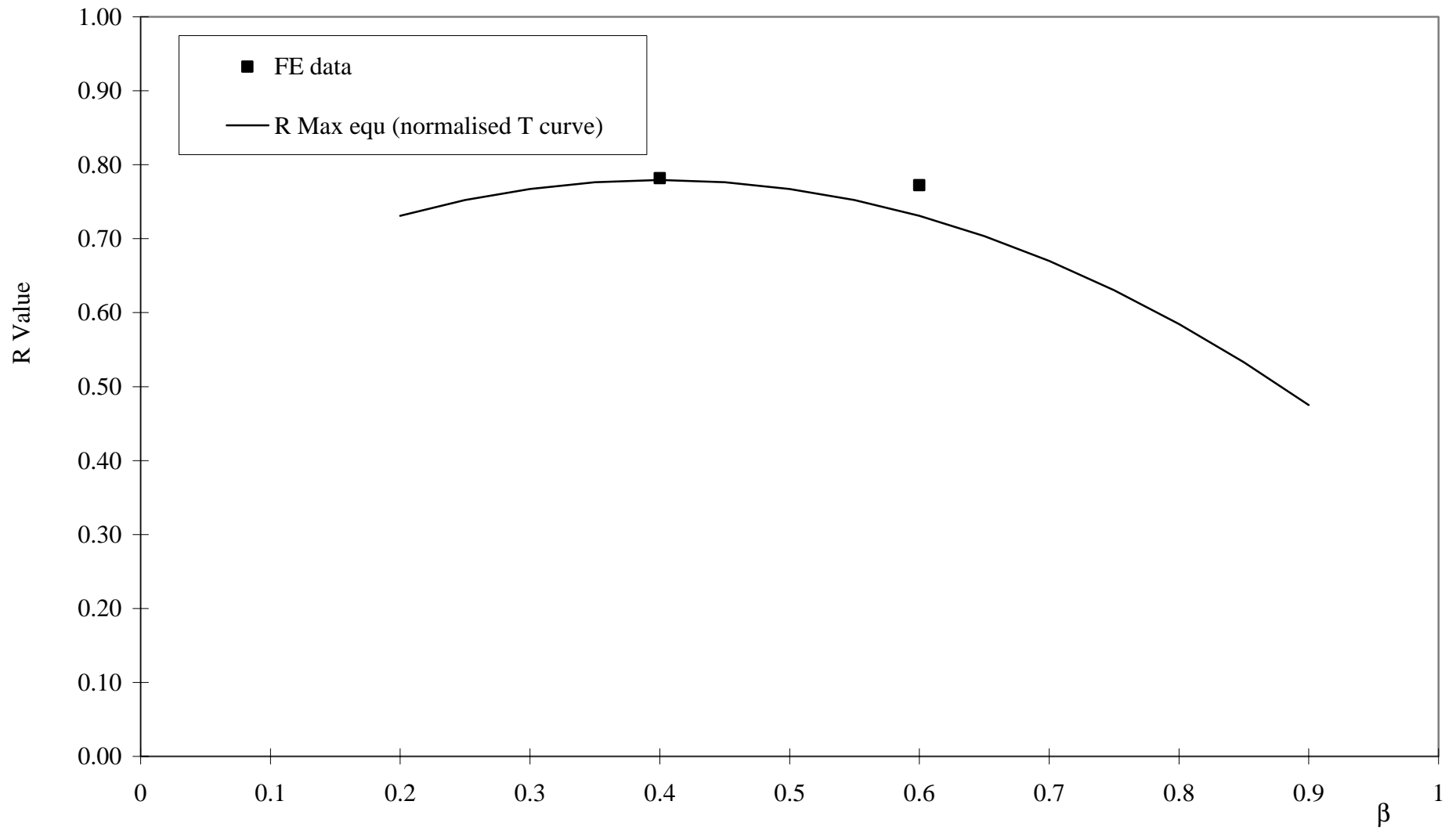


Figure 3.51: Y Joints under OPB loading, R v. β , $\gamma = 21.00$, $\tau = 0.35$, $\theta = 30^\circ$

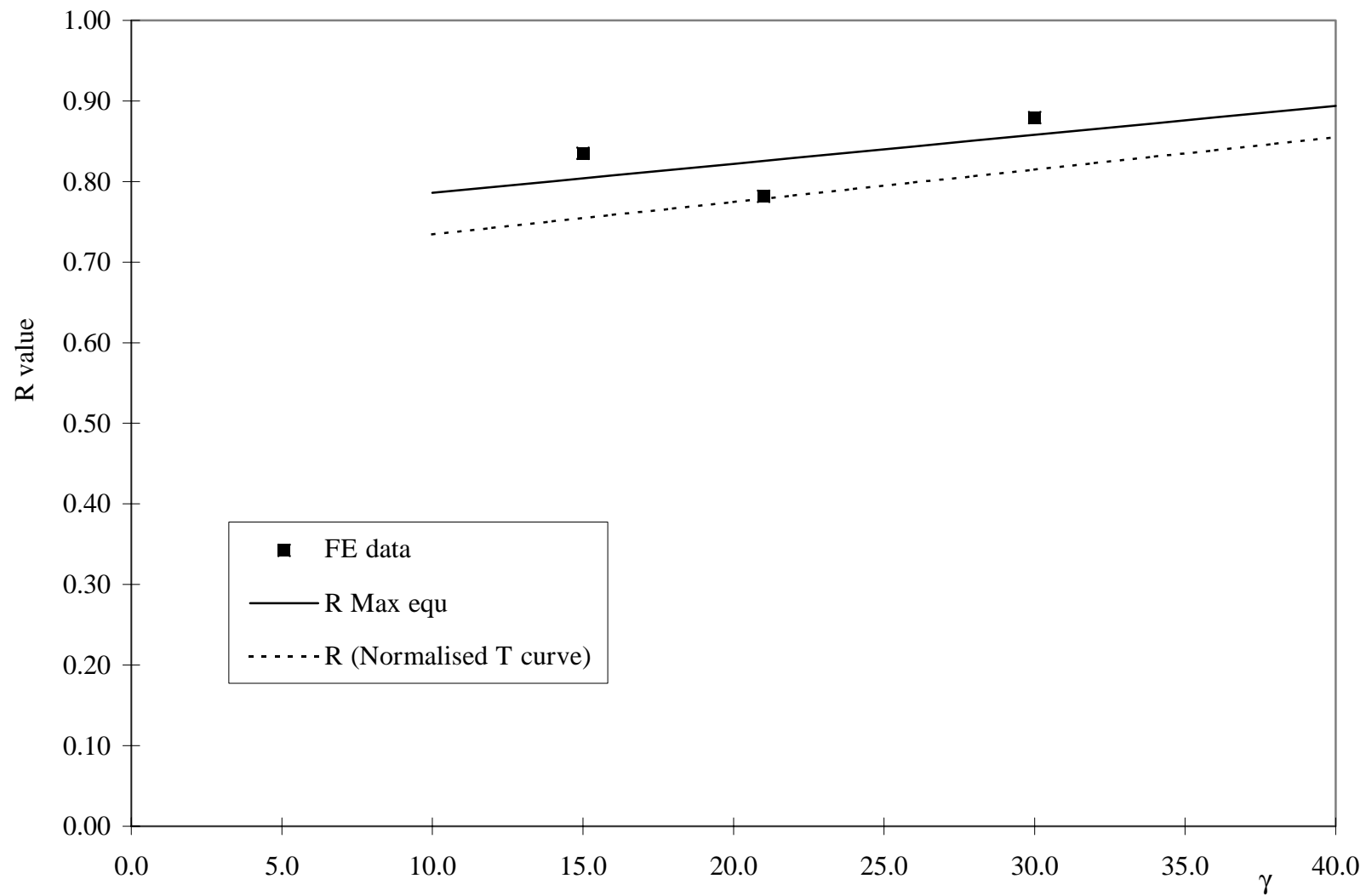


Figure 3.52: Y Joints under OPB loading, R v. γ , $\beta = 0.4$, $\tau = 0.35$, $\theta = 30^\circ$

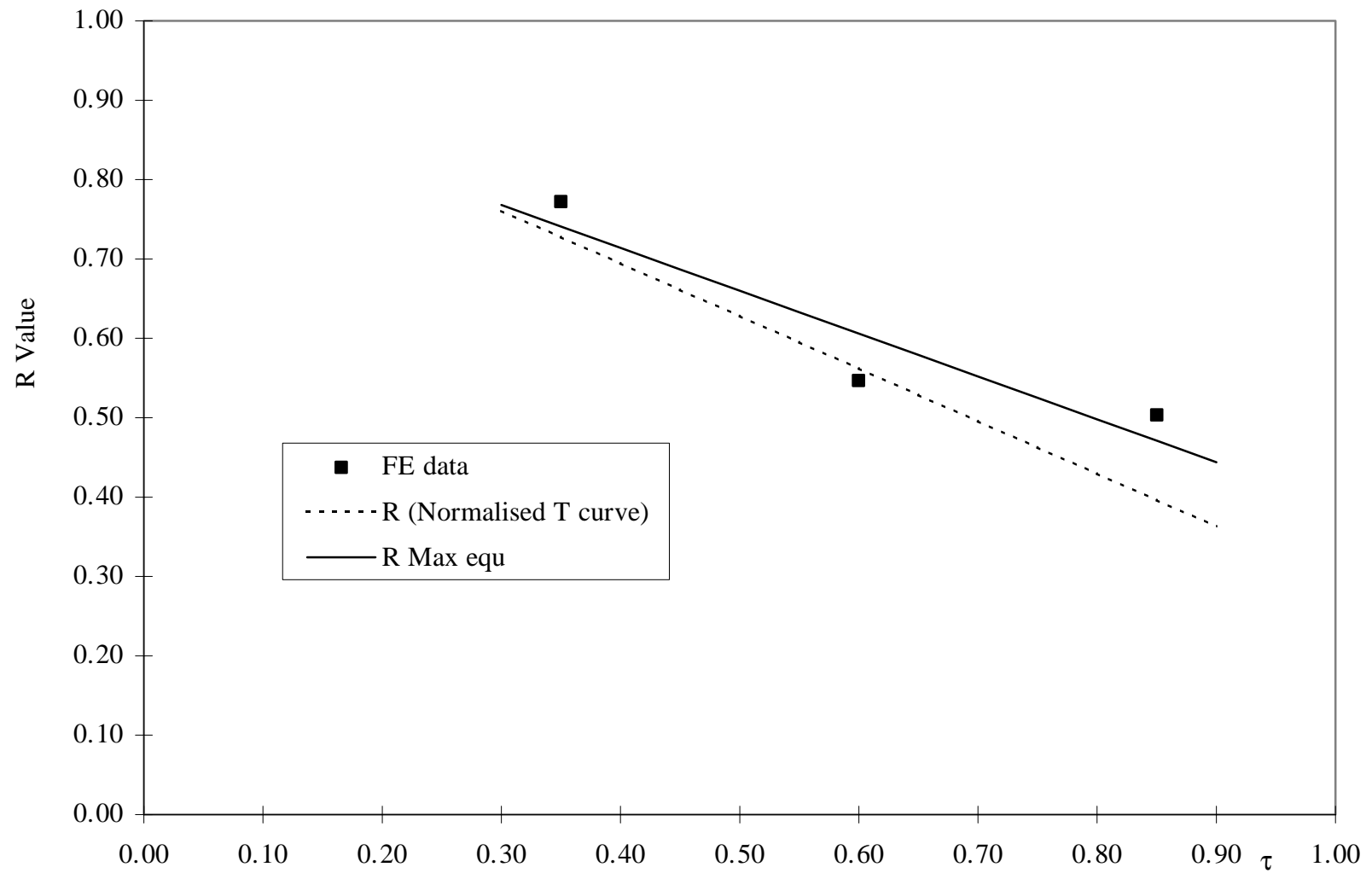


Figure 3.53: Y Joints under OPB loding, R v. τ , $\beta = 0.6$, $\gamma = 21.00$, $\theta = 30^\circ$

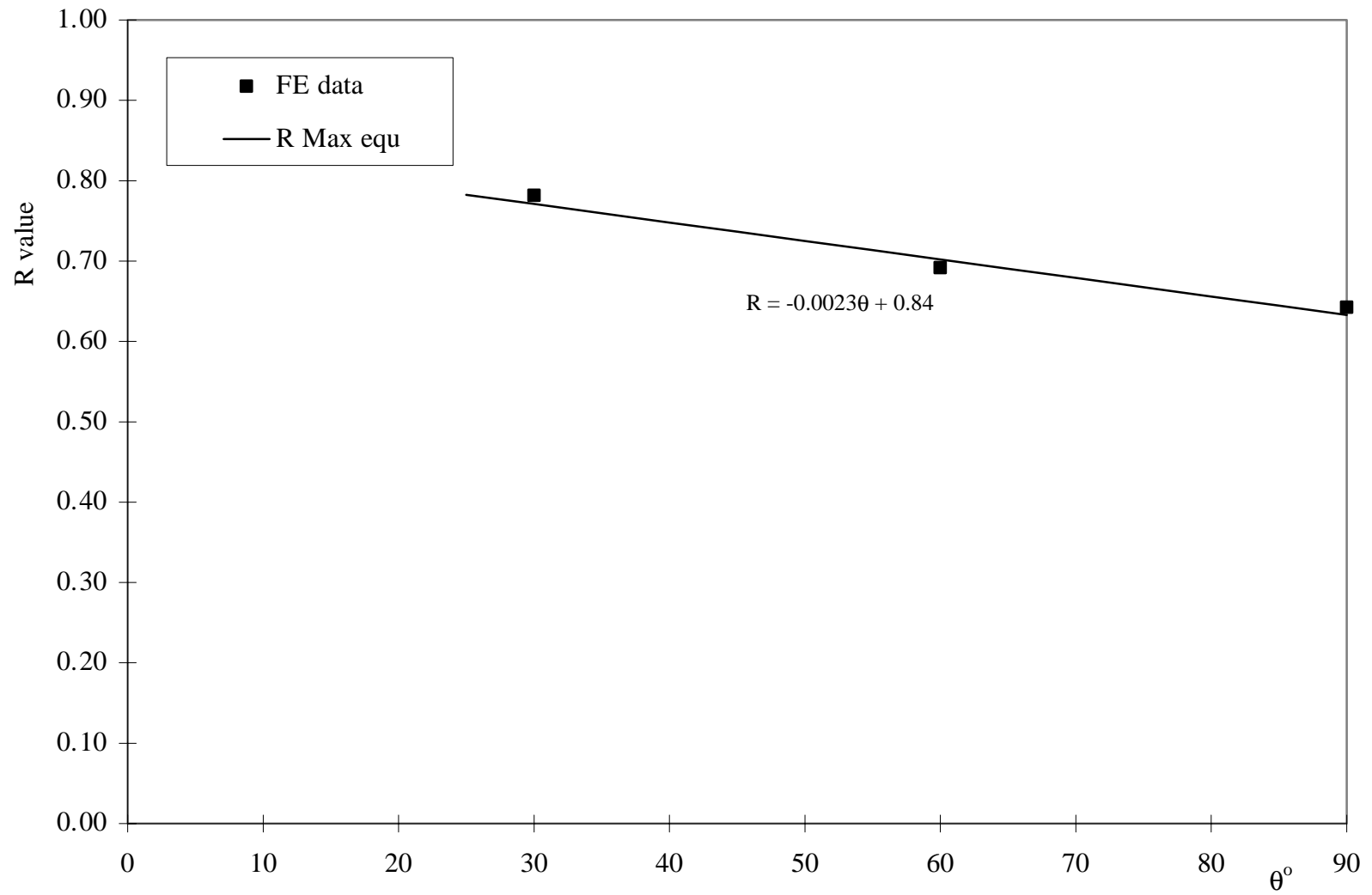


Figure 3.54: Y Joints under OPB loading, R v. θ , $\beta = 0.4$, $\gamma = 21.0$, $\tau = 0.35$

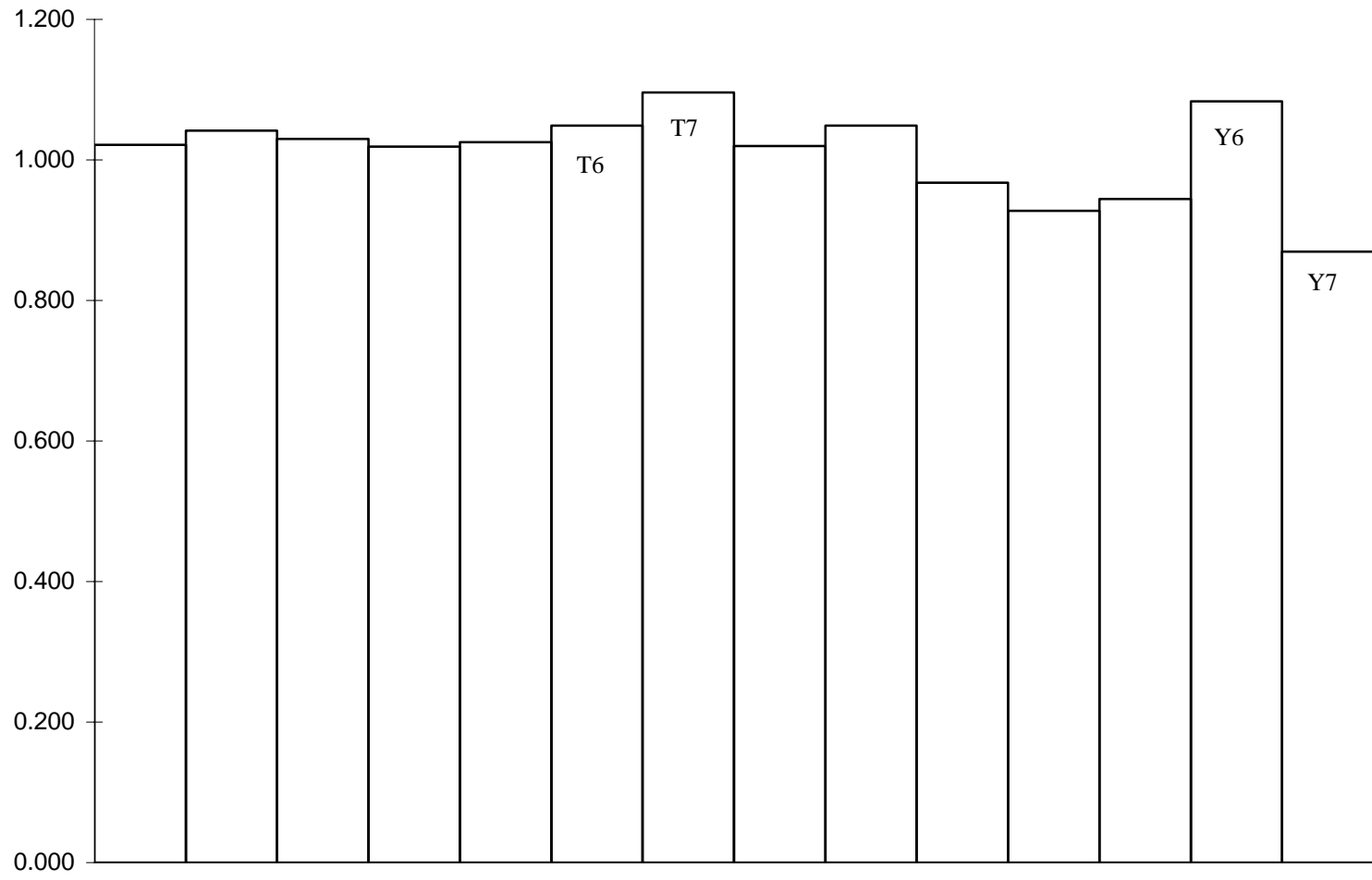


Figure 3.55: Y/T joints under OPB loading; Bar chart of predicted to calculated R values

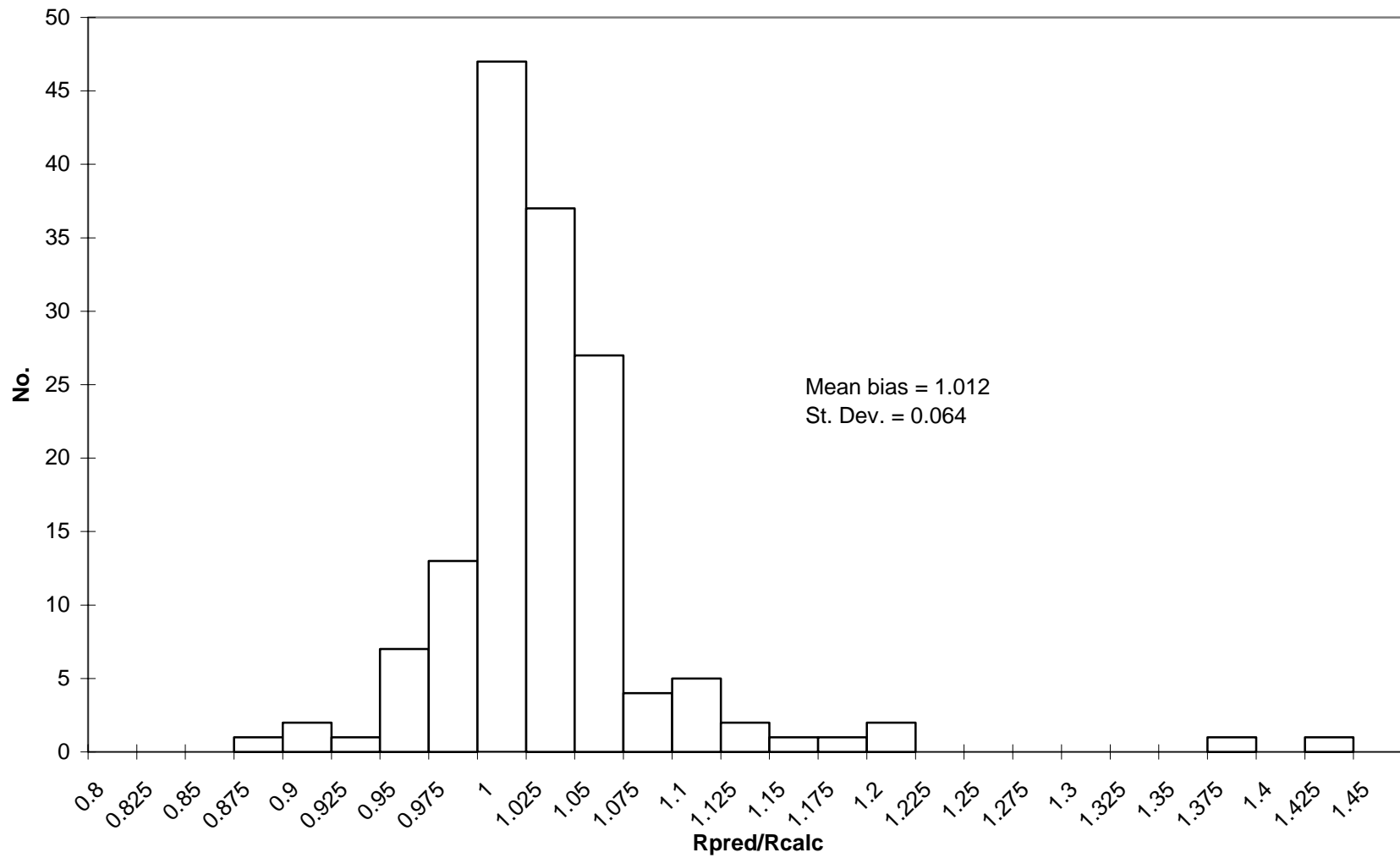


Figure 3.56: Histogram for all joint and load types

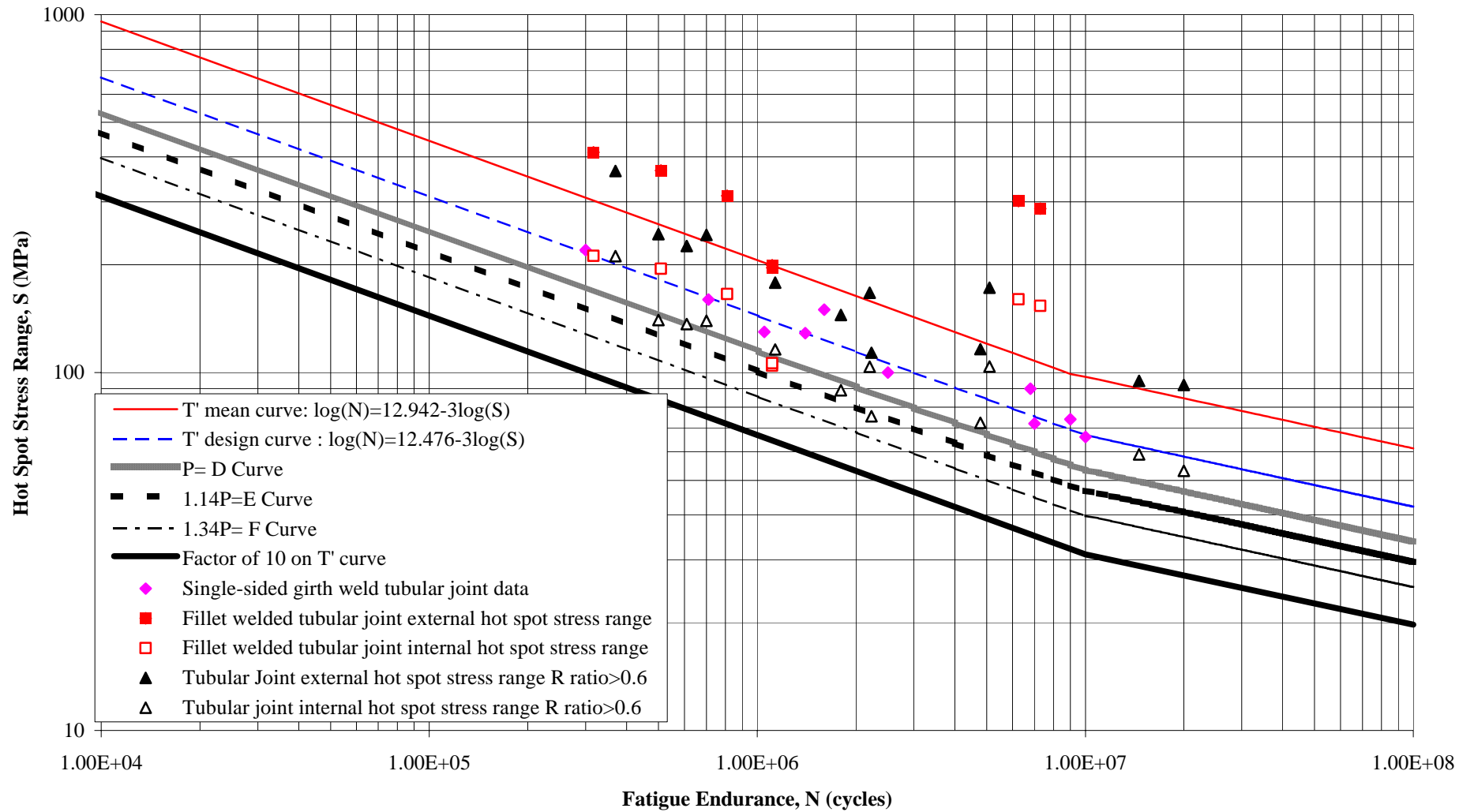


Figure 4.1: Comparison of tubular joint fatigue data with HSE S-N curves

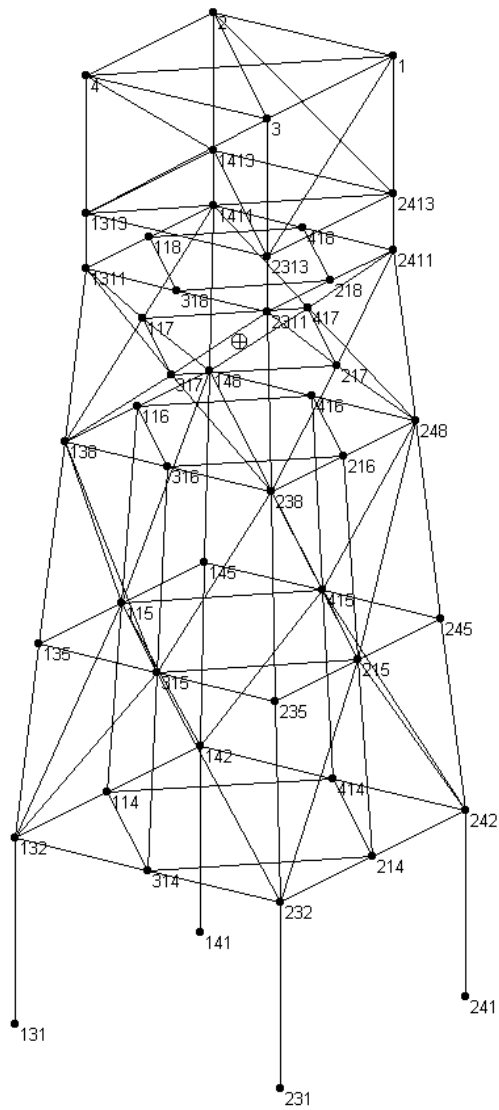


Figure 5.1: Node numbering for selected structure

APPENDIX A
Databases

K-Joints
Under Axial Loading

Ref No.	Joint Identification	θ	β	α	τ	γ	ζ	Maximum Calculated SCF's				R values			Efthymiou SCF Equations	
								Chord		Brace		Rchord	Rbrace	Rcrit	Balanced load	
								Internal	External	Internal	External	CH.int CH.ext	BR.int BR.ext	MAX.int MAX.ext	CH	BR
A1	K0	45	0.60	12.0	0.50	18.75	0.075	2.29	3.15	1.03	2.18	0.73	0.47	0.73	3.02	2.64
A1	K1	45	0.20	12.0	0.50	18.75	0.075	1.61	3.36	1.47	3.36	0.48	0.44	0.48	2.73	3.21
A1	K2	45	0.40	12.0	0.50	18.75	0.075	2.18	3.30	1.19	2.77	0.66	0.43	0.66	2.98	2.93
A1	K3	45	0.90	12.0	0.50	18.75	0.075	1.91	2.95	0.94	1.86	0.65	0.51	0.65	2.67	2.16
A1	K10	45	0.60	12.0	0.19	18.75	0.075	1.03	1.25	1.26	1.60	0.82	0.79	0.79	1.25	2.07
A1	K11	45	0.60	12.0	0.75	18.75	0.075	2.87	4.79	1.68	2.86	0.60	0.59	0.60	4.35	3.15
A1	K12	45	0.60	12.0	1.00	18.75	0.075	3.21	6.43	2.05	3.24	0.50	0.63	0.50	5.64	3.65
A1	K13	45	0.60	12.0	0.34	18.75	0.075	1.75	2.18	0.99	1.86	0.80	0.53	0.80	2.16	2.32
A1	K21	45	0.60	12.0	0.50	12.00	0.075	1.75	2.57	0.87	2.08	0.68	0.42	0.68	2.42	2.31
A1	K22	45	0.60	12.0	0.52	24.00	0.075	2.61	3.57	1.31	2.40	0.73	0.55	0.73	3.54	2.90
A1	K23	45	0.60	12.0	0.50	30.00	0.075	2.88	4.13	1.64	2.75	0.70	0.60	0.70	3.82	3.07
A1	K31	45	0.60	12.0	0.50	18.75	0.042	2.29	2.98	1.01	2.16	0.77	0.47	0.77	2.89	2.59
A1	K32	45	0.60	12.0	0.50	18.75	0.050	2.29	3.04	1.02	2.17	0.75	0.47	0.75	2.93	2.60
A1	K33	45	0.60	12.0	0.50	18.75	0.100	2.29	3.33	1.04	2.19	0.69	0.47	0.69	3.10	2.67
A1	K34	45	0.60	12.0	0.50	18.75	0.125	2.30	3.38	1.05	2.20	0.68	0.48	0.68	3.16	2.69
A1	K35	45	0.60	12.0	0.50	18.75	0.150	2.30	3.34	1.07	2.21	0.69	0.48	0.69	3.22	2.72
A1	K36	45	0.60	12.0	0.50	18.75	0.175	2.30	3.31	1.09	2.23	0.69	0.49	0.69	3.26	2.73
A1	K41	45	0.90	12.0	0.50	18.75	0.042	1.91	2.78	0.98	1.80	0.69	0.54	0.69	2.58	2.14
A1	K42	45	0.90	12.0	0.50	18.75	0.050	1.91	2.85	0.98	1.80	0.67	0.54	0.67	2.60	2.14
A1	K43	45	0.90	12.0	0.50	18.75	0.100	1.91	3.14	0.96	1.92	0.61	0.50	0.61	2.73	2.17
A1	K44	45	0.90	12.0	0.50	18.75	0.175	1.92	3.14	0.94	1.89	0.61	0.50	0.61	2.86	2.20
A1	K100	45	0.60	12.6	0.50	17.50	0.054	2.21	2.88	0.00	2.13	0.77	0.00	0.77	2.84	2.55
A1	K101	45	0.50	12.6	1.00	20.32	0.100	3.29	7.28	2.08	3.28	0.45	0.63	0.45	6.04	4.11
A1	K102	45	0.50	12.0	0.30	24.00	0.050	1.76	2.02	1.00	1.78	0.87	0.56	0.87	2.09	2.47
A1	Valid3	45	0.60	13.3	0.80	20.32	0.151	3.17	5.52	1.89	3.08	0.57	0.61	0.57	5.11	3.48

Ref. A1: Hansen, K. Single side welded tubular joints in offshore structures - A study of the stress concentrations at the weld root. HØGSKOLEN I STRAVANGER 1996.

Database A1: K joints under balanced axial loading (continued ...)

K-Joints
Under Axial Loading

								Maximum Calculated SCF's				R values			Efthymiou SCF Equations	
Ref No.	Joint Identification	θ	β	α	τ	γ	ζ	Chord		Brace		Rchord	Rbrace	Rcrit	Balanced load	
								Internal	External	Internal	External	CH.int CH.ext	BR.int BR.ext	MAX.int MAX.ext	CH	BR
A2	K13/1	30	0.6	12	0.34	18.75	0.075	1.43	1.43	1.09	1.70	1.00	0.64	0.84	1.52	1.77
A2	K13/2	45	0.6	12	0.34	18.75	0.075	1.63	2.09	0.89	2.09	0.78	0.43	0.78	2.16	2.32
A2	K13/3	60	0.6	12	0.34	18.75	0.075	1.66	2.52	0.72	2.71	0.66	0.27	0.61	2.64	2.76
A2	K36/2	45	0.6	12	0.50	18.75	0.175	2.06	3.31	0.92	2.26	0.62	0.41	0.62	3.26	2.73
A3	V1	45	0.6	12	0.50	17.5	0.054	2.18	2.59		2.00	0.84	0.00	0.84	2.84	2.55
A3	V2	45	0.9	12	0.50	17.5	0.054	1.85	2.49		1.74	0.74	0.00	0.74	2.53	2.11
A3	V3	45	0.5	12	0.40	18.0	0.054	1.86	2.13		2.06	0.87	0.00	0.87	2.36	2.49
A3	V4	45	0.8	12	0.40	18.0	0.107	1.86	2.49		2.27	0.75	0.00	0.75	2.35	2.17
A3	M1	45	0.8	12	0.50	14.0	0.054	1.69	2.24		1.73	0.75	0.00	0.75	2.40	2.13
A3	M2	45	0.8	12	0.50	9.0	0.054	1.26	1.80		1.67	0.70	0.00	0.70	1.93	1.90
A3	M3	45	0.8	12	0.40	14.0	0.054	1.53	1.91		1.63	0.80	0.00	0.80	1.97	2.01
A3	M4	45	0.8	12	0.50	17.5	0.054	2.07	2.65		1.83	0.78	0.00	0.78	2.69	2.26
A3	M5	45	0.8	12	0.78	14.0	0.054	2.12	3.38		2.15	0.63	0.00	0.63	3.58	2.48

Ref. A2: Stress concentrations in single - sided welds in offshore tubular joints. OTO 98 044, HSE Publication (Draft), May 1998

Ref. A3: Baerheim, M. Stress concentrations in tubular joints welded from one side. ISOPE, 1996

Database A1: K joints under balanced axial loading (...continued)

K-Joints
Under In-plane Bending

Ref No.	Joint Identification	θ	β	α	τ	γ	ζ	Maximum Calculated SCF's				R values			Efthymiou SCF Equations	
								Chord		Brace		Rchord	Rbrace	Rcrit	Balanced	
								Internal	External	Internal	External	CH.int CH.ext	BR.int BR.ext	MAX.int MAX.ext	CH	BR
A1	K0	45	0.60	12.0	0.50	18.75	0.075	1.56	2.79	1.00	2.18	0.56	0.46	0.56	2.57	2.89
A1	K1	45	0.20	12.0	0.50	18.75	0.075	1.44	1.80	1.24	2.77	0.80	0.45	0.52	1.67	2.55
A1	K2	45	0.40	12.0	0.50	18.75	0.075	1.52	2.44	1.38	2.51	0.62	0.55	0.61	2.39	2.97
A1	K3	45	0.90	12.0	0.50	18.75	0.075	1.44	2.76	0.79	1.77	0.52	0.45	0.52	2.34	2.44
A1	K10	45	0.60	12.0	0.19	18.75	0.075	0.84	1.30	0.86	1.82	0.65	0.47	0.47	1.12	2.27
A1	K11	45	0.60	12.0	0.75	18.75	0.075	1.73	3.93	1.43	2.46	0.44	0.58	0.44	3.63	3.22
A1	K12	45	0.60	12.0	1.00	18.75	0.075	1.68	4.94	1.57	2.47	0.34	0.64	0.34	4.64	3.49
A1	K13	45	0.60	12.0	0.34	18.75	0.075	1.27	2.04	0.77	2.00	0.62	0.39	0.62	1.87	2.62
A1	K21	45	0.60	12.0	0.50	12.00	0.075	1.41	2.39	1.06	2.25	0.59	0.47	0.59	1.98	2.64
A1	K22	45	0.60	12.0	0.52	24.00	0.075	1.75	3.04	1.05	2.19	0.58	0.48	0.58	3.08	3.00
A1	K23	45	0.60	12.0	0.50	30.00	0.075	1.91	3.27	1.12	2.21	0.58	0.51	0.58	3.40	3.00
A1	K31	45	0.60	12.0	0.50	18.75	0.042	1.56	3.40	1.00	2.18	0.46	0.46	0.46	2.62	2.89
A1	K32	45	0.60	12.0	0.50	18.75	0.050	1.56	3.20	1.00	2.18	0.49	0.46	0.49	2.61	2.89
A1	K33	45	0.60	12.0	0.50	18.75	0.100	1.57	2.53	1.00	2.18	0.62	0.46	0.62	2.54	2.89
A1	K34	45	0.60	12.0	0.50	18.75	0.125	1.57	2.38	1.00	2.18	0.66	0.46	0.66	2.52	2.89
A1	K35	45	0.60	12.0	0.50	18.75	0.150	1.57	2.31	1.00	2.18	0.68	0.46	0.68	2.49	2.89
A1	K36	45	0.60	12.0	0.50	18.75	0.175	1.57	2.30	1.01	2.18	0.68	0.46	0.68	2.46	2.89
A1	K41	45	0.90	12.0	0.50	18.75	0.042	1.43	3.38	0.80	1.83	0.42	0.44	0.42	2.40	2.44
A1	K42	45	0.90	12.0	0.50	18.75	0.050	1.43	3.18	0.80	1.78	0.45	0.45	0.45	2.39	2.44
A1	K43	45	0.90	12.0	0.50	18.75	0.100	1.44	2.53	0.80	1.76	0.57	0.45	0.57	2.30	2.44
A1	K44	45	0.90	12.0	0.50	18.75	0.175	1.45	2.35	0.80	1.77	0.62	0.45	0.62	2.20	2.44
A1	K100	45	0.60	12.6	0.50	17.50	0.054	1.51	3.04	0.00	2.17	0.50	0.00	0.50	2.50	2.85
A1	K101	45	0.50	12.6	1.00	20.32	0.100	1.61	4.36	1.62	2.47	0.37	0.66	0.37	4.77	3.66
A1	K102	45	0.50	12.0	0.30	24.00	0.050	1.27	2.12	0.78	2.11	0.60	0.37	0.60	1.95	2.71
A1	Valid3	45	0.60	13.3	0.80	20.32	0.151	1.81	3.56	1.49	2.47	0.51	0.60	0.51	3.89	3.32
A2	K1/1	30	0.20	12.0	0.50	18.75	0.075	0.02	0.92	1.28	0.86	0.02	1.49	1.39	1.31	2.57
A2	K1/2	45	0.20	12.0	0.50	18.75	0.075	0.57	1.78	1.23	1.27	0.32	0.97	0.69	1.67	2.55
A2	K1/3	60	0.20	12.0	0.50	18.75	0.075	0.88	2.32	0.78	1.57	0.38	0.50	0.38	1.93	2.54
A2	K13/2	45	0.60	12.0	0.34	18.75	0.075	0.86	2.08	1.04	2.09	0.41	0.50	0.50	1.87	2.62
A2	K36/1	30	0.60	12.0	0.50	18.75	0.175	0.18	1.84	2.05	1.60	0.10	1.28	1.11	1.93	2.91
A2	K36/2	45	0.60	12.0	0.50	18.75	0.175	0.69	2.22	1.18	1.76	0.31	0.67	0.53	2.46	2.89
A2	K36/3	60	0.60	12.0	0.50	18.75	0.175	1.04	2.74	0.90	2.16	0.38	0.42	0.38	2.84	2.87

Ref. A1: Hansen, K. Single side welded tubular joints in offshore structures - A study of the stress concentrations at the weld root. HØGSKOLEN I STRAVANGER 1996.

Ref. A2: Stress concentrations in single - sided welds in offshore tubular joints. OTO 98 044, HSE Publication (Draft), May 1998

Database A2: K joints under balanced in-plane bending

K-Joints
Under Out-of-plane Bending

Ref No.	Joint Identification	θ	β	α	τ	γ	ζ	Maximum Calculated SCF's				R values			Efthymiou SCF Equations	
								Chord		Brace		Rchord	Rbrace	Rcrit	Balanced	
								Internal	External	Internal	External	CH.int CH.ext	BR.int BR.ext	MAX.int MAX.ext	CH	BR
A1	K0	45	0.60	12.0	0.50	18.75	0.075	1.60	2.69	1.16	2.41	0.59	0.48	0.59	3.59	3.24
A1	K1	45	0.20	12.0	0.50	18.75	0.075	1.31	1.57	0.66	1.53	0.83	0.43	0.83	1.60	1.80
A1	K2	45	0.40	12.0	0.50	18.75	0.075	1.71	2.47	1.19	2.25	0.69	0.53	0.69	2.83	2.86
A1	K3	45	0.90	12.0	0.50	18.75	0.075	1.15	2.01	0.67	1.65	0.57	0.41	0.57	3.15	2.45
A1	K10	45	0.60	12.0	0.19	18.75	0.075	0.88	1.04	0.75	1.46	0.85	0.51	0.60	1.35	2.06
A1	K11	45	0.60	12.0	0.75	18.75	0.075	1.78	4.08	1.56	2.78	0.44	0.56	0.44	5.38	3.90
A1	K12	45	0.60	12.0	1.00	18.75	0.075	1.73	5.40	1.71	2.91	0.32	0.59	0.32	7.18	4.45
A1	K13	45	0.60	12.0	0.34	18.75	0.075	1.32	1.85	0.76	2.01	0.71	0.38	0.66	2.47	2.72
A1	K21	45	0.60	12.0	0.50	12.00	0.075	1.27	1.96	0.75	1.74	0.65	0.43	0.65	2.35	2.17
A1	K22	45	0.60	12.0	0.52	24.00	0.075	1.82	3.19	1.46	2.85	0.57	0.51	0.57	4.70	4.10
A1	K23	45	0.60	12.0	0.50	30.00	0.075	2.01	3.69	1.76	3.25	0.54	0.54	0.54	5.55	4.89
A1	K31	45	0.60	12.0	0.50	18.75	0.042	1.55	2.56	1.08	2.26	0.61	0.48	0.61	3.54	3.19
A1	K32	45	0.60	12.0	0.50	18.75	0.050	1.56	2.59	1.10	2.30	0.60	0.48	0.60	3.55	3.21
A1	K33	45	0.60	12.0	0.50	18.75	0.100	1.64	2.78	1.21	2.52	0.59	0.48	0.59	3.62	3.27
A1	K34	45	0.60	12.0	0.50	18.75	0.125	1.68	2.86	1.26	2.61	0.59	0.48	0.59	3.66	3.30
A1	K35	45	0.60	12.0	0.50	18.75	0.150	1.71	2.92	1.31	2.69	0.59	0.49	0.59	3.69	3.33
A1	K36	45	0.60	12.0	0.50	18.75	0.175	1.74	2.99	1.35	2.77	0.58	0.49	0.58	3.72	3.36
A1	K41	45	0.90	12.0	0.50	18.75	0.042	1.14	1.98	0.65	1.59	0.58	0.41	0.58	3.11	2.42
A1	K42	45	0.90	12.0	0.50	18.75	0.050	1.14	1.99	0.65	1.60	0.57	0.41	0.57	3.12	2.43
A1	K43	45	0.90	12.0	0.50	18.75	0.100	1.16	2.03	0.69	1.70	0.57	0.41	0.57	3.17	2.47
A1	K44	45	0.90	12.0	0.50	18.75	0.175	1.19	2.15	0.74	1.83	0.55	0.40	0.55	3.25	2.53
A1	K100	45	0.60	12.6	0.50	17.50	0.054	1.51	2.49	0.00	2.22	0.61	0.00	0.61	3.34	3.02
A1	K101	45	0.50	12.6	1.00	20.32	0.100	1.89	5.75	1.84	3.02	0.33	0.61	0.33	7.16	4.68
A1	K102	45	0.50	12.0	0.30	24.00	0.050	1.42	1.80	0.82	2.05	0.79	0.40	0.69	2.46	3.05
A1	Valid3	45	0.60	13.3	0.80	20.32	0.151	1.95	5.06	1.83	3.19	0.39	0.57	0.39	6.37	4.44
A2	K1/1	30	0.20	12.00	0.50	18.75	0.075	0.78	0.83	0.33	0.92	0.94	0.36	0.85	0.91	1.02
A2	K1/2	45	0.20	12.00	0.50	18.75	0.075	1.17	1.63	0.50	1.36	0.72	0.37	0.72	1.60	1.80
A2	K1/3	60	0.20	12.00	0.50	18.75	0.075	1.42	2.40	0.62	1.89	0.59	0.33	0.59	2.23	2.51

Ref. A1: Hansen, K. Single side welded tubular joints in offshore structures - A study of the stress concentrations at the weld root. HØGSKOLEN I STRAVANGER 1996.

Ref. A2: Stress concentrations in single - sided welds in offshore tubular joints. OTO 98 044, HSE Publication (Draft), May 1998

Database A3: K joints under balanced out-of-plane bending

X-Joints
Under Axial Loading

Ref No.	Joint Identification	θ	β	α	τ	γ	Maximum Calculated SCF's				R values			Efthymiou SCF Equations	
							Chord		Brace		Rchord	Rbrace	Rcrit	CH	BR
							Internal	External	Internal	External	CH.int CH.ext	BR.int BR.ext	MAX.int MAX.ext		
A2	X1'	90	0.40	12.0	0.345	20.69	6.20	9.41	1.46	9.04	0.66	0.16	0.66	10.03	9.90
A2	X2'	90	0.40	12.0	0.350	15.00	4.48	7.28	1.13	7.12	0.62	0.16	0.62	7.38	7.50
A2	X3'	90	0.40	12.0	0.333	25.00	7.09	9.92	1.65	9.94	0.71	0.17	0.71	11.71	11.57
A2	X4'	90	0.40	12.0	0.350	30.00	8.56	11.85	1.95	11.57	0.72	0.17	0.72	14.76	14.00
A2	X5'	90	0.20	12.0	0.345	20.69	4.51	7.84	1.42	6.90	0.58	0.21	0.58	5.77	6.56
A2	X6'	90	0.60	12.0	0.345	20.69	6.32	8.97	1.31	9.64	0.70	0.14	0.66	11.62	10.77
A2	X7'	90	0.85	12.0	0.345	20.69	3.08	5.43	1.12	7.71	0.57	0.15	0.40	8.30	7.61
A2	X8'	90	0.40	12.0	0.207	20.69	3.55	4.81	0.68	5.79	0.74	0.12	0.61	6.02	7.89
A2	X9'	90	0.40	12.0	0.586	20.69	9.02	16.94	2.07	12.10	0.53	0.17	0.53	17.04	12.60
A2	X10'	90	0.40	12.0	0.862	20.69	9.50	25.57	2.05	12.89	0.37	0.16	0.37	25.06	15.07
A4	X1	90	0.27	12.0	0.300	8.500	1.51	2.29	1.51	2.29	0.66	0.66	0.66	2.68	3.67
A4	X2	90	0.50	12.0	0.480	13.98	5.40	10.10	5.40	10.10	0.53	0.53	0.53	10.55	8.71
A4	X3	90	0.60	12.0	0.300	18.75	4.58	6.53	4.58	6.53	0.70	0.70	0.70	9.16	9.26
A4	X4	90	0.60	12.0	0.500	18.75	7.05	12.50	7.05	12.50	0.56	0.56	0.56	15.27	11.66
A4	X5	90	0.60	12.0	0.800	18.75	8.43	22.00	8.43	22.00	0.38	0.38	0.38	24.43	14.49
A4	X6	90	0.60	12.0	0.500	10.00	3.77	7.46	3.77	7.46	0.51	0.51	0.51	8.14	6.69
A4	X7	90	0.60	12.0	0.500	30.00	10.90	22.70	10.90	22.70	0.48	0.48	0.48	24.43	18.06
A4	X8	90	0.30	12.0	0.500	18.75	5.90	9.94	5.90	9.94	0.59	0.59	0.59	10.73	9.19
A4	X9	90	0.80	12.0	0.500	18.75	4.09	12.20	4.09	12.20	0.34	0.34	0.34	12.50	9.36
A4	X10	52.68	0.60	12.0	0.500	18.75	4.64	9.53	4.64	9.53	0.49	0.49	0.49	10.34	7.01
A4	X11	74.27	0.60	12.0	0.500	18.75	7.20	13.60	7.20	13.60	0.53	0.53	0.53	14.31	10.69
A4	X12	45	0.60	12.0	0.500	18.75	4.57	7.00	4.57	7.00	0.65	0.65	0.65	8.47	5.48

Ref. A2: Stress concentrations in single - sided welds in offshore tubular joints. OTO 98 044, HSE Publication (Draft), May 1998

Ref. A4: Baerheim, M. et. al. Single sided welded tubular joints-Stress concentrations at the weld root. OMAE, 1998

Database A4: X joints under axial loading

X-Joints
Under In-plane Bending

							Maximum Calculated SCF's				R values			Efthymiou SCF Equations	
Ref No.	Joint Identification	θ	β	α	τ	γ	Chord		Brace		Rchord	Rbrace	Rcrit		
							Internal	External	Internal	External	<u>CH.int</u> CH.ext	<u>BR.int</u> BR.ext	<u>MAX.int</u> MAX.ext	CH	BR
A2	X1'	90	0.40	12.0	0.345	20.69	1.57	2.28	0.78	2.53	0.69	0.31	0.62	2.13	2.82
A2	X2'	90	0.40	12.0	0.350	15.00	1.33	1.85	0.42	2.23	0.72	0.19	0.60	1.71	2.42
A2	X3'	90	0.40	12.0	0.333	25.00	1.75	2.39	1.01	2.66	0.73	0.38	0.66	2.37	3.08
A2	X4'	90	0.40	12.0	0.350	30.00	2.03	2.77	1.20	2.86	0.73	0.42	0.71	2.83	3.44
A2	X5'	90	0.20	12.0	0.345	20.69	1.41	2.09	0.35	2.29	0.67	0.15	0.62	1.61	2.45
A2	X6'	90	0.60	12.0	0.345	20.69	1.62	2.05	0.52	2.31	0.79	0.23	0.70	2.12	2.71
A2	X7'	90	0.85	12.0	0.345	20.69	1.63	1.80	0.33	2.12	0.91	0.16	0.77	1.79	2.35
A2	X8'	90	0.40	12.0	0.207	20.69	1.12	1.42	0.42	2.31	0.79	0.18	0.48	1.38	2.48
A2	X9'	90	0.40	12.0	0.586	20.69	1.87	3.52	0.97	2.70	0.53	0.36	0.53	3.34	3.24
A2	X10'	90	0.40	12.0	0.862	20.69	1.70	4.78	0.67	2.63	0.36	0.25	0.36	4.64	3.62

Ref. A2: Stress concentrations in single - sided welds in offshore tubular joints. OTO 98 044, HSE Publication (Draft), May 1998

Database A5: X joints under in-plane bending

X-Joints
Under Out-of-plane Bending

							Maximum Calculated SCF's				R values			Efthymiou SCF Equations	
Ref No.	Joint Identification	θ	β	α	τ	γ	Chord		Brace		Rchord	Rbrace	Rcrit	Balanced	
							Internal	External	Internal	External	<u>CH.int</u> CH.ext	<u>BR.int</u> BR.ext	<u>MAX.int</u> MAX.ext	CH	BR
A2	X1'	90	0.40	12.0	0.345	20.69	3.46	5.32	1.42	5.23	0.65	0.27	0.65	4.35	5.35
A2	X2'	90	0.40	12.0	0.350	15.00	2.42	3.92	0.68	3.77	0.62	0.18	0.62	3.20	3.97
A2	X3'	90	0.40	12.0	0.333	25.00	4.15	5.92	1.81	6.20	0.70	0.29	0.67	5.09	6.30
A2	X4'	90	0.40	12.0	0.350	30.00	5.20	7.42	2.88	7.67	0.70	0.38	0.68	6.41	7.66
A2	X5'	90	0.20	12.0	0.345	20.69	2.07	3.43	0.31	2.91	0.60	0.11	0.60	2.22	3.04
A2	X6'	90	0.60	12.0	0.345	20.69	3.73	5.42	1.76	6.04	0.69	0.29	0.62	5.93	6.51
A2	X7'	90	0.85	12.0	0.345	20.69	1.97	3.40	1.08	4.60	0.58	0.23	0.43	5.22	5.04
A2	X8'	90	0.40	12.0	0.207	20.69	2.28	3.14	0.99	3.88	0.73	0.26	0.59	2.61	4.23
A2	X9'	90	0.40	12.0	0.586	20.69	4.38	8.54	1.83	6.17	0.51	0.30	0.51	7.40	6.82
A2	X10'	90	0.40	12.0	0.862	20.69	4.19	11.87	1.75	6.01	0.35	0.29	0.35	10.88	8.15

Ref. A2: Stress concentrations in single - sided welds in offshore tubular joints. OTO 98 044, HSE Publication (Draft), May 1998

Database A6: X joints under out-of-plane bending

Y-Joints
Under Axial Loading

							Maximum Calculated SCF's				R values			Efthymiou SCF Equations	
Ref No.	Joint Identification	θ	β	α	τ	γ	Chord		Brace		Rchord	Rbrace	Rcrit	Fixed chord ends	
							Internal	External	Internal	External	CH.int CH.ext	BR.int BR.ext	MAX.int MAX.ext	CH	BR
A2	T1	90	0.40	12.0	0.345	20.69	5.01	7.69	1.34	7.57	0.65	0.18	0.65	6.84	8.05
A2	T2	90	0.40	12.0	0.350	15.00	3.49	5.87	0.92	5.89	0.59	0.16	0.59	5.04	6.23
A2	T3	90	0.40	12.0	0.350	30.00	7.24	10.27	1.28	9.97	0.70	0.13	0.70	10.09	11.16
A2	T4	90	0.60	12.0	0.345	20.69	4.41	6.66	1.03	7.30	0.66	0.14	0.60	7.00	8.06
A2	T5	90	0.85	12.0	0.345	20.69	1.98	3.86	0.93	5.84	0.51	0.16	0.34	5.02	5.90
A2	T6	90	0.40	12.0	0.586	20.69	7.13	13.64	1.74	9.92	0.52	0.18	0.52	12.27	10.19
A2	T7	90	0.40	12.0	0.862	20.69	7.54	20.14	1.96	10.45	0.37	0.19	0.37	18.75	12.17
A2	Y1	30	0.40	12.0	0.350	21.00	1.79	2.64	0.94	3.28	0.68	0.29	0.55	2.33	2.45
A2	Y2	60	0.40	12.0	0.350	21.00	4.33	6.81	1.31	6.72	0.64	0.19	0.64	5.61	6.06
A2	Y3	30	0.60	12.0	0.350	21.00	1.51	2.76	0.98	2.99	0.55	0.33	0.51	2.38	2.46
A2	Y4	30	0.40	12.0	0.350	15.00	1.40	2.58	0.87	3.30	0.54	0.26	0.42	1.66	2.12
A2	Y5	30	0.40	12.0	0.350	30.000	2.38	2.98	1.05	3.16	0.80	0.33	0.75	3.33	2.95
A2	Y6	30	0.60	12.0	0.600	21.00	2.45	5.03	1.27	4.21	0.49	0.30	0.49	4.31	2.83
A2	Y7	30	0.60	12.0	0.850	21.00	3.00	7.77	1.69	5.26	0.39	0.32	0.39	6.32	3.14

Ref. A2: Stress concentrations in single - sided welds in offshore tubular joints. OTO 98 044, HSE Publication (Draft), May 1998

Database A7: Y joints under axial loading

Y-Joints
Under In-plane Bending

							Maximum Calculated SCF's				R values			Efthymiou SCF Equations	
Ref No.	Joint Identification	θ	β	α	τ	γ	Chord		Brace		Rchord	Rbrace	Rcrit		
							Internal	External	Internal	External	CH.int CH.ext	BR.int BR.ext	MAX.int MAX.ext	CH	BR
A2	T1	90	0.40	12.0	0.345	20.69	1.57	2.28	0.78	2.53	0.69	0.31	0.62	2.13	2.82
A2	T2	90	0.40	12.0	0.350	15.00	1.33	1.87	0.40	2.24	0.71	0.18	0.59	1.71	2.42
A2	T3	90	0.40	12.0	0.350	30.00	2.02	2.95	1.12	2.90	0.68	0.39	0.68	2.83	3.44
A2	T4	90	0.60	12.0	0.345	20.69	1.61	2.04	0.52	2.31	0.79	0.23	0.70	2.12	2.71
A2	T5	90	0.85	12.0	0.345	20.69	1.61	1.79	0.32	2.09	0.90	0.15	0.77	1.79	2.35
A2	T6	90	0.40	12.0	0.586	20.69	1.86	3.52	0.97	2.70	0.53	0.36	0.53	3.34	3.24
A2	T7	90	0.40	12.0	0.862	20.69	1.70	4.77	0.67	2.63	0.36	0.25	0.36	4.64	3.62
A2	Y1	30	0.40	12.0	0.350	21.00	0.48	2.28	2.85	2.68	0.21	1.06	1.06	1.34	2.72
A2	Y2	60	0.40	12.0	0.350	21.00	1.09	2.06	0.94	2.45	0.53	0.38	0.44	1.97	2.82
A2	Y3	30	0.60	12.0	0.350	21.00	0.16	1.46	1.44	1.66	0.11	0.87	0.87	1.33	2.62
A2	Y4	30	0.40	12.0	0.350	15.00	0.43	1.80	2.51	2.35	0.24	1.07	1.07	1.05	2.70
A2	Y5	30	0.40	12.0	0.350	30.00	1.40	2.81	3.10	2.99	0.50	1.04	1.04	1.74	2.57
A2	Y6	30	0.60	12.0	0.600	21.00	0.11	1.91	2.03	1.40	0.06	1.45	1.06	2.10	3.01
A2	Y7	30	0.60	12.0	0.850	21.00	0.15	2.25	2.31	1.41	0.07	1.64	1.03	2.83	3.31

Ref. A2: Stress concentrations in single - sided welds in offshore tubular joints. OTO 98 044, HSE Publication (Draft), May 1998

Database A8: Y joints under in-plane bending

Y-Joints
Under Out-of-plane Bending

Y-Joints Under Out-of-plane Bending							Maximum Calculated SCF's				R values			Efthymiou SCF Equations			
							Chord		Brace		Rchord	Rbrace	Rcrit	CH		BR	
							Internal	External	Internal	External	CH.int CH.ext	BR.int BR.ext	MAX.int MAX.ext				
Ref No.	Joint Identification	θ	β	α	τ	γ											
A2	T1	90	0.40	12.0	0.345	20.69	3.45	5.37	1.44	5.28	0.64	0.27	0.64	4.66	5.72		
A2	T2	90	0.40	12.0	0.350	15.00	2.43	3.98	0.70	3.82	0.61	0.18	0.61	3.43	4.24		
A2	T3	90	0.40	12.0	0.350	30.00	5.15	7.78	2.72	7.73	0.66	0.35	0.66	6.86	8.20		
A2	T4	90	0.60	12.0	0.345	20.69	3.81	5.65	1.86	6.31	0.67	0.29	0.60	6.31	6.92		
A2	T5	90	0.85	12.0	0.345	20.69	2.59	4.54	1.47	5.92	0.57	0.25	0.44	6.40	6.18		
A2	T6	90	0.40	12.0	0.586	20.69	4.31	8.60	1.82	6.21	0.50	0.29	0.50	7.92	7.30		
A2	T7	90	0.40	12.0	0.862	20.69	4.11	11.97	1.72	6.04	0.34	0.28	0.34	11.65	8.72		
A2	Y1	30	0.40	12.0	0.350	21.00	1.79	2.29	1.40	1.93	0.78	0.73	0.78	1.58	1.93		
A2	Y2	60	0.40	12.0	0.350	21.00	2.94	4.23	1.69	4.25	0.70	0.40	0.69	3.81	4.64		
A2	Y3	30	0.60	12.0	0.350	21.00	2.00	2.56	1.49	2.59	0.78	0.58	0.77	2.14	2.33		
A2	Y4	30	0.40	12.0	0.350	15.00	1.67	2.00	1.40	1.79	0.84	0.78	0.84	1.13	1.40		
A2	Y5	30	0.40	12.0	0.350	30.000	2.04	2.32	1.45	2.11	0.88	0.69	0.88	2.26	2.70		
A2	Y6	30	0.60	12.0	0.600	21.00	1.98	3.62	1.93	2.88	0.55	0.67	0.55	3.67	2.99		
A2	Y7	30	0.60	12.0	0.850	21.00	1.80	4.27	2.15	2.97	0.42	0.72	0.50	5.21	3.51		

Ref. A2: Stress concentrations in single - sided welds in offshore tubular joints. OTO 98 044, HSE Publication (Draft), May 1998

Database A9: Y joints under out-of-plane bending

APPENDIX B
SCF Plots

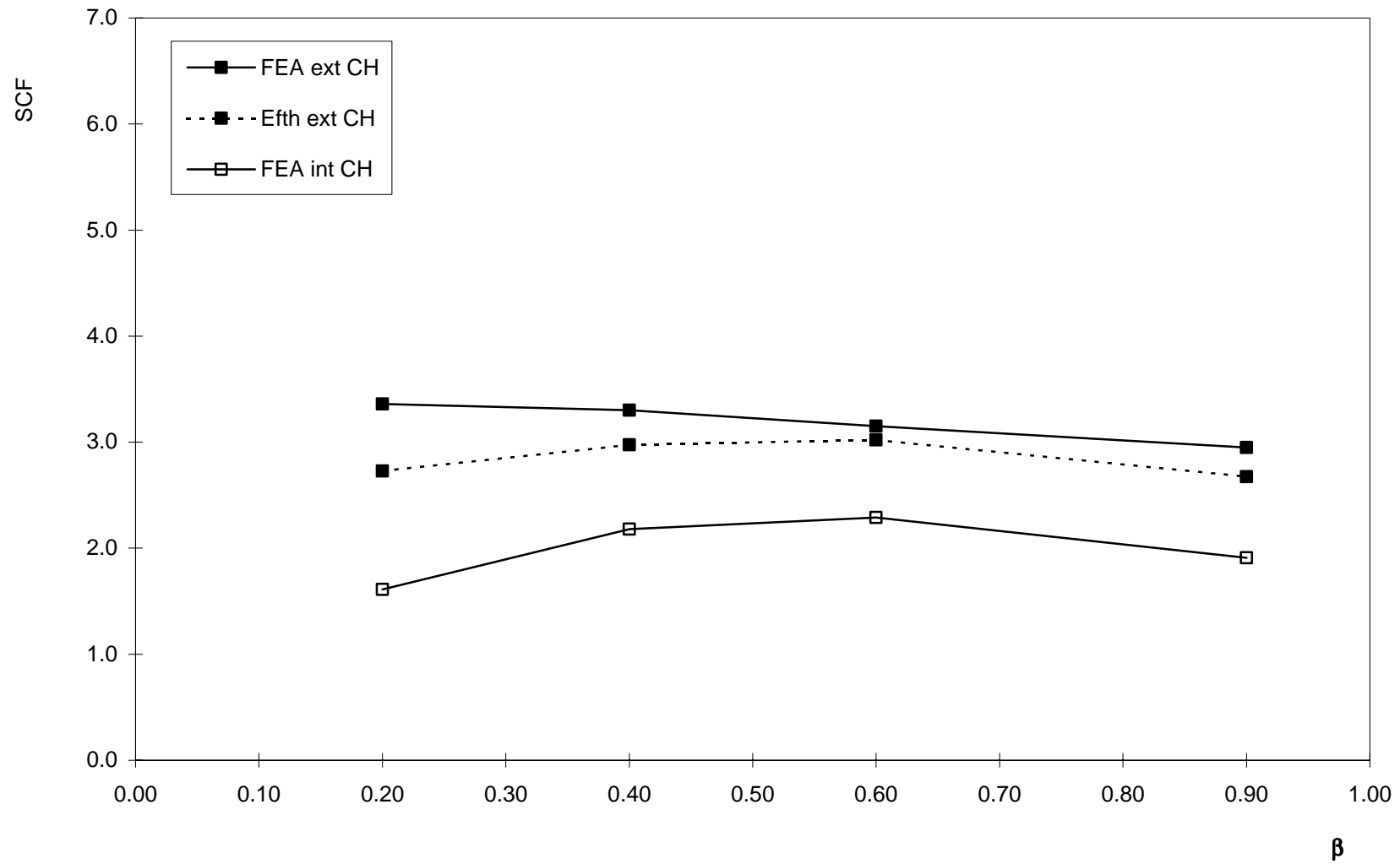


Figure B1: K joints (balanced axial), $\gamma = 18.75$, $\tau = 0.5$, $\zeta = 0.075$, $\theta = 45^\circ$

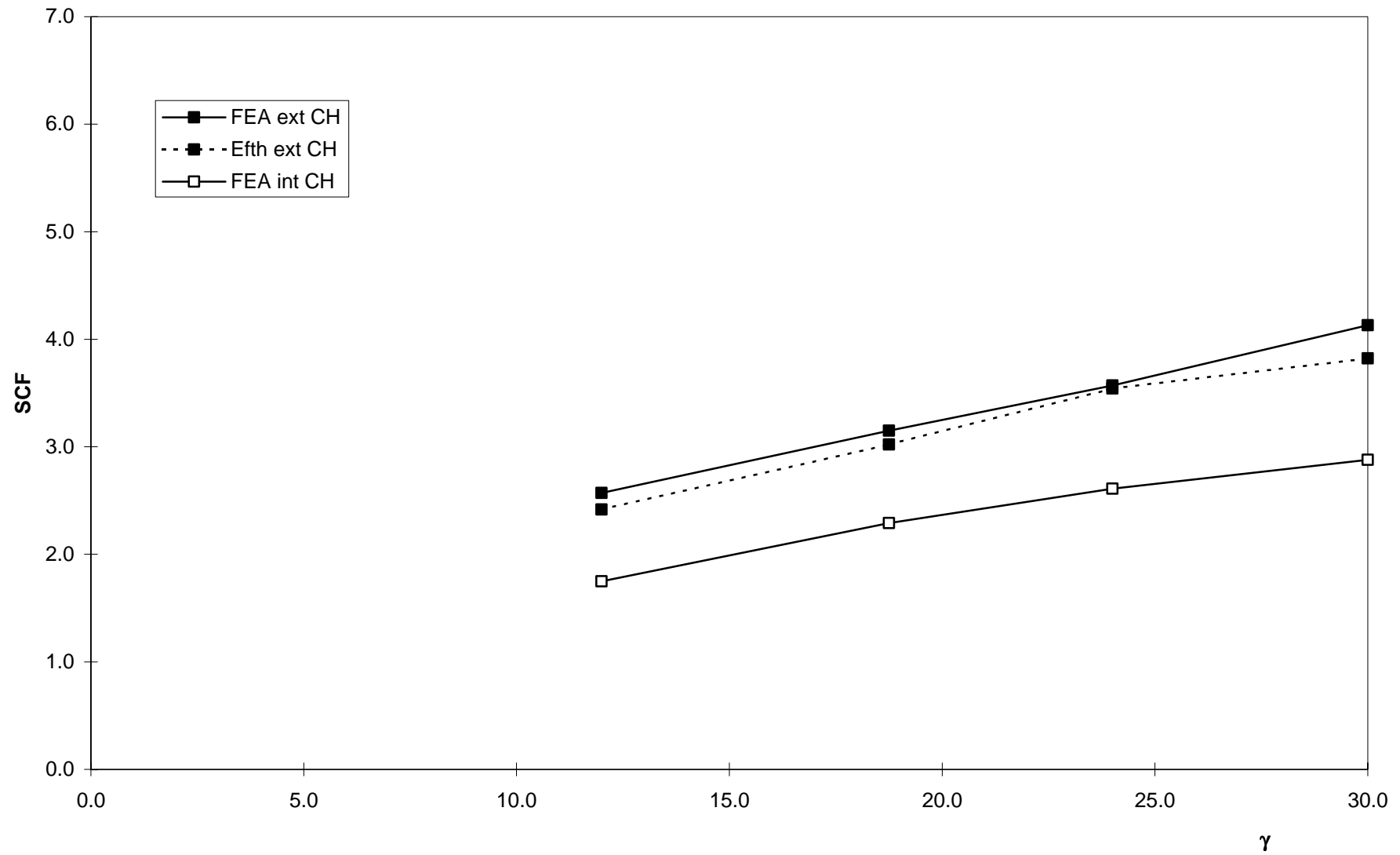


Figure B2: K joints (balanced axial), $\beta = 0.6$, $\tau = 0.5$, $\zeta = 0.075$, $\theta = 45^\circ$

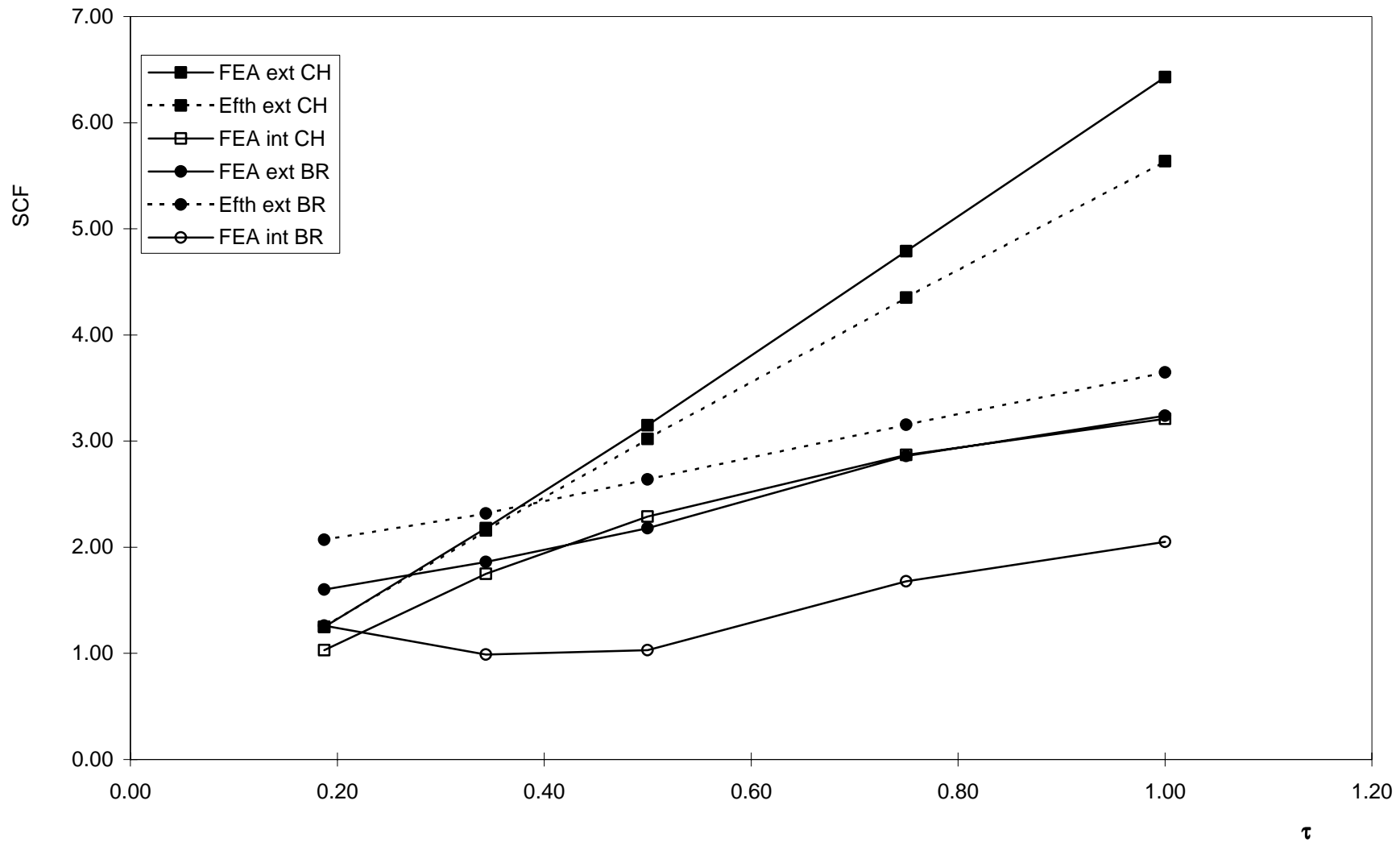


Figure B3: K joints (balanced axial), $\beta = 0.6$, $\gamma = 18.75$, $\zeta = 0.075$, $\theta = 45^\circ$

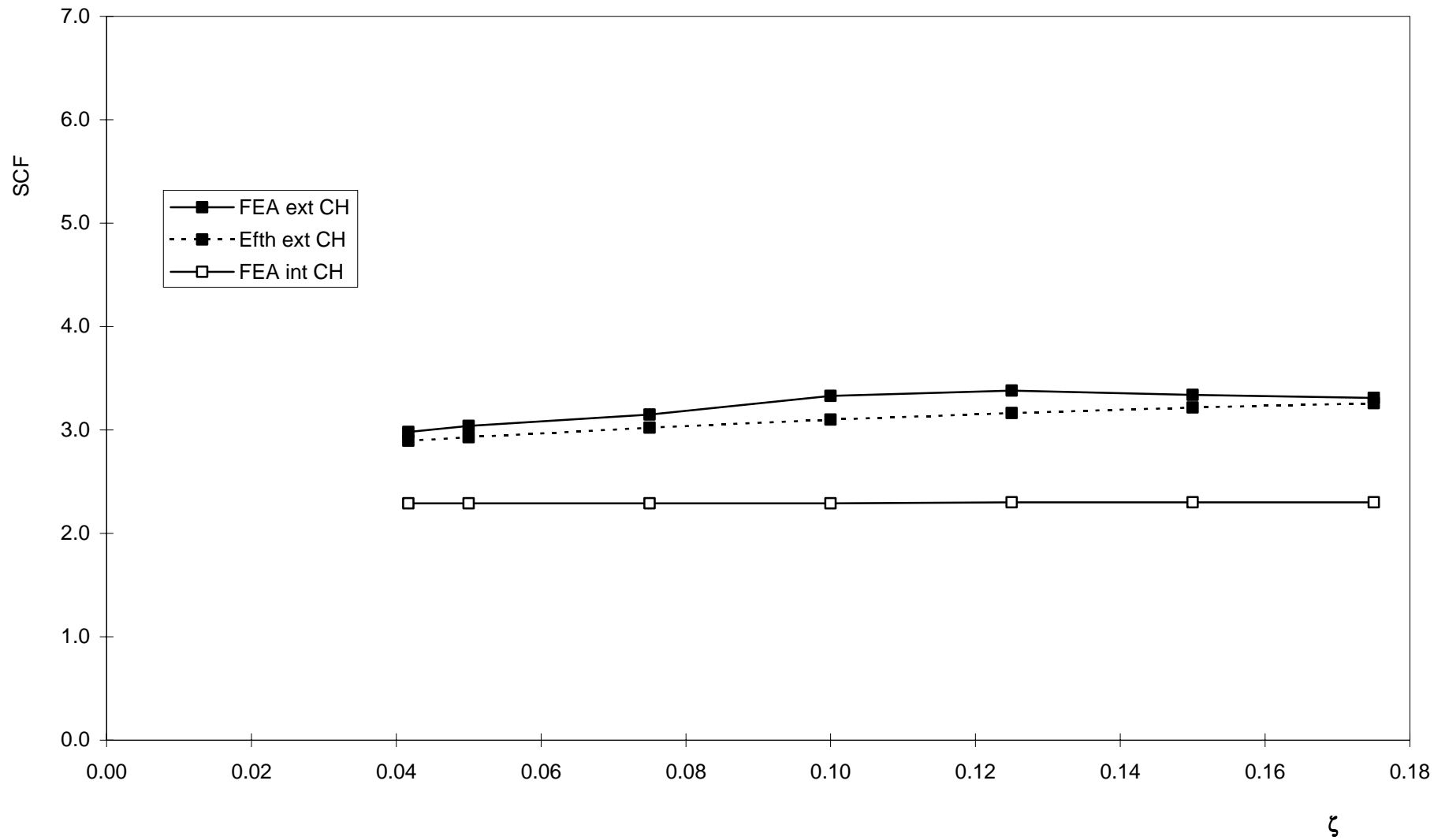


Figure B4: K joints (balanced axial), $\beta = 0.6$, $\gamma = 18.75$, $\tau = 0.5$, $\theta = 45^\circ$

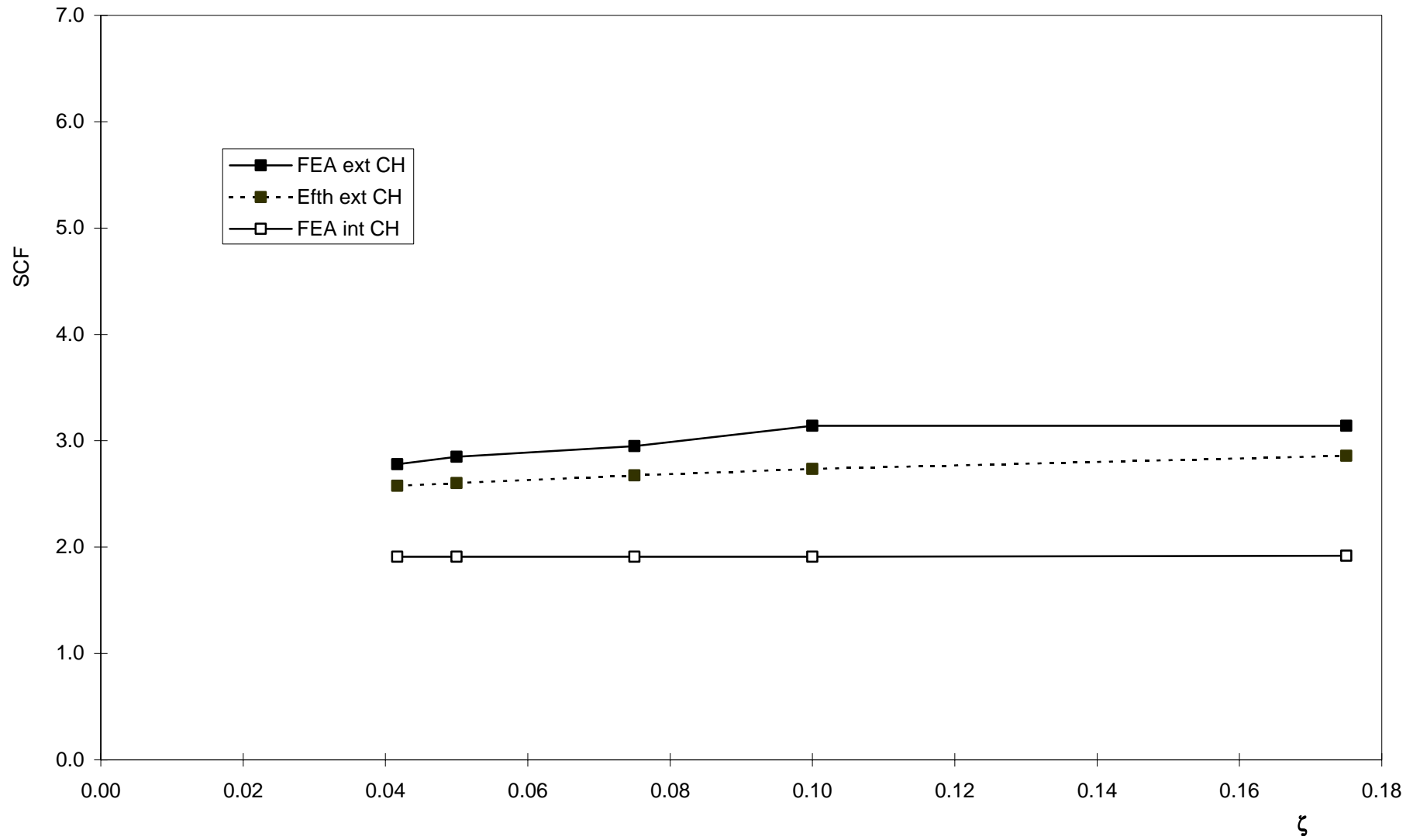


Figure B5: K joints (balanced axial), $\beta = 0.9$, $\gamma = 18.75$, $\tau = 0.5$, $\theta = 45^\circ$

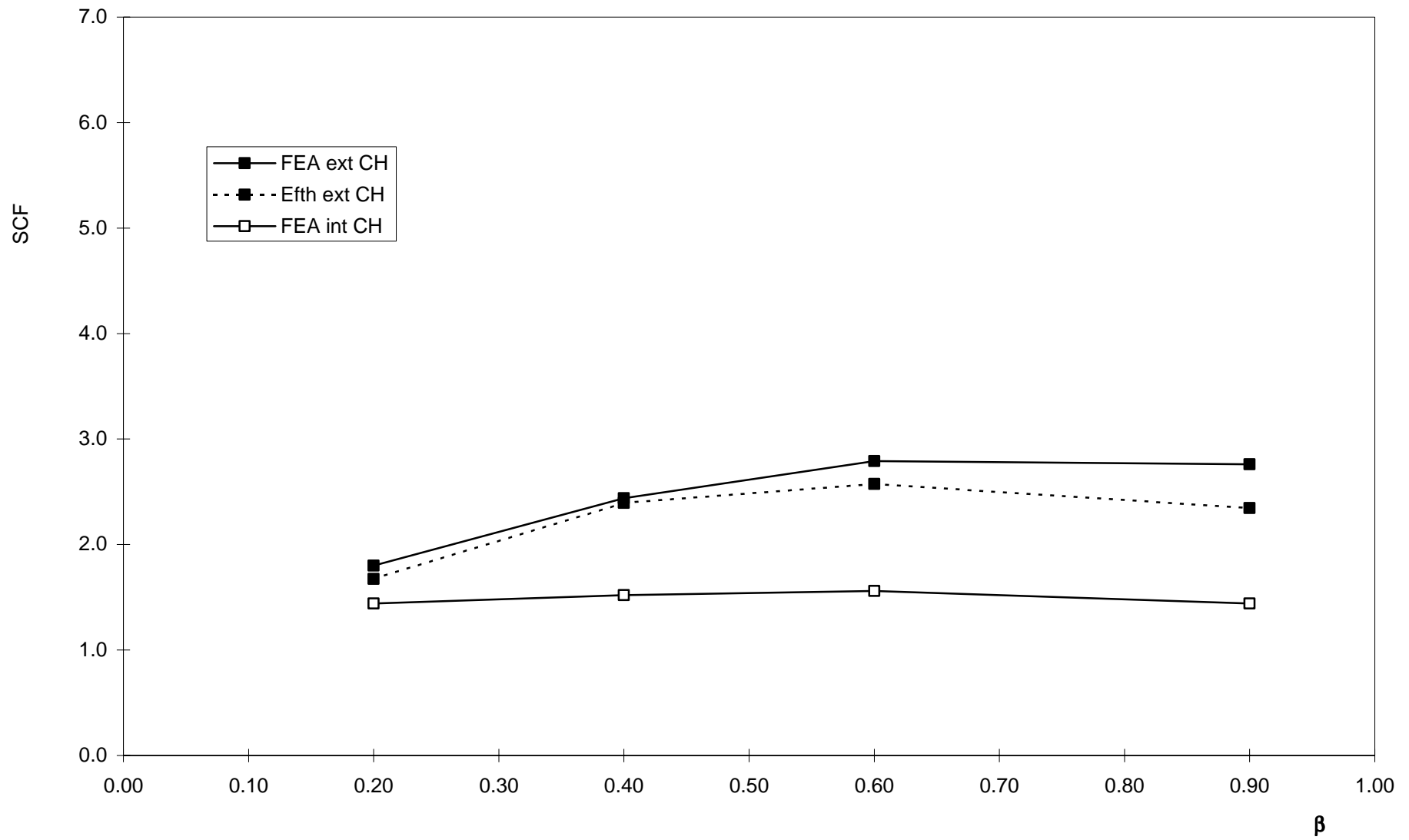


Figure B6: K joints (IPB), $\gamma = 18.75$, $\tau = 0.5$, $\zeta = 0.075$, $\theta = 45^\circ$

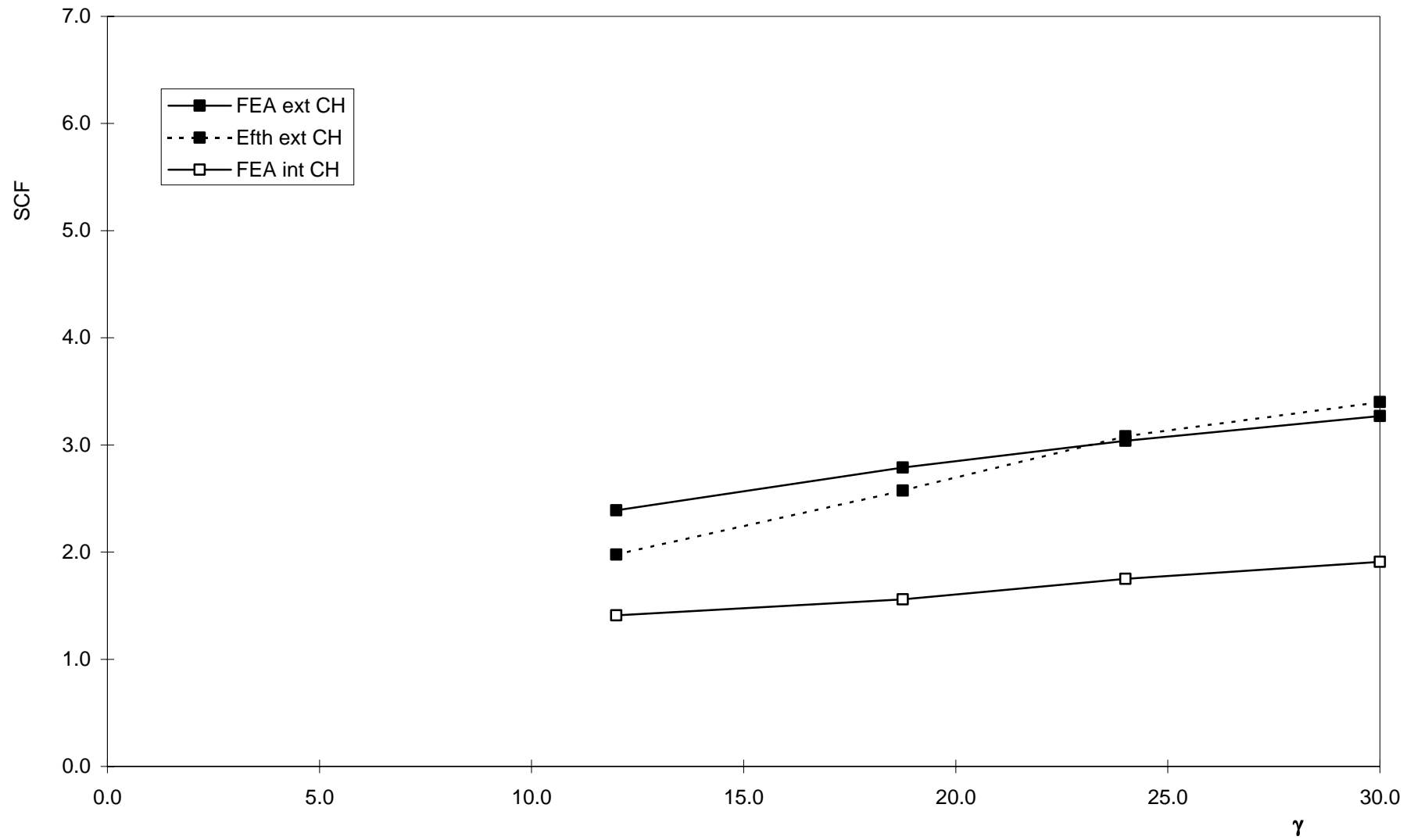


Figure B7: K joints (IPB), $\beta = 0.6$, $\tau = 0.5$, $\zeta = 0.075$, $\theta = 45^\circ$

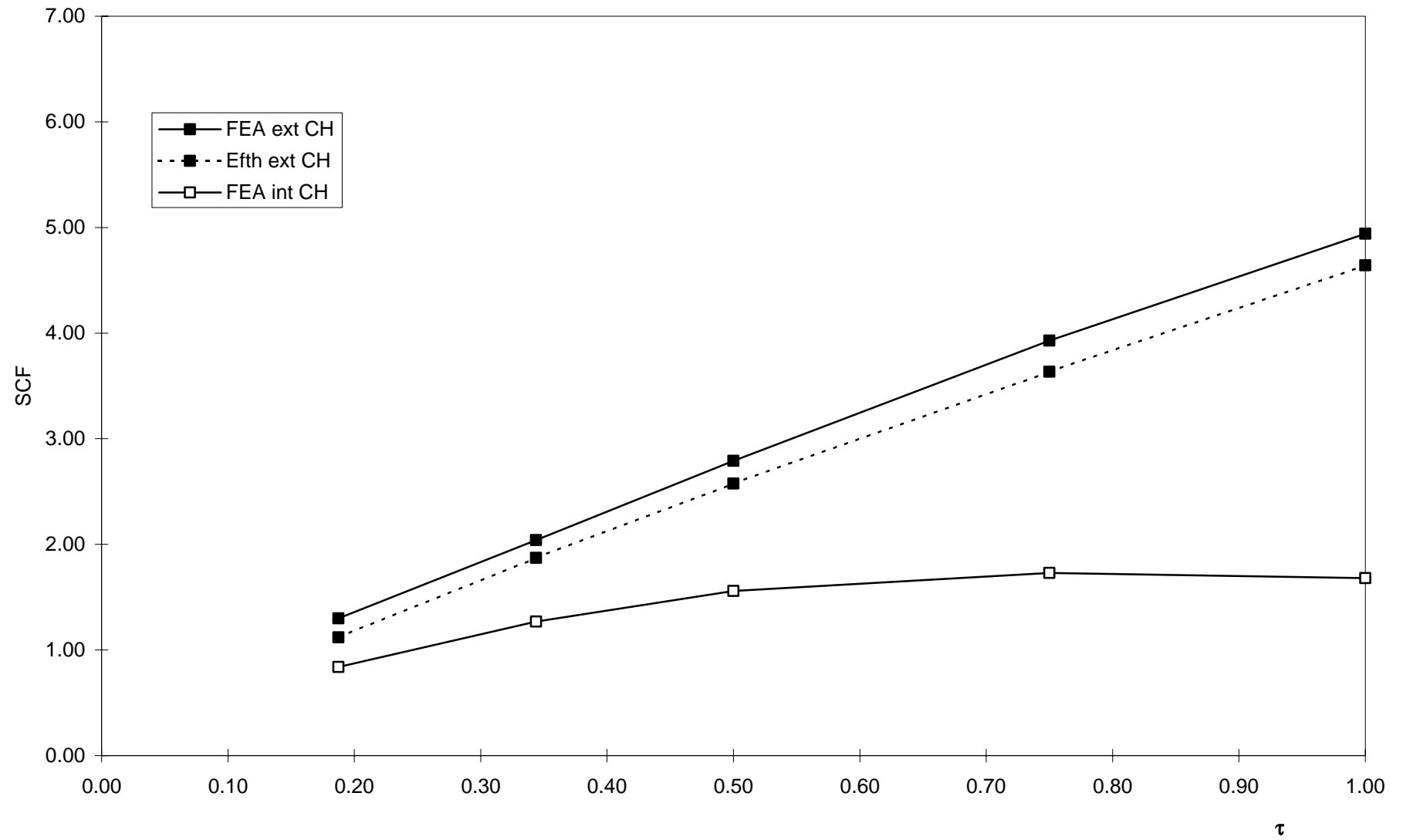


Figure B8: K joints (IPB), $\beta = 0.6$, $\gamma = 18.75$, $\zeta = 0.075$, $\theta = 45^\circ$

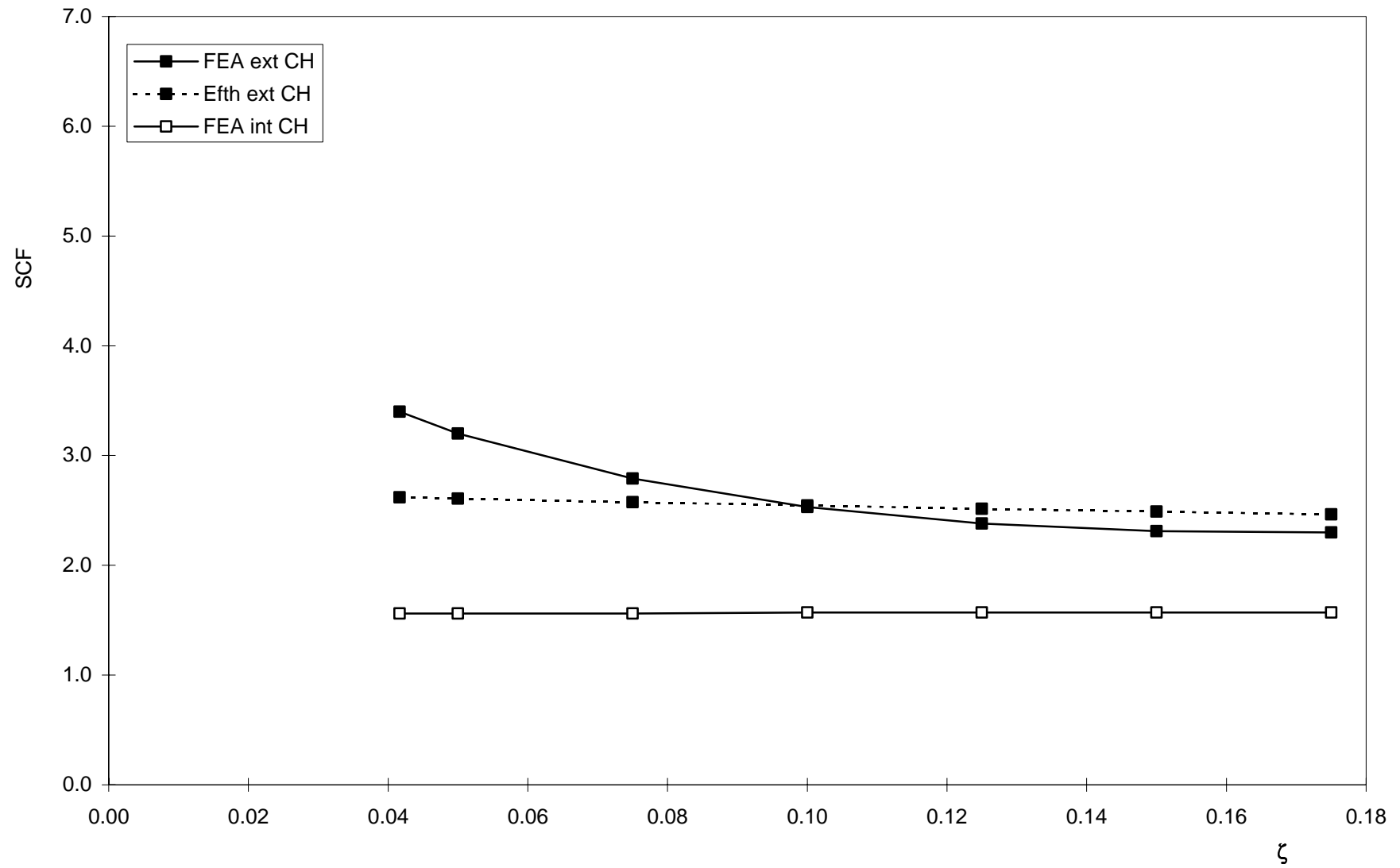


Figure B9: K joints (IPB), $\beta = 0.6$, $\gamma = 18.75$, $\tau = 0.5$, $\theta = 45^\circ$

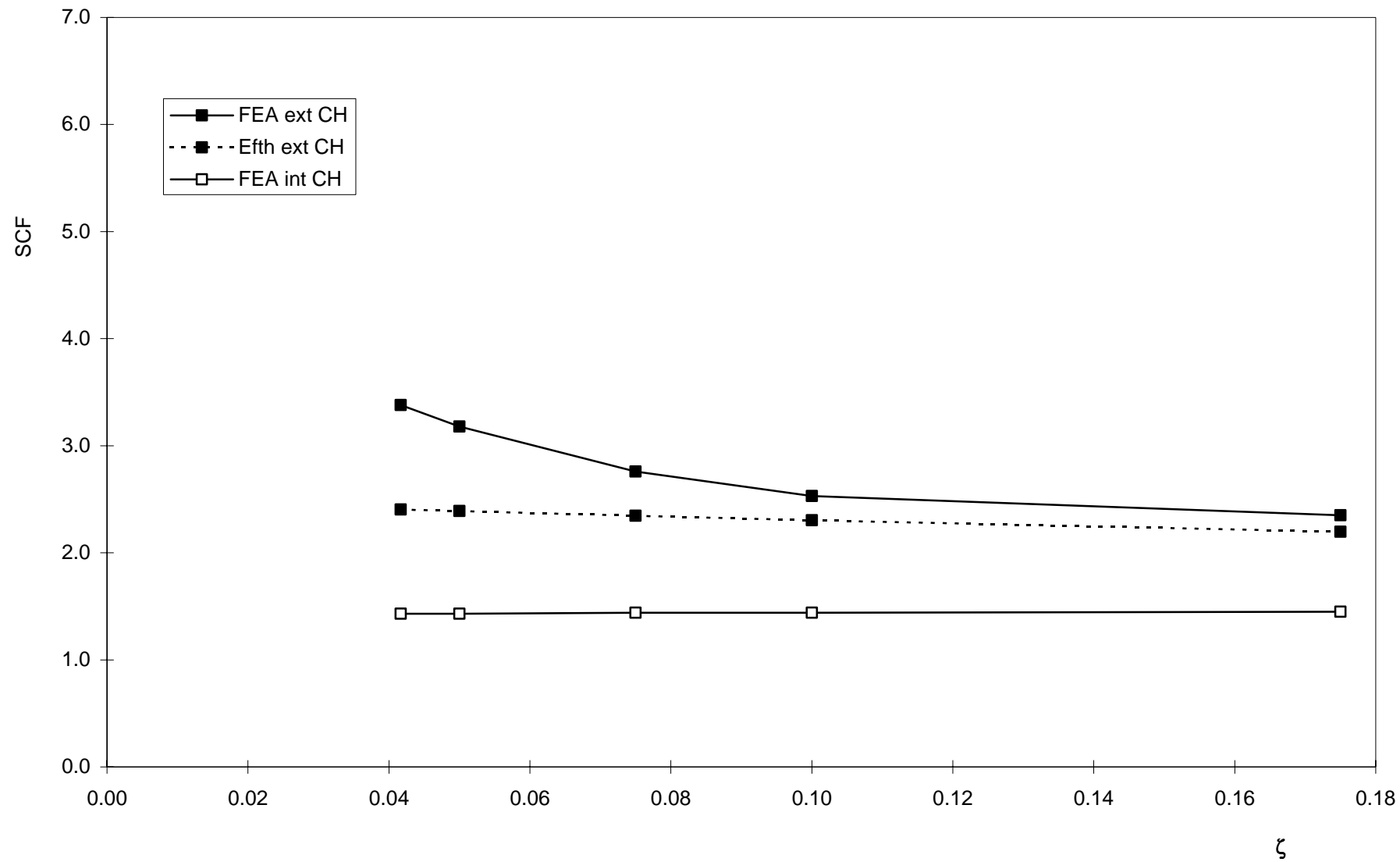


Figure B10: K joints (IPB), $\beta = 0.9$, $\gamma = 18.75$, $\tau = 0.5$, $\theta = 45^\circ$

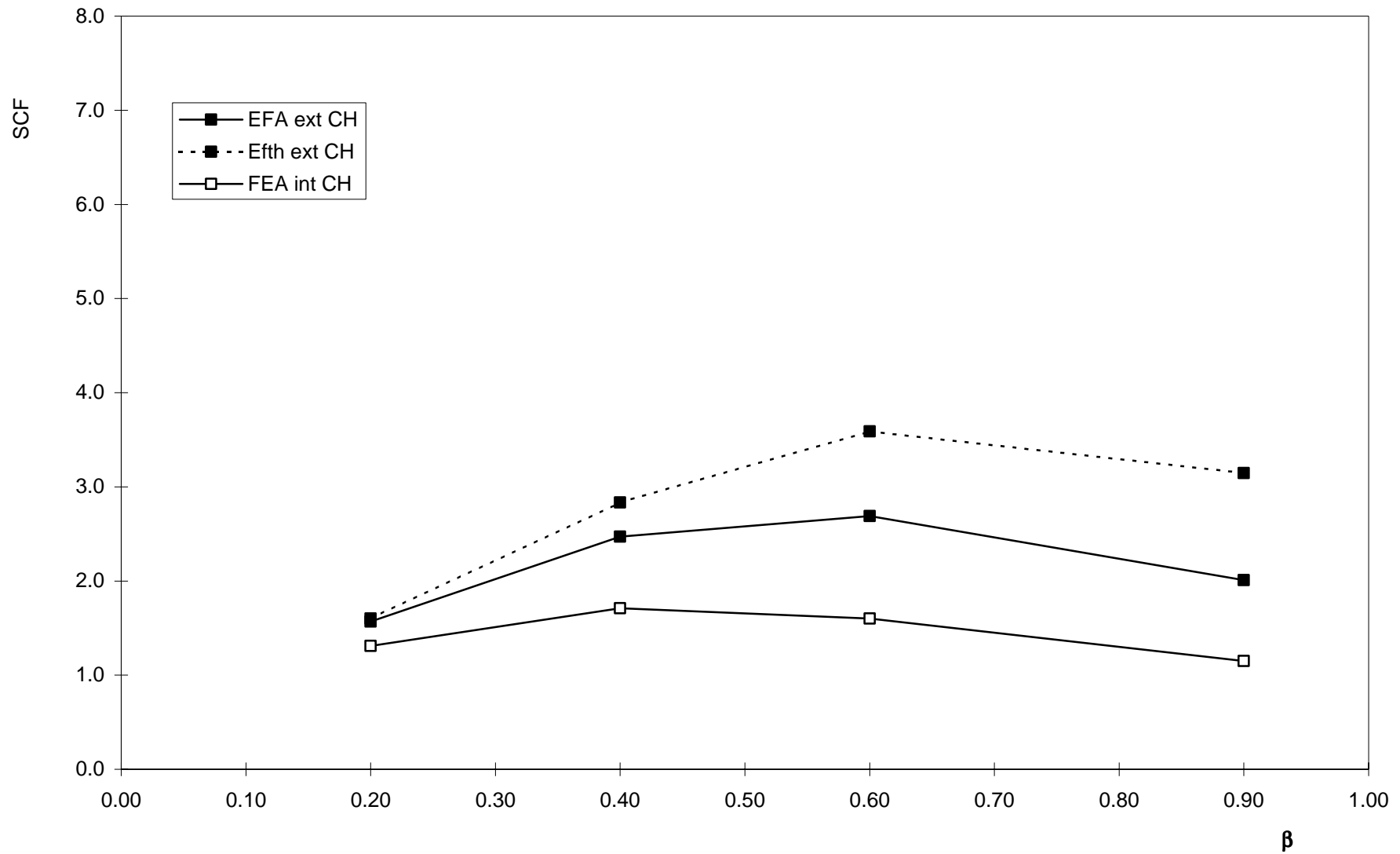


Figure B11: K joints (OPB), $\gamma = 18.75$, $\tau = 0.5$, $\zeta = 0.075$, $\theta = 45^\circ$

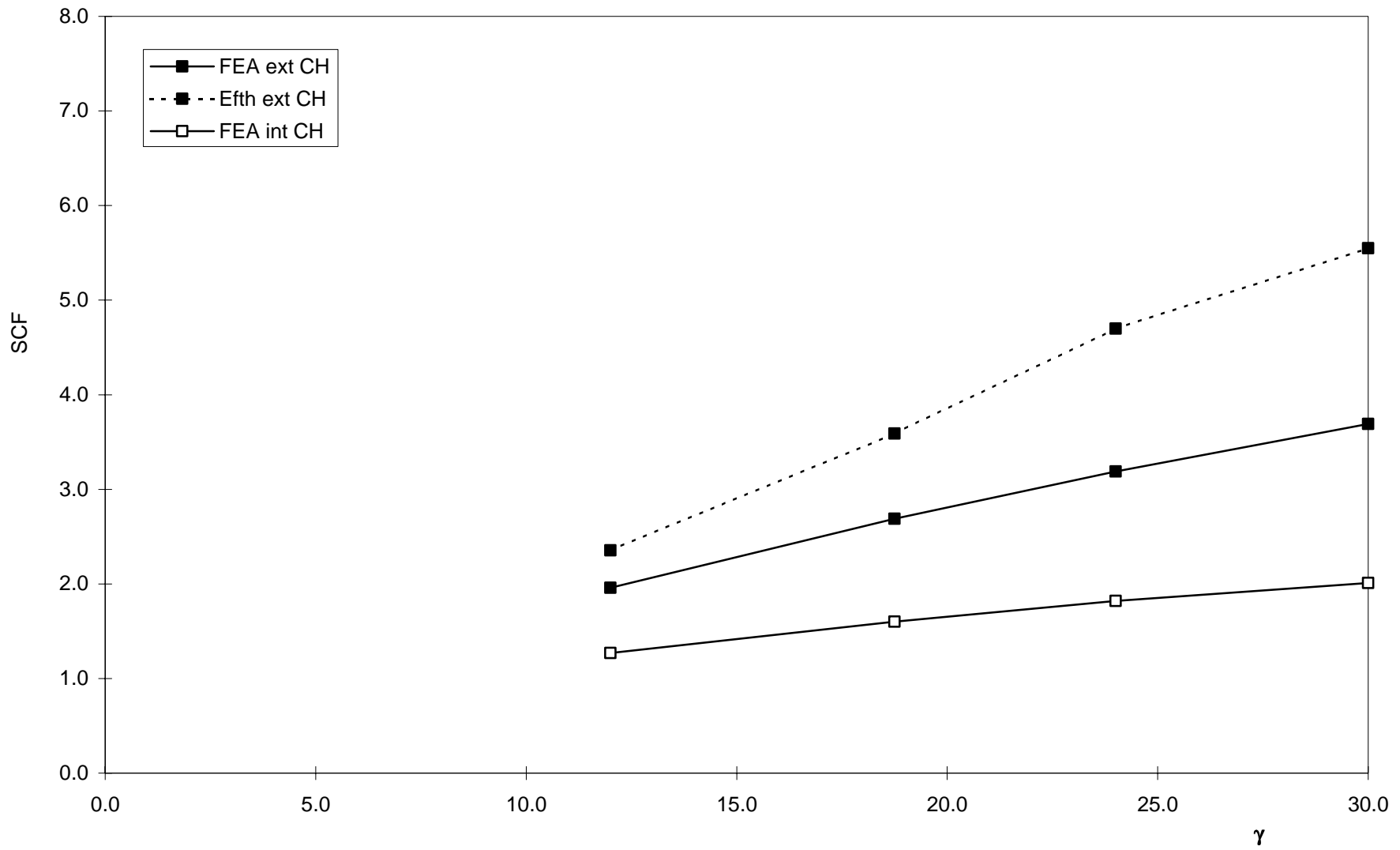


Figure B12: K joints (OPB), $\beta = 0.6$, $\tau = 0.5$, $\zeta = 0.075$, $\theta = 45^\circ$

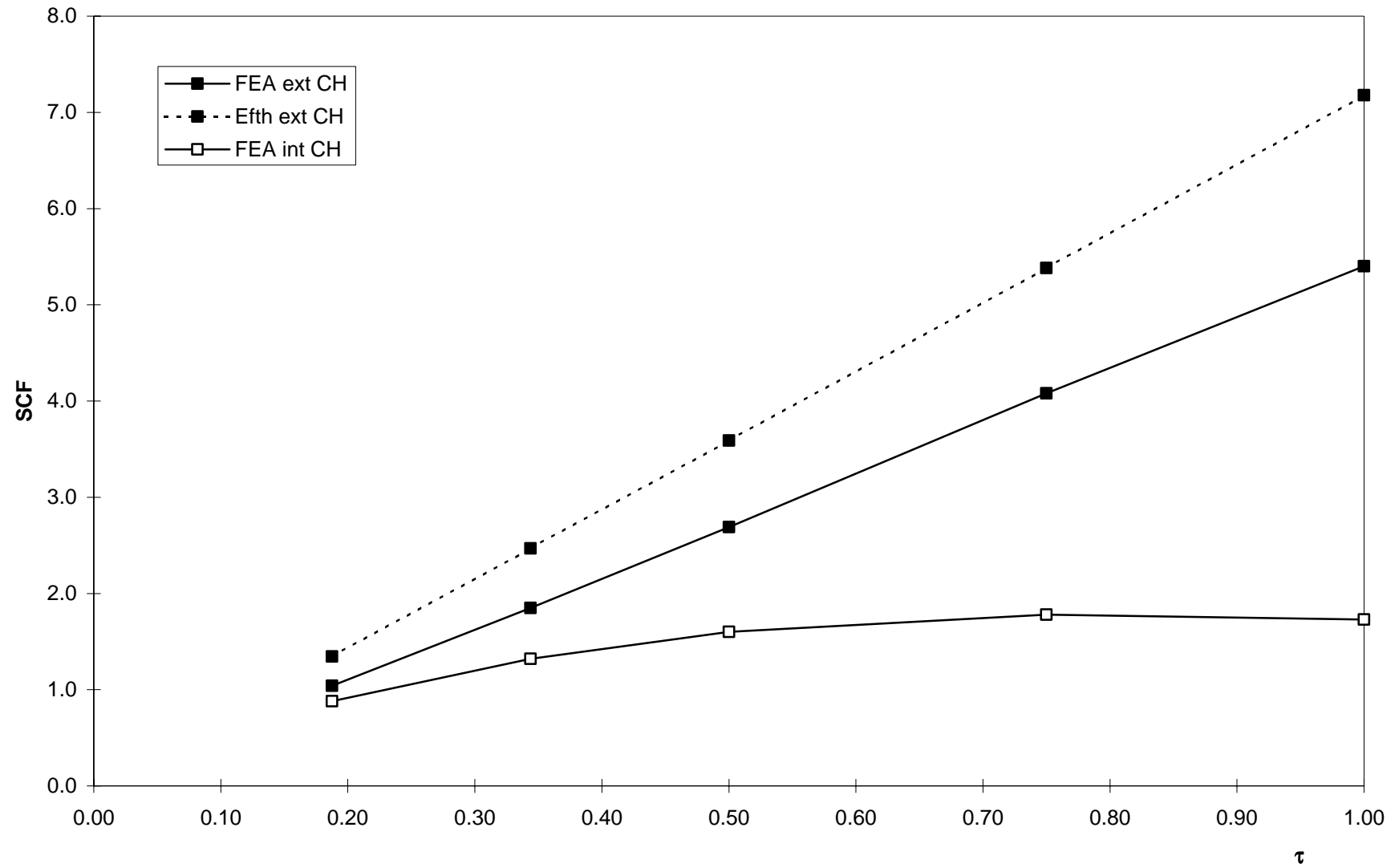


Figure B13: K joints (OPB), $\beta = 0.6$, $\gamma = 18.75$, $\zeta = 0.075$, $\theta = 45^\circ$

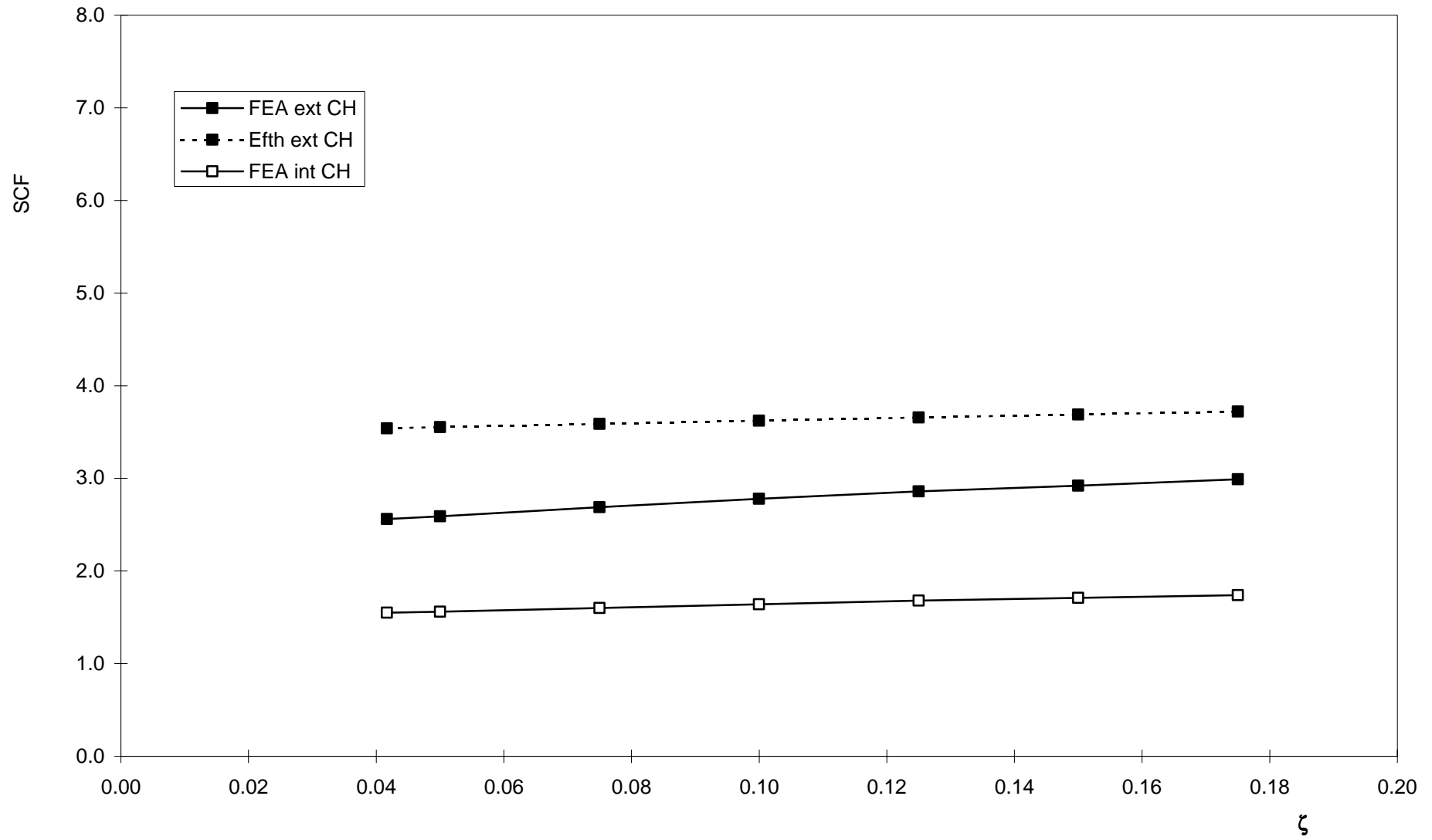


Figure B14: K joints (OPB), $\beta = 0.6, \gamma = 18.75, \tau = 0.5, \theta = 45^\circ$

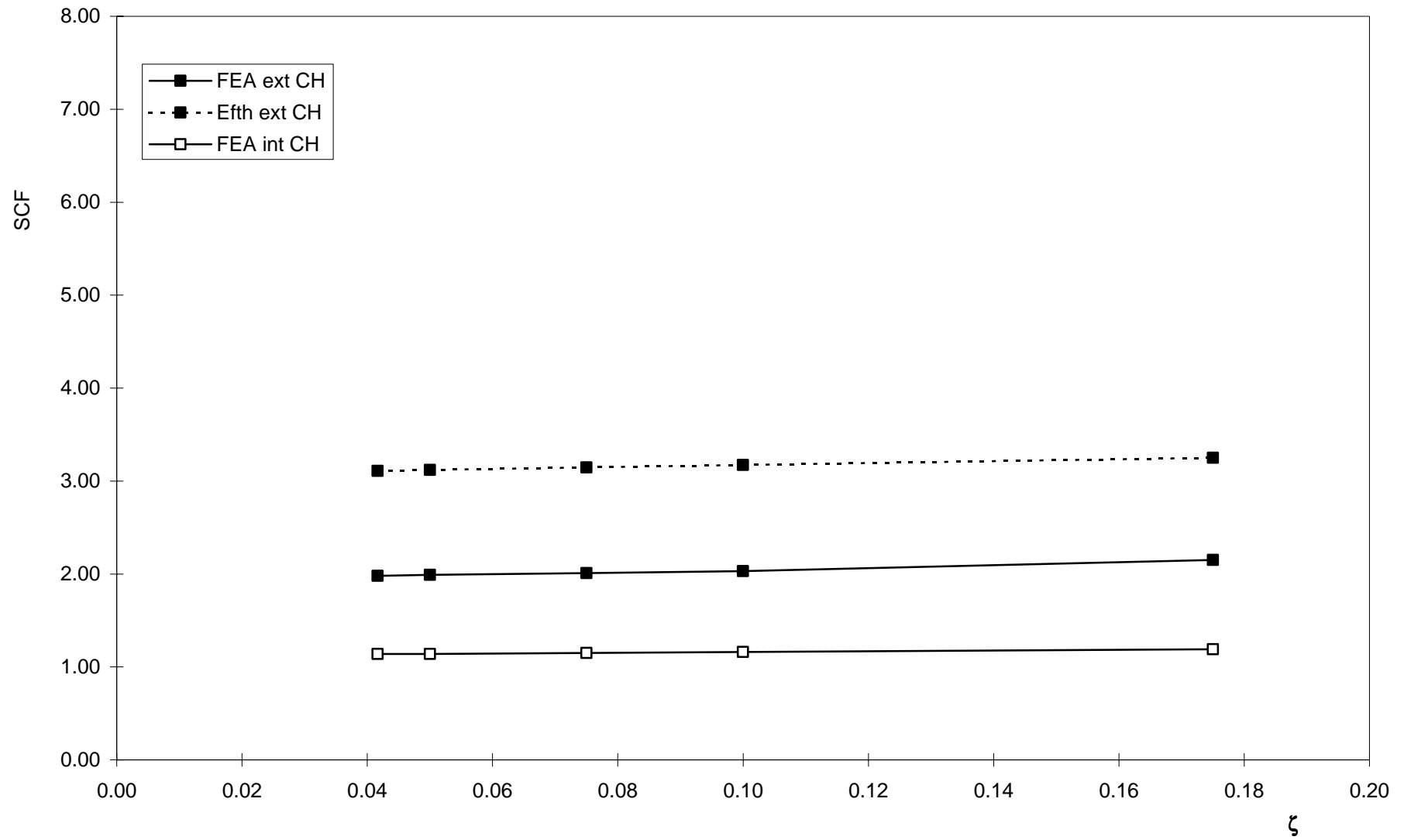


Figure B15: K joints (OPB), $\beta = 0.9$, $\gamma = 18.75$, $\tau = 0.5$, $\theta = 45^\circ$

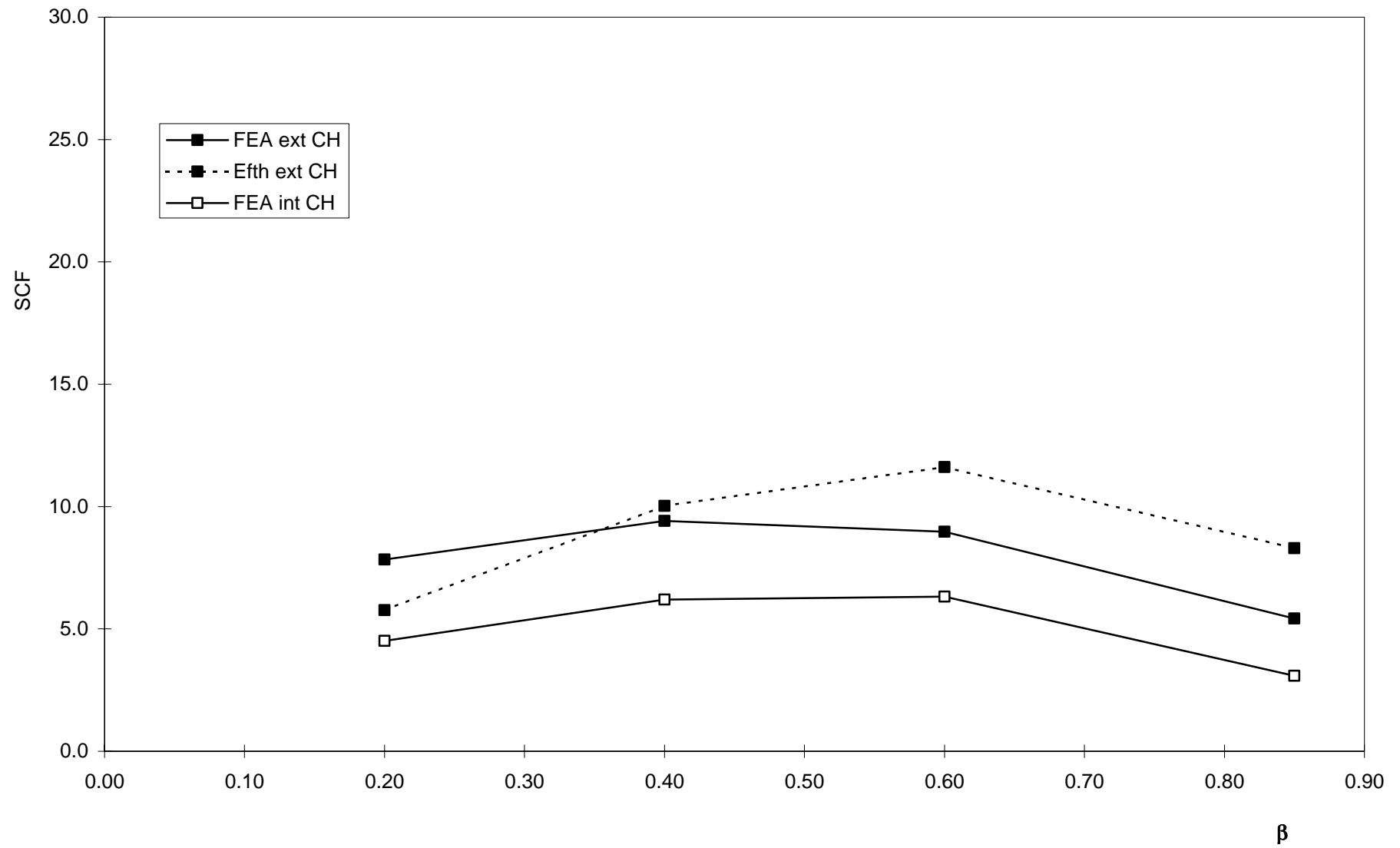


Figure B16: X joints (axially loaded tension), $\gamma = 21$, $\tau = 0.35$, $\theta = 90^\circ$

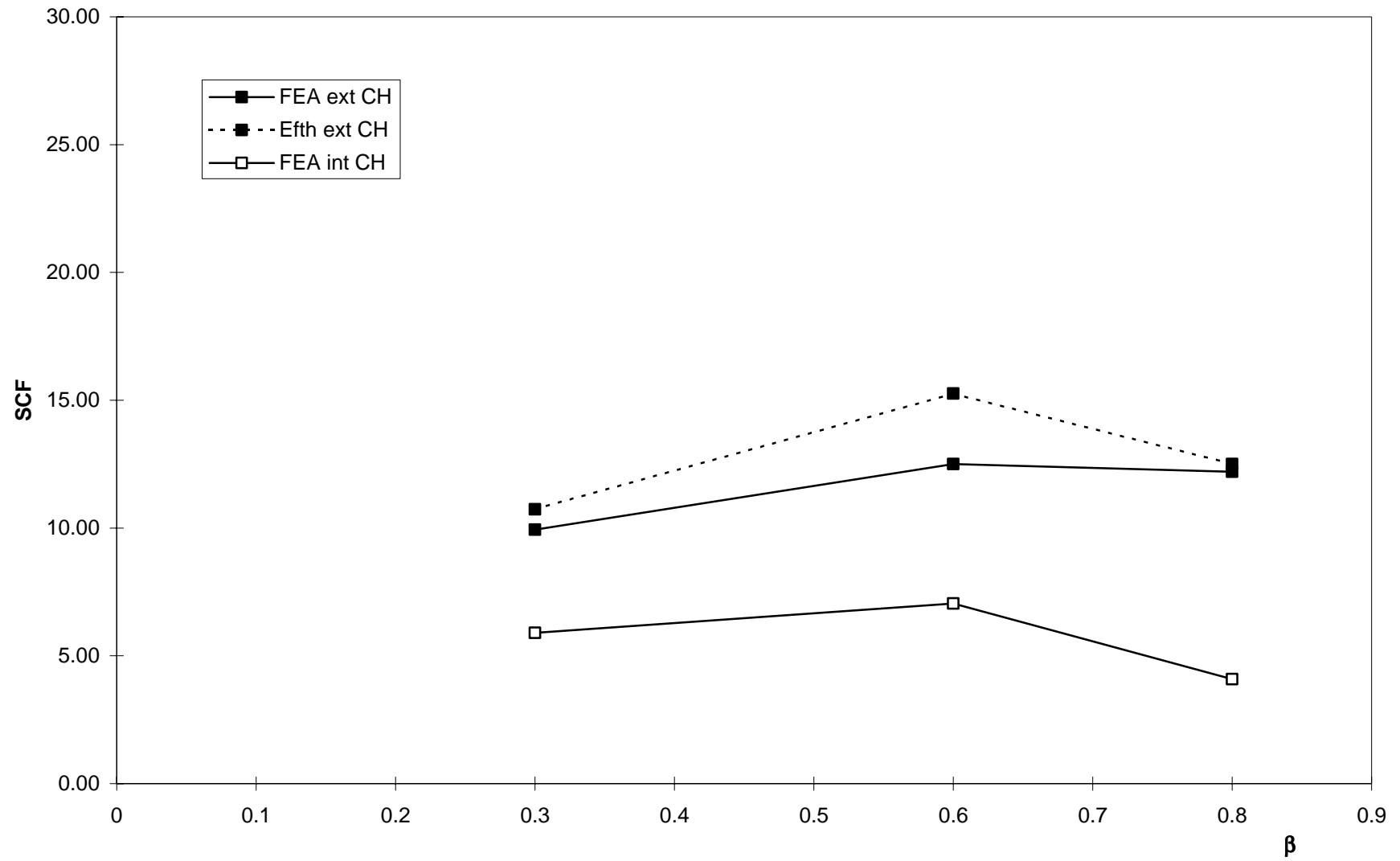


Figure B17: X joints (axially loaded compression), $\gamma = 18.75$, $\tau = 0.5$, $\theta = 90^\circ$

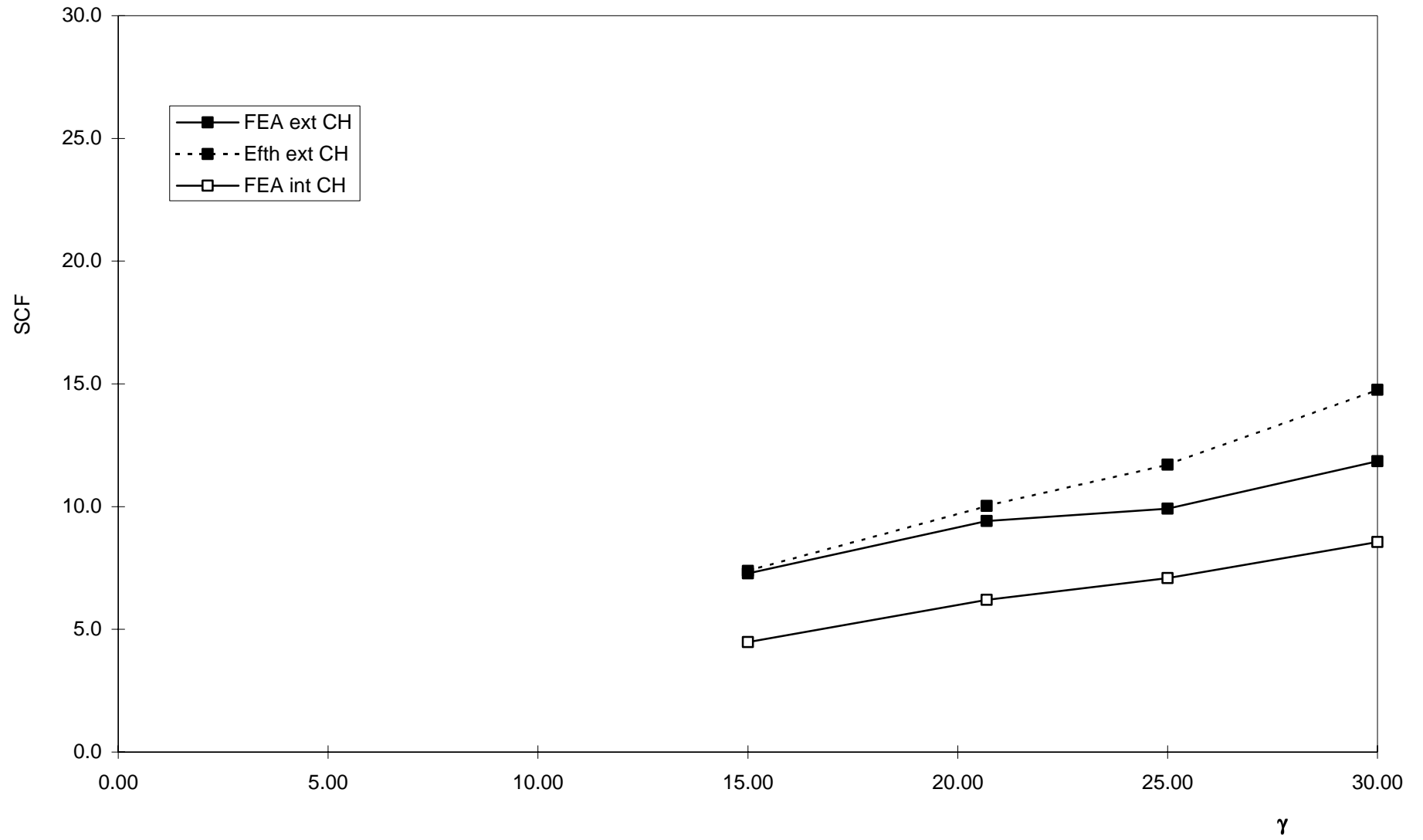


Figure B18: X joints (axially loaded tension), $\beta = 0.4$, $\tau = 0.35$, $\theta = 90^\circ$

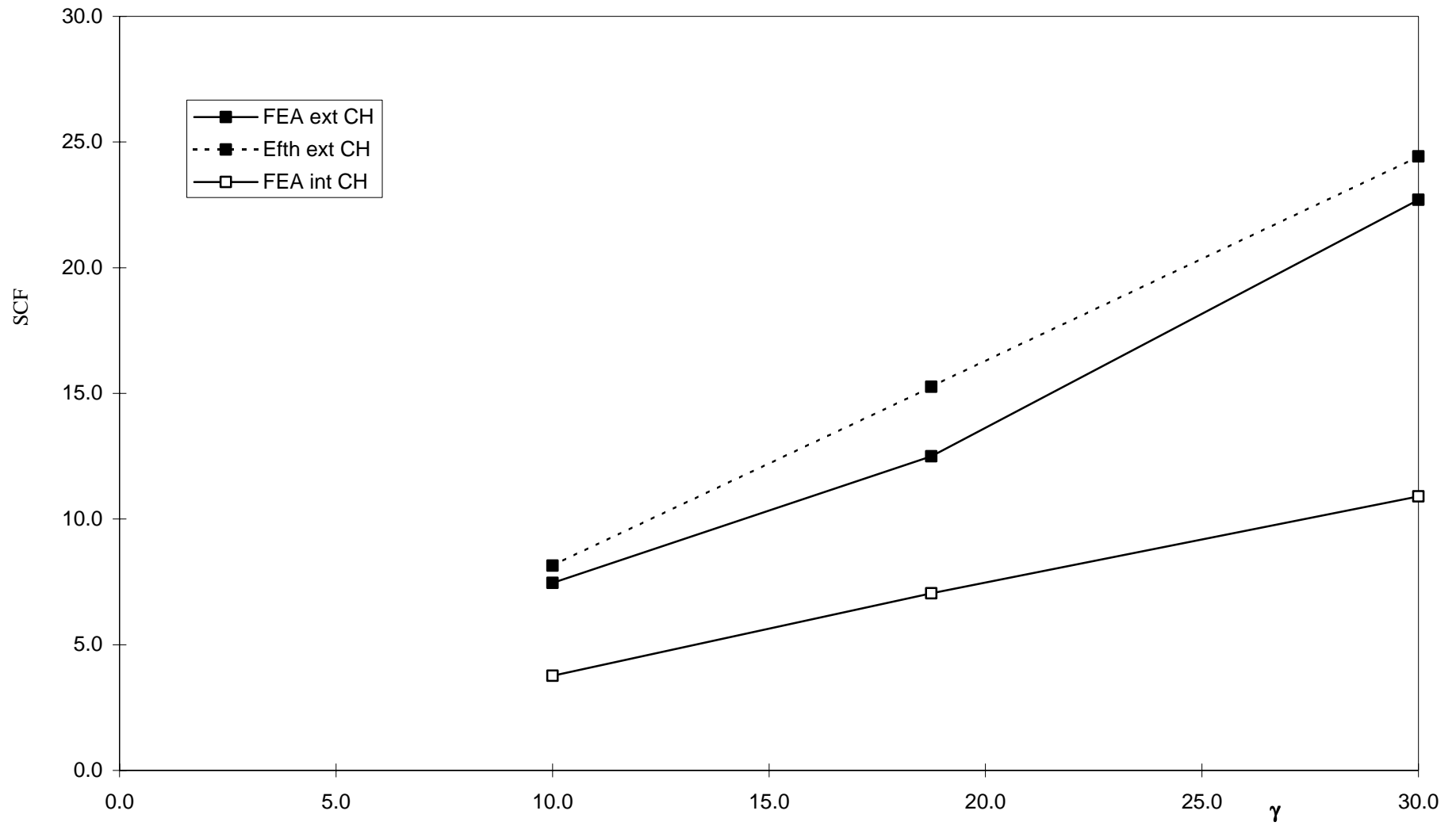


Figure B19: X joints (axially loaded compression), $\beta = 0.6$, $\tau = 0.5$, $\theta = 90^\circ$

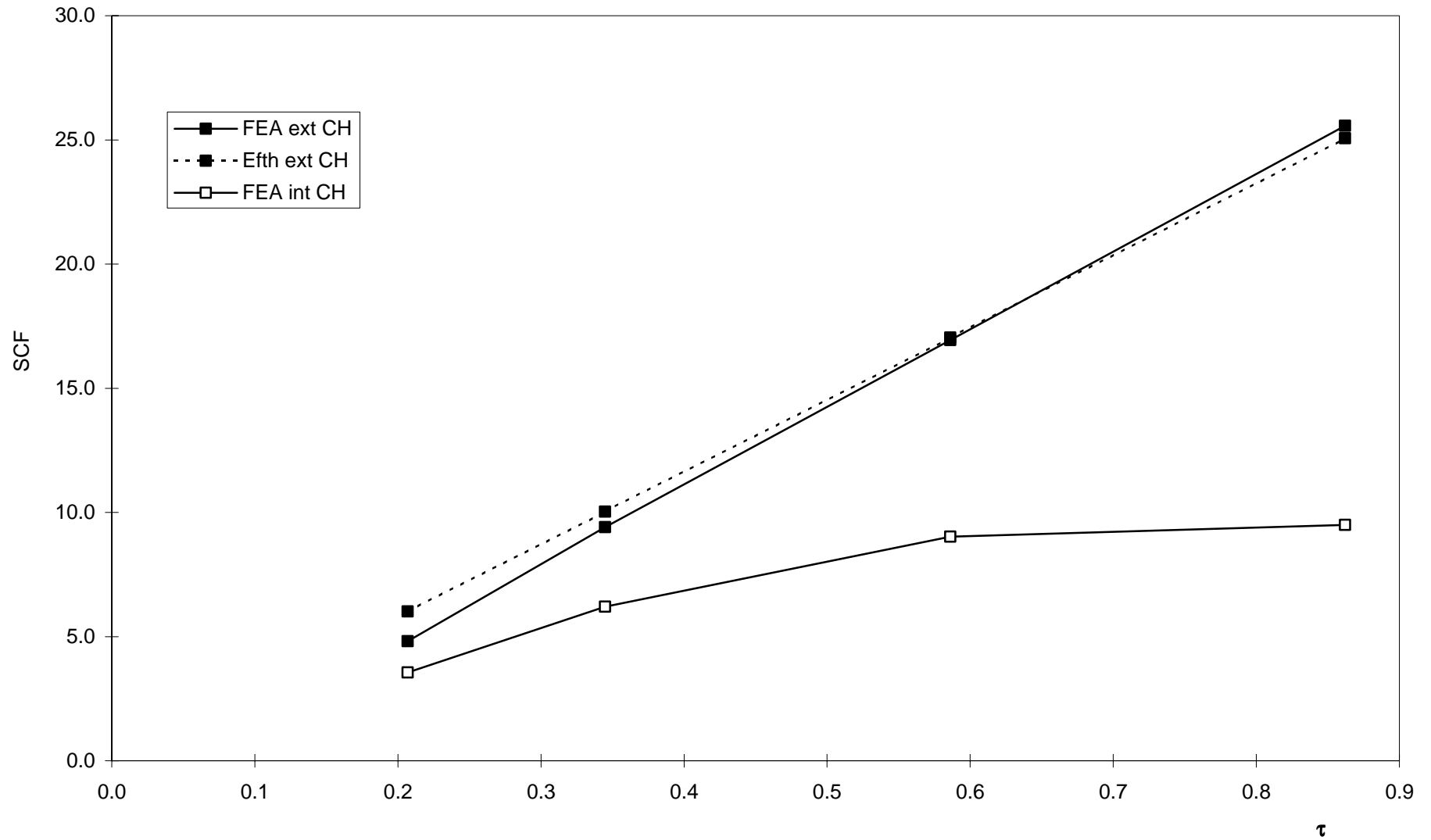


Figure B20: X joints (axially loaded tension), $\beta = 0.4$, $\gamma = 21$, $\theta = 90^\circ$

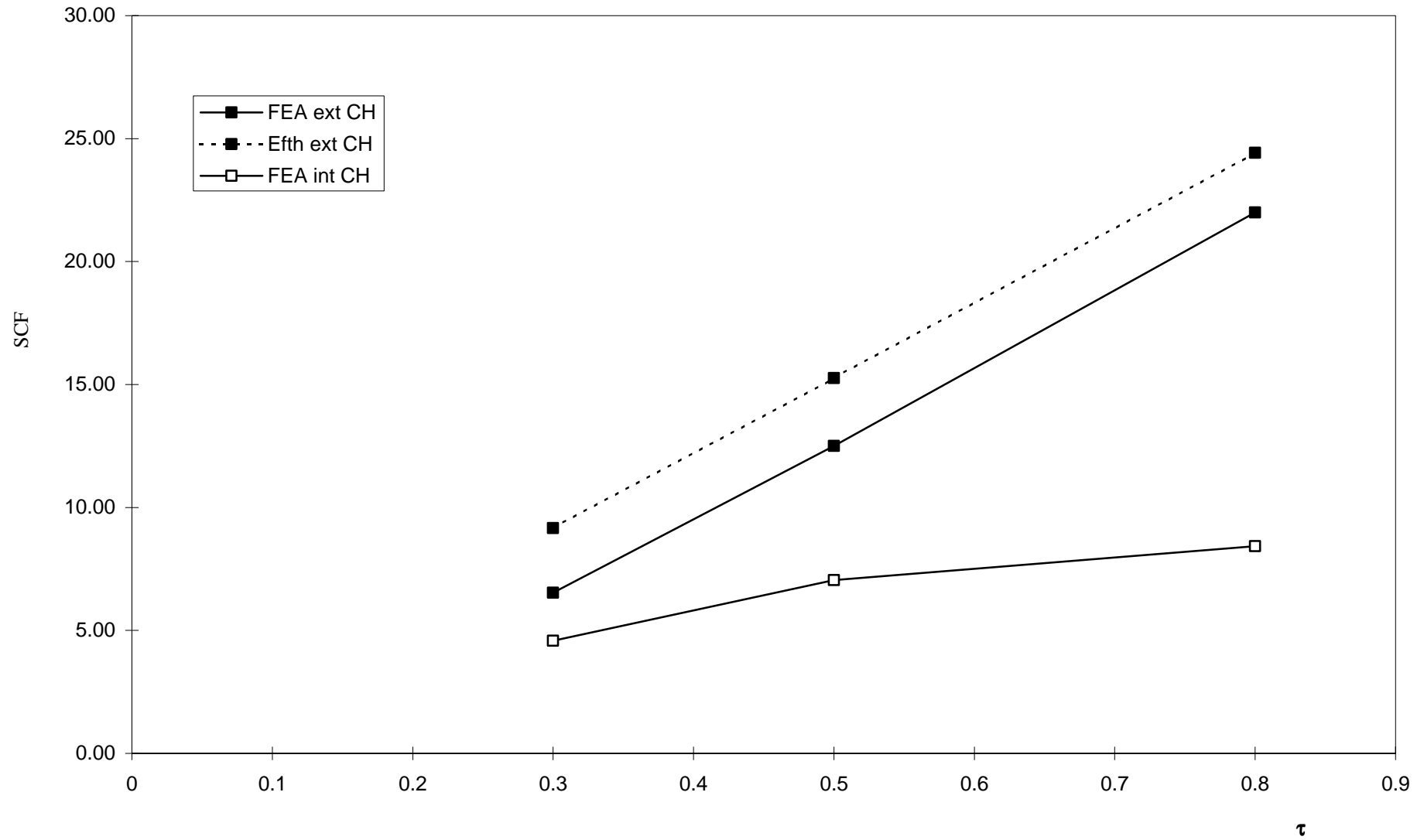


Figure B21: X joints (axially loaded compression), $\beta = 0.6$, $\gamma = 18.75$, $\theta = 90^\circ$

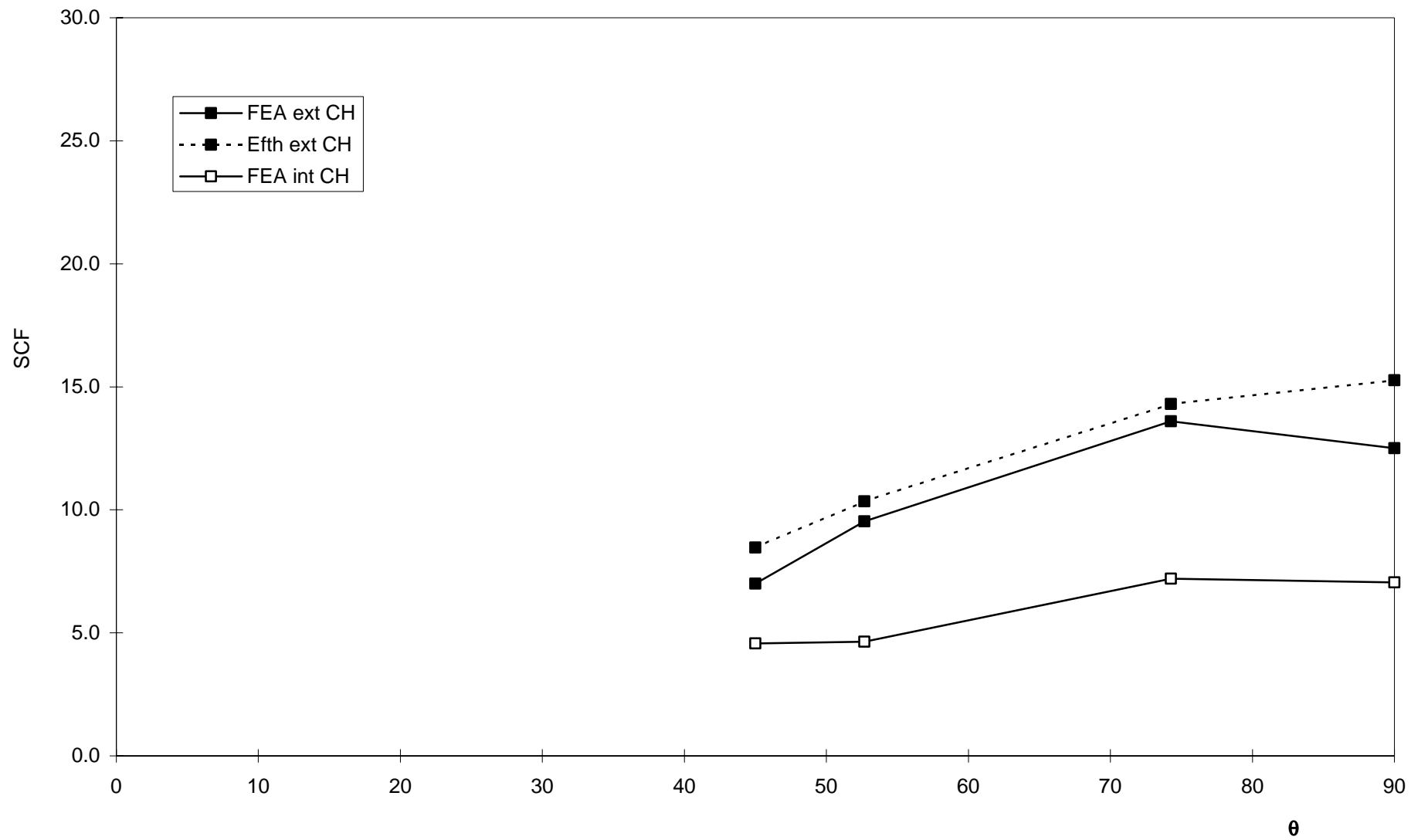


Figure B22: X joints (axially loaded compression), $\beta = 0.6$, $\gamma = 18.75$, $\tau = 0.5$

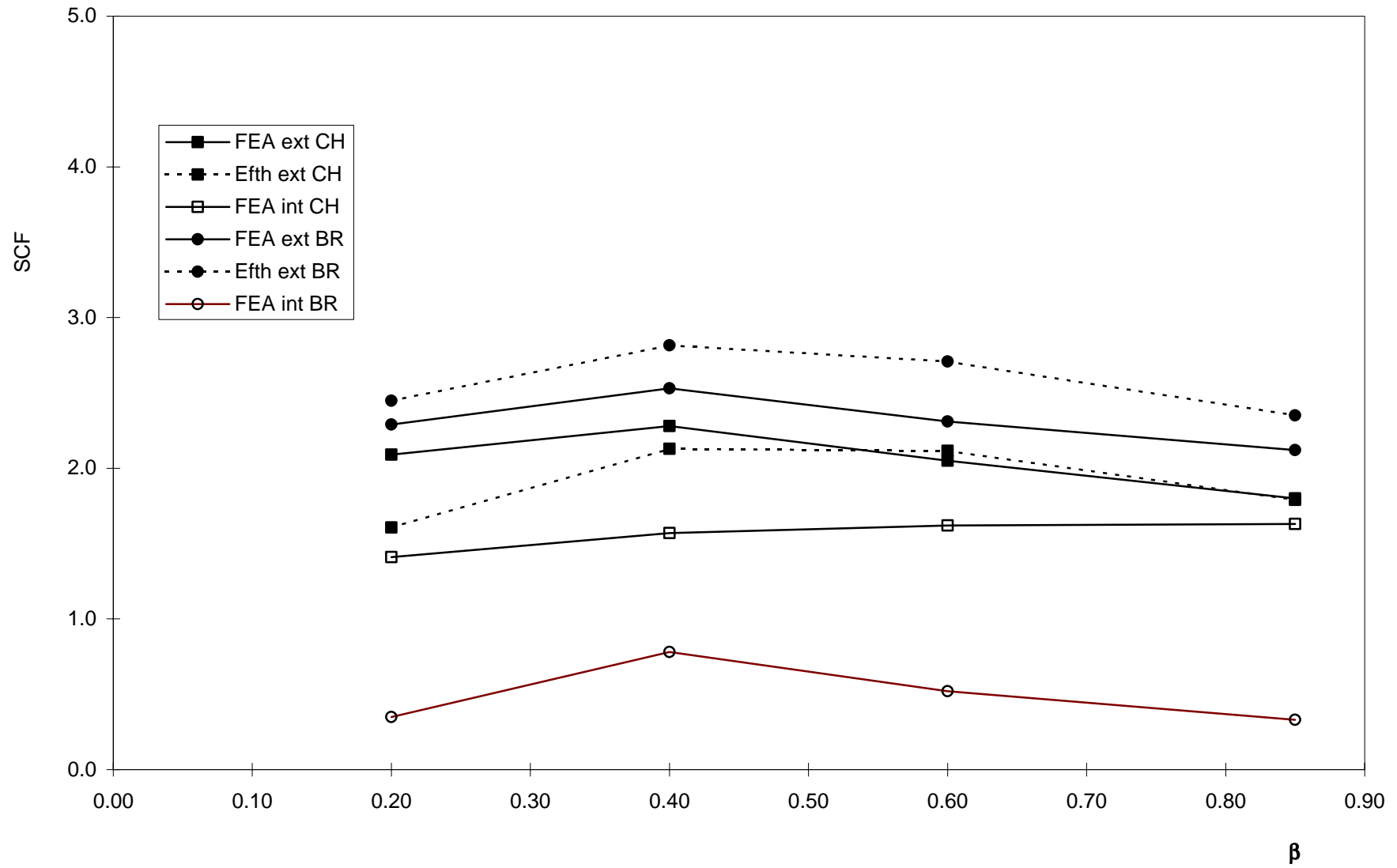


Figure B23: X joints (IPB), $\gamma = 21$, $\tau = 0.35$, $\theta = 90^\circ$

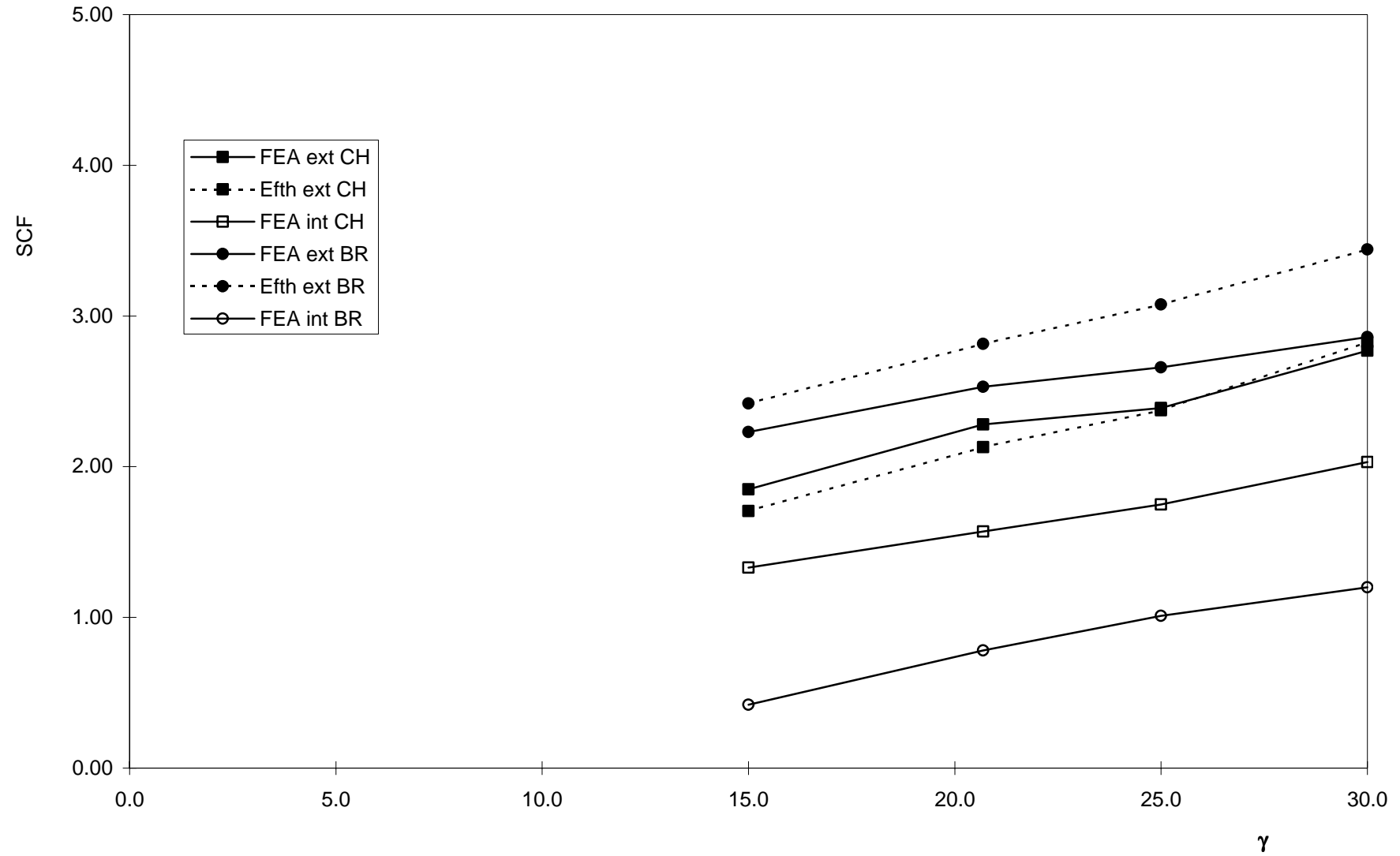


Figure B24: X joints (IPB), $\beta = 0.4$, $\tau = 0.35$, $\theta = 90^\circ$

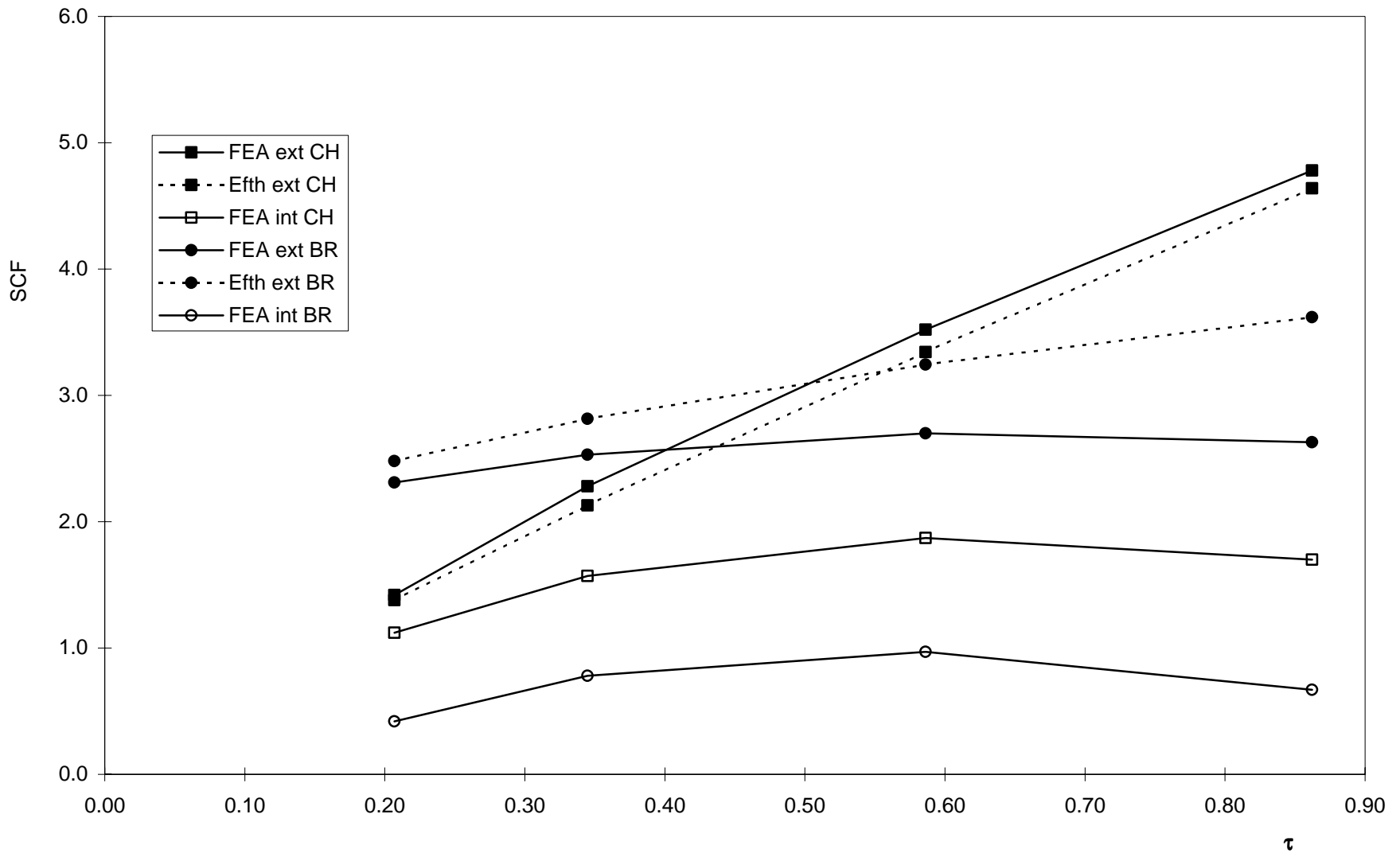


Figure B25: X joints (IPB), $\beta = 0.4$, $\gamma = 21$, $\theta = 90^\circ$

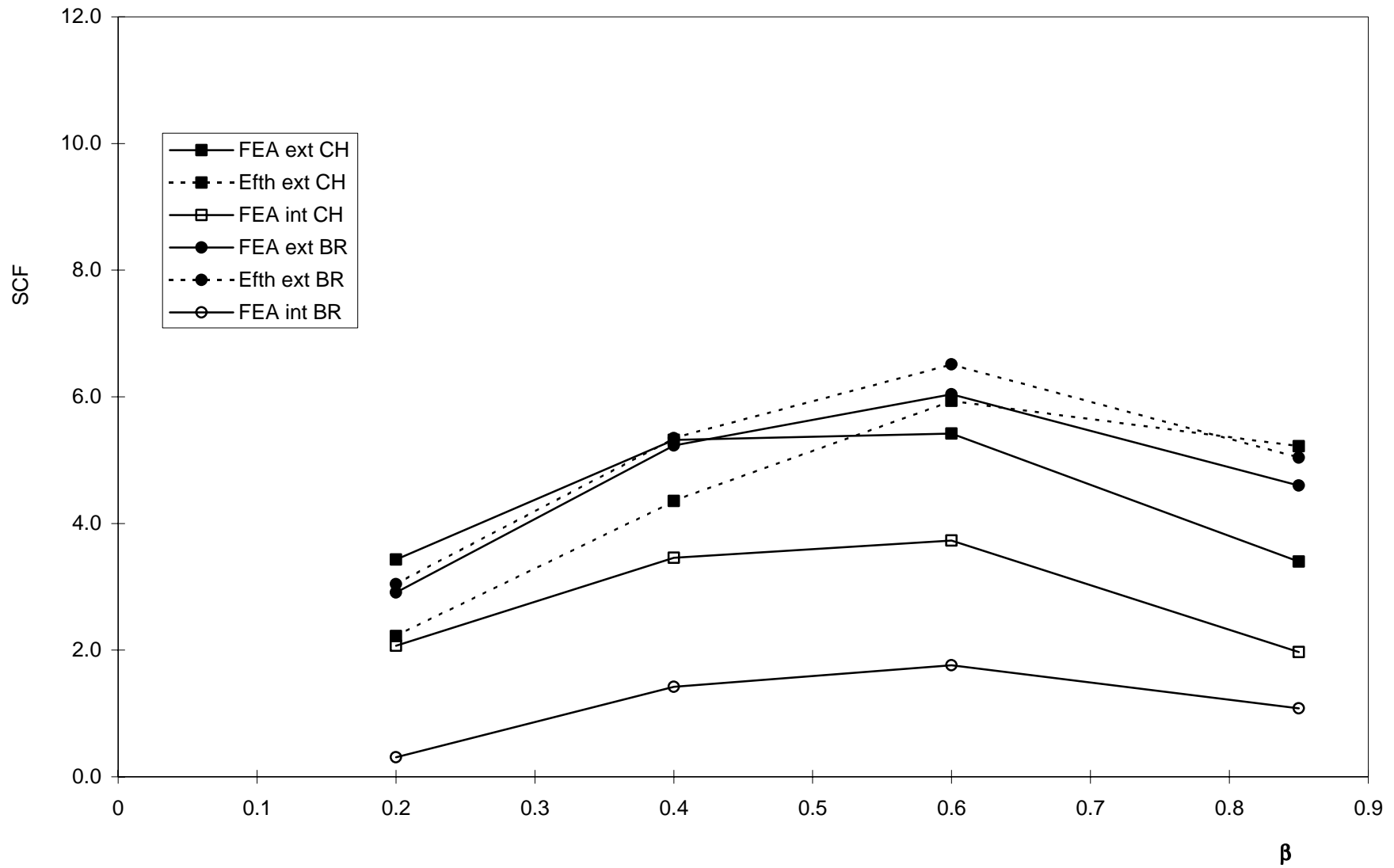


Figure B26: Xjoints (OPB), $\gamma = 21$, $\tau = 0.35$, $\theta = 90^\circ$

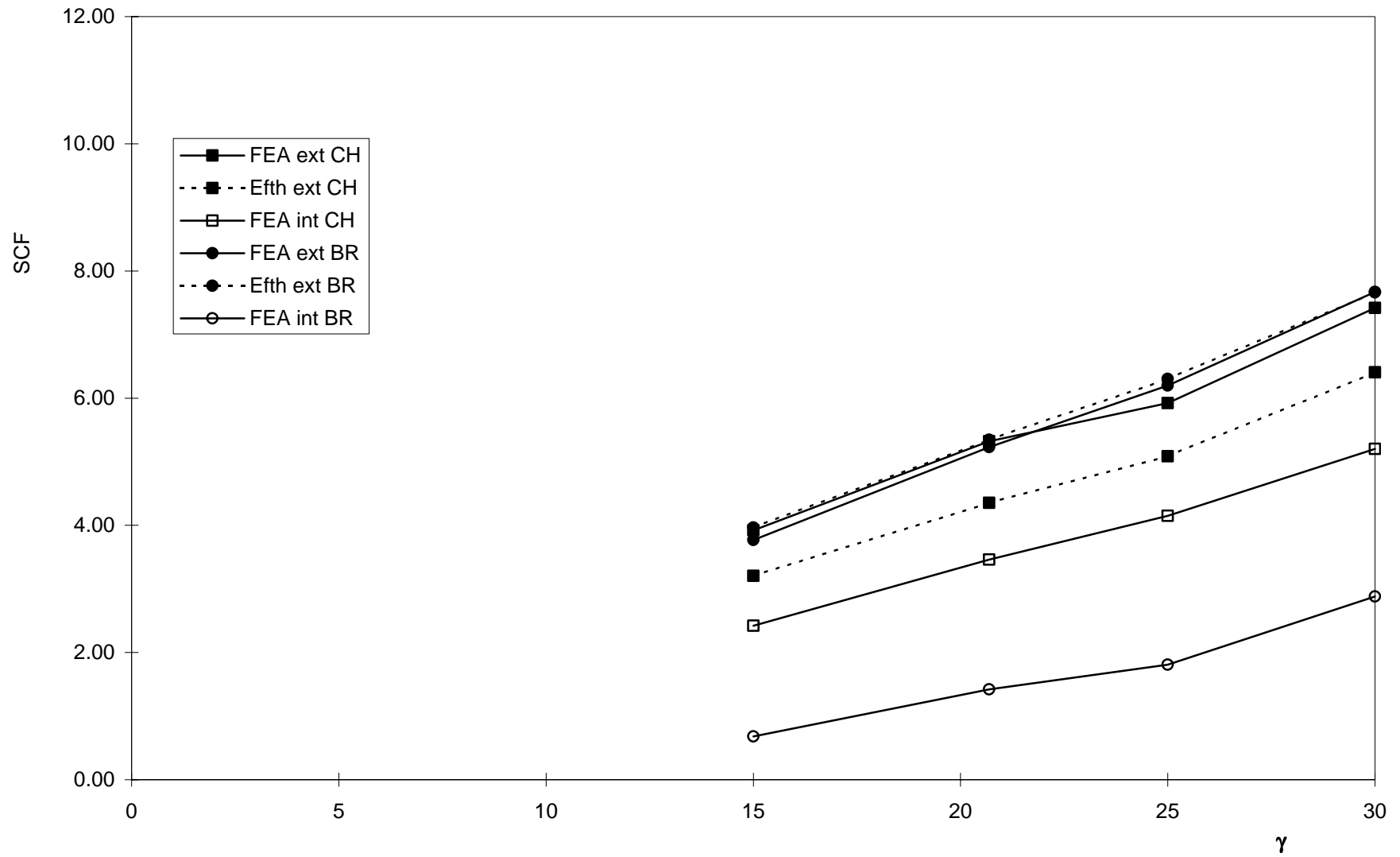


Figure B27: X joints (OPB), $\beta = 0.4$, $\tau = 0.35$, $\theta = 90^\circ$

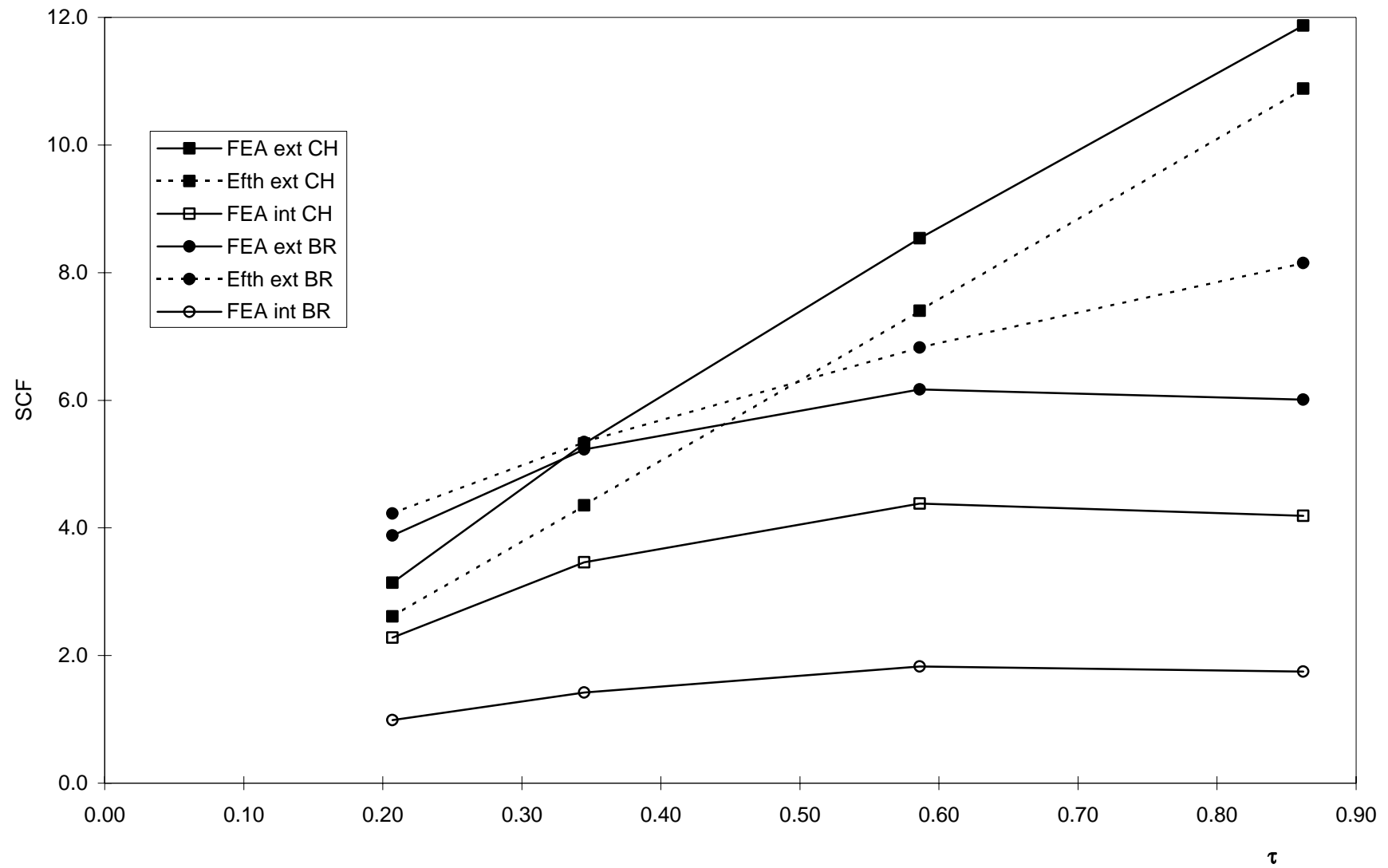


Figure B28: X joints (OPB), $\beta = 0.4$, $\gamma = 21$, $\theta = 90^\circ$

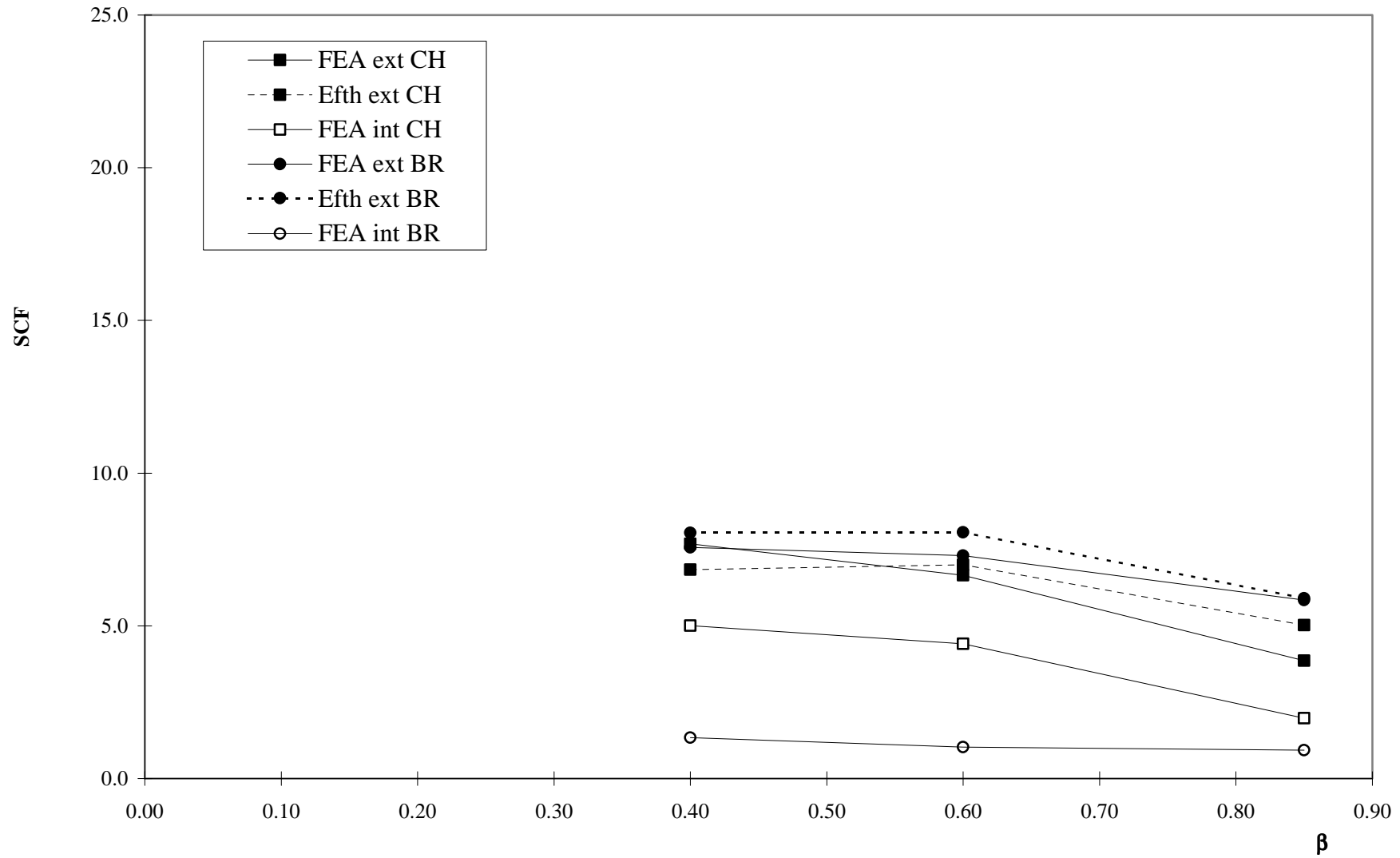


Figure B29: T-Joints (axially loaded) $\gamma = 20.69$, $\tau = 0.34$, $\theta = 90^\circ$

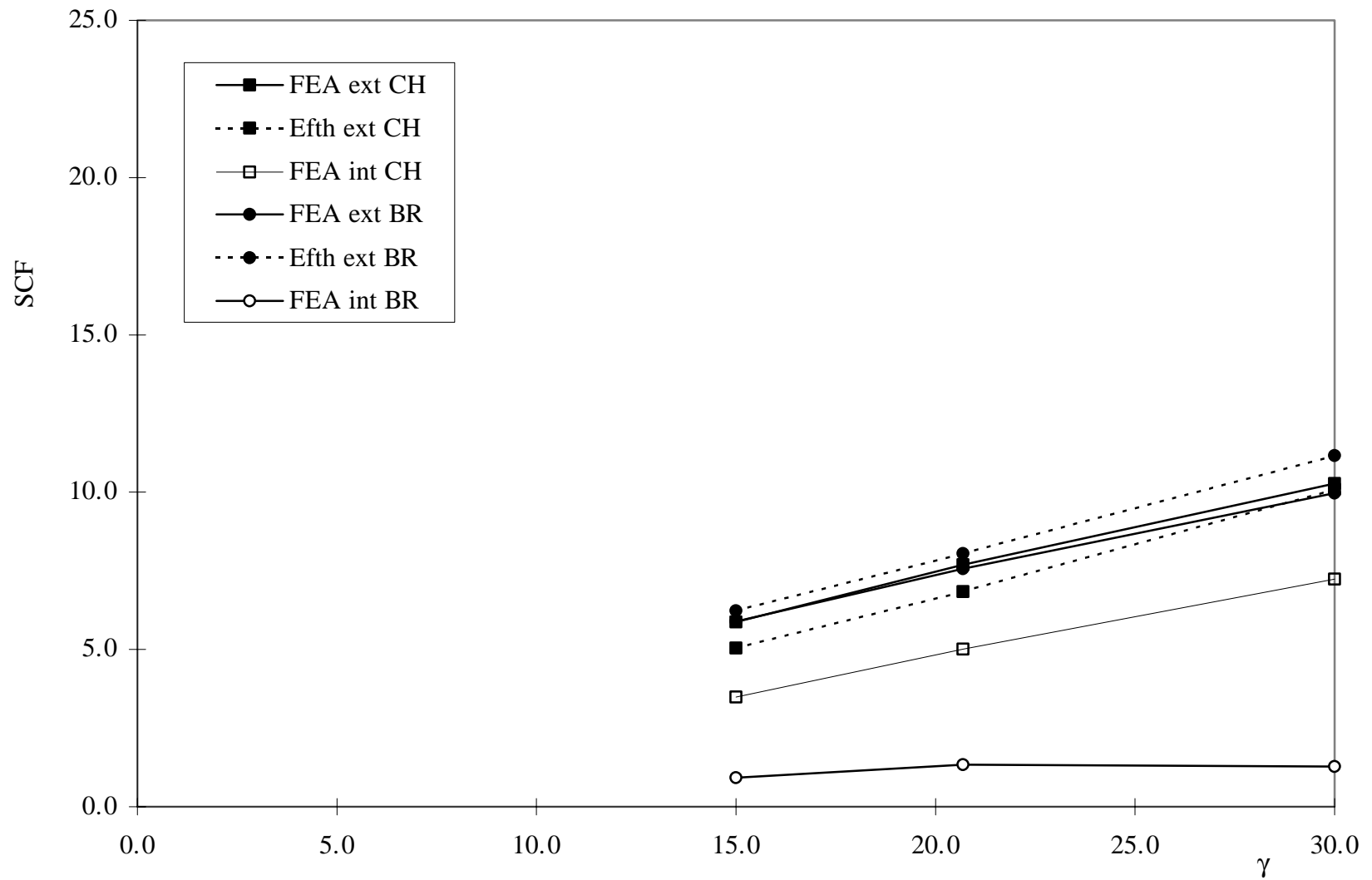


Figure B30: T-Joints (axially loaded) $\beta = 0.4$, $\tau = 0.35$, $\theta = 90^\circ$

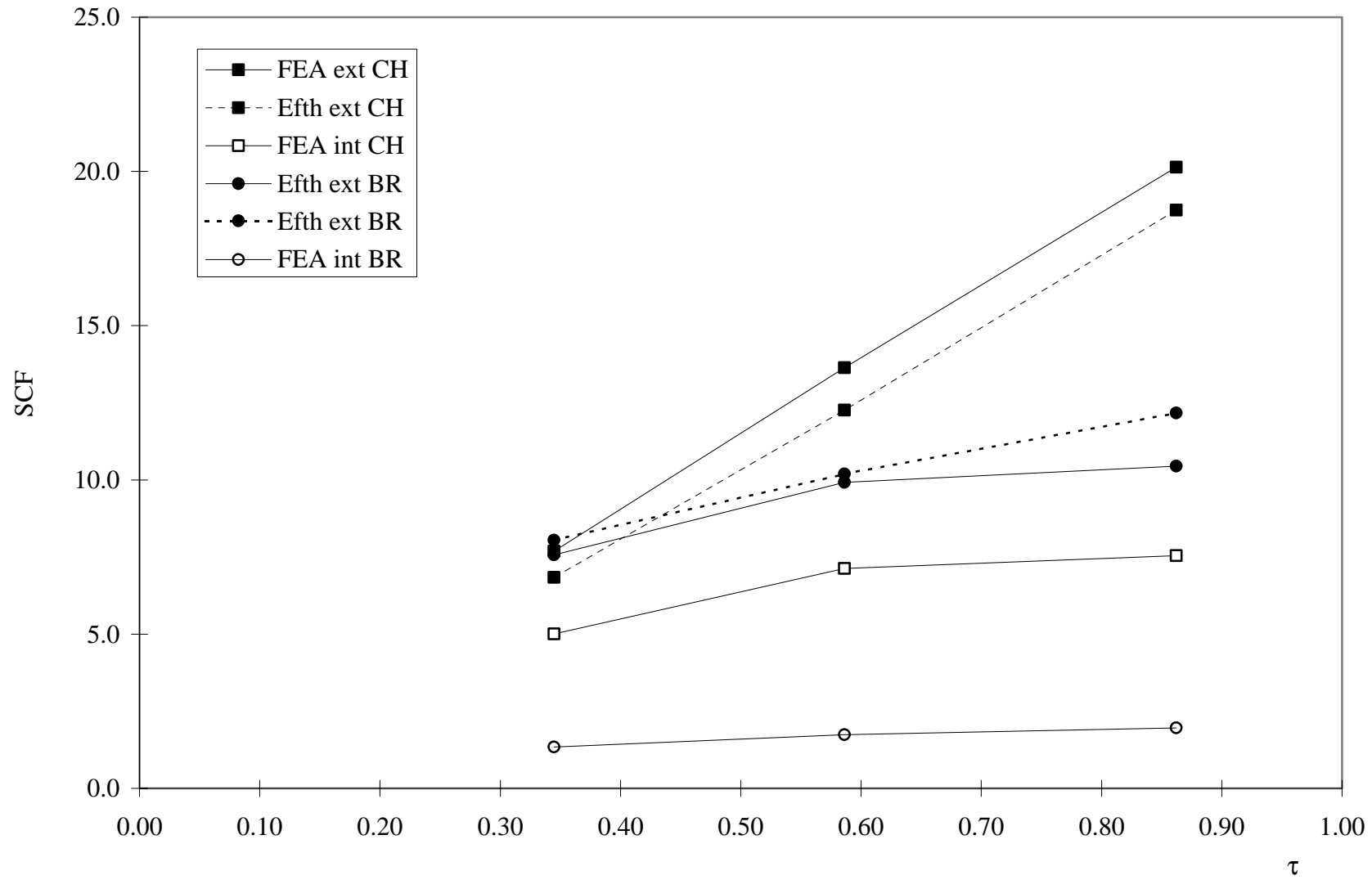


Figure B31: T-Joints (axially loaded), $\beta = 0.34$, $\gamma = 20.69$, $\theta = 90^\circ$

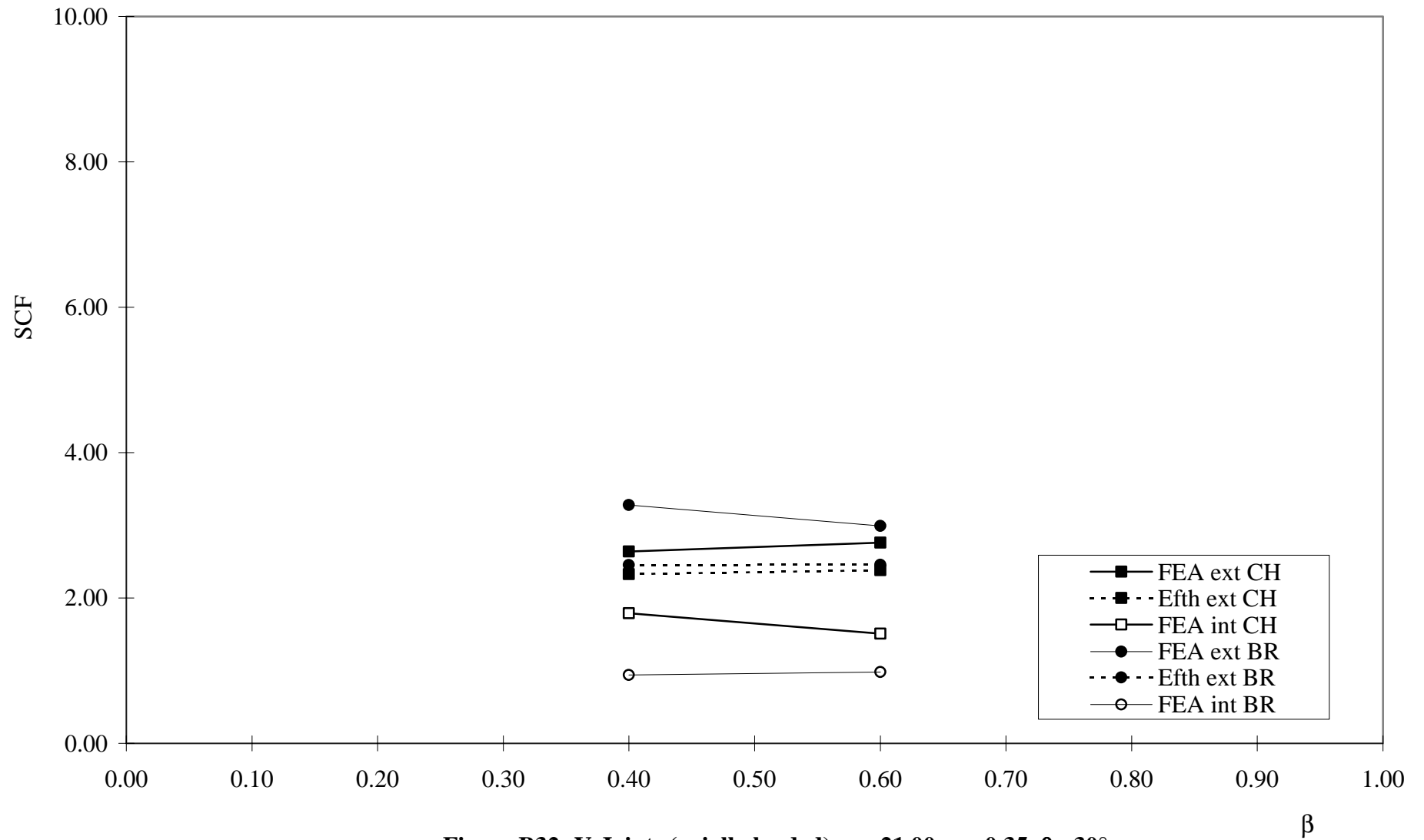


Figure B32: Y-Joints (axially loaded), $\gamma = 21.00$, $\tau = 0.35$, $\theta = 30^\circ$

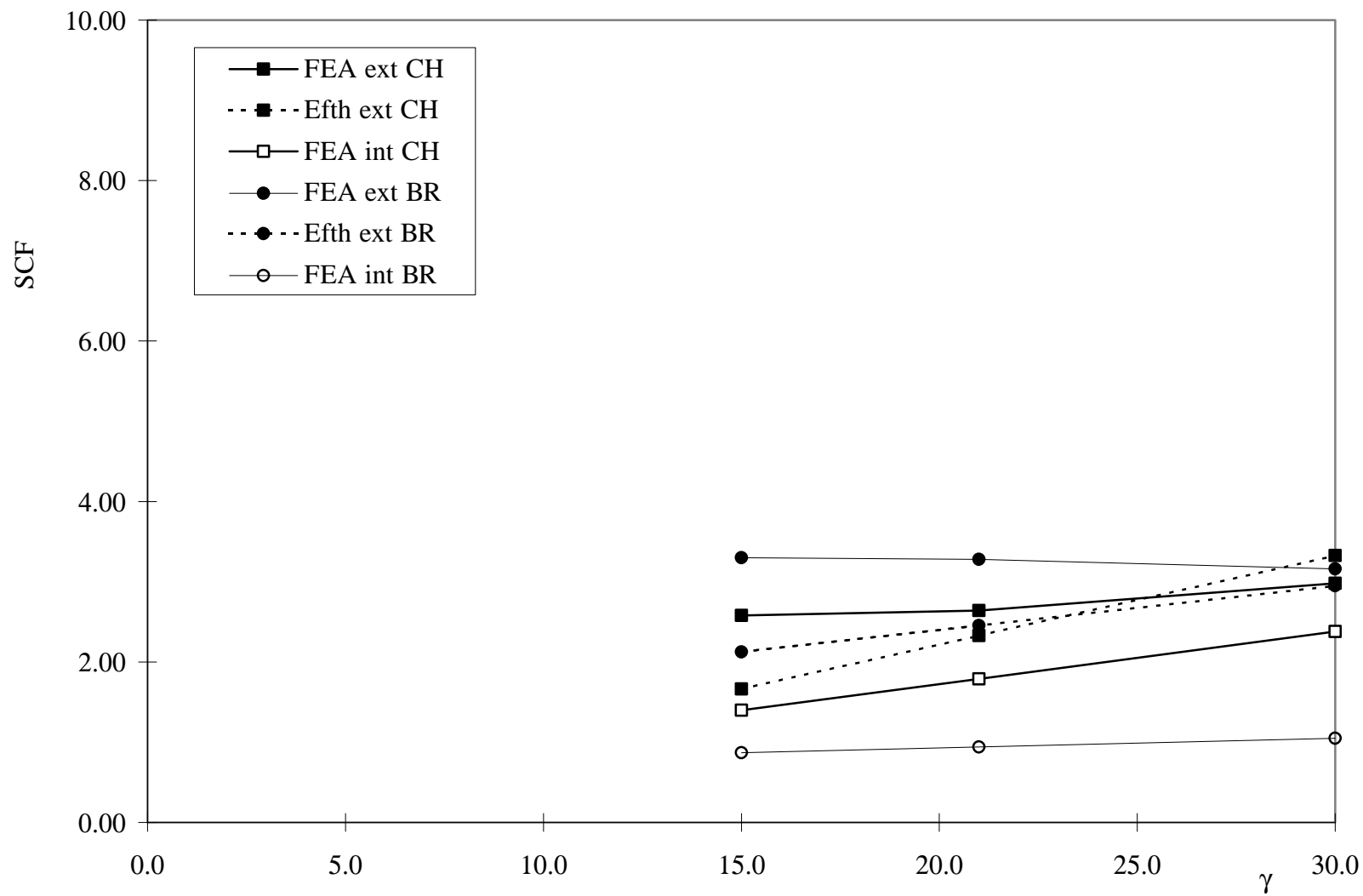


Figure B33: Y-Joints (axially loaded), $\beta = 0.4$, $\tau = 0.35$, $\theta = 30^\circ$

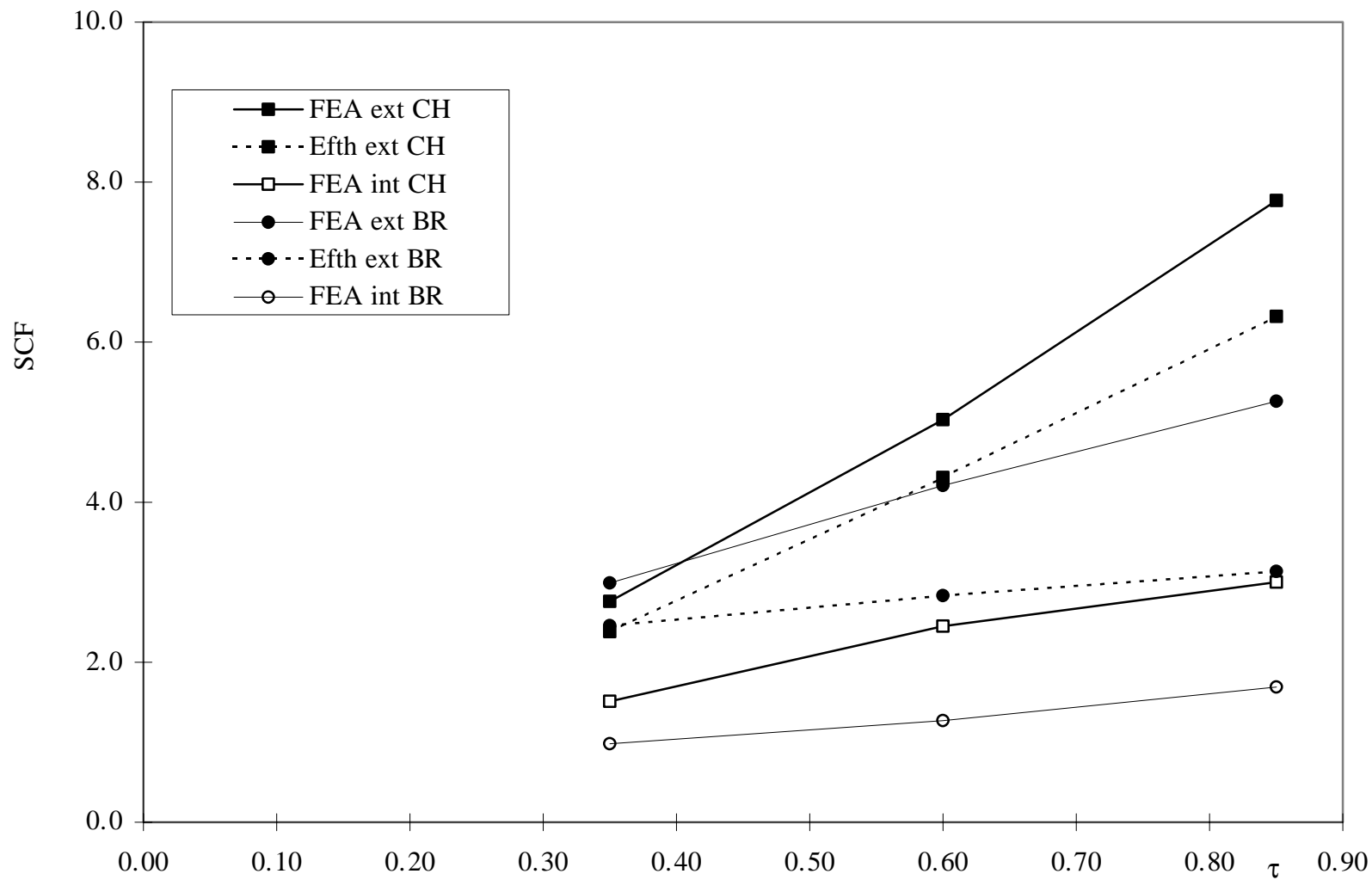


Figure B34: Y-Joints (axially loaded), $\beta = 0.6$, $\gamma = 21.00$, $\theta = 30^\circ$

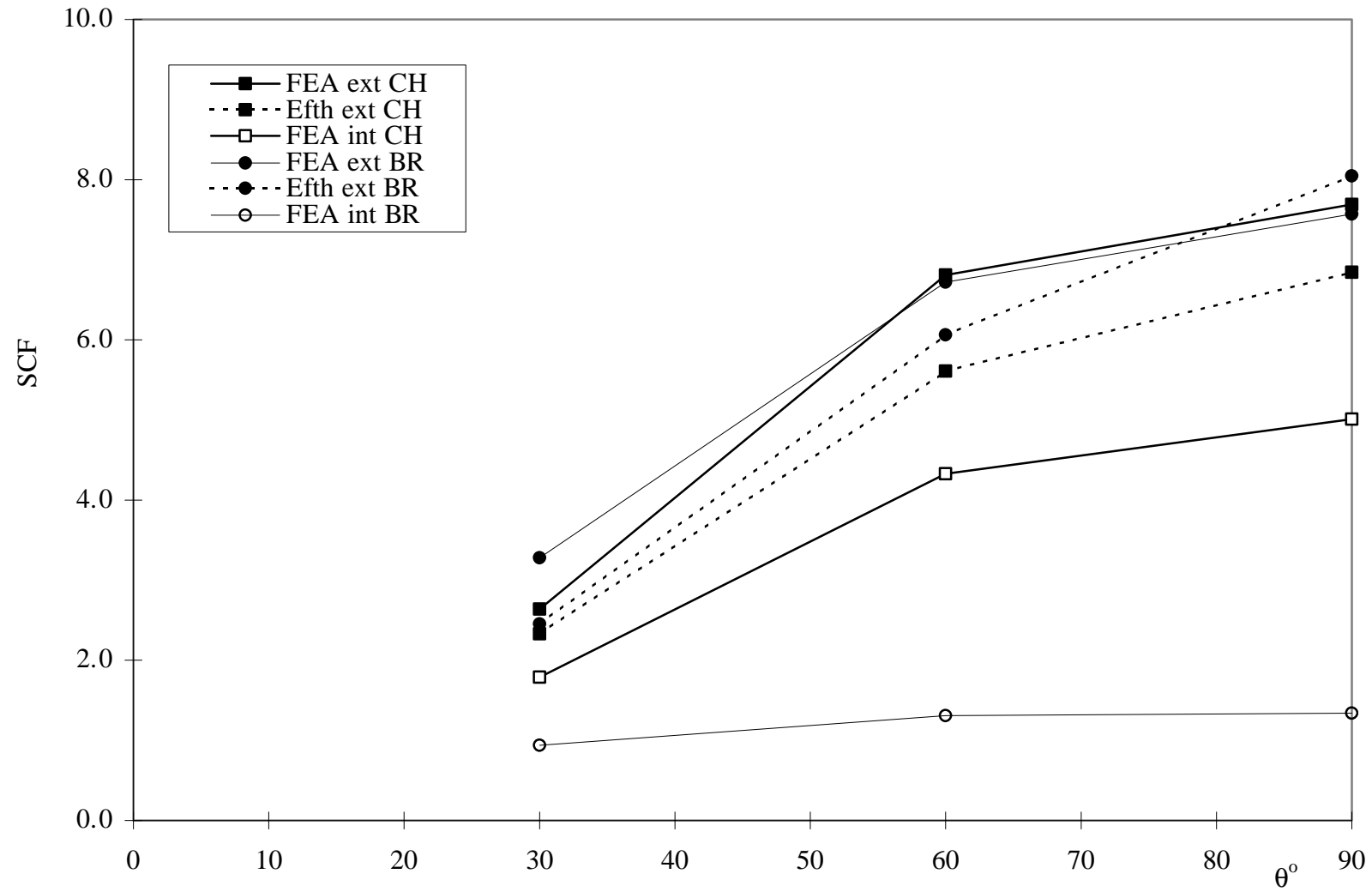


Figure B35: Y-Joints (axially loaded), $\beta = 0.4$, $\gamma = 21.0$, $\tau = 0.35$

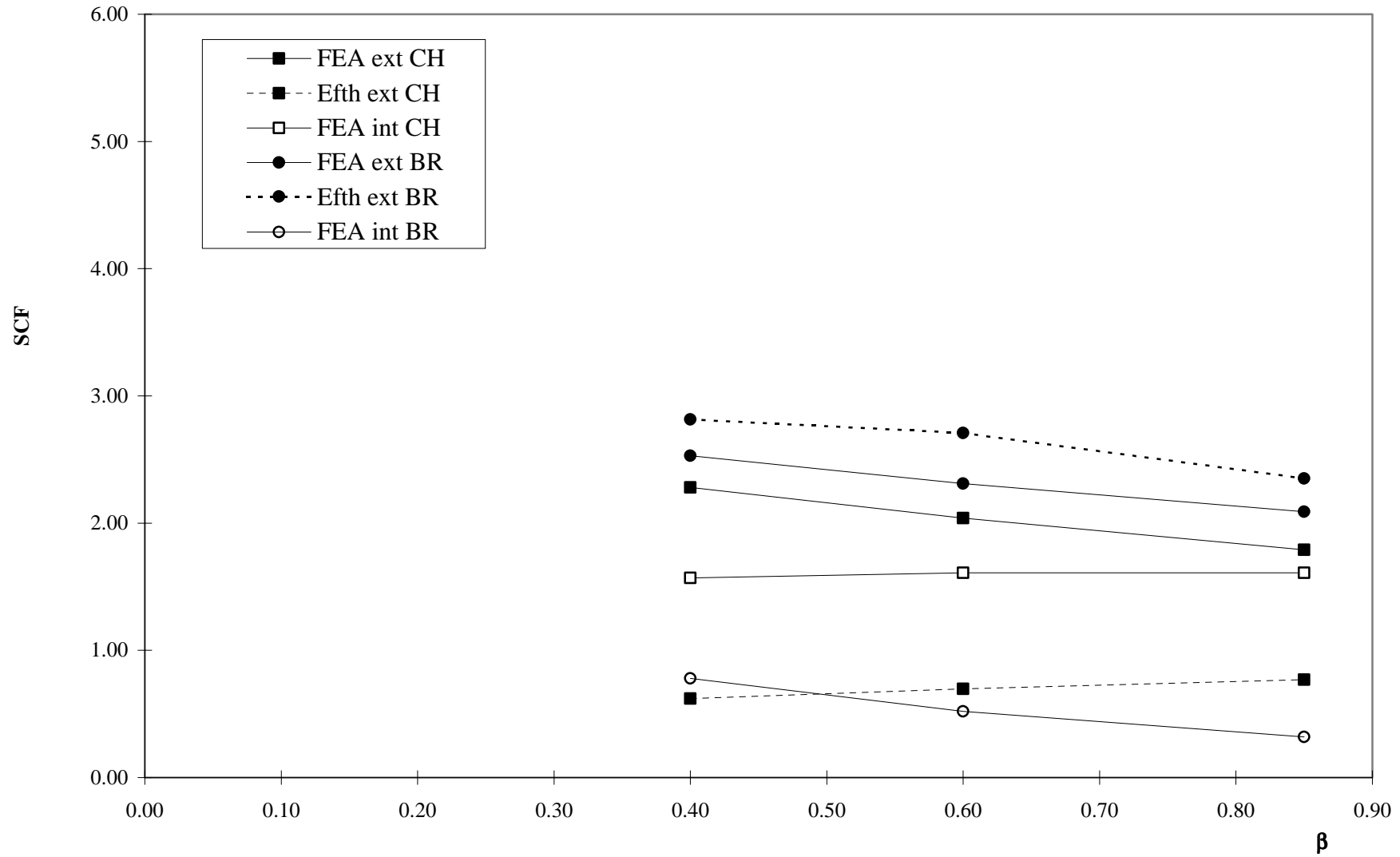


Figure B36: T-Joints (IPB), $\gamma = 20.69$, $\tau = 0.34$, $\theta = 90^\circ$

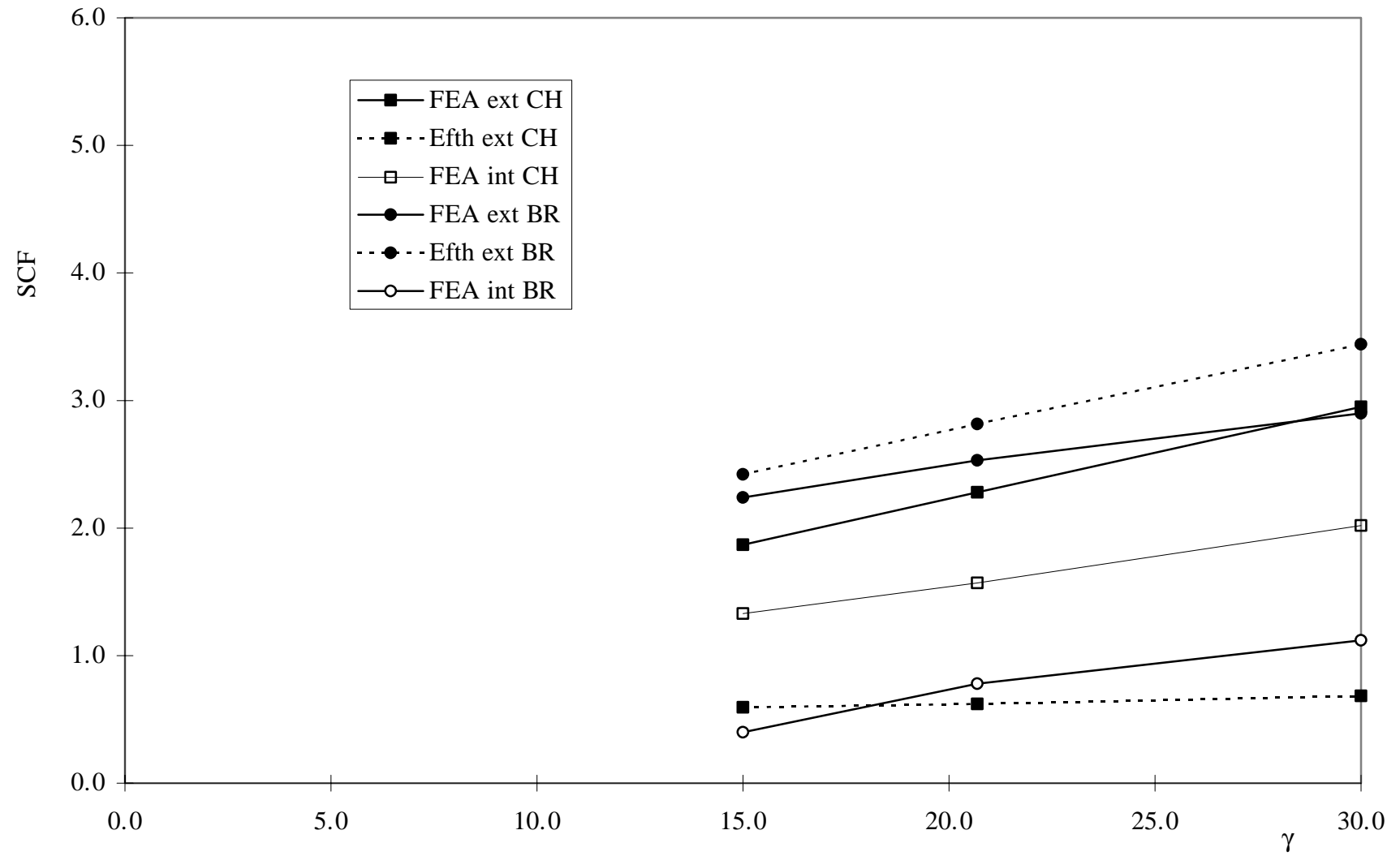


Figure B37: T-Joints (IPB), $\beta = 0.4$, $\tau = 0.35$, $\theta = 90^\circ$

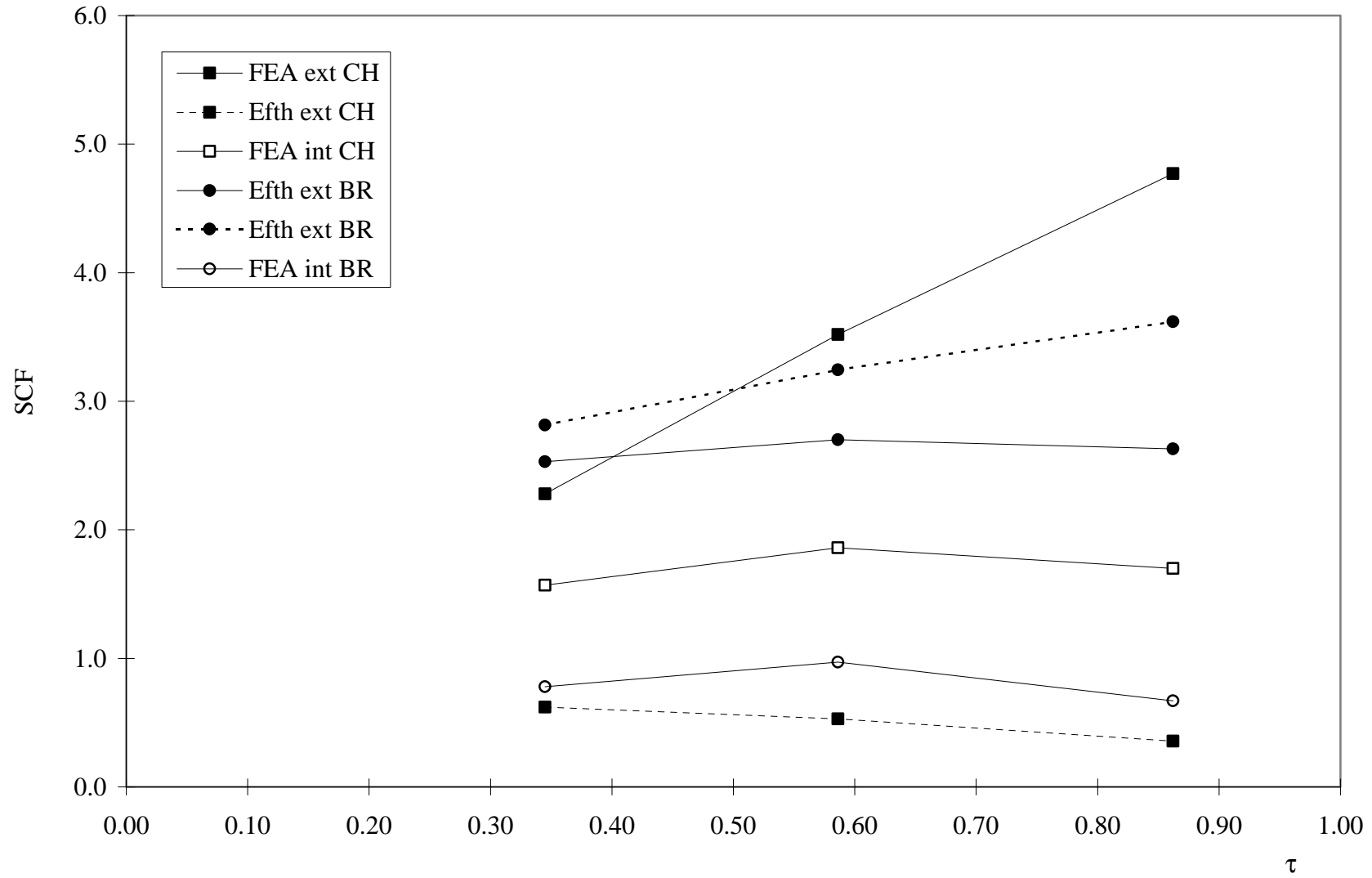


Figure B38: T-Joints (IPB), $\beta = 0.34$, $\gamma = 20.69$, $\theta = 90^\circ$

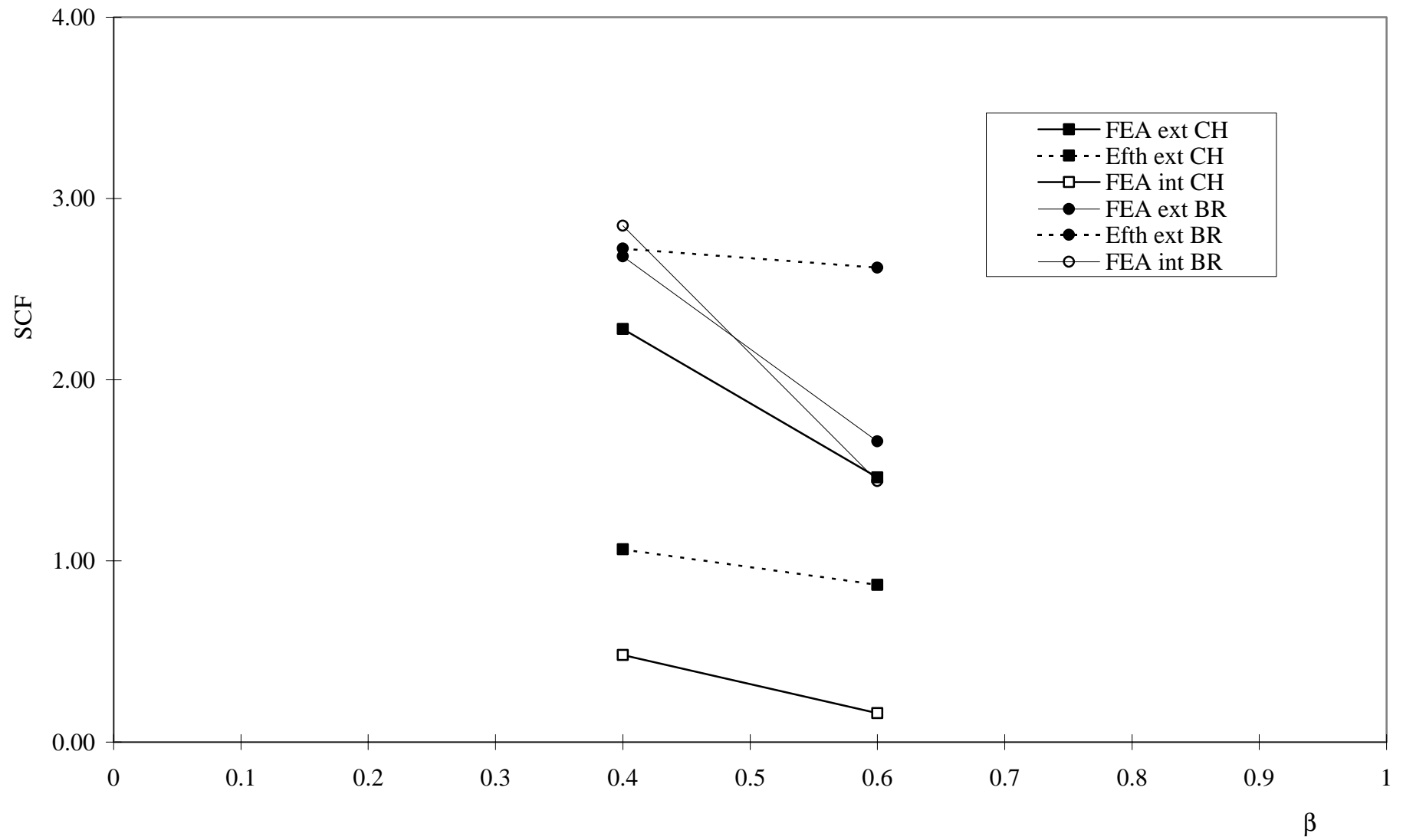


Figure B39: Y-Joints (IPB), $\gamma = 21.00$, $\tau = 0.35$, $\theta = 30^\circ$

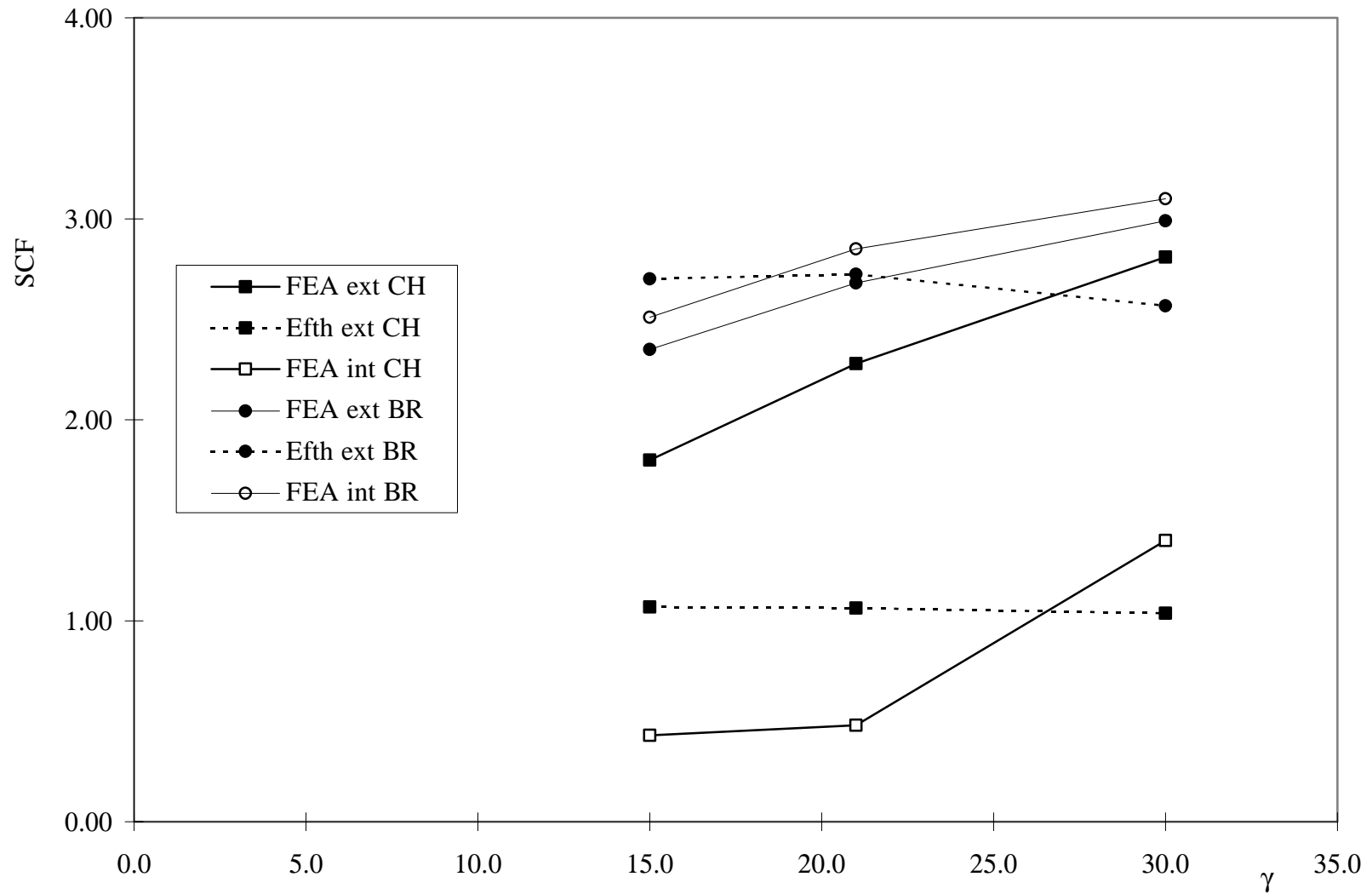


Figure B40: Y-Joints (IPB), $\beta = 0.4$, $\tau = 0.35$, $\theta = 30^\circ$

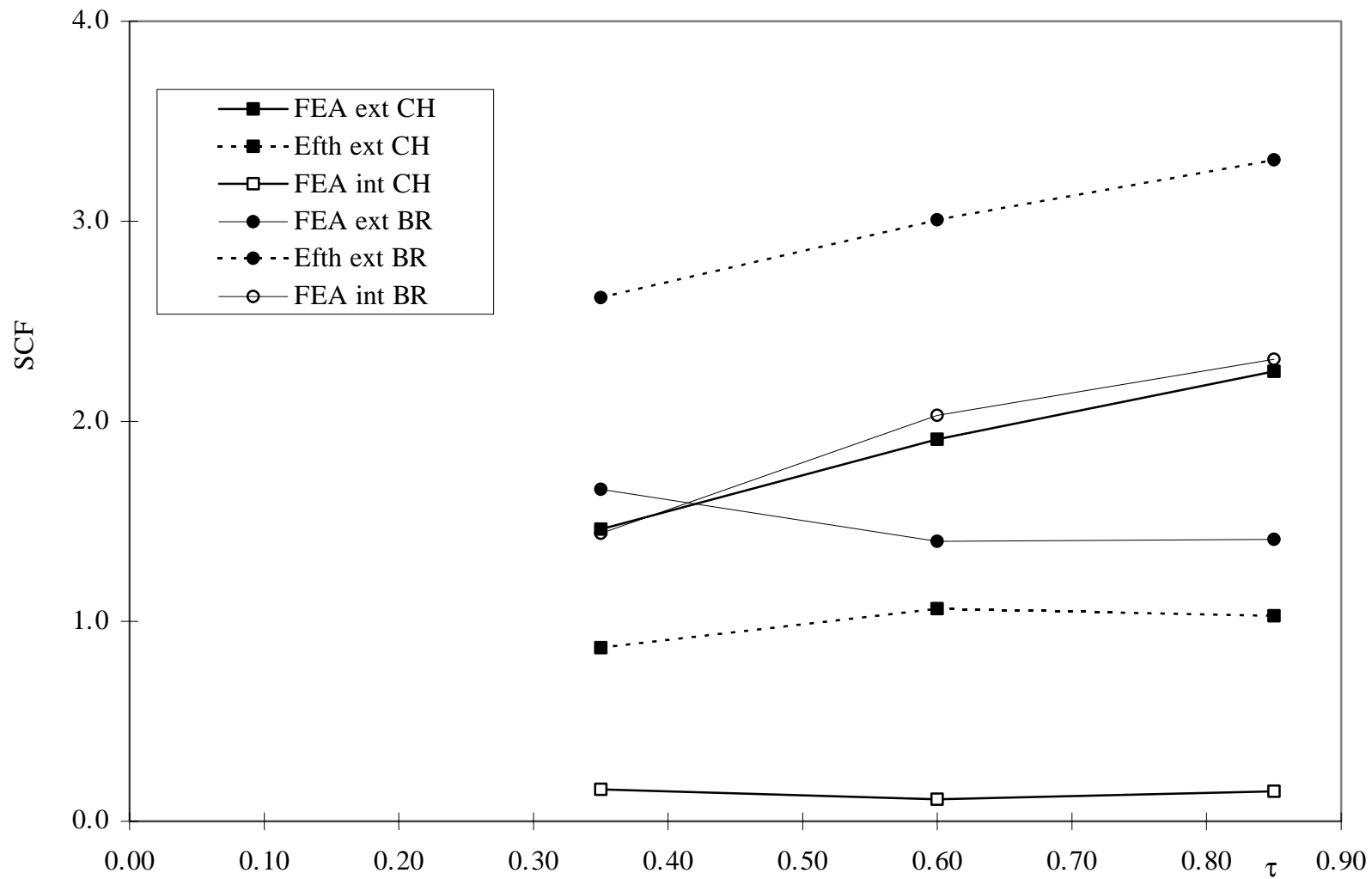


Figure B41: Y-Joints (IPB), $\beta = 0.6$, $\gamma = 21.00$, $\theta = 30^\circ$

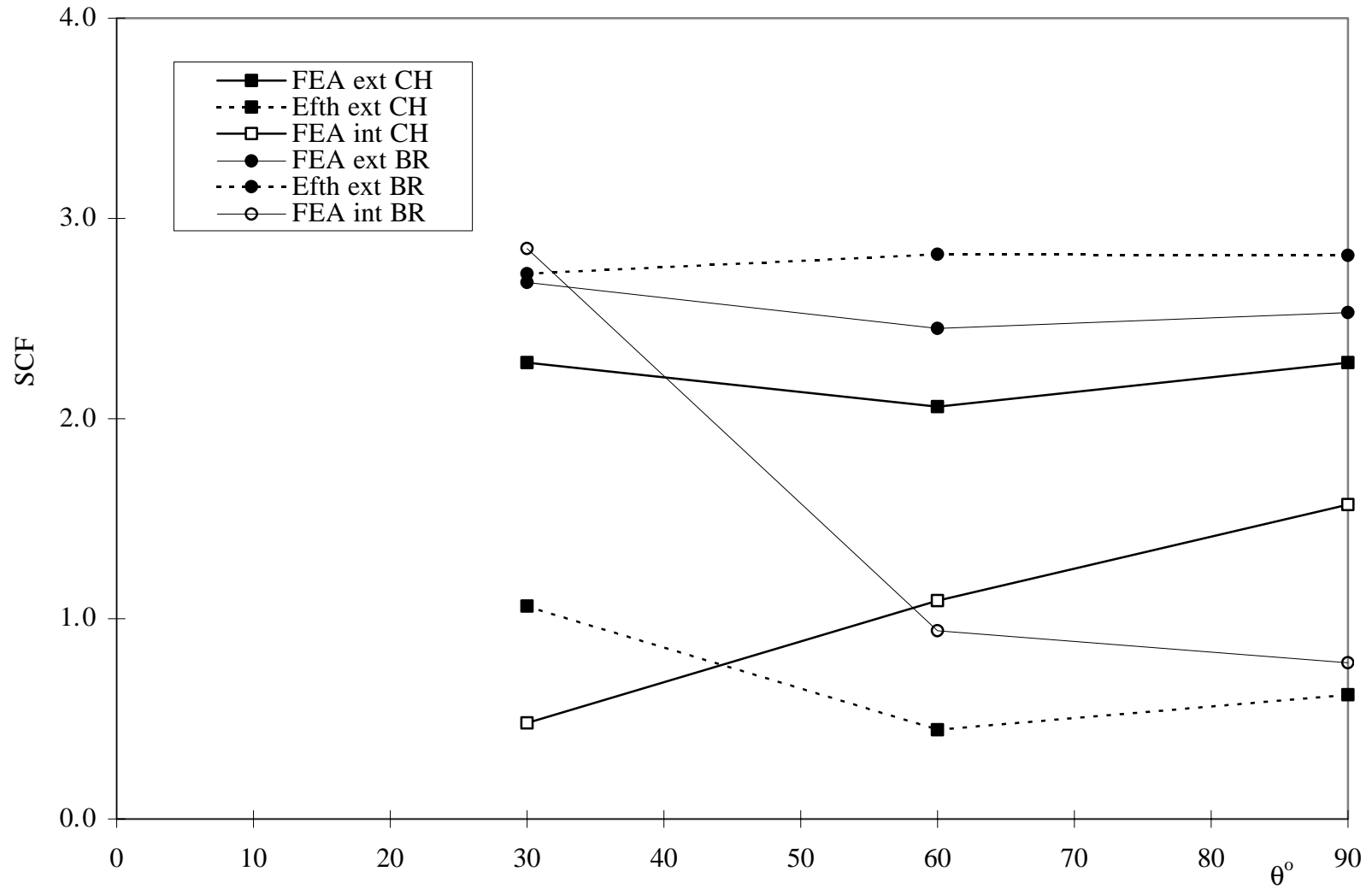


Figure B42: Y-Joints under IPB $\beta = 0.4$, $\gamma = 21.0$, $\tau = 0.35$

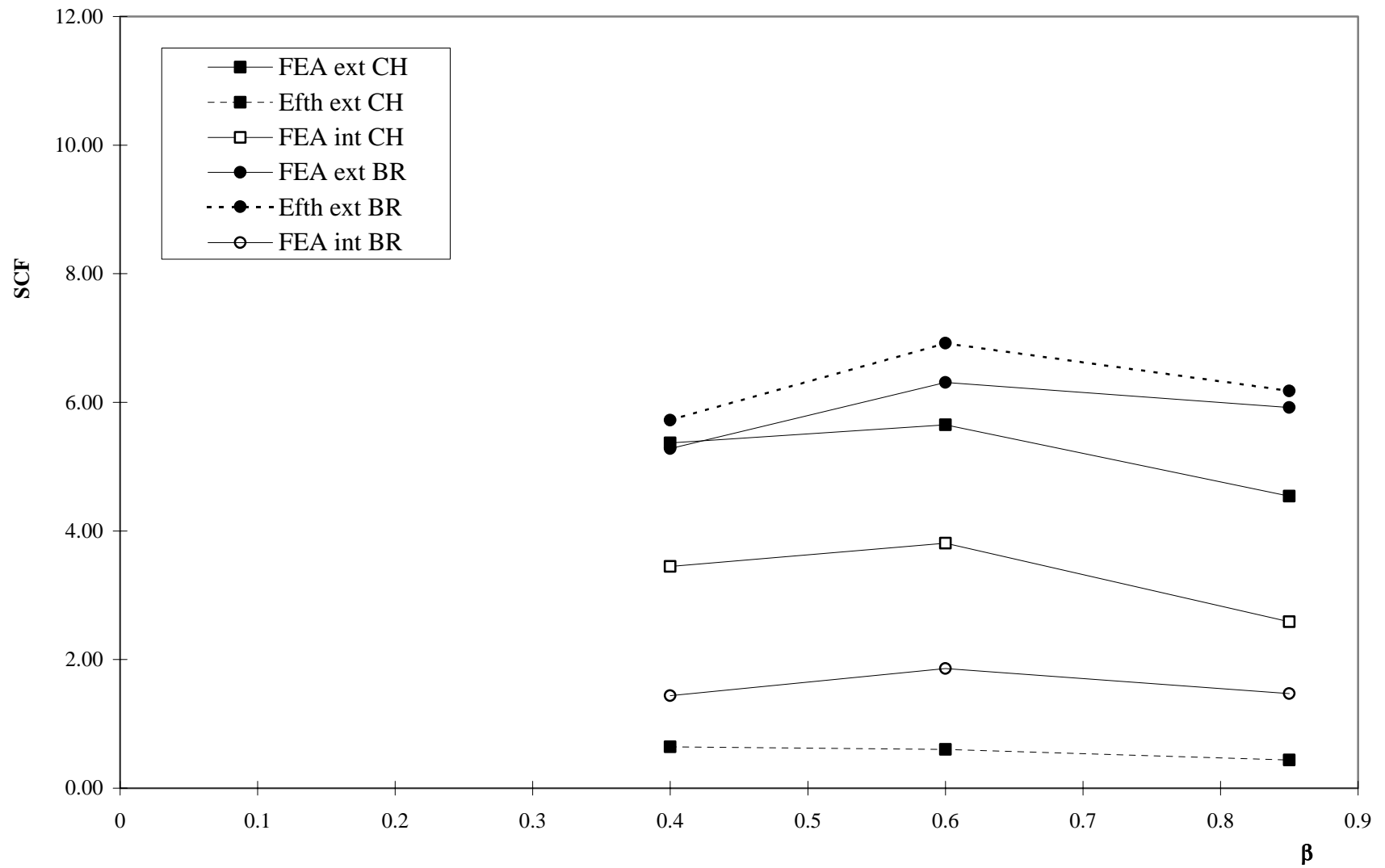


Figure B43: T-Joints (OPB), $\gamma = 20.69$, $\tau = 0.34$, $\theta = 90^\circ$

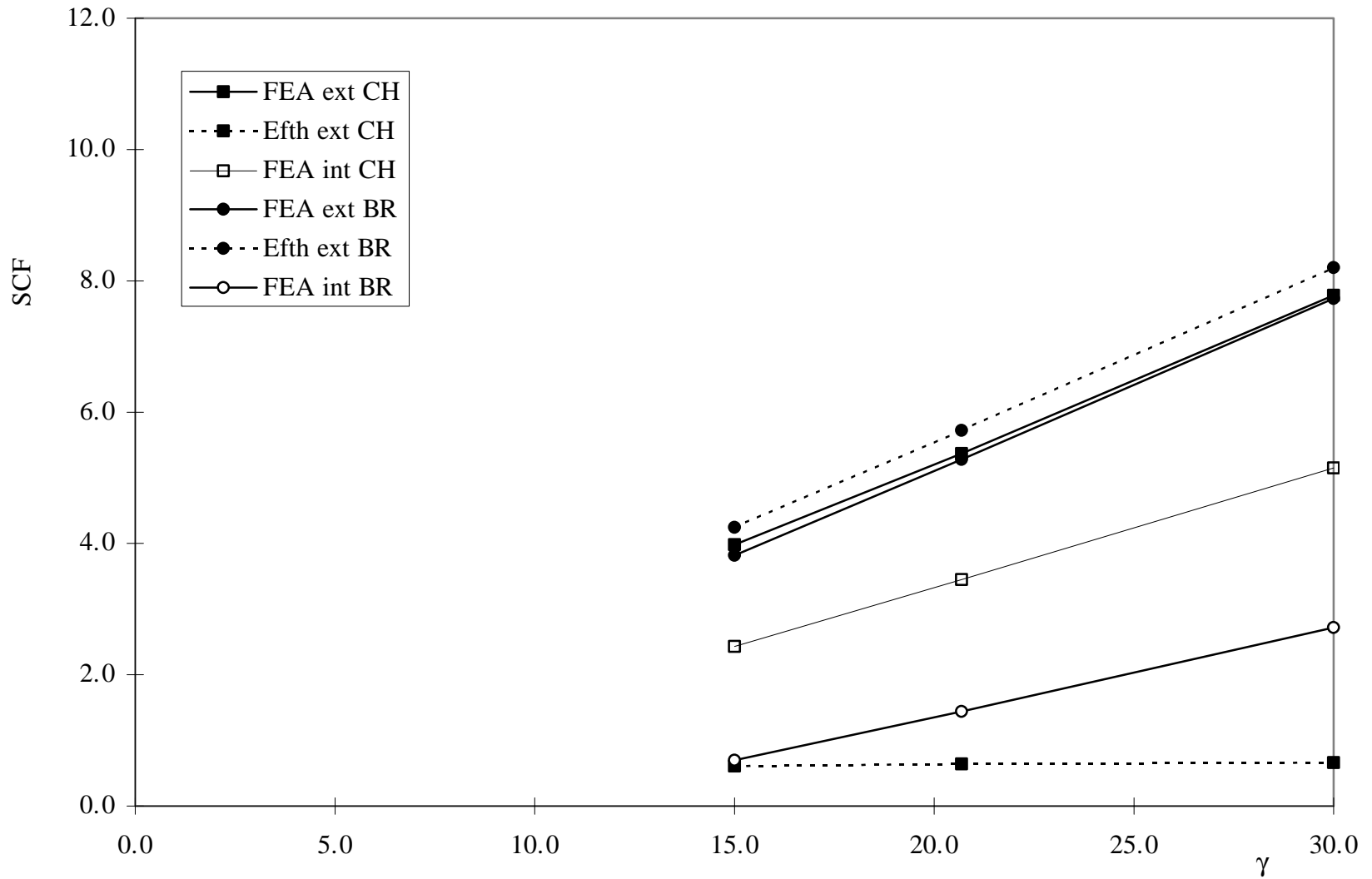


Figure B44: T-Joints (OPB), $\beta = 0.4$, $\tau = 0.35$, $\theta = 90^\circ$

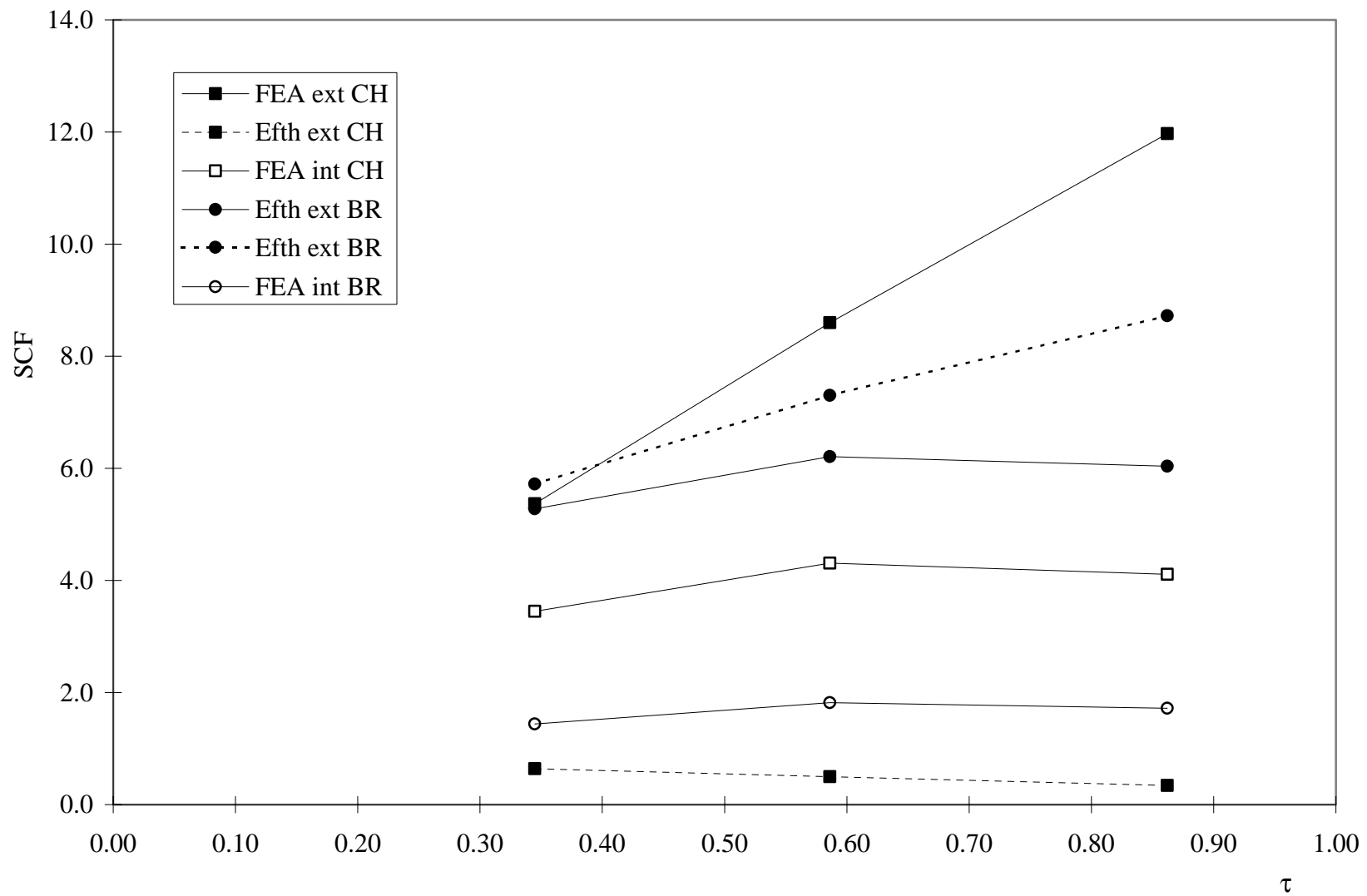


Figure B45: T-Joints (OPB), $\gamma = 20.69$, $\beta = 0.34$, $\theta = 90^\circ$

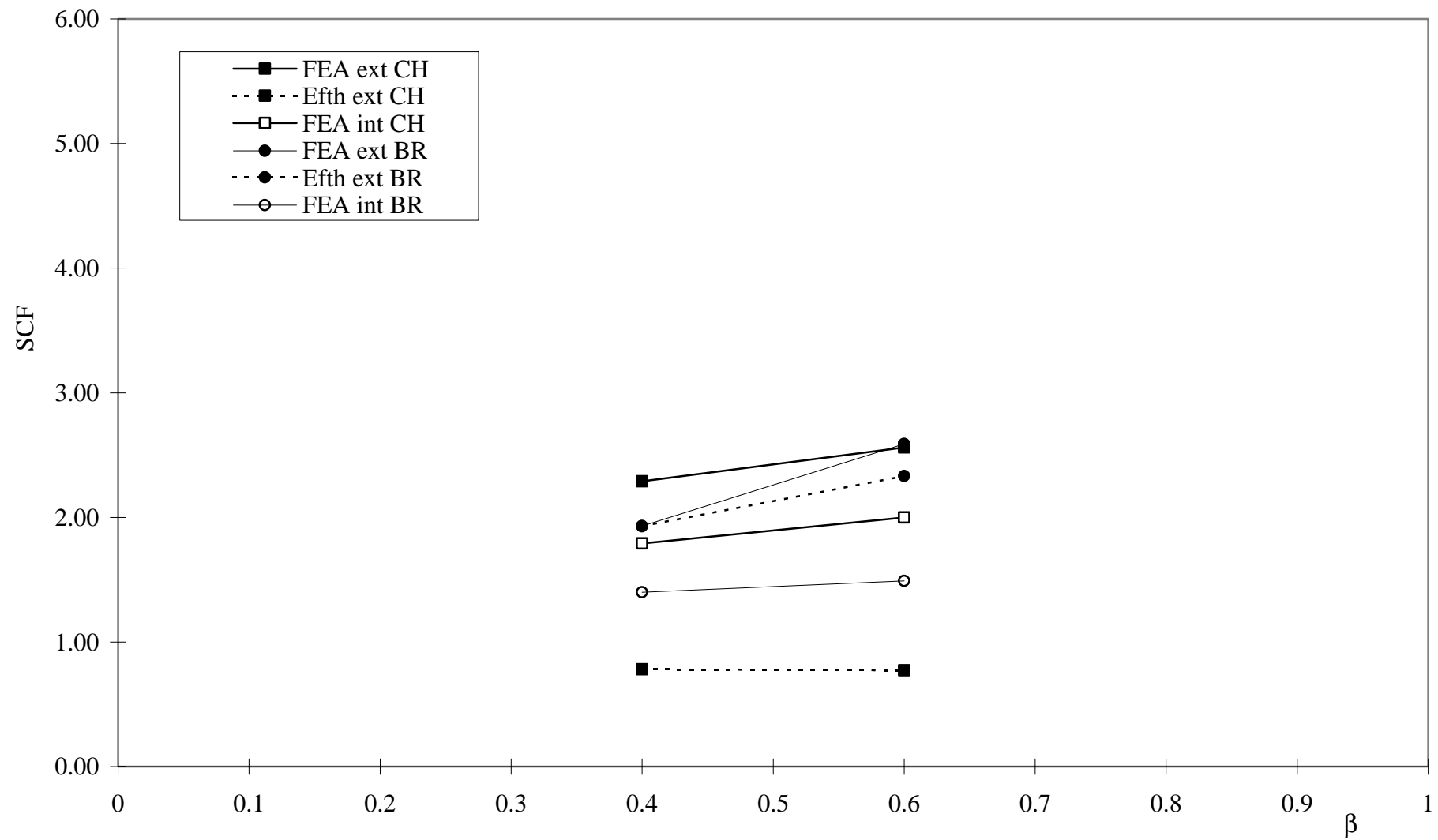


Figure B46: Y-Joints (OPB), $\gamma = 21.00$, $\tau = 0.35$, $\theta = 30^\circ$

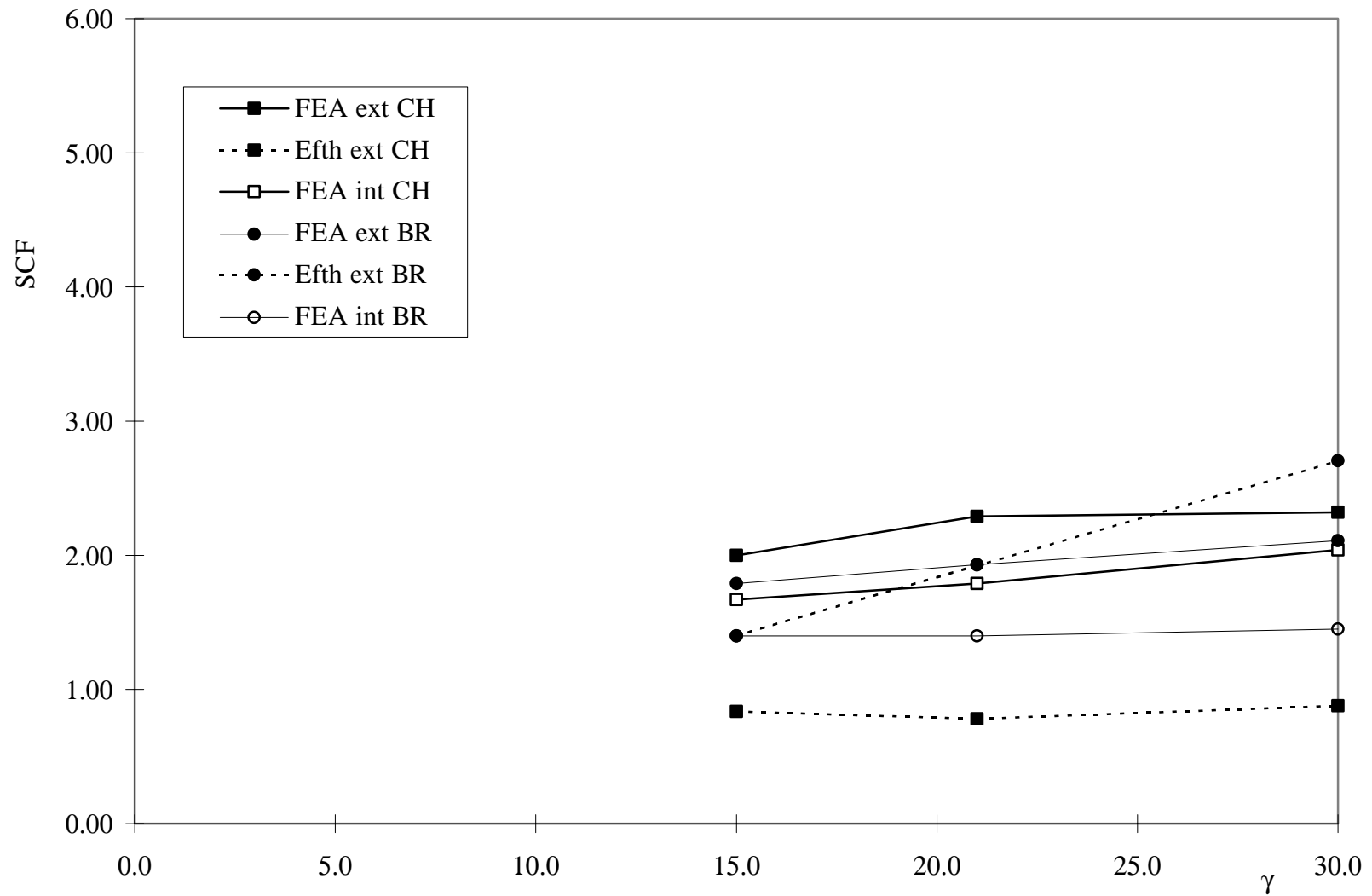


Figure B47: Y-Joints (OPB), $\beta = 0.4$, $\tau = 0.35$, $\theta = 30^\circ$

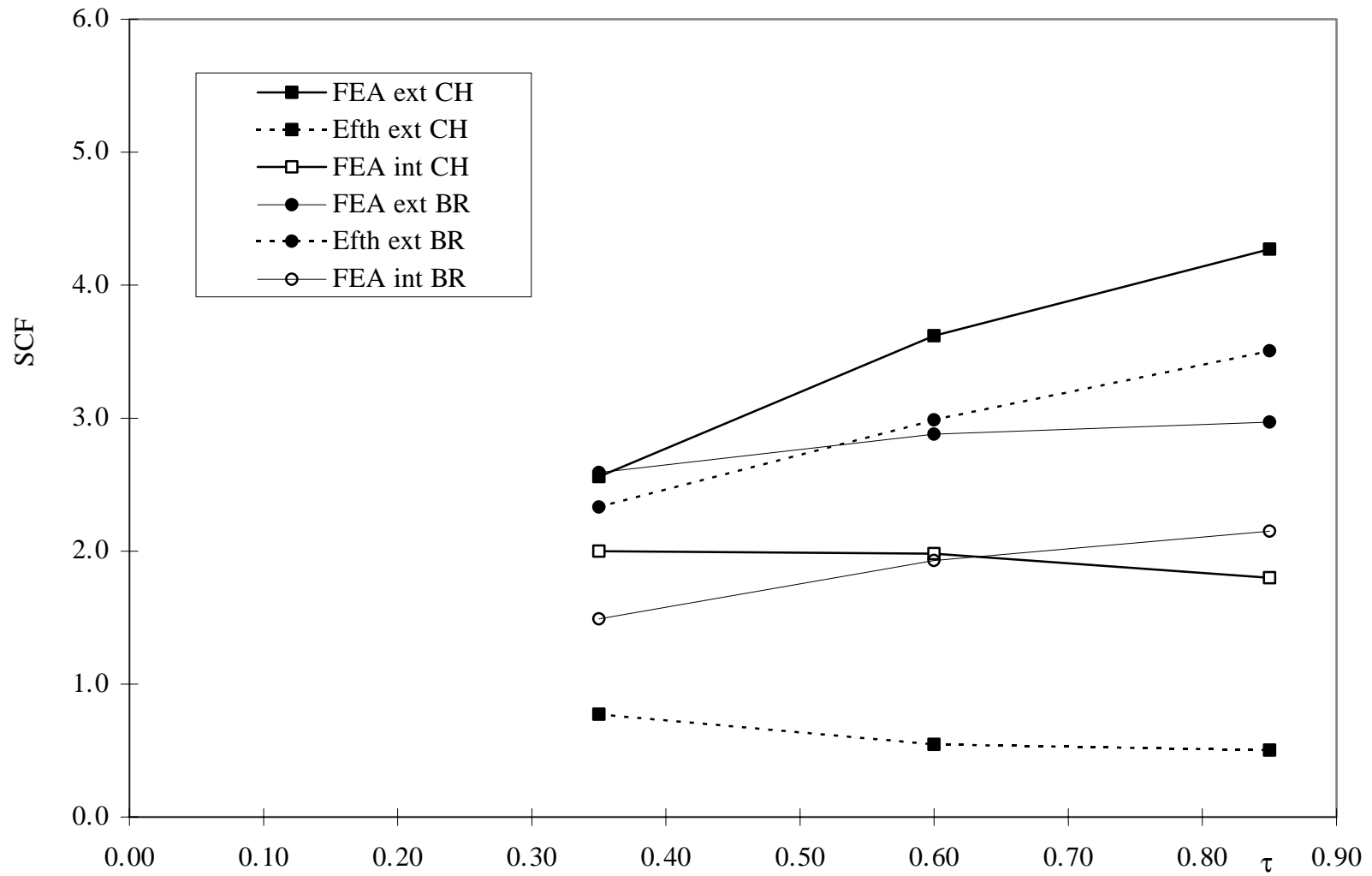


Figure B48: Y-Joints (OPB), $\beta = 0.6$, $\gamma = 21.00$, $\theta = 30^\circ$

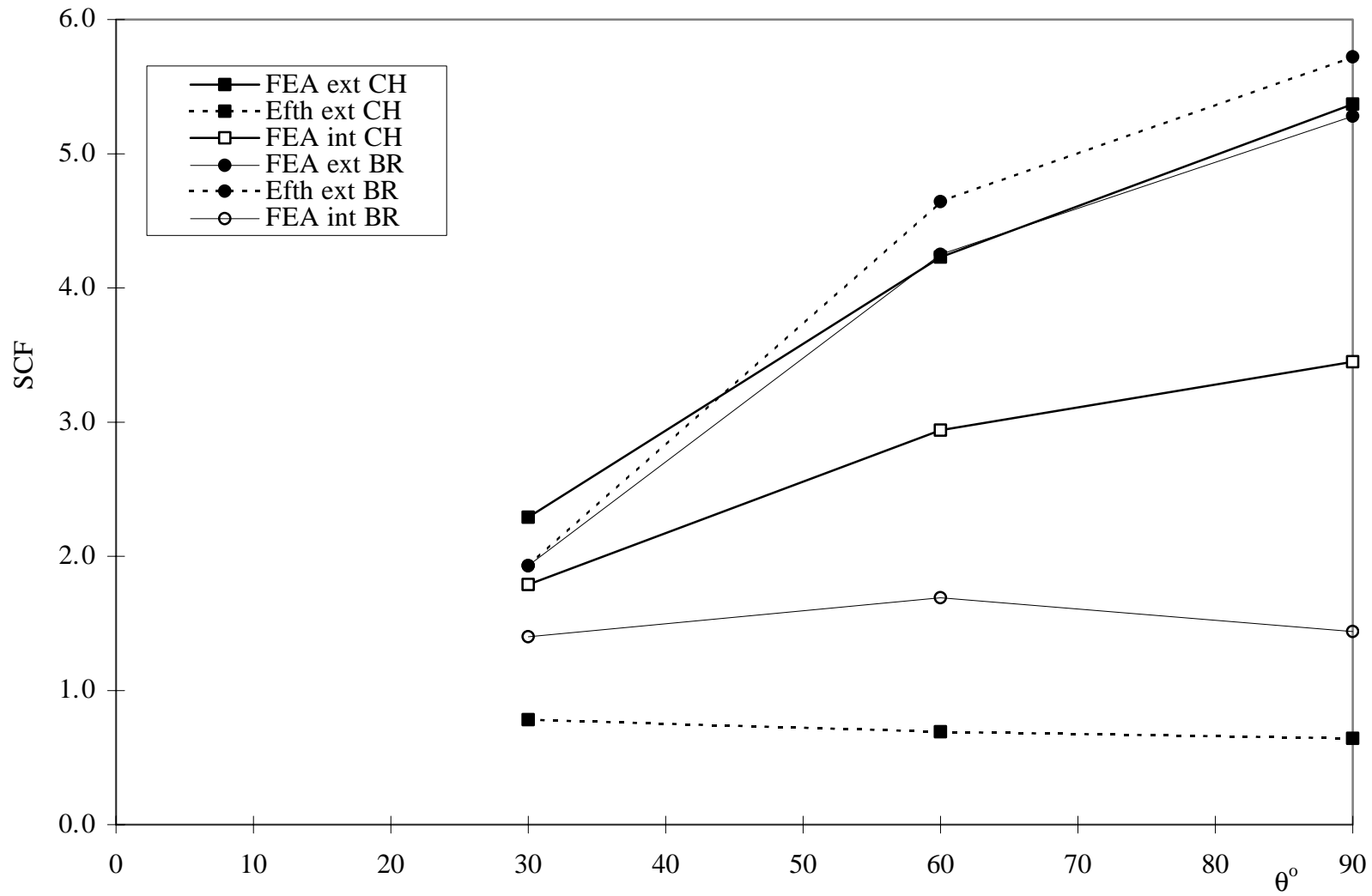


Figure B49: Y-Joints (OPB), $\beta = 0.4$, $\gamma = 21.0$, $\tau = 0.35$